TU Graz

Dipl.-Ing. Martin Tscherner

Opto-Chemical Sensing Technology for Measuring Oxygen Transmission Rates of Ultra-Barrier Membranes

Development and First Applications

DISSERTATION

zur Erlangung des akademischen Grades

Doktor der technischen Wissenschaften

eingereicht an der

Technischen Universität Graz

Betreuer

Em.Univ.-Prof. Dipl.-Ing. Dr.techn.Franz Stelzer

Institut für Chemische Technologie von Materialien

Graz, Oktober 2017

EIDESSTATTLICHE ERKLÄRUNG

Ich erkläre an Eides statt, dass ich die vorliegende Arbeit selbstständig verfasst, andere als die angegebenen Quellen/Hilfsmittel nicht benutzt, und die den benutzten Quellen wörtlich und inhaltlich entnommenen Stellen als solche kenntlich gemacht habe. Das in TUGRAZonline hochgeladene Textdokument ist mit der vorliegenden Dissertation identisch.

18·10·2017
Datum
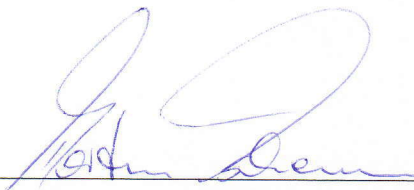
Unterschrift

DEDICATED TO

MY DAUGHTER LUISA

BORN 7TH OF OCTOBER, 2016

ACKNOWLEDGEMENT

ABSTRACT

In the 2000 decade, worldwide activities dedicated to preparation of cost-effective, flexible and transparent ultra-barrier membranes (such as the project "Flexonics" funded by the European commission) intensified significantly. Research is, however, aggravated by lack of sufficiently sensitive yet easily operated analytical tools covering the full range of ultra-low permeation rates relevant in the field of organo-electronics encapsulation. Some reports consider barriers with oxygen transmission rates ("OTR") as low as 10^{-6} [cm^3 m^{-2} day^{-1} atm^{-1}] and water vapour transmission rates ("WVTR") of 10^{-7} [g m^{-2} day^{-1}] mandatory for sufficient durability of organo-electronic components, enabling their application in the first place. Although renowned manufacturers of analytical instruments have meanwhile reacted to the challenges, the detection limits of the best commercial devices are still behind these worst-case-scenario demands by orders of magnitude. The topic was investigated and discussed intensively in the first stages of the conducted work.

Ultimately, a highly sensitive alternative for measuring oxygen transmission rates of ultra-barrier membranes is presented in this doctoral thesis. The key concept involves an opto-chemical sensing scheme, thus using a luminescent dye immobilized in a matrix as the actual sensitive element. The luminescent response of the sensor to modulated light, altered in the presence of oxygen, is non-invasively evaluated by opto-electronic instrumentation. Such sensing systems offer unique advantages over electrochemical sensors, above all the capability for consumption-less detection and the extraordinary sensitivity of some luminophore/ matrix combinations. Based on opto-chemical detection, an autonomously operating stand-alone permeation instrument was developed. Unlike in conventional devices using a continuous purge flow passing the analyte into a detector, the permeating oxygen is accumulated in a sealed cavity in the immediate vicinity of the sample membrane while permeation is being monitored simultaneously.

In the development process, which was embedded in "Flexonics", the key aspects, determining the attainable device performance, were identified and, if applicable, subject of improvement. After countless modifications addressing the entire measuring chain and requiring chemical, mechanical, electronic, mathematical modelling and programming skills, the demonstrator instruments achieve a limit of detection in the 10^{-5} [cm^3 m^{-2} day^{-1} atm^{-1}] regime. They are therefore among the most sensitive O_2 permeability testers and outperforming commercial instruments by an order of magnitude, yet offering similar convenience in operation. Unresolved issues, meanwhile dominating detection limit and accuracy, include surface-chemical effects inside the stainless-steel permeation cell and the time-scale of diffusion kinetics inside the accumulation cavity.

KURZFASSUNG

Ab 2000 wurden weltweit Aktivitäten, die der Herstellung von günstigen, flexiblen und transparenten Ultrabarrierefolien gewidmet sind (wie auch das von der europäischen Kommission finanzierte Projekt „Flexonics"), bedeutend intensiviert. Durch die Nichtverfügbarkeit von ausreichend empfindlichen und zugleich leicht anwendbaren analytischen Werkzeugen, die den gesamten Bereich extrem niedriger, im Gebiet der Verkapselung von Organoelektronik relevanter Permeationsraten abdecken, wird allerdings die Forschung dazu erheblich erschwert. Manche Quellen erachten Barrieren mit Sauerstofftransmissionsraten von 10^{-6} [cm^3 m^{-2} day^{-1} atm^{-1}] und Wasserdampftransmissionsraten von 10^{-7} [g m^{-2} day^{-1}] für eine ausreichende Haltbarkeit von organoelektronischen Komponenten, die deren praktischen Einsatz überhaupt erst erlaubt, für erforderlich. Obwohl namhafte Hersteller analytischer Instrumente inzwischen auf die Herausforderungen reagiert haben, liegen die Nachweisgrenzen der besten kommerziellen Geräte nach wie vor um Größenordnungen über diesen Worst-Case-Anforderungen. Die Thematik wurde in den ersten Phasen der durchgeführten Arbeit intensiv untersucht und diskutiert.

Die vorliegende Dissertation stellt schlussendlich eine hochempfindliche Alternative für die Messung von Sauerstofftransmissionsraten durch Ultrabarrieremembranen vor. Das Konzept baut auf optochemischer Sensorik und damit auf der Verwendung eines lumineszenten, in einer Matrix immobilisierten Farbstoffs als sensitives Element auf. Dabei wird die sauerstoffabhängige Lumineszenzantwort des Sensors auf moduliertes Anregungslicht von optoelektronischer Instrumentierung nicht-invasiv ausgewertet. Solche Sensorsysteme bieten einzigartige Vorteile gegenüber elektrochemischen Sensoren, insbesondere durch die Fähigkeit zur verbrauchsfreien Detektion und die außerordentliche Empfindlichkeit mancher Luminophor/ Matrix-Kombinationen. Auf optochemischer Detektion basierend wurde so ein eigenständiges, autonom arbeitendes Permeationsmessinstrument entwickelt. Im Gegensatz zu konventionellen Geräten, in denen ein kontinuierlicher Gasstrom den Analyten zum Detektor transportiert, wird in diesem Fall der diffundierende Sauerstoff in einer versiegelten Kavität in unmittelbarer Nähe zur Probenmembran akkumuliert und gleichzeitig permanent gemessen.

In dem in "Flexonics" eingebetteten Entwicklungsprozess wurden Aspekte, die die erreichbare Geräteperformance limitieren, identifiziert und, wenn möglich, einer Verbesserung unterzogen. Nach zahlreichen und die gesamte Messkette betreffenden, dabei chemische, mechanische, elektronische, mathematische oder Programmierfähigkeiten erfordernden Modifikationen erreichen die Demonstratorgeräte die Nachweisgrenze im Bereich von 10^{-5} [cm^3 m^{-2} day^{-1} atm^{-1}]. Sie gehören damit zu den empfindlichsten Testgeräten für die Messung der Sauerstoffpermeation und übertreffen kommerzielle Geräte um eine Größenordnung, bei gleichzeitig ähnlicher Bedienerfreundlichkeit. Ungelöste Problemaspekte, die inzwischen die Nachweisgrenze dominierend bestimmen, betreffen beispielsweise oberflächenchemische Effekte in der aus rostfreiem Stahl gefertigten Permeationszelle oder die Diffusionskinetik im Inneren der Akkumulationskavität.

TABLE OF CONTENTS

INTRODUCTION:

MOTIVATION AND TASK OVERVIEW

THE DEMAND FOR ULTRA-BARRIER TESTING

The development of organo-electronic devices such as OLEDs or OPVs is producing continuous successes, steering towards a conquest of a wide field of applications. Organic light emitting diodes, for instance, are considered to provide the display and lighting technology of the future. Components made of organic semiconductors are cheap in their production because the active substances can be applied and structured by simple processes like inkjet printing. Furthermore, they are mechanically flexible and lightweight, opening up new perspectives. Visions of the future include large-area photovoltaic modules that can be deployed from large rolls onto otherwise unusable desert soil by agricultural machinery, the so-called "e-paper" which is a flexible electronic device capable of displaying news and entertainment, or RFID tags that are cost-effective enough to allow the labelling and automatic localisation of every single, even low-value item in a large-scale warehouse.

One of the major drawbacks of the technology, however, is the extraordinary sensitivity of the main functional parts of state-of-the-art organo-electronic devices (extremely thin and corrosive metal contacts and the organic semiconductors themselves) to oxygen and, even more pronounced, water vapour. These molecules cause the immediate degradation of the sensitive substances and hence destroy the device.

A competitive employment of organo-electronics, taking advantage of all their favourable properties, demands a sufficiently airtight yet flexible and transparent encapsulation, using highly sophisticated barrier materials. Before the evolution of organo-electronics, apparently there was little demand for such membranes showing barrier properties exceeding those of polymer films such as PET typically used in the packaging industry. When necessary, the films were cast with an additional barrier layer (sputtered aluminium, for instance) to reduce the permeability, but at the cost of transparency. For most packaging applications (food packaging or the encapsulation of LCDs [1], for instance) barriers with oxygen permeation rates of 0.1 [$cm^3\,m^{-2}\,day^{-1}\,atm^{-1}$] proved sufficient, however.

Along with the appearance of organo-electronics, the requirements to barrier materials became much more demanding, defined mainly through stoichiometric considerations and on the basis of a minimum operation time and shelf-life for a successful technical application of OLED and OPV devices. Although the numbers in literature are diverging somewhat, barrier materials with oxygen transmission rates ("OTR")[1] as low as 10^{-5} - 10^{-6} [$cm^3\,m^{-2}\,day^{-1}\,atm^{-1}$] and water vapour transmission rates ("WVTR") of 10^{-6} - 10^{-7} [$g\,m^{-2}\,day^{-1}$] are required now in a worst-case scenario [1-9, 10 {pp. 26‑28}]. Moreover, the barrier materials shall be transparent, weather-resistant (particularly for an employment in photovoltaics), flexible, lightweight and economically competitive.

The barrier performances necessary for specific applications are shown more clearly in Fig. 0-1. Remarkably, there is hardly any demand for barriers in the intermediate range, that is, between the

---

[1] For a more detailed definition of the terms OTR and WVTR see section 1.1.1

permeation rates typically accepted by the food packaging industry and those now required for organo-electronics encapsulation.
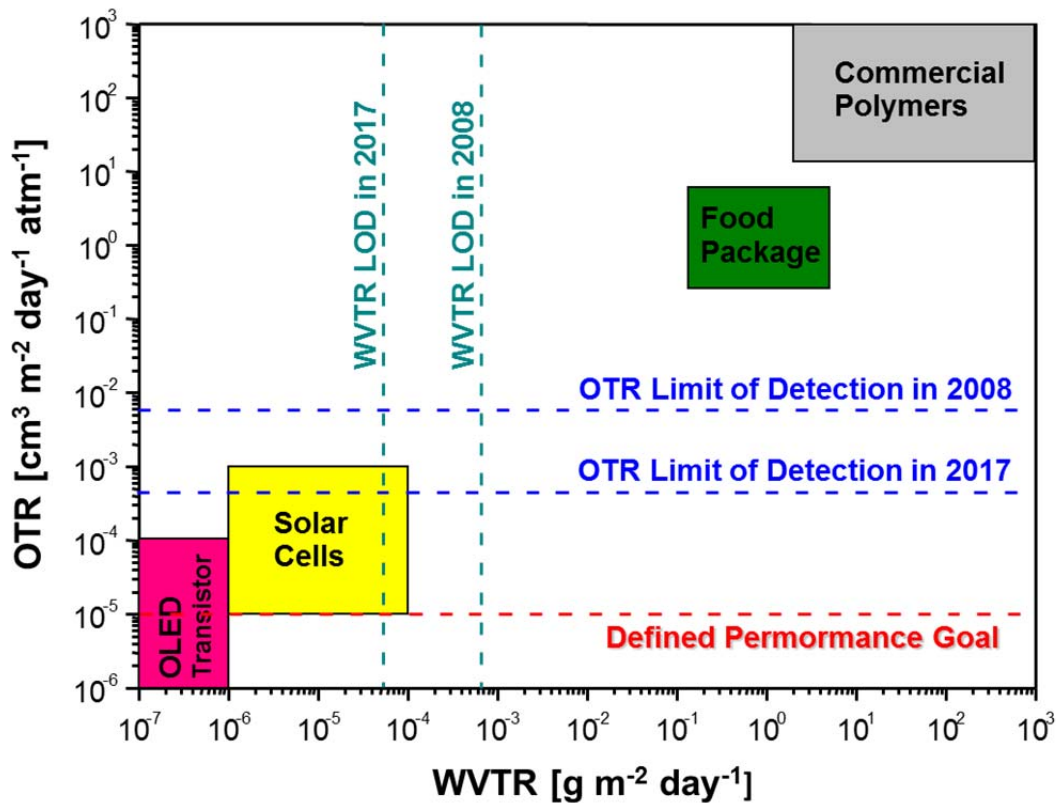
Fig. 0-1:   Barrier Requirements to encapsulation materials for different fields of application [1-7, 10 {pp. 26‑28}]. *Blue and Green:* Limits of detection of commercially available instruments in 2008 and 2017 [11-14]. *Red:* Performance goal specified within the Flexonics project [15].

Driven by the large potential of organo-electronics, worldwide research activities are focusing on the development and fabrication of according packaging membranes showing the required properties [15, 16]. Although the preparation of transparent materials with water vapour transmission rates as low as 10^{-6} [g m^{-2} day^{-1}] was reported already by 2006 [17-19], the manufacture of such membranes in large-scale roll-to-roll processes was lagging behind the performance demands by orders of magnitude.

Research dealing with high-performance barriers is confronted with a number of obstacles, most of which are inherent to the preparation of the required, defect-free barrier layers themselves. In addition, the proper characterisation of such low permeation rates proves extremely difficult, since manufacturers of respective equipment were apparently taken by surprise by the rapid evolution of organo-electronics and the associated research in the field of ultra-barriers. As yet, commercially available instruments attend well upon the food packaging industry, but are still not capable of quantifying the full range of the nowadays required barriers. So far, material testing in the high-end ultra-barrier regime is commonly achieved via time- and labour-intensive, laboratory-dependent analytical methods (the "calcium degradation test" for instance, see section 3.5), which are in-house developed by the groups working with ultra-barriers themselves in many cases. By 2008 and thus the

end of Flexonics, a standardised method for ultra-barriers was lacking, however, and even more so were commercially available, reusable and fast instruments. Meanwhile in 2017, notably MOCON (see section 3.4.1) has improved the detection limits of the instruments and now provides a method to cover at least a part of the regime of ultra-barriers.

To overcome the shortage by construction and development of a stand-alone system capable of detecting such very small permeation rates with respect to oxygen represents the central intention of this doctoral thesis. The development task was embedded in the inter-institutional research venture "Flexonics", funded by the European commission [15, 20] The consortium was concerned with the (intended industrial) preparation of flexible and transparent ultra-barrier membranes by means of roll-to-roll processes.

The predominant part of the development was accomplished within the 39 months of Flexonics, thus, from February 2005 until April 2008. The author followed a job offer and joined Joanneum Research, and activities related to finish writing the thesis which was more than half-complete were largely suspended until 2017.

Nevertheless, modifications and improvements on the instruments were still performed occasionally, and within the 9 years that have passed since the end of Flexonics, the enhancements were summing up significantly. However, competitors haven't been dormant either in the meanwhile, and the role of being an absolute pioneer using an opto-chemical detection scheme for the analysis of oxygen permeation properties in a commercialised device had to be granted to OxySense (section 3.4.7) in 2011.

In 2017, writing was resumed, literature was reviewed and a survey about the state-of-the-art commercial instruments was carried out. The activities culminated in this text at hand.

SCOPE OF THIS THESIS

First and foremost, the interdisciplinary nature of the development task originating from the complexity of the developed instrument is rather unusual in the context of a chemistry doctoral thesis. Although eager and according to the self-awareness flexible and skilled in many fields of science and technology, the author had to get acquainted with a fairly large number of topics that were not related in any way to what was in the "mental toolbox" so far.

The complexity of the project and the distinct interdependence between chemistry, mechanics, optics, electronics, software and data processing algorithms, which all play a key role in the functionality of the instrument did furthermore not always permit a straightforward advancement in research and development. On the contrary, investigations often took place in parallel, and the findings frequently resulted in a distinct adjustment of requirements of something completely different within all the aspects of the development. Although the best was attempted to illustrate the development in a comprehensible way, the segmentation of the report on the development process in detail is only appreciable with a large number of cross-references, as will be noticed in section 5.

The task set within the thesis is summarized as follows:

- Demonstration of the feasibility using an opto-chemical oxygen sensor for oxygen permeation measurement,

- Definition of requirements for a test-setup capable of ultra-barrier characterisation with respect to the oxygen transmission rate,

- Design and construction of a laboratory demonstrator instrument on the basis of the findings,

- Characterisation of barrier samples prepared by partners within the context of the Flexonics project.

The thesis is structured into two parts and 7 major sections.

Part I: The Background is based on a literature- and web survey about physical and chemical fundamentals associated with the development task as well as about the state-of-the art regarding barrier analysis with a focus on commercially available instruments.

Section 1 provides the physical background to diffusion phenomena in membranes. A detailed involvement with the complicated physics in organic-inorganic hybrid multilayer barriers is, however, not within the scope of this thesis.

Section 2 addresses the fundamentals of spectrofluorimetry as the basis for the comprehension of opto-chemical oxygen sensors.

Section 3 provides an overview of possibilities to measure permeation and of the state-of-the-art methods to do so with a certain level of detail.

Part II: The Work is illustrating the functionality, design, development, and performance of the opto-chemical permeation testing instrument created in the project.

Section 4 is basically a description of the functionality of the instrument in general. It was attempted to limit the level of detail to a large degree in order to maintain comprehensibility to the best possible extend. Section 4 furthermore provides a fundamental understanding of the instrument as it will be required in the detailed discussions bundled in section 5.

Section 5 now provides very detailed insight in all relevant aspects of the functionality and the development process. As already mentioned, the sub-structure of this section is, regarding the complex interdependence of practically all aspects of the device, a compromise which is amenable only in combination with a large number of cross-references.

Section 6 reports on the performance accomplished by the permeation measuring instrument by the end of the Flexonics project and as a result of development and permanent enhancement.

Section 7 finally summarizes conclusions and provides recommendations for any future development of an improved instrument based on the development presented.

PART I:

THE BACKGROUND

1 GAS DIFFUSION IN MEMBRANES

1.1 INTRODUCTION

The first recorded experiments on the transport of gases in solid membranes were conducted by Thomas Graham in 1829. He observed that a wet pig bladder inflated to the bursting point when being exposed to carbon dioxide. Thereby, Graham became the founder of membrane science and technology and was also the first one to develop and employ a permeation-rate[2] measuring device [21 {p. 19}]. Nevertheless, membranology was of rather academic interest until about 1960. The importance of membrane science began to grow as the first asymmetric integrally skinned cellulose acetate RO membranes to be developed made applications such as desalination by reverse osmosis possible [21, 22 {p. 272}]. Since then, significant progress was made in virtually every aspect of membranology, and membranes conquered a wide field of technical applications. Accordingly, the appropriate research tools developed at the same pace [21 {pp. 7‑19}].

Still, one of the main application fields is the employment of membranes for gas separation. Consequently, application-inherently critical properties like permeation rates and gas selectivity (that is, the differences in permeation rates of different gases through a specific membrane) are meanwhile well investigated and the relevant mechanisms well understood. Accounting for the large number of different production and design approaches for gas separation membranes, a large number of models for the description of transport phenomena in solid materials exist.

In contrast to gas *separation* membranes, where a *selective*, controllable permeation of one gas component is desired, the membranes used in the packaging industry are designed to provide a good barrier against permeation, ideally regardless of the permeant. The term "packaging" hereby refers to applications such as food packaging, the fabrication of containers for medical applications, fuel tanks, but also the encapsulation of technical components (mainly electronics) to protect them from atmospheric influences, namely oxygen and water vapour. The development of according materials relies mainly on the same mechanistic considerations that are used to describe the processes in gas separation membranes.

Before the application of semi-conducting polymers in devices like flexible photovoltaic modules or OLED displays became a subject of major interest, there was little demand for membranes with barrier properties (with respect to oxygen and water vapour) that would drastically exceed those of single-layered PET foils. Sometimes, such PET substrates were cast with an additional barrier layer of, e. g., sputtered aluminium to further reduce the permeability, but at the cost of sacrificing the transparency. However, barriers with oxygen permeation rates of 0.1 [$cm^3\,m^{-2}\,day^{-1}\,atm^{-1}$] were sufficient for most packaging applications.

Along with the rapidly growing interest for thin-film photovoltaics and organo-electronic applications, the requirements to barrier materials increased drastically. All at once, barrier materials

---

[2] The migration of molecules through solid materials such as polymers is called "permeation".

with permeation rates (O_2) as low as 10^{-5} - 10^{-6} [$cm^3\,m^{-2}\,day^{-1}\,atm^{-1}$] are in great demand, and the needs concerning the water vapour barrier are no smaller. Moreover, the materials sought *must be* transparent to allow the penetration of light, have to be weather-resistant (UV and temperature changes), flexible, lightweight and cheap. Consequently, intensive research activities worldwide are currently focusing on the development and fabrication of barrier membranes showing the required properties, a goal that has yet to be achieved at all. To date, some groups and manufacturers claim the preparation of transparent barrier materials with water vapour transmission rates as low as 10^{-6} [$g\,m^{-2}\,day^{-1}$], but these values are apparently only achieved either in batch or laboratory roll-to-roll production [17-19]. Generally, the manufacture of barriers in a large-scale roll-to-roll process is lagging behind the demands by orders of magnitude.

In addition, the characterisation of the desired ultra-high barrier properties proves extremely difficult. Until recently, only laboratory-dependent and complicated, therefore time- and labour-intensive analytical methods were known. The rapid emergence of research activity in the field of ultra-barriers struck the manufacturers of respective equipment fairly unprepared. To date, commercial instruments serve the demand for barrier characterisation in the food packaging industry, but are still unable to measure the full range of the recently required barriers. Consequently, laboratories working on ultra-barriers have, in many cases, developed their own analytical methods to characterize the membranes under investigation [23, 24]. Commonly, the analysis is based on the degradation of a thin calcium mirror by the permeating oxygen and water vapour (for details see section 3.5). The degradation is assessed either optically (measuring the fraction area of degraded calcium) or via the decreasing electric conductivity of the film as a result of the degradation. Despite the sensitivity, the calcium degradation methods are not particularly suitable for routine measurements due to the elaborate preparation of the substrates in an inert atmosphere. Furthermore, the tests are generally unable to discriminate between oxygen and water vapour permeation.

The central objective of the doctoral thesis at hand is the development of a method and the construction of a reusable stand-alone system capable of the detection of such very small permeation rates with respect to oxygen, so-called "oxygen transmission rates" (OTR). The OTR is one of a number of quantities often encountered in the discussion of gas diffusion through membranes.

1.1.1   The Terminus "Oxygen Transmission Rate"

The concept of the "oxygen transmission rate" (OTR) refers to the amount of oxygen migrating through a unit area of any kind of membrane per unit time under a given set of conditions. Although a number of unit dimensions are found for the OTR in literature, it is commonly expressed in terms of [$cm^3\,m^{-2}\,day^{-1}\,atm^{-1}$], that is, the volume of pure oxygen referred to standard conditions (0 °C, 1013.25 mbar) penetrating one square meter of membrane per day and atmosphere of oxygen partial pressure drop across the membrane. Alternatively, [$cm^3\,m^{-2}\,day^{-1}\,bar^{-1}$] is sometimes used as

the unit denominator[3], and a number of other unit dimensions exist [25 {p. 545}]. In analogy to the OTR, the water vapour transmission rate, WVTR, is usually given in terms of [g m^{-2} day^{-1}].

The temperature during the experiment (commonly 23 °C, but frequently also 25 °C) must be quoted for a full description of the permeation behaviour, since the OTR is a property dependent of it. In some cases, elevated temperatures (38 °C or 65 °C) are employed for so-called "accelerated measurements". The results obtained are converted to the standard temperature of 23 °C according to empirically determined acceleration factors. In comparisons between membranes, the "standardized" OTRs must be, however, used with great care because the factors are dependent of the membrane material and permeation mechanisms.

The oxygen transmission rate is addressing the properties of a given membrane as a whole, regardless of its constitution, namely its thickness, uniformity, shape, the presence or absence of defects, whether it is composed of a homogenous polymer or a stack of many *different* materials, and so forth. Although the *permeability coefficient P* (see section 1.3), is a related and very similar quantity, it addresses, in contrast, the properties of a *material* rather than the properties of the completed membrane.[4]

The importance of the oxygen transmission rate is justified by the technical application of the membranes. In a food package, for instance, the amount of oxygen ending up inside after e. g. a month will have an impact on the durability and shelf-life of the contained product, while the mechanisms responsible for its intrusion are of little interest at the end of the day.

In materials research, on the other hand, the emphasis is on the properties of the membrane material itself. It shall be noted that a direct determination of the permeability coefficient is possible only in simple cases (e. g., a homogenous polymeric membrane above its glass transition temperature, see section 1.3.1), where the permeability coefficient is the OTR multiplied by the film thickness.

As already explained, the OTR is an overall result, composed of the permeation properties of every constituent part of the membrane. In the case of a non-homogeneous membrane (most commonly a multi-layered composite, hence a stack of different materials), the OTR arises from the combination of a number of different permeation mechanisms with different permeation parameters. The OTR is thus a comparably "macroscopic" property, and, in contrast to the permeability coefficient which is always addressing the properties of *one* coherent and homogeneous layer only, a simple correlation to the thickness of the membrane is no longer possible. For a fundamental understanding of the coherences, some selected permeation processes commonly contributing to the overall "sum" of the transmission rate are considered in the following sections.

---

[3] The difference between bar and atm is merely 1.3 % and therefore, in fact, insignificant in the context of permeation properties.
[4] However, the concept of a constant permeability coefficient as a universal material property ceases to be valid if there are specific interactions between the gas and the polymer. For permanent gases like O_2, N_2, H_2 or He this is rarely the case.

1.1.2   Remarks on Ultra-Barrier Membranes

Although they do play a crucial role in membranology, the manufacture of packaging, gas separation and barrier membranes is, of course, not limited to polymeric materials. In the production of barrier membranes, for instance, inorganic layers of Al, SiO_x or AlO_x are often applied with a thickness of several ten nanometres by appropriate means (sputtering, etc.) to form the actual barrier against permeation. The inorganic material is thereby thought to be absolutely airtight, and the remaining permeation rates which are *always* observed are due to *inevitably* present defect sites ("pinholes") in the inorganic layers. The diffusion processes therefore only occur in the polymeric material and through the defects.

Interestingly, already a relatively small number of pinholes are able to annihilate the barrier properties to a large extent. An improvement of the barriers is often sought by the application of multiple inorganic layers, separated by sophisticated organic intermediate layers (e. g. Ormocer® varnishes) which are supposed to "repair" the defect sites. In an ideal case, the defects of the individual layers are non-aligned relative to each other as to create long, "tortuous" diffusion pathways through the thickness of the membrane.

The according mathematical treatment, however, is very complicated, compared to the description of diffusion processes in bare polymeric materials, since many geometric aspects and physical interactions must be taken into account. Although substantial research was performed already some decades ago [26, 27], according models are largely under development thus far.

A detailed treatment of multilayer systems shall therefore not be subject to the doctoral thesis at hand. The focus of this introductory section will be constrained to the diffusion mechanisms inherent to polymeric materials, because some fundamental insight is thus attained and the building blocks for more elaborate theories dealing with multilayers are provided.

A number of models were developed for the description of gas permeation mechanisms through polymers, depending on the nature of the membrane material. A first, very fundamental discrimination is necessary between porous membranes and dense membranes, whose inherent permeation properties are very different. In the following sections, both types of permeation processes are discussed in detail.

1.2   DIFFUSION IN POROUS MEMBRANES

Expectedly, porous membranes are mainly used for (gas) separation processes rather than for packaging purposes, due to their inherent permeability properties, in particular with respect to small permeants of low molecular weight. Nevertheless, a description of the mechanisms encountered in the context of porous membranes shall be given since they include valuable information relevant to

constructional details of the OTR measurement device which was developed in the course of the presented project (see section 5.5.3)

The migration of gas molecules through porous membranes is generally described by transport equations through capillary tubes based on the kinetic theory of gases. It is driven simultaneously by two different processes, namely the Knudsen (or free molecule) diffusion and the Poiseuille (or viscous) flow. The proportions of Knudsen to Poiseuille flow are depending on the relative magnitude of pore radius of the capillary r and the mean free path of the gas molecules λ, thus, on the ratio r/λ. The mean free path λ is obtained as in Equation 1-1 [21 {p. 21}, 28 {p. 15}].

$$\lambda = \frac{3\eta}{2p}\sqrt{\frac{\pi RT}{2M}}$$

λ	mean free path
η	viscosity of the gas
p	pressure
R	universal gas constant
T	temperature
M	molecular weight

Equation 1-1: The mean free path λ of gas molecules.

1.2.1 Knudsen Flow

The migration of gas molecules is predominantly governed by the Knudsen flow, if the ratio r/λ is significantly less than 1, indicating that there are significantly more collisions with the pore walls than with other gas molecules. In every collision with the wall, the gas molecules are reflected in a random direction. Molecule-to-molecule collisions occur rarely in between the wall collisions. Hence, each gas molecule can be thought to move independently of all the others. As a result, a separation of gas mixtures is achieved because different gas species move at different velocities, depending on the molecular weight. This is referred to as the Present-deBethune effect [28 {p. 16}]. The mean molecular velocity is given by Equation 1-2.

$$\overline{\mu} = \sqrt{\frac{8RT}{\pi M}}$$

$\overline{\mu}$	mean molecular velocity
R	universal gas constant
T	temperature
M	molecular weight

Equation 1-2

For the description of the Knudsen diffusion, as already mentioned, the membrane pores are considered as long and parallel capillary tubes (a detailed derivation of the model is found in [21 {pp. 21-23}]), defining the Knudsen's diffusion coefficient D_K according to Equation 1-3 and the gas flow J in the membrane made of cylindrical capillaries as in Equation 1-4.

$$D_\kappa = \frac{4r}{3} \sqrt{\frac{2RT}{\pi M}}$$

D_κ	Knudsen's diffusion coefficient
r	radius of capillary
R	universal gas constant
T	temperature
M	molecular weight

Equation 1-3

$$J = D_\kappa \frac{P_0 - P_1}{lRT}$$

J	gas flux in g mol^{-1} cm^{-2} s^{-1}
D_κ	Knudsen's diffusion coefficient
P_0	pressure on the upstream end of the pores
P_1	pressure on downstream end of the pores
l	pore length
R	universal gas constant
T	temperature

Equation 1-4

However, since the pores in a real membrane have a finite length and are random in direction, the diffusive transport of gases in porous membranes differs from the predictions by the capillary tube model. Consequently, an effective diffusion coefficient D_e, as defined in Equation 1-5, corrects the Knudsen diffusion coefficient, accounting for the effects of porosity and tortuosity. The tortuosity τ is considered as a correction factor, combining experimental and theoretical values, but a physical meaning has not been given [21 {p. 23}]. Other authors account the deviations from the ideal capillary tube model to the negligence of the interactions between the penetrant gas and the membrane material. In according models, a "surface flow" on the capillary walls is used to correct for the non-ideal behaviour [28 {p. 17}].

$$D_e = \frac{\varepsilon}{\tau} D_\kappa$$

D_e	effective diffusion coefficient
ε	porosity
τ	tortuosity
D_κ	Knudsen's diffusion coefficient

Equation 1-5

1.2.2   Poiseuille Flow

When r/λ becomes much larger than 1, the movement of the gas species is coupled with all the other species present in the mixture, since there are more collisions among the gas molecules than with the walls of the pores. Consequently, all molecules move with the same average velocity, and gas separation is no longer possible. Poiseuille's law is now predominantly governing the flow (Equation 1-6). In contrast to the Poiseuille law for liquids, an additional term $\left(P_0 + P_1\right)$ is arising from the expansion of a gas as it moves down the pressure gradient [21, 28].

For the intermediate range, where r and λ are comparable and neither the Knudsen diffusion nor the Poiseuille flow are able to satisfactorily describe the permeation behaviour, in some text books a third type of "mechanism" is introduced as a correction term, referred to as "slip flow" [28 {p. 16}].

$$J = \frac{r^2\left(P_0 - P_1\right)\left(P_0 + P_1\right)}{8\eta lRT} = \frac{r^2\left(P_0^2 - P_1^2\right)}{8\eta lRT}$$

J	gas flux in g mol^{-1} cm^{-2} s^{-1}
r	radius of capillary
P_0	pressure on the upstream end of the pores
P_1	pressure on downstream end of the pores
η	viscosity of the gas
l	pore length
R	universal gas constant
T	temperature

Equation 1-6

1.2.3 Gas Separation Utilizing Porous Membranes

To make the Knudsen flow the predominant effect and obtain gas separation, the ratio *r/λ* has to be sufficiently small. The mean free path *λ* of gases at atmospheric pressures is in the range of 100 – 200 nm, hence the pore size must be smaller than 50 nm [21 {p. 24}].

As mentioned before, the Knudsen flow is molecular weight dependent. Therefore, the separation of the species in a mixture of gases results from their differences in molecular weight. For a pair of gases, Equation 1-4 can be rewritten for each component, given that the downstream pressure is negligible (see Equation 1-7).

$$J_1 = \frac{KP_0 x}{\sqrt{M_1}} \qquad J_2 = \frac{KP_0(1-x)}{\sqrt{M_2}}$$

J	flux for gas 1 in g mol^{-1} cm^{-2} s^{-1}
K	combination of constants from Equation 1-4, excluding the molar mass *M*
P_0	pressure on the upstream end of the pores
x	upstream mole fraction of gas 1
M	molecular weight

Equation 1-7

The separation factor *α* is defined as in Equation 1-8.

$$\alpha = \frac{J_1/J_2}{x/(1-x)}$$

α	separation factor
J	flux for gases 1 and 2 in g mol^{-1} cm^{-2} s^{-1}
x	upstream mole fraction of gas 1

Equation 1-8

Substitution of J_1 and J_2 with Equation 1-7 leads to Equation 1-9 [21 {p. 24}, 28 {p. 15}].

$$\alpha = \sqrt{\frac{M_2}{M_1}}$$

α	separation factor
M_1	molar mass of gas 1
M_2	molar mass of gas 2

Equation 1-9

Gas separations on the basis of molecular weight are particularly common where differences in the chemical behaviour do not exist, namely in the separation of isotopes of the same element. Unfortunately, the weight *difference* of isotopes is generally very small compared to the element's weight itself. The difficulty is best exemplified considering a technically important process such as the enrichment of uranium. In theory, a separation factor as small as 1.0043 is attainable between $U^{235}F_6$ and $U^{238}F_6$, provided an idealised behaviour in the separation. In real separations, however, not even this value is obtained due to a number of adverse effects like non-ideal membranes, back diffusion, etc. Since the selectivity obtained is so small, a large number of cascaded stages are required for sufficient separation. As a consequence, this approach to gas separations is highly uneconomical, and it is therefore used only in processes in which economics is not a primary factor. The manufacture of nuclear weapons shall be mentioned as one important example. Thus, 10276 stages are used in American gas diffusion plants for the production of U^{235} [21 {p. 25}].

1.3   DIFFUSION IN DENSE MEMBRANES

In contrast to micro-porous membranes, in which the gases traverse pores by Knudsen diffusion or Poiseuille flow and separation is achieved on the basis of their different molecular weights, the permeation through nonporous membranes happens in a fundamentally different way. In the latter case, the gas molecules actually have to penetrate the molecular structure of the solid, dense membrane matrix (that is, to *dissolve*) rather than just to travel through a system of (in molecular terms) "macroscopic" voids (we will, however, consider an important exception of mechanistic relevance to this generalised "preface").

The simplest way to describe and predict the permeation of gas molecules through solid, non-porous membranes is to utilize the solution-diffusion model. In this model the mechanism of permeation is considered to comprise three subsequent steps [21, 28-30]:

1. Absorption of the gas on the upstream, high-pressure boundary of the membrane,

2. activated diffusion through the membrane material down a concentration gradient and

3. desorption or evaporation from the downstream, low-pressure boundary of the membrane.

It is assumed that the adsorption and desorption processes at the interfaces are fast compared to the rate of diffusion in the bulk of the polymer. Consequently, the gas phase is in equilibrium with the polymer interface at either side of the membrane. The driving force for the solution-diffusion mechanism is found in the difference in thermodynamic activity existing at the opposite boundaries of the membrane, which causes a concentration difference, leading to diffusion in the direction of decreasing activity [21, 28, 29].

The ability of a given gas to permeate through a given dense membrane material is expressed in terms of the *permeability coefficient P*, which is defined in Equation 1-10 (a more detailed derivation is given in the following sections).

$$P = D \cdot S$$

P	permeability coefficient
D	diffusion coefficient
S	gas solubility coefficient

Equation 1-10: The Permeability Coefficient.

Besides the kinetic term diffusivity *D* (~mobility), a thermodynamic term is determining the permeability *P*, namely the amount of gas that can be accommodated per unit volume of the matrix, thus the solubility *S*. [21, 28 {p. 17}, 29]

The model just introduced is valid only in some ideal cases and must thus be accompanied by more thorough considerations. Before a proper description of the permeation processes observed in many polymer membranes is possible, a fundamental discrimination with respect to the thermodynamic state of the polymer is necessary. The mechanistic treatment of the permeation through dense membranes strongly depends on whether the membrane material is in the "rubbery" or "glassy" state, that is, *above* or *below* its *glass transition temperature T_g*.

Polymer molecules in rubbers adjust immediately to a new equilibrium situation (e. g. when a penetrant species is absorbed and transported through the polymer matrix). The time required to reach a new state of equilibrium is very much shorter than the time-scale of typical diffusion processes through a membrane. The "micro-pores" or "free volume" thought to be responsible for the transport of molecules (see 1.3.3) are in permanent "movement" and thus of constantly varying dimensions.

Glassy polymers, on the other hand, are never in a true equilibrium, because the motion of the polymer chains is much more constrained than it is in the rubbery state. The "micro-pores" are fixed in this case and a complete homogenisation of the penetrant's environment is not attained within the time-scale of the permeation process [28 {p. 20}, 31 {pp. 126‑127}].

1.3.1   Diffusion in "Rubbery" Materials

The treatment of permeation processes in polymers above their glass transition temperature T_g is relatively straightforward. Thus, the solubility of a gas in a rubbery polymer is described by Henry's law (Equation 1-11), which is particularly accurate at low concentrations of low molecular weight gases (O_2, CO_2, N_2, etc.), that is, when interactions of the gas and the polymer can be neglected:

$$C = S \cdot p$$

C	equilibrium concentration of gas in the polymer
S	solubility constant for the gas/ polymer pair
p	(partial) pressure of the gas

Equation 1-11: Henry's law.

According to Henry's law, the gas concentration in the polymer is linearly dependent on the external pressure, although both positive and negative deviations from this relationship can be observed at high pressures [21, 28, 29, 32, 33].

A dependence of the solubility of simple gases on the type and structure of the membrane polymer is hardly pronounced, as it can be seen in Table 1-1.

Table 1-1: O₂ Solubility in polymers [25, 32].

Polymer	O_2 Solubility $[10^{-5}\ cm^3\ (at\ STP^{[a]})\ cm^{-3}\ Pa^{-1}]$
Polybutadiene [elastomeric]	0.097
Polyurethane rubber [elastomeric]	0.048
Polyethylene L.D. [semi-crystalline]	0.065
Poly (ethylene terephthalate) [semi-crystalline]	0.069
Polystyrene [amorphous]	0.055
Poly (vinyl acetate) [amorphous]	0.040

[a] STP: Standard Temperature and Pressure

Once the gas molecules are dissolved in rubbery polymers, diffusion is mathematically obeying Fick's first law (Equation 1-12).

$$J = \frac{dm}{dt \cdot A} = -D \left(\frac{dC}{dx} \right)$$

J	permeation flux
m	mass of permeant
t	time
A	membrane area
D	diffusion coefficient ("diffusivity")
C	local concentration of permeant in the membrane
x	coordinate direction of permeation

Equation 1-12: Fick's first law

Hereby, the diffusivity D is the amount of matter traversing a unity area per second at a unity concentration gradient. In contrast to the solubility coefficient, the diffusion coefficient of simple gas molecules strongly depends on the structure of the polymer [28 {p. 18}, 32 {p. 189}]. Examples for different polymers are given in Table 1-2.

Table 1-2: O₂ Diffusion coefficient in polymers [25, 32].

Polymer	O₂ Diffusion Coefficient [10⁻⁶ cm² s⁻¹]
Polybutadiene *[elastomeric]*	1.5
Polyurethane rubber *[elastomeric]*	0.24
Polyethylene L.D. *[semi-crystalline]*	0.46
Poly (ethylene terephthalate) *[semi-crystalline]*	0.0036
Polystyrene *[amorphous]*	0.11
Poly (vinyl acetate) *[amorphous]*	0.05

Given steady-state conditions[5], Fick's law may be integrated from the upstream boundary (point 0) to the downstream boundary (point 1), because the flux J is constant throughout the thickness of the membrane [32 {p. 189}]. The resulting Equation 1-13 may be rewritten as in Equation 1-14.

$$J = -D \frac{[C_0 - C_1]}{[x_0 - x_1]}$$

J	permeation flux
D	diffusion coefficient ("diffusivity")
C_0, C_1	gas concentration in the polymer at the membrane boundaries
x_0, x_1	coordinates of the membrane boundaries

Equation 1-13

$$J = -D \frac{[C_0 - C_1]}{l}$$

J	permeation flux
D	diffusion coefficient ("diffusivity")
C_0, C_1	gas concentration in the polymer at the membrane boundaries
l	membrane thickness

Equation 1-14

By substitution of Henry's law into Equation 1-14, the expression as in Equation 1-15 is obtained [28 {p. 18}, 32 {p. 189}].

$$J = D \cdot S \cdot \frac{(p_0 - p_1)}{l} = P \cdot \frac{(p_0 - p_1)}{l} = \frac{P \cdot \Delta p}{l}$$

J	permeation flux
D	diffusion coefficient ("diffusivity")
S	solubility constant for the gas/ polymer pair
l	membrane thickness
p_0, p_1	external partial pressures of the permeant gas at the membrane boundaries
P	permeability coefficient

Equation 1-15

---

[5] A steady-state is on hand, if there is a constant diffusive flux in the direction ("x-axis") perpendicular to the membrane's surface, regardless of the location in the x-direction. Thus, the existence of a stable concentration gradient in the direction of diffusion is demanded.

The quantity *P* is the so-called permeability coefficient (also permeability) and reflects the steady-state flux through a planar, isotropic and homogeneous polymer membrane at constant temperature [28 {p. 18}]. As it was shown in the introduction of this section, it is given by Equation 1-16.

$$P = D \cdot S$$

P	permeability coefficient
D	diffusivity
S	solubility

Equation 1-16

It is noted that there are many dimensions and units found in literature for the general expression "permeability". The text at hand shall refer to it as the *permeability coefficient* with the dimensions [25 {p. 543}]:

$$P = \frac{(quantity\ of\ permeant) \times (film\ thickness)}{(area) \times (time) \times (pressure\ drop\ across\ the\ membrane)}$$

P is a quantitative descriptor of the mass transport through a polymer and most commonly given in "Barrer", which is defined as *[10^{-10} cm^3(STP)*cm*cm^{-2}*s^{-1}*$cmHg^{-1}$]*, named after R.M. Barrer [29 {p. 41}]. Alternatively, *[cm^3(STP)*cm*cm^{-2}*s^{-1}*Pa^{-1}]* or shorter *[cm^2*s^{-1}*Pa^{-1}]* are regularly used. "STP" hereby refers to "standard temperature and pressure" (273.15 K and 1.013×10^5 Pa, respectively) [21 {pp 26-27}, 25 {p. 544}]. The according SI unit is *[mol*m*m^{-2}*s*Pa]*, corresponding to 3.03×10^{15} Barrers.

For polymer-gas combinations lacking specific interactions between the gas and the polymer, the permeability coefficients are characteristic constants [25 {p. 544}] which can be found in tabulated data [25 {p. 545}, 28 {p. 9}, 34 {p. 241}, 35].

For most gases, the permeability coefficient P is independent from pressure for all practical purposes, and Equation 1-16 is equivalent to Equation 1-17:

$$P = \frac{J \cdot l}{p_0 - p_1} = \frac{J \cdot l}{-(p_1 - p_0)} = \frac{J \cdot l}{-\Delta p}$$

P	permeability coefficient
J	permeation flux
l	membrane thickness
p_0, p_1	external partial pressures of the permeant gas at the membrane boundaries

Equation 1-17

However, non-ideal gas effects are observed in many cases, leading to a concentration-dependent permeability coefficient. Such behaviour is found for gases with high boiling points, at temperatures

below the critical temperature. Hereby, the permeability increases with pressure, reflecting an increasing solubility as the pressure increases. According mathematical models are readily found in literature [21 {pp. 26‑27}].

The three physical quantities in Equation 1-16 all show a temperature-dependence, which is, in each case, expressed by the Van't Hoff-Arrhenius-Equation (Equation 1-18).

$$P(T) = P_0 * e^{\frac{-E_P}{RT}}$$

$$D(T) = D_0 * e^{\frac{-E_D}{RT}}$$

$$S(T) = S_0 * e^{\frac{-\Delta H_S}{RT}}$$

D	diffusivity
P	permeability
S	solubility
D_0, P_0, S_0	pre-exponential factors
E_P	apparent activation energy of permeation
E_D	apparent activation energy of diffusion
ΔH_S	molar solution enthalpy
R	universal gas constant
T	temperature

Equation 1-18 [21 {p. 43}, 25 {p. 544}, 28 {p. 26}, 32, 36]

For a given temperature, the permeability coefficient P for a number of gases in a number of polymers (and analogously D and S) can be estimated using P_0 and E_p from tabulated data which are readily available in according literature [25 {p. 544}, 35].

Normally, the effects of temperature changes on the diffusivity and solubility coefficients have opposite signs. Thus, the diffusivity is increasing with increasing temperature, whereas the solubility is decreasing. The overall effect of temperature variations on the permeability coefficient is hence a composite of the two contributions. In most cases, however, the predominant influence is acting on the diffusivity and the permeability coefficient increases with temperature. Nevertheless, at low temperatures the solubility can become sufficiently high as to reverse the described behaviour [28].

1.3.2 Diffusion in "Glassy" Materials – Dual Mode Sorption Theory

This rather complex section is a summary of the respective sections found in the textbooks consulted in this context [21, 28, 31, 33]. The sources are in agreement with each other, and reference to specific sources is only given when appropriate.

When a polymer is cooled through its glass transition temperature T_g, some intersegmental packing defects are frozen into the structure of the polymer bulk [21], and the polymer is "trapped" in a permanent non-equilibrium situation. The molecular chains are unable to react to new chemical and physical conditions within the time-scale of typical permeation processes [31 {p. 127}]. The non-equilibrium and the presence of such defects cause the Henry's law solubility model (see Equation 1-11), which is valid in case of rubbery materials, to fail for glassy polymers, resulting in a non-linear

dependence of the amount of dissolved gas on the applied pressure. The sorption of gases in glassy polymers is thus more complex, but well described by a combination of Henry's law and so-called Langmuir terms, leading to what is called the "dual mode sorption theory".

In this model, the existence of two types of sorption sites in a glassy polymer is assumed. One type of sorption site is accommodating mobile gas molecules into normally densified regions of the polymer in a just analogous way as in case of a rubbery polymer, hence obeying Henry's law. The sorption process involves dilation of the polymer matrix to accommodate the sorbed gas molecules.

The second type, the so-called "Langmuir sorption sites" are unique to glassy polymers. They are associated with microscopic voids and excess free volumes which are formed as the temperature drops through the glass transition temperature and packing defects are fixed in the polymer structure. When heated above T_g, permanent Langmuir sites disappear because of anew relaxation of the polymer. Molecules in the Langmuir sites are much less mobile than in the Henry's law sorption sites, but the two populations are in rapid equilibrium with each other.

In analogy to the treatment of rubbers, the transport phenomena in glassy polymers are mathematically expressed in terms of a sorption process, followed by the migration of the sorbed species in the bulk of the polymer. However, in the case of glassy polymers an additional "hole-filling process" associated with the Langmuir sites has to be considered [31].

Sorption is described by Equation 1-19. Thereby, C'_H is representing the limit sorption capacity of the Langmuir sites. Its value increases as the temperature decreases below the glass transition temperature. The hole affinity constant b reflects the ratio of rate constants of sorption and desorption in the Langmuir sites, hence the tendency of a given gas molecule to sorb in the Langmuir mode. The parameter b is depending on the gas of interest. For H and He, the constants are small, while becoming much larger for condensable penetrants such as benzene.

$$C = C_D + C_H = S \cdot p + \frac{C'_H \cdot b \cdot p}{1 + b \cdot p}$$

C	solubility
C_D	Henry-site solubility
C_H	Langmuir-site solubility
S	Henry's law solubility constant
p	pressure
C'_H	hole saturation constant
b	hole affinity constant

Equation 1-19

At low pressures (that is, $b*p$ <<1), Equation 1-19 simplifies to Equation 1-20, which is consistent with a linear behaviour, as also predicted by Henry's law (see Equation 1-11).

$$C = \left(S + C'_H \cdot b\right) \cdot p$$

C	solubility
C	solubility
S	Henry's law solubility constant
C'_H	hole saturation constant
b	hole affinity constant
p	pressure

Equation 1-20

At sufficiently high pressures, when $b*p>>1$, the micro-voids become saturated, and additional gas molecules can no longer be accommodated. Thus, the saturation limit C'_H of the Langmuir sites is reached and Equation 1-19 again reduces to a linear expression (Equation 1-21).

$$C = S \cdot p + C'_H$$

C	solubility
S	Henry's law solubility constant
p	pressure
C'$_H$	hole saturation constant

Equation 1-21

Eventually, it is concluded that the solubility C is linearly depending on the pressure at both low and high pressures, with a non-linear part connecting the linear portions of the dependence.

For a determination of S and C'_H, the "Langmuir term" (see Equation 1-22) is rearranged to Equation 1-23. At high pressures, the slope and intercept of the plot p/C_H against p are leading to [$1/C'_H$] and [$1/C'_H*b$], respectively. The gas solubility in the Langmuir sites is finally calculated according to Equation 1-24.

$$C_H = \frac{C'_H \cdot b \cdot p}{1 + b \cdot p}$$

Equation 1-22

$$\frac{p}{C_H} = \frac{1}{C'_H \cdot b} + \frac{p}{C'_H}$$

Equation 1-23

C$_H$	Langmuir-site solubility
C'$_H$	hole saturation constant
b	hole affinity constant
p	pressure
C	solubility
C$_D$	Henry-site solubility
S	Henry's law solubility constant

$$C_H = C - C_D = C - S \cdot p$$

Equation 1-24

As it may be concluded from the existence of additional sorption sites, the solubility of gases in glassy polymers is higher than in rubbers. The sorption enthalpies ΔH_D for the Henry-type sorption and ΔH_H for the Langmuir-type sorption are determined in Equation 1-25.

$$S = S_0 \cdot e^{-\Delta H_D / RT} \qquad b = b_0 \cdot e^{-\Delta H_H / RT}$$

S	Henry's law solubility constant
b	hole affinity constant
S$_0$ b$_0$	pre-exponential factors
ΔH_D	Henry-type sorption enthalpy
ΔH_H	Langmuir-type sorption enthalpy
R	universal gas constant
T	temperature

Equation 1-25 [21 {p. 24}, 28]

For the Henry-type sorption, the enthalpy ΔH_D is comparable to that in rubbers. The sorption into Langmuir-type sites is, however, much more exothermic, which is reflected by a higher enthalpy ΔH_H. This is consistent with the fact that the Langmuir sites are pre-existing prior to the sorption, unlike the Henry-type sites which must, just like in rubbers, be formed by molecular re-orientation of the polymer chains in the course of the sorption.

The diffusion of species sorbed in glassy polymers is treated on the basis of the following postulates:

1.) The sorption of the gas into the micro-heterogeneous medium follows two concurrent mechanisms.

2.) The sorption mechanism leading to mobile species obeys a linear law (Henry's law for glassy polymers). Only the mobile species can take part in the permeation process, driven by a concentration gradient.

3.) The second mode of sorption, expressed by a non-linear Langmuir term, leads to species completely immobilised into a fixed number of sites within the medium, which do not contribute to the diffusive flux.

4.) The rate of immobilisation/ mobilisation from the Langmuir sites is very rapid in comparison with the rate of migration. Thus, a local equilibrium between mobile and immobilised species is always maintained throughout the medium and the diffusion is rate-determining.

5.) The true diffusion coefficient is a constant independent of the position in the medium or the concentration of the permeant.

Since only the gas dissolved in the Henry-type sites is able to diffuse, the unidirectional flux is given by Fick's law (compare also Equation 1-12):

$$J = \frac{dm}{dt \cdot A} = -D\left(\frac{dC_D}{dx}\right)$$

J permeation flux
m mass of permeant
t time
A membrane area
D diffusion coefficient ("diffusivity")
C_D Henry-site solubility
x coordinate direction of permeation

Equation 1-26

The substitution of Equation 1-26 into the equation of continuity of the gas (Equation 1-27) leads to a modification of Fick's second law (Equation 1-28), accounting for accumulation in the polymer by both immobilisation and "simple" dissolution.

$$\frac{dC}{dt} = \frac{d(C_D + C_H)}{dt} = -\frac{dJ}{dx}$$

Equation 1-27

J	permeation flux
C	solubility
C_D	Henry-site solubility
C_H	Langmuir-site solubility
t	time
x	coordinate direction of permeation

$$\frac{d}{dt} \cdot (C_D + C_H) = \frac{d}{dx}\left(D \frac{dC_D}{dx} \right)$$

Equation 1-28

Since there is always a rapidly adjusting equilibrium between the immobilised and mobile gas molecules in the polymer, a relationship between C_D and C_H can be derived from the Henry's law and Langmuir isotherms via the partial pressure *p*.

$$C_H = \frac{(C_H' \cdot b/S) \cdot C_D}{[1 + (b/S) \cdot C_D]}$$

Equation 1-29

C_H	Langmuir-site solubility
C_H'	hole saturation constant
b	hole affinity constant
S	Henry's law solubility constant
C_D	Henry-site solubility

Inserting Equation 1-29 into Equation 1-28 and factoring out the diffusion coefficient *D* leads to the "unsteady state diffusion equation" which describes the transient sorption of a penetrant into the polymer according to the dual mode sorption model (Equation 1-30).

$$\left[1 + \frac{C_H' \cdot (b/S)}{[1 + (b/S) \cdot C_D]^2} \right] \cdot \frac{dC_D}{dt} = D \cdot \frac{d^2 C_D}{dx^2}$$

Equation 1-30

C_H'	hole saturation constant
b	hole affinity constant
S	Henry's law solubility constant
C_D	Henry-site solubility
D	diffusion coefficient ("diffusivity")

At very low pressures (that is, in one of the two limiting cases of the dual mode sorption diffusion model), Equation 1-30 may be written in the forms of Equation 1-31 to Equation 1-33 (a detailed derivation is found in [21 {pp. 36-37}]).

$$D_{eff} \frac{d^2 C_D}{dx^2} = \frac{dC_D}{dt}$$

Equation 1-31

D_{eff}	true diffusion coefficient
C_D	Henry-site solubility
x	coordinate direction of permeation
t	time
D	diffusion coefficient
K	Parameter defined in Equation 1-33
C'_H	hole saturation constant
b	hole affinity constant
S	Henry's law solubility constant

$$D_{eff} = \frac{D}{1+K}$$

Equation 1-32

$$K = \frac{C'_H \cdot b}{S}$$

Equation 1-33

The result predicts that the measured diffusion coefficient D_{eff} is the true diffusion coefficient reduced by *1/(1+K)*. The factor *K* is thus reflecting the amount of immobilised gas molecules which do not participate in the diffusion process.

The second limiting case of the dual mode sorption diffusion model occurs at high pressures. Thus, Equation 1-30 reduces to Fick's second law, predicting that the experimentally determined diffusivity is equal to the true diffusivity, as expressed in Equation 1-34.

$$D \frac{d^2 C_D}{dx^2} = \frac{dC_D}{dt}$$

D	diffusion coefficient
C_D	Henry-site solubility
x	coordinate direction of permeation
t	time

Equation 1-34

The mathematical treatment presented above is limited to the ideal case that gas molecules in the Langmuir sorption sites are completely immobilised. This is, however, not necessarily the case. Further refinement of the model thus deals with two populations of gas molecules in the polymer, moving with different inherent mobility. According mathematical relations are found in literature [21 {p. 38}, 28 {p. 27}].

1.3.3 Free Volume Theory

Again, the rather complex section is a summary of [21 {pp. 42f}, 31 {pp. 133-136}, 33], and the sources are in agreement with each other. Reference to specific sources is only given when appropriate.

In addition to the phenomenological dual sorption model, gas diffusion in polymers was explained on a molecular basis, according to the disciplines of classical, quantum and statistical mechanics. The respective models include (1) the lattice vacancy (or "hole") theory, (2) the activated complex theory and (3) the fluctuation theory. In (1) a certain amount of work is necessary on a matrix to create or expand a void to accommodate the penetrant gas molecule, while in (2) work is necessary for the penetrant to overcome a potential energy barrier separating it from a lower energy region in the matrix. In (3), finally, energy is needed to activate density fluctuations in the matrix, allowing a movement of the penetrant down a gradient of chemical potential. From all of these approaches, expressions of a very similar functional form are derived (see Equation 1-35). The Arrhenius-like equations were already introduced in section 1.3.1. The expression for the solubility is obtained through Equation 1-16 (*P=D*S*). In addition to these approaches, the energy of diffusion was explained on the basis of the penetrant size instead of the mass to account for observed relationships. All of the presented models are commonly classified as either molecular models or free-volume theories [31 {p. 127}]. The latter terminus shall be considered in more detail in the following.

$$D = D_0 e^{-E_D / RT}$$

$$P = P_0 e^{-E_P / RT}$$

$$S = S_0 e^{-\Delta H_S / RT}$$

$$\Delta H_S = E_P - E_D$$

D	diffusivity
P	permeability
S	solubility
D_0, P_0, S_0	pre-exponential factors
$E_D, E_P, \Delta H_S$	apparent activation energies
R	universal gas constant
T	temperature

Equation 1-35 [21 {p. 43}, 25 {p. 544}, 28 {p. 26}, 36]

The free volume theories are most commonly explained departing from the nature of the glass transition temperature T_g, at which the thermal expansion coefficient changes and the polymer is undergoing a transition from the rubbery to the glassy state. While the polymer is a comparably brittle solid below T_g, it behaves like a viscous liquid at temperatures above T_g. The glass transition demarks the onset of a cooperative movement of significant portions of the polymer backbone, which does not occur at lower temperatures.

Most interestingly, T_g is dependent on the rate of heating or cooling. Along with the glass transition temperature, also the specific volume occupied by the polymer at a given temperature below T_g changes as a function of the cooling rate. Fast cooling leads to a glass transition at a higher temperature and results in a higher specific volume.

For a given polymer, a volume contained within the van der Waals' radii of the molecular chains and an additional volume "occupied" through molecular vibrations may be assigned. The sum of these volumes (occupied volume V_0), however, is always somewhat smaller than the specific volume of the polymer, leaving a certain amount of "excess" or "free" volume. The free volume is resulting from motional constraints on account of the high molecular weight of the polymer segments and is depending on the cooling rate at which the temperature drops below T_g, bringing the polymer into the glassy state. [6]

Theories in which the free volumes mentioned are playing a crucial role were first developed to describe viscosity and diffusivity in liquids. However, free volume is also responsible for the diffusive transport in polymeric membranes. The according transport properties are thus seen as a function of the free volume V_f, which is defined by Equation 1-36.

$$V_f = V - V_0(T)$$

V_f	free volume
V	total macroscopic volume
V_0	volume occupied by molecules

Equation 1-36

The "occupied" volume $V_0(T)$ is calculated from the extrapolated volume of the glassy polymer at absolute zero, according to its thermal expansion coefficient (see Equation 1-37).

$$V_0 = V' + \beta_g T$$

V_0	volume occupied by molecules
V'	extrapolated volume at 0 K
B_g	thermal expansion coefficient

Equation 1-37

In case of many polymers, the fraction $f = V_f/V$ is around 0.025 at the glass transition temperature. Since below T_g the polymer is in its glassy state and the fraction of free volume stays virtually constant, this value represents a minimum amount (disregarding a further decrease due to possible ageing effects). Above T_g, the fractional free volume increases as a function of temperature.

---

[6] Assuming an idealized free volume equal to zero for the glassy state, an imaginary minimum glass transition temperature $T_{g\infty}$ may be deduced from the intersection of the "occupied volume" and the specific volume of the rubbery state, both plotted as a function of temperature.

$$f = f_g + \beta_f \left(T - T_g \right)$$

f free volume fraction
f_g fractional free volume at Tg
β_f expansion coefficient of free volume
T temperature
T_g glass transition temperature

Equation 1-38

The total macroscopic volume *V* is finally predicted as in Equation 1-39.

$$V = V_0 \cdot \left[1 + e^{(\varepsilon_h + p\gamma_h)RT} \right]$$

V total macroscopic volume
V_0 volume occupied by molecules
ε_h energy of the free volume "holes"
γ_h volume of the free volume "holes"
p pressure

Equation 1-39

According to the free volume theory, the temperature-dependence of transport properties is described on the basis of the Williams-Landel-Ferry equation (WLF equation, see Equation 1-40). A detailed derivation of the expression is found in literature [21 {p. 46}].

$$\log \frac{\eta_T}{\eta_{T_g}} = \frac{C_1 \left(T - T_g \right)}{C_2 + \left(T - T_g \right)}$$

η_T viscosity at temperature T
η_{Tg} viscosity at glass transition temperature
T temperature
T_g glass transition temperature
C_1, C_2 constants

Equation 1-40

The values of the constants C_1 = -17.44 and C_2 = 51.6 are nearly universal for amorphous polymers. The viscosity itself is related to the fractional free volume according to the Doolittle viscosity equation (Equation 1-41):

$$\eta = a \cdot e^{(b/f)}$$

η_T viscosity at temperature T
f fractional free volume
a, b constants

Equation 1-41: The Doolittle viscosity equation.

Insertion of the universal constants into Equation 1-40 leads to the suggestion that at a temperature $T = T_g$ *-51.6* the viscosity of the polymer becomes infinite. At and below this temperature, diffusion thus depends solely on the free volume and on the mobility of the penetrant molecules within the "frozen" polymer, which is reflected by the mobility M_D in Equation 1-42, an expression strikingly similar to Equation 1-41. A_D and B_D are constants depending on the geometry, that is, the size and shape of the penetrant molecules, but not on the temperature anymore.

Expectedly, the mobility of the gas molecules increases with increasing free volume, a dependency just inverted to that of the viscosity (see Equation 1-41).

$$M_D = A_D \cdot e^{(-B_D / f)}$$

M_D	mobility of the penetrant
A_D, B_D	constants reflecting size and shape of penetrant
f	fractional free volume

Equation 1-42

At temperatures above the glass transition, the mobility at a certain temperature is related to the mobility at T_g according to Equation 1-43 (valid in the range from T_g to $T_g + 100$ °C).

$$\ln \frac{M_D(T)}{M_D(T_g)} = -B_D \left[\frac{1}{f} - \frac{1}{f_g} \right]$$

$M_D (T)$	mobility at temperature T
$M_D (T_g)$	mobility at glass transition
B_D	constant
f	fractional free volume at T
f_g	fractional free volume at T_g

Equation 1-43

Eventually, a relation of the terminus "mobility" and the thermodynamic diffusion coefficient, a property similar to that encountered in the previous sections, is attained by multiplication of M_D with the temperature and the gas constant, as follows in Equation 1-44.

$$M_D = \frac{D_T}{RT}$$

M_D	Mobility of the penetrant
D_T	Thermodynamic diffusion coefficient at temperature T
R	Gas constant

Equation 1-44

By means of appropriate derivation [21 {p. 48}], Equation 1-45 and Equation 1-46 are obtained, where the parameter K (see Equation 1-47) is understood as a measure of the "efficiency or inefficiency of utilisation of free volume by a mass transport process…". It thus reflects the size and shape of the penetrant molecules and ranges from very small values to unity. Without specific interactions between the penetrant gas molecules and the polymer, the thermodynamic diffusion coefficient can be replaced by the diffusion coefficient according to Fick's law.

$$\log \frac{D_T / T}{D_g / T_g} = K \cdot \log \frac{\eta}{\eta_g}$$

D_T	thermodynamic diffusion coefficient at temperature T
D_g	thermodynamic diffusion coefficient at glass transition
T	temperature
T_g	glass transition temperature
K	parameter (Equation 1-47)
η_T	viscosity at temperature T
η_{Tg}	viscosity at glass transition temperature

Equation 1-45

$$\log \frac{D_T T_g}{T} = -\frac{K \cdot C_1 (T - T_g)}{C_2 + (T - T_g)} + \log D_g$$

D_T	diffusion coefficient at temperature T
D_g	diffusion coefficient at glass transition
T	temperature
T_g	glass transition temperature
K	parameter (Equation 1-47)
C_1, C_2	constants

Equation 1-46:   A form of the WLF equation in terms of the diffusion coefficient *D*.

$$K = \frac{B_D}{b}$$

K	parameter
B_D, b	constants

Equation 1-47:   The parameter K as a measure of the efficiency of free volume utilisation by mass transport.

Molecular theories (such as the model of Pace and Daytner [31 {p. 131}]) imagine the transport phenomena on the basis of specific motions of the polymer backbone. It is assumed that in an amorphous polymer, regions of semi-crystalline order exist, with chain bundles that are oriented in parallel over distances of several nanometres.[7] The adjacent polymer chains are thought to form "tubes", along whose axis a dissolved penetrant is able to move with relatively little activation energy. However, the movement is interrupted at the end of the tubular structures. The permeating molecules are thus quickly moving back and forth in the confining "tubes", unless they are given the energy to separate two adjacent polymer chains and travel perpendicular to the tube axis into an adjoining tube. During the separation, the polymer chains are assumed to bend like flexible rods.

Since diffusion rates along the tube axis are more than three orders of magnitude higher than the macroscopically observed permeability, for a transfer through the polymer bulk, both processes (parallel and perpendicular migration) are thought to occur in series. The tube length determines the effective "jump length of diffusion" (about half of the effective tube length, since the penetrant may leave a tube at any point along the axis), while the activation energy necessary for a movement perpendicular to the axis determines the "jump frequency". Expectedly, the amount of required energy is depending on the kinetic diameter of the penetrant, thus, how pronounced the separation of the polymer chains must be to allow the transition of the diffusing molecule.

The mathematical treatment of the theory is complicated and in some aspects not subject to analytical solution. According computational approaches are found in literature [21 {pp. 50-53}].

---

[7] To account for the lower packing density of amorphous polymers, each polymer chain is thought to be surrounded by four nearest neighbours instead of six in a crystalline arrangement.

1.3.4   Convergence of Models – A Summary

In all theories, the diffusion processes in polymers are thought to depend on the free volume in the polymer bulk [21, 28, 31, 34]. There are, however, distinct differences in how the available free volume influences the diffusivity, depending on whether the polymer is above or below its glass transition temperature T_g. For a polymer in the rubbery state, that is, above T_g, the free volume increases as a function of temperature and the mathematical treatment of the diffusion process is fairly straight forward.

Below T_g, however, the polymer is in the glassy state and the free volume is "frozen" into the polymer bulk, thus, micro-voids or defects are created as the polymer is cooled through the glass transition. In addition to the Henry type sorption sites which are also present in a rubber, these Langmuir type sites are accommodating penetrant molecules which are not able to participate directly in the permeation process. As a result, Arrhenius plots on the basis of diffusion measurements below and above T_g show pronounced discontinuities, with the energy of activation being always higher for rubbery polymers. The additional energy is required for the chain separation permitting the migration of the penetrant.

In contrast to rubbery polymers, the free volume and hence the diffusion coefficients of glasses are strongly history-dependent with respect to temperature. In the first place, the rate of cooling the polymer through the glass transition is determining the amount of free volume "frozen" into the glass. Consequently, the specific volume of the non-equilibrium glassy state is higher than it would be in the liquid state and the free volume is hence slowly reduced by ageing effects. The rate of ageing is again depending on the temperature [21 {p. 4}].

The history-dependence follows a few rules-of-thumb. In a rapidly quenched polymer, for instance, when more free volume is frozen into the bulk than in a smoothly cooled one, the diffusivity will be higher. Ageing gradually reduces the free volume, with ageing rates being higher at temperatures close to T_g than at lower temperatures. At temperatures much lower than T_g, the loss of free volume will become negligible. As expected, polymer membranes undergoing a longer period of ageing will contain less free volume than such which were just quenched from the rubbery state.

The amount of free volume is a property of major interest for the application of polymers in gas separation membranes. If the polymer is kept at a temperature sufficiently below T_g, the amount of free volume remains virtually constant over commercially significant periods of time. In the according membrane production process, the free volume and hence also the size and diameter of the micro-voids are governed by the rate of cooling through the glass transition. In such a manner, the separation properties of membranes can be precisely adjusted, allowing gas separation on the basis of the kinetic diameter of the gas species in a mixture. However, only small alterations in the molecular scale environment are required to effect significant changes in the performance, as it can be deduced from the kinetic diameters of various penetrants shown in Table 1-3.

Table 1-3:   **Kinetic (sieving) diameter of various penetrants [21 {p. 55}, 34 {p. 255}]**

The dimensions given represent the minimum zeolite window dimension that will allow sorption to occur for the indicated molecule.

Molecule	Kinetic Diameter (Å)
He	2.6
H_2	2.89
NO	3.17
CO_2	3.3
O_2	3.46
N_2	3.64
CO	3.76
CH_4	3.8
C_2H_4	3.9
Xe	3.96
C_3H_8	4.3
$n\text{-}C_4H_{10}$	4.3
CF_4	4.7
$i\text{-}C_4H_{10}$	5.0

1.3.5   The Gas Selectivity of Dense Membranes

In a simplified model, the selectivity of a dense polymer membrane regarding a gas A relative to another gas B is given by Equation 1-48.

$$\alpha_{AB} = \frac{P_A}{P_B} = \frac{D_A}{D_B} \times \frac{S_A}{S_B}$$

α_{AB}	selectivity with respect to the gases A and B
P	permeability coefficient
D	diffusivity
S	solubility

Equation 1-48: The ideal selectivity of dense membranes.

Hereby, the ratio D_A/D_B can be considered as mobility selectivity, and S_A/S_B as solubility selectivity. Both mobility selectivity and solubility selectivity for a given pair of gases are determined by chemical and physical properties of the polymer. The relationships between polymer structure, the nature of the gases and transport properties are not quite straight forward, although there are some general rules [29 {p. 42}].

The diffusivity D decreases as the size of the gas molecules increases, and the extent of the decrease is dependent on the flexibility of the polymer backbone. The mobility selectivity for a given gas pair, which is dominant for most glassy polymers, hence increases with an increasing rigidity of the polymer structure, and the transport of smaller molecules is, in comparison, favoured more strongly [29 {p. 42}].

The solubility *S*, on the other hand, increases with the permeant's molecular size, due to the growing intermolecular forces between the polymer and the gas. Rubbers with their flexible polymer chain exhibit little mobility selectivity. Gas separation is attained mainly via solubility selectivity in this case. For gas separation processes, solubility is strongly related to condensability. Large organic vapour molecules may therefore permeate much faster through some rubber-type polymers than "permanent gases", that is, symmetric and hardly polar low molecular weight molecules like N_2 or O_2 [21 {p. 3}].

Solubility selectivity and mobility selectivity are generally reverse. Depending on the physical state of the polymer, one of the two may outnumber the other and become the predominant one. As already mentioned, most polymers in the rubbery state behave according to their solubility selectivity, while glassy polymers effect gas separations via a mobility selectivity mechanism.

1.4 "TRANSIENT" PERMEATION EXPERIMENTS

Both the permeability coefficient *P* and the diffusivity coefficient *D* of rubbers (and hence also the solubility coefficient *S*) can be determined in a single, so-called "transient permeation experiment" [19, 21, 34 {p. 250}, 37].

In such a measurement, a thoroughly degassed membrane is subjected to a partial pressure gradient with respect to the permeant of interest. In other words, a certain partial pressure of the permeant is applied in an according apparatus in the form of a "test gas" on one side of the membrane. On the opposite side of the membrane, the increasing partial pressure of the permeant is recorded as a function of time. Since the membrane has been thoroughly degassed prior to the experiment, a certain "time lag" ϑ is observed, which is related to the time required by the gas molecules to traverse the membrane. Eventually, steady-state conditions with a stable concentration gradient across the thickness of the membrane are eventually established. The "time lag" (or, alternatively, "onset-time" or "time-before-breakthrough") is given by Equation 1-49.

$$\theta = \frac{l^2}{6D}$$

ϑ	"time lag" or "onset time"
l	membrane thickness
D	Diffusivity

Equation 1-49

ϑ is found by extrapolation of the linear portion of the recorded partial pressure plot (as a function of time) to the time axis. The linearity is observed after the stationary state has been attained. It has been shown that this occurs after a period three times the time lag [21, 37]. Only data points recorded after that time should be considered in the extrapolation procedure. The permeability coefficient is derived from the slope of the linear portion of the curve. The solubility is, eventually, obtained by division of the permeability by the diffusivity.
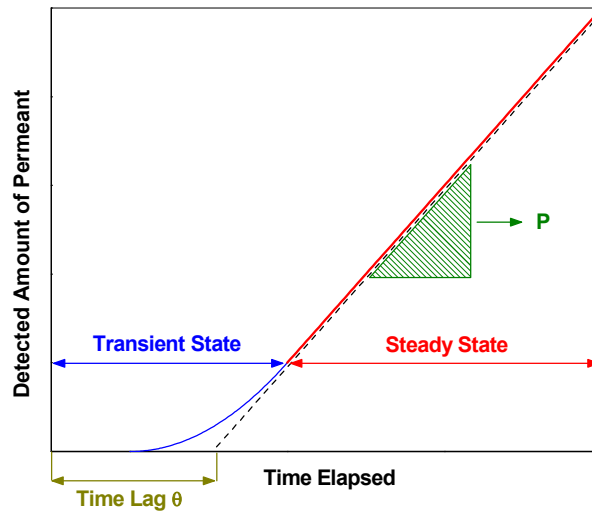
Fig. 1-1: Transient permeation experiment [21 {p. 28}, 37].

The method is valid only in case of rubbery polymers, that is, when the temperature is above the glass transition temperature T_g of the polymer. Below T_g the polymer is in its glassy state and the dual mode sorption diffusion model applies, leading to a more complicated form of the time lag expression which becomes a function of a number of parameters introduced in section 1.3.2.

The general conclusion drawn from a detailed treatment [21 {pp. 40-42}] is that true diffusion constants cannot be obtained in glassy polymers. In one of the two limits of the dual sorption mode model, total immobilisation of the gas molecules is obtained as the result, predicting that the permeability is constant and the time-lag is pressure dependent. In the other limit, no distinction between sorption mechanisms is possible and the time lag is predicted to be constant, but the permeability is very pressure-dependent. In true polymers, however, incomplete immobilisation is observed and both the time lag and permeability are decreasing with increasing pressure.

In regard of the inability to obtain diffusion constants not even for polymers below their glass transition, an according attempt appears even more obsolete in case of ultra-barrier membranes which usually comprise a multilayer structure formed of polymers and inorganic coatings. Transient permeation experiments therefore do not appear useful with such samples.

1.5   GUIDELINES FOR DIFFUSION PROPERTIES OF POLYMERS

Besides the experimental determination, the permeability coefficient of a polymer can be roughly estimated from the properties of the structural units which it comprises. Both purely empirical rules-of-thumb and mathematical procedures are known and shall be briefly presented in the following sections.

1.5.1 Estimation of the Gas Solubility

The solubility of gases in a polymer is in a first approximation depending on the gas molecule's diameter, given that there are no specific interactions between the gas and the polymer. Thus, when the solubility of a certain gas is in a polymer is known, the solubility of another gas can be estimated by multiplication with a factor *x* characteristic for the gas of interest. For example, in a given polymer O_2 has got twice the solubility and CO_2 the 25-fold solubility of N_2 (compare Table 1-3) [36, 38]. Together with increasing polarity and molecular weight of the gas molecules, the condensability and tendency for specific interactions with functional groups on the polymer increase, and the "rule-of-thumb" just introduced ceases to be valid [21 {p. 3}].

1.5.2 Influence of Polymer Structure

The permeability coefficients of polymers with respect to simple gases can be predicted to a degree in accordance with a number of empirical guidelines regarding the composition and structural properties of the membrane material. These rules-of-thumb provide valuable hints for the selection of a suitable polymer when specific permeation rates shall be achieved. The diffusion behaviour can furthermore be tailored to a wide range by copolymerisation or physical mixing with other polymers, and generally the same guidelines apply (see Table 1-4, where descriptive examples for polymers and their distinct properties responsible for different permeability coefficients are given, and compare from Pos. 9 to Pos. 12). The most important rules for an estimation of the diffusion properties are listed as follows [25 {p. 544}, 38, 39]:

Density: The density of a given polymer can be seen as an indicator for the free volume between the molecules of the polymer structure. A larger free volume is equivalent with a greater variety of diffusion pathways for the gas molecules. Generally, the permeability coefficient decreases with increasing density (see Table 1-4; compare Pos. 1 with Pos. 2).

Crystallinity: A semi-crystalline polymer has normally a higher density than its totally amorphous pendant. Hence the permeability coefficient is an inverse function of the degree of crystallisation (see Table 1-4; compare Pos. 3 with Pos. 4).

Orientation: A higher density is usually attained by orientation of the polymer chains (e. g. as a result of stretching). The higher degree of organisation among the molecules hence reduces the permeability coefficient (see Table 1-4; compare Pos. 5 with Pos. 6).

Fillers and Plasticisers: Fillers can, in certain cases, improve the barrier properties of a polymer. Nano-composite materials of a polymer and inorganic particles (e. g. Ormocers®) or silicates with a layered structure (e. g. nano-clays) are particularly interesting. In contrast, the utilisation of plasticisers normally has a negative effect on the barrier properties, since the mobility of the molecular chains is increased (see Table 1-4; compare Pos. 7 with Pos. 8).

<u>Functional Groups:</u> Introduction of polar functional groups, particularly fluorine and sulphonyl groups, can in some cases improve the barrier properties (see Table 1-4; compare Pos. 9 with Pos. 13).

Table 1-4: Permeability coefficients of polymers – structural influence [25]

Pos.	Polymer	Distinct properties	P[a]
1	Polyethylene LDPE	Density 0.914 g cm^{-3}	2.2
2	Polyethylene HDPE	Density 0.964 g cm^{-3}	0.3
3	Polyethylene terephthalate)	Amorphous	0.0444
4	Polyethylene terephthalate)	40 % crystalline	0.0257
5	Polyethylene [Hizex 7000F]	Deg. of stretch = 8	1.46
6	Polyethylene [Hizex 7000F]	Deg. of stretch = 20.5	0.129
7	Poly(trifluorochloroethylene)		0.03
8	Poly(trifluorochloroethylene)	With plasticizer [b]	0.42
9	Polystyrene		1.9
10	Polymethacrylnitrile		0.0009
11	Poly(methacrylnitrile-co-styrene)	97/3	0.0018
12	Poly(methacrylnitrile-co-styrene)	18/82	0.81
13	Poly(styrene-co-styrenesulfonic acid)	27 mol-% acid	0.315

[a] Permeability coefficient [10^{13} cm^2*s^{-1}*Pa^{-1}] for oxygen
[b] Plasticiser: Poly(trifluorochloroethylene) of low molecular weight

Except in case of a very low degree of polymerisation, the molecular weight of the polymer has little impact on the permeability coefficient. Cross-linkage of the polymer chains, on the other hand, generally reduces the permeation rates [39].

1.5.3   Numerical, Structure-Based Estimation of the Permeability Coefficient

A more numerically emphasised prediction method for the permeability coefficient is based on the consideration of the structural units forming the polymer too. The respective physical parameter, the permachor π, is determining the permeability coefficient as in Equation 1-50 [36, 39].

$$P(298) = P^*(298) * e^{(-s*\pi)}$$

$P_{(298)}$ permeability coefficient
$P^*_{(298)}$ permeability coefficient in the standard polymer
S scale factor
π permachor

Equation 1-50

$P_{(298)}$ represents the permeability coefficient of any simple gas in any polymer, $P^*_{(298)}$ is the permeability of the same gas in a certain standard polymer while s is a scale factor depending on the type of gas and the standard polymer [36]. The permachor is calculated from tabulated data for the present functional groups according to Equation 1-51:

$$N * \pi = \Sigma \left(N_i * \Pi_i \right)$$

N	number of characteristic groups per structural unit
π	permachor
Π_i	Increment of group i

Equation 1-51

N represents the total number of characteristic groups per structural unit, with Π_i being the so-called increment of the characteristic group i. The contributions Π_i to the permachor are readily available in literature [36].

1.5.4   Permeation through Multi-Layered Membranes

When the apparent permeability coefficient (technically the OTR) of a stack of different polymer materials shall be estimated, the permeation properties of each layer must be known. The permeability can thereby be imagined as a property reciprocal to a "diffusion resistance" (just like the properties electrical conductivity and resistance are reciprocal). In a multilayer membrane, the "diffusion resistors" are in series; their values are therefore added to obtain the "total diffusion resistance". Since the apparent total permeability coefficient P_{tot} is the reciprocal property, it is calculated from the permeability coefficients of the individual layers (P_1, P_2, …) as in Equation 1-52 [34].

$$P_{tot}^{-1} = P_1^{-1} + P_2^{-1} + ...$$

P_{tot}	total permeability coefficient
$P_1, P_2,...,P_n$	permeability coefficients of the individual layers

Equation 1-52

In case of barrier membranes comprising organic and inorganic materials in combination (multi-layer structures, polymers filled with inorganic particles), the situation is much more complicated, however. In case of fillers but also in case of areal inorganic layers which will inevitably have defect sites, the improvement in the barrier properties may be regarded as a result of a significant elongation of the path that a permeating molecule needs to migrate on its way through the material (see also the introductory section 1.1.2).

The concept of a "tortuous path" is frequently encountered in the context of contemporary ultra-barrier materials. According research regarding the mathematical modelling of such materials has been attempted some decades ago already [26, 27], and in the 2000 decade, research activities concerned with the preparation and understanding of multi-layered ultra-barriers were intensified distinctly. Detailed background is meanwhile found abundantly in literature therefore [16].

1.6 Ultra-high free volume polymers

In the recent decades, a number of polymeric materials were developed, showing unusually high permeation rates, which aroused much interest in the field of membrane research. Since the gas permeability is also of major interest for the fabrication of opto-chemical sensor matrices, a brief overview of such materials shall be given in this section.

Until the physical properties of poly(1-trimethylsilyl-1-propyne) (PTMSP) were published in 1983, the rubbery poly(dimethylsiloxane) was believed to have by far the highest gas permeability of all known polymers. However, the permeability coefficient of PTMSP was found to be 10 times higher than that of PDMS. The discovery triggered intensive research in this field, and thus a number of ultra-high free volume polymers with outstandingly high permeability coefficients were introduced. Generally, the extreme diffusivities are attributed to a very high fractional free volume, with a high degree of *interconnection* of the free volume elements [29 {pp. 45-47}]. Noteworthy that a frequently used method to determine the free volume of a polymer is positron annihilation lifetime spectroscopy (PALS) [40].

Until recently, the free volume was commonly controlled by introduction of bulky side chain groups into the polymer, acting as *permanent templates* or spacers. A simultaneous increase of the rigidity of the polymer backbone is desired to accomplish favourable selectivity properties [21 {p. 3}]. According polymers show many similarities with nano-porous materials [41] and are sometimes referred to as "super glassy polymers" on account of the high glass transition temperature necessary to prevent ageing effects from decreasing the free volume.

In Fig. 1-2 the structures of three important ultra-high free volume polymers are shown. The driving force for the development of such materials is found in their favourable properties for the manufacture of gas separation membranes, particularly in the field of hydrocarbon dew-pointing[8] of natural gas [29]. One of them, DuPont's TeflonAF® 2400, is a perfluorinated random copolymer of 87 mol-% 2,2-bistrifluoromethyl-4,5-difluoro-1,3-dioxole and 13 mol-% tetrafluoroethylene. It was used in the project at hand (see section 5.4.1) as a highly permeable matrix material for an extremely sensitive opto-chemical oxygen sensor. All of the shown polymers have a very high fractional free volume and a very high glass transition temperature.

As it can be seen in Table 1-5, these ultra-high free volume polymers have extreme permeability coefficients, compared to PDMS and other common polymer materials employed in gas separation membranes. Related physical parameters are abundantly found in literature [42-45].

Although manufactured in a completely different way and designed mainly to provide favourable liquid separation, it is worth mentioning that a well-known membrane material, namely "Goretex®" consists of poly(tetrafluoroethylene) and is thus chemically similar to TeflonAF®. In analogy, the Goretex® membrane obtains its distinct properties from a highly porous, interconnected

---

[8] The terminus "hydrocarbon dewpointing" refers to the separation of higher hydrocarbons like butane present in natural gas from methane.

microstructure. Water vapour is able to travel through the pores, while liquid water is repelled at the highly hydrophobic membrane surface and therefore unable to moisten the membrane. On account of this behaviour, the Goretex® membrane is commercially very successful in the textile industry, where it is used for water-impermeable but respiratory (outdoor and adventure) clothing. The microstructure is accomplished by paste extrusion of a mixture of the polymer with a volatile lubricant, such as naphta or kerosene, followed by uniaxial or biaxial stretching [29 {p. 32}].
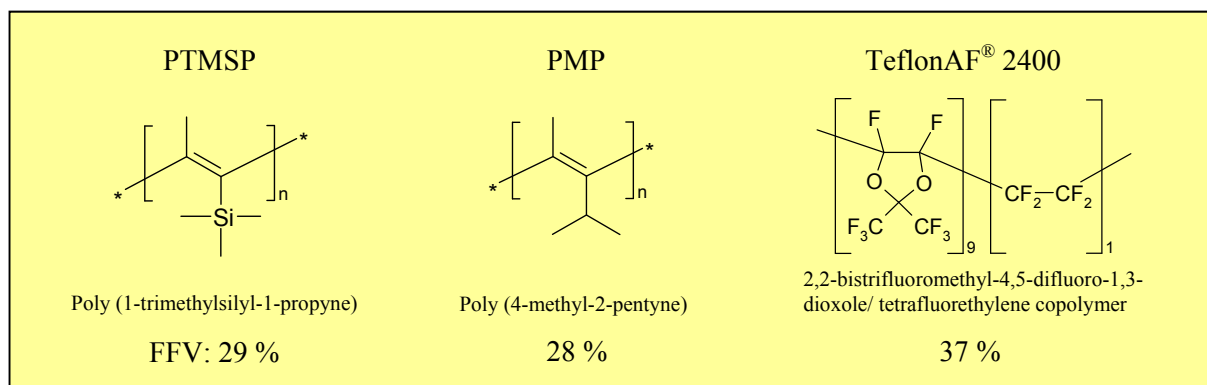
Fig. 1-2:   **Chemical structures and fractional free volume of selected ultra-high free volume polymers.**

Table 1-5:   **Oxygen permeability and oxygen/ nitrogen selectivity of high-free-volume polymers compared with conventional polymers [29, 44].**

Polymer	Oxygen Permeability [Barrer]	Oxygen-Nitrogen Selectivity
PTMSP	9700	1.5
PMP	2700	2.0
TeflonAF® 2400	1300	1.7
PDMS	600	2.2
Poly(methylpentene)	37	4.2
Poly(phenyleneoxide)	17	4.4
Ethylcellulose	11	3.4
Polycarbonate	1.4	4.7

2 PHOTOCHEMICAL OXYGEN SENSING

2.1 INTRODUCTION

The methodology for the measurement of oxygen transmission rates presented in the doctoral thesis at hand is fundamentally depending on the favourable properties of opto-chemical oxygen sensors. Roughly speaking, this type of sensors consists of luminescent metal-complex dyes which are immobilised in a suitable matrix material and brought into contact with the environment whose analyte concentration shall be analysed. During the measurement, the luminescence of the sensor, which is dependent on the analyte concentration, is characterised by an appropriate opto-electronic setup. The relevant parameters thus attained (luminescence *intensity* and *lifetime*) are processed to yield the analyte concentration according to experimentally determined calibration characteristics.

Not exclusively in the context of oxygen transmission rate measurements (and also the transmission rates of other permeants, given there is an appropriate sensor dye) the opto-chemical methodology offers some important advantages [46].

First, since the sensor itself comprises simply an immobilised dye, the mechanical dimensions may be downscaled to a wide extend. The sensor element merely needs to cover the area required by the optical setup for a sufficient luminescence excitation and emission measurement, generally a few millimetres in diameter.[9] The thickness of the sensor, however, is usually in the range of a few micrometres. Thus*, the volume of such a sensor element is effectively negligible*, even when compared to the interior of an already quite small apparatus, and any dead volumes associated with mechanical properties of the sensor are a priori circumvented in this way.

A second and very valuable property of opto-chemical sensors is that information about the analyte concentration is transmitted in the form of light, which can be detected through a transparent window of an otherwise sealed container. No electrical lines or interconnections of any kind penetrating the boundaries of the sensor compartment are required. *Non-invasive measurements* are therefore possible. Difficulties not to be underestimated are thus avoided, arising from insufficient gas tightness of electrical insulations and other constructional details which were otherwise necessary.

The most eminent advantage of many luminescent sensors is emerging from the mechanism of analyte detection. Commonly, the luminescence of the sensor is affected by analytes like oxygen via simple collision processes, thus liberating the chemically unchanged analyte after the "detection" (see section 2.2.1.5.2). As a consequence, the mechanism does not involve analyte *consumption*, as it is the case with many electrochemical sensors (see section 3.3.2). *Accumulation* of the analyte in the vicinity of the sensor and *simultaneous, continuous* measurements of the concentration increase resulting from membrane permeation are therefore accessible, exploiting the sensor performance to the best possible extend.

---

[9] If necessary, the utilisation of according fiber optics permits a much more efficient miniaturisation.

With the valuable virtues of opto-chemical oxygen sensors in mind and an according, in-house developed measuring system at hand (see section 4.3 and section 5) an apparatus was constructed "around" the sensor allowing a very sensitive determination of oxygen transmission rates through barrier membranes. One may thus say that the presented project is indispensably interwoven with the properties of luminescent sensor dyes.

The detection of analytes based on an alteration of the luminescence behaviour of certain fluorophores is a special case in the wide field of *fluorescence spectroscopy* [47]. Fluorescence technologies are used by scientists from many disciplines and meanwhile provide dominant research tools in the areas of biochemistry, biophysics, biotechnology, DNA sequencing, genetic analysis, forensics and medical diagnostics, to point out a few. Most according techniques are highly sensitive and thus allow, for instance, the intracellular imaging of biological molecules, even at the level of single-molecule detection in some cases [47, 48].

Since the term fluorescence spectroscopy covers a vast number of techniques and possibilities, each associated with a large amount of specific physical and chemical background, a comprehensive review is by far out of the scope of this doctoral thesis. Therefore, this section focuses mainly on aspects directly relevant to opto-chemical oxygen sensing techniques on which the project is based.

2.2 LUMINESCENCE

The concept of *luminescence* or, more precisely, *photoluminescence*, refers to the emission of radiation (most commonly in the form of visible light) from a substance, some of whose molecules are situated in electronically excited states. The excited state commonly results from initial absorption of an incident photon carrying sufficient energy. Formally, luminescence is divided into two categories, depending on the nature of the excited states [47, 48].

It is spoken of *fluorescence*, if the electronically excited atom or molecule is in the *singlet* state, that is, if the electron in the excited orbital is spin-paired to the second electron in the ground state. A return of the excited electron to the ground state orbital is therefore spin allowed and occurs rapidly with typical rates in the range of $10^8 \, s^{-1}$. The average time spent by the electron in the excited state (the so-called lifetime" τ, see section 2.2.1.4) consequently amounts about 10 ns. The energy of the excited state cannot be accommodated in the ground state and is therefore released to the surroundings by the emission of a fluorescent photon in the course of the transition.[10]

If the excited electron is in a so-called *triplet* state, its spin orientation is parallel to the electron in the ground state. Since, according to Hund's law, no two electrons with identical spins can be accommodated in the same orbital, a return of the excited electron is spin-forbidden, which results in much lower transition rates (typically $10^3 \, s^{-1}$ - $1 \, s^{-1}$). It is spoken of *phosphorescence* in this case. The according lifetimes typically range from milliseconds to seconds, but even longer lifetimes are

---

[10] Dissipation mechanisms devoid of the emission of photons exist and form a vital aspect when thinking about the employment of luminescent dyes as sensors. They will be discussed in the following sections.

observed. However, a distinction between fluorescence and phosphorescence is not always clear, because some luminescent species display mixed singlet and triplet states, leading to intermediate lifetimes [47].
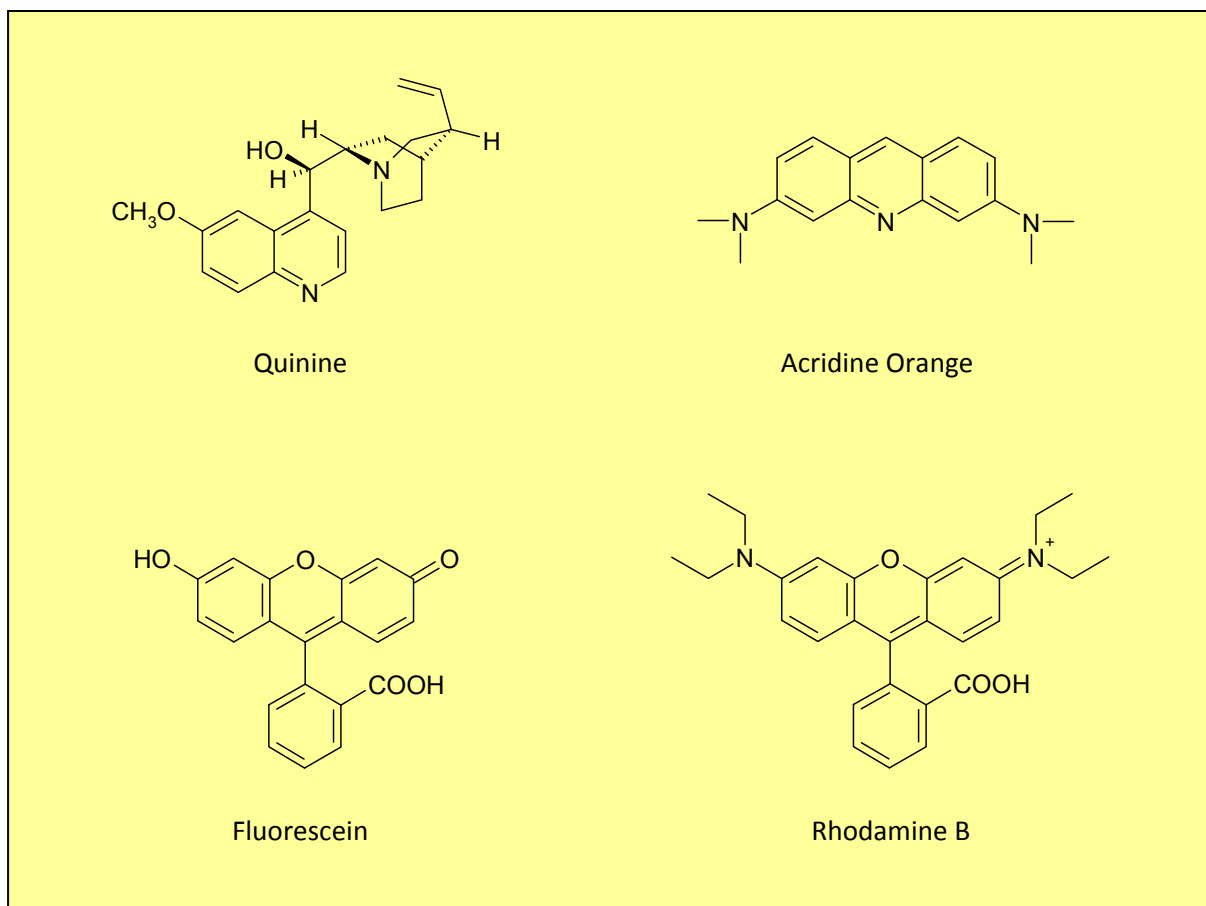
Fig. 2-1: Structures of fluorescent aromatic substances [47].

Substances which exhibit fluorescent behaviour ("*fluorophores*") typically comprise aromatic structures, as does the first fluorophore to be discovered by Sir John Frederick William Herschel in 1845, quinine. In Fig. 2-1 the structures of typical fluorophores are shown. The property of fluorescence inherent to aromatic compounds is, for instance, used in environmental monitoring of oil pollution due to the fluorescent behaviour of components such as anthracene or perylene [47].

In contrast to organic molecules, atoms generally do not exhibit fluorescence in the condensed phase, with the elements of the lanthanide group being one important exception.

2.2.1   Fundamental Luminescence Processes

Luminescence is the result of a number of mechanisms associated with the interaction of light and matter. A very useful starting point for the discussion of relevant processes is the so-called Jablonski diagram (see Fig. 2-2), named after Prof. Alexander Jablonski, who is considered as the father of fluorescence spectroscopy. Jablonski diagrams may be constructed in a variety of forms and illustrate

the electronic and molecular transitions that can occur when photons transfers their energy to molecules and vice versa [47, 48]. For simplicity, in the diagram shown in Fig. 2-2 a number of possible interactions were omitted.

Beginning with the initial absorption of an incident photon, a number of mechanisms may apply until the thus excited molecule arrives in the ground state again. These processes are formally categorised into *primary* and secondary *processes*. Primary processes involve the initial absorption of a photon hv_A of incident radiation and the resulting excitation of the absorbing atom or molecule. All contemplable events in which the energy just absorbed is transferred or dissipated are considered secondary processes.

At the beginning of a primary process, the molecules are in the singlet ground state (S_0). Pairs of electrons, which possess anti-parallel spins according to Hund's law, occupy the molecular orbitals. The electronic energy level of the ground state (as well as the other electronic levels) disperse into a number of vibrational energy levels, as it is indicated in the Jablonski diagram by the indices 0, 1, 2, and so forth. At room temperature, excited vibrational levels are not significantly populated due to the energy spacing of 1500 cm^{-1} (too large to be thermally excited at this temperature), and consequently, the primary processes originate in the lowest vibrational energy level of the ground state.

The absorption of a photon of hv_A causes the molecules to undergo a transition into an excited electronic energy level, which is initially also a singlet state (S_1, S_2, etc.). The absorption, illustrated by an upward arrow, occurs within about 10^{-15} s. After the excitation, the electron occupies an orbital which is further away from the atom's nucleus. In the course of the very short absorption process, the distances between the atomic nuclei in the molecule do not change significantly according to the Frank-Condon principle, and the transition is said to be "vertical". However, the entire molecule is now in a state of higher energy and the oscillating movements of the atoms relative to each other have change to in accordance with the altered electronic environment [47, 48].

In condensed phases, the molecules relax to the lowest vibrational level of the excited state very rapidly in a process called *internal conversion*, in which excess energy is dissipated to the surroundings in the form of heat [48]. The thermally equilibrated state is attained within 10^{-12} s or less. Any subsequent processes therefore have their provenance in the lowest vibrational level of the excited state in which the electron remains for typically 10^{-8} s. At this point, the primary processes are completed.

Secondary processes are of a greater variety. The excited electron may return from the excited state S_1 to the ground state S_0 following a number of different mechanisms. If during the transition a photon of energy hv$_F$ is emitted, the process is termed *fluorescence* (spectroscopically, *fluorescence* refers to a luminescence emission *without* a change in multiplicity during the transition [48]). The energy of the emitted photon is always smaller than the energy of the absorbed photon (see section 2.2.1.1). In analogy to the absorption process, the molecule commonly arrives at an excited vibrational level of the electronic ground state due to the Frank-Condon principle. The vibrational

energy is again very quickly dissipated in the form of heat and the molecule is in the ground state again [47].

Besides the direct emission of a photon, electrons in the excited level S_1 may also undergo *spin conversion* in a process called *inter-system crossing*, resulting in a triplet state T_1, which is the starting point of the emission process named *phosphorescence (*which spectroscopically addresses an emission *involving a change* in multiplicity [48]). Since the transition back to the ground state is now spin forbidden, the rates of emission from triplet states are by several orders of magnitude smaller than those from singlet states. Furthermore, the energy of T_1 is smaller than the energy of S_1, and likewise is the energy of the emitted photons. Phosphorescence emission is therefore shifted towards smaller wavenumbers, compared to fluorescence emission. Molecules are often phosphorescent if they contain heavy atoms such as bromine or iodine. Besides emissive transitions, the triplet states may dissipate their energy to the surroundings also in radiation-less processes such as internal conversion [47, 48].

Although rare exceptions are known, fluorescence and phosphorescence most commonly display a number of general characteristics, which are outlined in the following sections.

2.2.1.1 *The Stokes Shift*

As it is illustrated in the Jablonksi diagram in Fig. 2-2, the energy of the emitted fluorescent or phosphorescent photons is lower than the energy of the photons absorbed during the excitation. This energy difference is referred to as the *Stokes shift*. Compared to the incident radiation, the emitted light is shifted towards smaller wavenumbers, as it was first discovered by Sir G.G. Stokes in 1852 [47, 48]. The "loss" of energy in the form of heat between excitation and emission is, in solution, universally observed. A dominant energy "sink" is attributed to the rapid decay from the excited to the lowest vibrational level of S_1. In addition, the molecule is commonly in an excited vibrational level of the ground state after the emission of a photon. The vibrational energy again decays to the lowest level very rapidly. Furthermore, interactions with the solvent, reactions of the excited state, the formation of complexes and energy transfer processes can lead to a decrease of the emitted photon's energy.
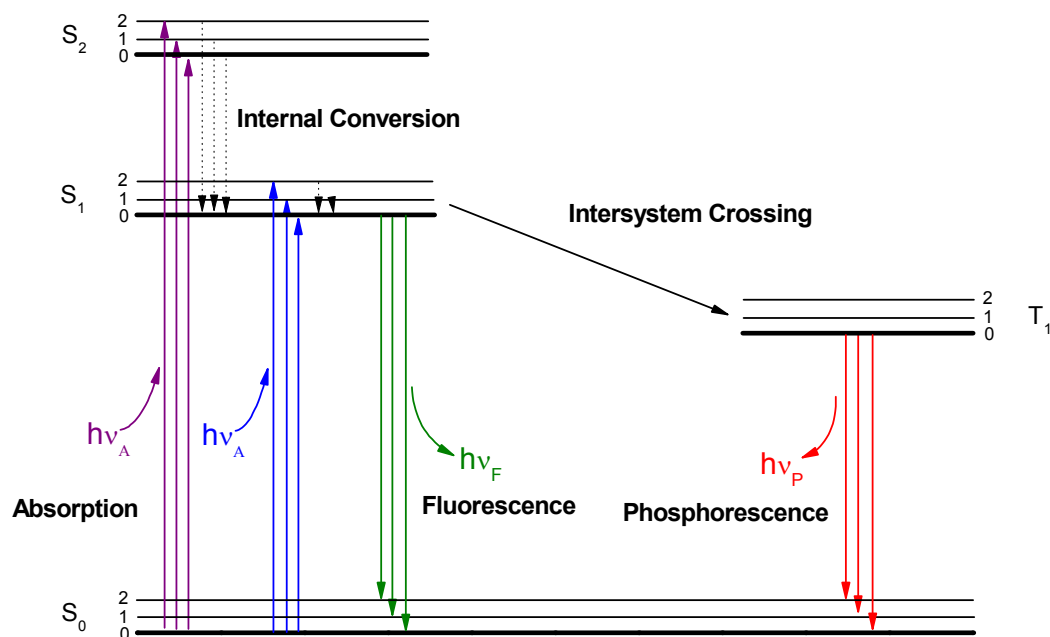
Fig. 2-2:   Fundamental luminescence processes illustrated in a Jablonski diagram [47].

2.2.1.2   Independence of Excitation and Emission Wavelength

Another, nearly universal property of fluorescence is delineated by Kasha's rule, which states that the emission spectrum is independent of the wavelength of excitation. If the incident photons carry more energy than necessary to reach S_1, the initial excited state is in a higher vibrational level or even a higher electronic state (S_2, for instance). However, within typically 10^{-12} s, the excess energy is dissipated in the form of heat and the fluorophore arrives in the lowest vibrational level of S_1. Since fluorescence emission virtually always occurs from this energy level, the energy difference to the ground state is always the same and the wavelength of emission consequently independent of the wavelength of the incident radiation. Exceptions to Kasha's rule exist (such as fluorophores displaying two ionisation states or molecules which are able to emit from S_2), but such emissions are rarely observed [47].

2.2.1.3   The Mirror-Image Rule

In many cases, the spectra of absorption and emission of a given fluorophore are very similar in shape but behave like mirror images.

The appearance of the absorption spectrum is determined by the electronic and vibrational energy levels that can be reached from the ground state S_0, and the probability that a specific transition occurs. Commonly, the accessible states consist of the different vibrational levels of S_1 (see the Jablonksi diagram in Fig. 2-2). Multiple absorption maxima, separated by the energy spacing of the vibrational levels are thus observed, with the strongest absorption normally corresponding to a

transition from the 0th level of S_0 to the 1st level of S_1 (that is, the transition with the highest probability is to the level immediately above the *lowest* in terms of energy).

As it was explained in the previous sections, molecules in higher vibrational levels quickly relax to the lowest vibrational state of S_1, in which they remain for a certain period of time before the emission of a fluorescent photon occurs. In the transition to the ground state, different destination vibrational levels are again accessible. In analogy to absorption, the transition from the 0th vibrational level of S_1 to the 1st vibrational level of S_0 is commonly the most probable one. However, in the case of emission the energy of this transition is the first to the *highest* in energy. The energy sequence of transitions to the other vibrational levels is likewise reversed.

The spacing of the absorptions peaks reflects the energy difference of the vibrational levels of the excited state S_1. The spacing in emission spectra, on the other hand, refers to the ground state's vibrational levels. Since the vibrational levels of the ground and excited states are very similar in spacing, a mirror-image-like appearance of the absorption and emission spectra is attained [47].

There are, however, fluorophores whose spectra are devoid of the mirror image behaviour. Excitation occurs into S_2 in many of such cases, which is followed by fast relaxation into S_1. The emission spectrum is thus the mirror image of the $S_0 \rightarrow S_1$ transition, not of the overall absorption spectrum. Besides excitation into higher electronic levels, reactions of the excited state such as proton dissociation (as a result of a change of the pK_a) or the formation of charge-transfer complexes can void the mirror image rule. In these cases, the reactions are specific to the excited state and do not occur in the ground state.

The formation of such charge-transfer complexes of excited states is of importance in a number of technical applications. If the process involves a reaction partner of a different molecular species than the excited state molecule, the complex is referred to as *exciplex* ("excited complex"). Some fluorophores form complexes also with themselves, and the resulting complex is called *excimer* ("excited-state dimer"). Exciplexes and excimers are molecule which can exist exclusively in the excited state [47].

2.2.1.4   Luminescence Lifetime and Quantum Yield

In the quantitative description of the luminescence behaviour of a fluorophore, the terms *lifetime* and *quantum yield* represent the most important characteristics [47, 48].

Besides the emission of a luminescent photon, molecules in the excited state S_1 can undergo a radiation-less transition to the ground state. Hereby, the electronic energy of S_1 is initially transferred by internal conversion into vibrational energy of the ground state S_0. As it was explained in section 2.2.1, the higher vibrational levels seek the equilibrium with the surroundings and quickly relax to the lowest level. The energy discharged in this event is dissipated by collision processes in the form of heat.

In addition to fluorescence and radiation-less processes based on internal conversion, a number of events may annihilate the energy acquired in the absorption and depopulate the excite state S_1. Consequently, not every photon absorbed results in an emitted fluorescent photon. The fraction of the absorbed photons "utilised" for luminescence itself is reflected by the *quantum yield Q,* which is defined according to Equation 2-1 [47, 48].

$$Q = \frac{N_{Emission}}{N_{Absorption}}$$

Q	quantum yield
$N_{Absorption}$	number of absorbed photons
$N_{Emission}$	number of emitted photons

Equation 2-1: The quantum yield.

A discussion about the meanings of quantum yield and lifetime is assisted by a simplified Jablonski diagram (see Fig. 2-3), in which the individual relaxation events leading to the lowest excited state S_1 are omitted and the focus is on the processes responsible for a return to the ground state. As mentioned before, these involve the emission of photons with a rate Γ as well as a non-radiative decay with a rate k_{nr}.[11]
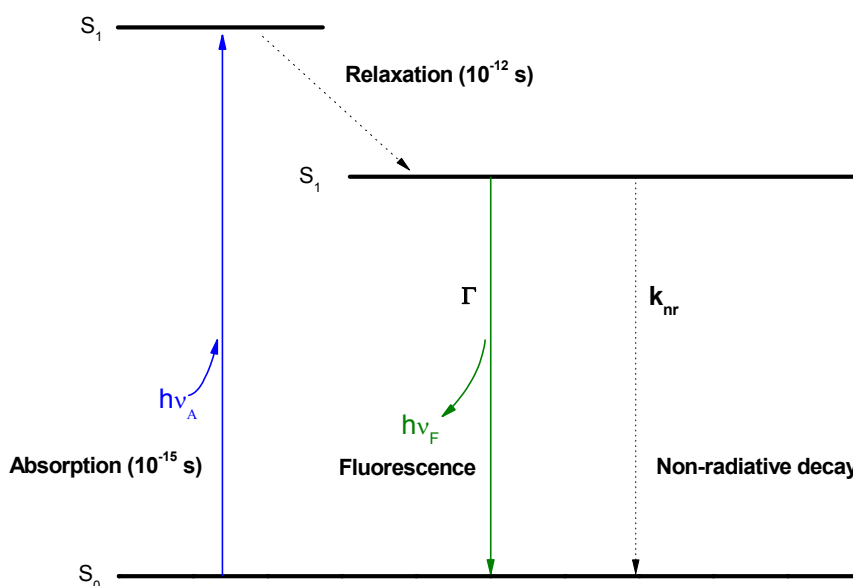
Fig. 2-3: Simplified Jablonski diagram illustrating the meaning of quantum yield and lifetime [47].

---

[11] It is noted that for reasons of convenience all non-radiative processes are grouped in k_{nr} at this point of the discussion.

Both radiative and non-radiative processes depopulate the excited state. In terms of rates, Equation 2-1 may be rewritten into Equation 2-2.

$$Q = \frac{\Gamma}{\Gamma + k_{nr}}$$

Q	quantum yield
Γ	rate of emissive depopulation
k_{nr}	rate of non-radiative depopulatio

Equation 2-2: The quantum yield in terms of depopulation rates

The quantum yield may range from very small values for virtually non-fluorescent molecules to unity for the best fluorophores displaying the brightest emissions. The theoretical maximum value of 1 is attained in the complete absence of non-radiative decay. It shall be pointed out that the *energy yield* of fluorescence is generally smaller than 1 because in numerous relaxation processes energy is lost, resulting in a more or less pronounced stokes shift [47, 48].

Besides the quantum yield, the *lifetime τ* of the excited state is a property of importance, as it determines the time available for the fluorophore to interact with the environment (typically in the range of 10 ns). It is defined as the average time the molecule spends in the excited state prior to the emissive or non-radiative relaxation to the ground state, and, in terms of decay rates, it is expressed as in Equation 2-3. The reciprocal value of the lifetime can thus be seen as the sum of the rates depopulating the excited state [47, 48].

$$\tau = \frac{1}{\Gamma + k_{nr}}$$

τ	lifetime
Γ	rate of emissive depopulation
k_{nr}	rate of non-radiative depopulation

Equation 2-3: The luminescence lifetime as a function of depopulation rates

The depopulation is a random process and follows 1st order kinetics. Hence an exponential decay is observed, if the excited state is not continuously re-populated. As it follows from the exponential decay function, 63 % of the excited species are deactivated at a time t< τ, while only 37 % populate the excited state for a period longer than the lifetime [47, 48].

In the imaginary absence of non-radiative processes, a theoretical maximum of the lifetime can be defined, called the *intrinsic* or *natural lifetime* τ_n (see Equation 2-4). The natural lifetime can, in theory, be calculated from the extinction coefficient and the absorption and emission spectra of the fluorophore [47].

$$\tau_n = \frac{1}{\Gamma} \qquad \tau_n = \frac{\tau}{Q}$$

τ_n natural lifetime
Γ rate of emissive depopulation
τ lifetime
Q quantum yield

Equation 2-4: The natural or intrinsic lifetime

Two molecules with the same rate of emissive decay (and consequently the same natural lifetime) do not necessarily display the same fluorescence lifetime and quantum yield. In fact they may be very different, as it is the case with eosin and erythrosine B, for instance. These fluorophores have a very similar rate of fluorescent emission. However, there is a pronounced difference in quantum yield, caused by different rates of non-radiative energy dissipation [47].

2.2.1.5 Interaction: The Concept of Donor and Acceptor

In the previous sections, two general types of processes depopulating the excite state were encountered, namely radiative and non-radiative transitions to the ground state. However, the non-radiative processes, some of which have their origin in the fluorophore itself (e. g. internal conversion) were grouped into one rate constant for reasons of simplicity. In fact, there is a wide variety of possible mechanisms arising from the interaction of fluorophores with the environment, contributing to a radiation-less depopulation of excited states and hence a reduction of the intensity and lifetime of the observable luminescence. In some of these processes, new excited state species are created which are in turn able to emit a photon upon a transition to the ground state. Thus, the original luminescent emission of the fluorophore may be accompanied or even replaced by another emission at different wavelength and with different lifetimes and quantum yields [47].

In the context of a fluorophore's interaction with the environment, the concepts of *donor* and *acceptor* shall be introduced. A *donor* is a fluorophore which transfers the energy it acquired in the absorption process to another molecule, the so-called *acceptor*, whose excited state energy is somewhat lower than that of the donor. Thereby, the acceptor molecule does not need to be a fluorophore by itself. If the acceptor is unable to absorb the incident radiation on its own, the donor is also referred to as the *photosensitizer* in the particular donor/ acceptor pair.[12]

The energy transfer can either proceed from the donor's singlet or triplet states. In the latter case, the donor molecules are given more time for effective encounters with other molecules on account of the extended lifetimes of the triplet states. According mechanisms are therefore more important than those involving exclusively singlets. During such triplet-singlet energy transfers, the donor is returning to a singlet ground state while the acceptor arrives in an excited triplet state [47].

---

[12] Photosensitised processes play an important role in nature and technology. Photosynthesis and preparatory photo-oxidation are resulting from sensitizer action, for instance.

2.2.1.5.1 Resonance Energy Transfer

An important example for donor-acceptor mechanisms that depopulate the excited state of a fluorophore is the so-called resonance energy transfer (RET).[13] It occurs when the emission spectrum of a fluorophore named *donor* in this context is overlapping with the absorption spectrum of another species, the *acceptor*, which does not need to be a fluorophore by itself. A very important aspect of RET is that it *does not* involve intermediate emission of a photon by the donor and re-absorption by the acceptor. Instead, the energy is transferred via a dipole-dipole interaction mechanism. The acceptor is in an excited state after the energy transfer and may now emit a photon upon return to the ground state [47, 48]. The RET mechanism is schematically shown in Fig. 2-4 (see next section).

The efficiency of resonance energy transfer is depending on the donor-acceptor distance and the extent of spectral overlap. The latter is expressed in terms of the Förster distance R_0. Generally, RET can act over distances of a macromolecular scale. The rate of resonance energy transfer and its efficiency for a donor-acceptor pair at a fixed distance are given by Equation 2-5.

$$k_T(r) = \frac{1}{\tau_D} \cdot \left(\frac{R_0}{r} \right)^6 \qquad E = \frac{R_0^6}{R_0^6 + r^6}$$

$k_T(r)$	rate of energy transfer
τ_D	donor lifetime in absence of RET
R_0	Förster distance
r	distance between donor and acceptor
E	efficiency of energy transfer

Equation 2-5

Resonance energy transfer comprehends a wide and complex field. The mechanism is of importance, for instance, in the development of a water-sensitive luminescent dye in a project related to the presented one [49].

2.2.1.5.2 Quenching

There are countless examples in which the acceptor molecules annihilate the energy they have just received from the donor molecules devoid of the emission of light. The according processes are subsumed by the terminus *quenching* and represent the key property when thinking of an employment of luminescent substances as sensors. More generally, quenching refers to any process that decreases the fluorescence intensity of a sample. It does not necessarily involve a donor-acceptor interaction. Thus, quenching mechanisms include excited-state reactions, molecular rearrangements or ground state complex formation [47].

Quite commonly and most important in the context of analyte detection, the deactivation occurs upon contact with some other molecule in the course of a simple *collision*, in which neither the fluorophore (=donor) nor the *quencher* (=acceptor) are chemically altered. The process is therefore

---

[13] The term "resonance energy transfer" (RET) is preferred over "fluorescence resonance energy transfer" (FRET) due to the absence of intermediate fluorescent photons. Some scientists read FRET as "Förster resonance energy transfer", which appears to be the most accurate interpretation.

not a photochemical reaction. During the diffusive encounter with the quencher, however, the excited fluorophore is returned to the ground state without the emission of a fluorescent photon, as it is shown in the Jablonski diagram in Fig. 2-4. Thereby, the energy of the excited state is accepted by the quencher and dissipated into the environment in the form of heat [47, 48].

$$k_T(r) = \frac{1}{\tau_D} \cdot \left(\frac{R_0}{r} \right)^6$$
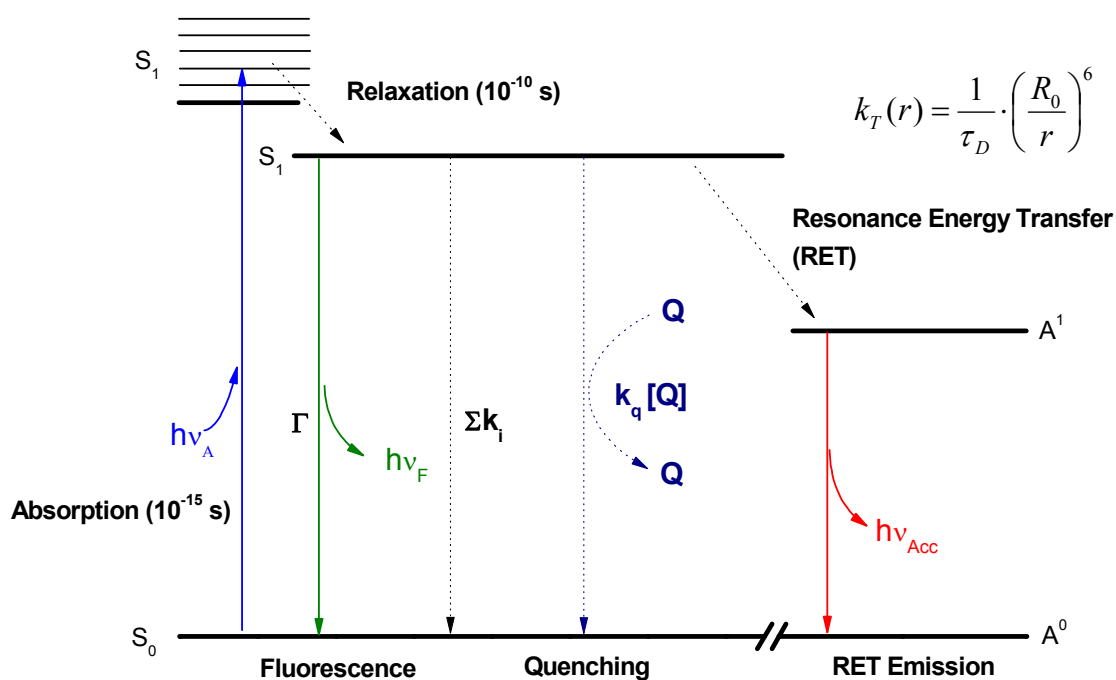
Fig. 2-4: Jablonski diagram illustrating the processes of quenching and resonance energy transfer [47].

Many molecules, including halogens, amines and, first of all, *oxygen* can act as *collisional quenchers.* The individual quenching mechanism upon collision is depending on the fluorophore-quencher pair and may, among others, involve electron exchange (*Dexter interaction*), photo-induced electron transfer and spin-orbit coupling including intersystem crossing to the triplet state. The complex formation with ground state fluorophore molecules is known as *static quenching*. Collision processes besides static quenching are commonly subsumed as *dynamic quenching* [47, 48].

For both static and dynamic quenching an intimate molecular contact between the excited-state fluorophore and the quencher is required for an efficient energy exchange (within 2 Å). Furthermore, the "permitted" distance increases with the lifetime of the fluorophore. These properties represent an important difference to the resonance energy transfer mechanism (see section 2.2.1.5.1) which can act over distances on a macromolecular scale, and the distance is furthermore independent from the donor lifetime [47 {p. 333}]. However, the requirement of molecular contact enables a number of possible applications. Quenching may, for instance, reveal the accessibility of the fluorophore to the quencher molecules. Thus, the diffusivity of the quencher through a cell membrane or the position of a fluorophore within a macromolecule such as a protein may be determined. Conversely, the

diffusivity of an analyte in a matrix material has a direct influence on the sensitivity of a luminescent chemical sensor towards the quenching analyte [47, 50]. This is of importance when appropriate sensor/ matrix combinations are selected. In the presented project, a highly permeable, ultra-free volume polymer was tested and employed as a matrix material to attain one of the greatest possible sensitivities to traces of oxygen (see sections 1.6 and 5.4.1).

The decrease in fluorescence intensity resulting from the quenching process is mathematically delineated by the Stern-Volmer equation (see Equation 2-7), which derives from the consideration of the fluorescence intensities in the presence and absence of the quencher. The observed fluorescence intensity of a fluorophore is proportional to the concentration of excited states $[F^*]$. Under constant illumination, the excited state population is also constant and therefore $d[F^*]/dt = 0$. The concentration $[F^*]$ in the absence (A) and presence (B) of the quencher is described by the differential equations given in Equation 2-6. In the absence of quenching, the excited state is depopulated with a rate $\gamma = (\Gamma + k_{nr})$ by radiative (rate Γ) and non-radiative (rate k_{nr}) processes. In the presence of the quencher, an additional process with a rate $k_q[Q]$ contributes to the overall depopulation. Since the population is constant under constant illumination, the derivatives of Equation 2-6 are set zero. Subsequent division of B by A and rearrangement leads to the Stern-Volmer equation (Equation 2-7) [47, 51].

(A)
$$\frac{d[F^*]}{dt} = f(t) - \gamma [F^*]_0 = 0$$

$[F^*]_0$	equilibrium concentration of excited state fluorophores in the absence of the quencher
$[F^*]$	equilibrium concentration of excited state fluorophores in the presence of the quencher
$f(t)$	rate of excitation due to constant illumination
γ	decay rate in absence of quencher ($\gamma = \tau_0^{-1}$)
k_q	bimolecular quenching constant
$[Q]$	concentration of quencher
τ_0	unquenched lifetime
t	time

(B)
$$\frac{d[F^*]}{dt} = f(t) - (\gamma + k_q[Q])[F^*] = 0$$

Equation 2-6

$$\frac{F_0}{F} = 1 + K[Q] = 1 + k_q \tau_0 [Q]$$

F_0	unquenched luminescence intensity
F	quenched luminescence intensity
K	Stern-Volmer quenching constant
$[Q]$	concentration of quencher
k_q	bimolecular quenching constant
τ_0	unquenched lifetime

Equation 2-7: The Stern-Volmer equation [47, 51]

Since dynamic quenching is a process that depopulates the excited state with an additional rate, the lifetimes in the absence (τ_0) and presence (τ) of the quencher may be written as in Equation 2-8. Division of τ_0 by τ again leads to the Stern-Volmer equation (Equation 4-1). The thus expressed equivalence of the decrease in fluorescence intensity *and* lifetime is an important characteristic of

dynamic quenching. Static quenching, in contrast, leads to a decrease of *intensity* but does *not* cause a decrease of the observable lifetime [47, 48 {p. 17}]. In this case, only from non-complexed fluorophore molecules luminescent excited states may be formed at all, which thereafter emit with an unperturbed decay rate τ_0.

$$\tau_0 = \frac{1}{\gamma}$$

(A)

$$\tau = \frac{1}{\gamma + k_q [Q]}$$

(B)

τ_0	unquenched lifetime
γ	decay rate in absence of quencher
τ	quenched lifetime
k_q	bimolecular quenching constant
[Q]	concentration of quencher

Equation 2-8: Lifetimes in the absence and presence of the quencher.

$$\frac{\tau_0}{\tau} = 1 + k_q \tau_0 [Q] = \frac{F_0}{F}$$

τ_0	unquenched lifetime
τ	quenched lifetime
k_q	bimolecular quenching constant
[Q]	concentration of quencher
F_0	unquenched luminescence intensity
F	quenched luminescence intensity

Equation 2-9: Equivalence of decrease in lifetime and decrease in intensity.

In Equation 2-7, the Stern-Volmer quenching constant *K* represents the sensitivity of the fluorophore towards the quencher. If the quenching is known to be dynamic, the Stern-Volmer constant is often represented by K_D, otherwise by K_{SV}. However, *K* is not only depending on the fluorophore-quencher pair but also on the environment in which the collisions occur. Fluorophores hidden in the bulk of a polymer are, for instance, hardly accessible to water-soluble quenchers and *K* is hence small. In solution, on the other hand, much larger values for *K* are obtained for the same fluorophore-quencher combination. Other molecules like oxygen are readily penetrating certain polymeric matrices, and large Stern-Volmer constants are attained even when the fluorophore is immobilised in the polymer bulk [47, 48]. Such behaviour is exploited with the oxygen sensors used for the construction of the oxygen transmission rate measuring device developed in this project (see section 1.6 and section 5.4.1).

A further important characteristic of dynamic quenching is the proportionality of the Stern-Volmer constant (thus, the extent to which the fraction F_0/F is affected by a change in the quencher concentration) and the unquenched lifetime τ_0, as it can be concluded from Equation 2-7. Since for dynamic quenching the fluorophore and quencher must come into intimate molecular contact, the efficiency of quenching rapidly vanishes with increasing distance between the two molecules. However, such direct encounters between two molecules occur seldom, compared to typical rates of fluorescent decay. If the unquenched lifetime increases, molecules in the excited state are given more time for a deactivating collision with a quencher. Consequently, the probability for radiation-less deactivation by quenching is increased. Thus, phosphorescent fluorophores with typical lifetimes

in the microsecond or even millisecond regime are particularly conceptive to collisional quenching, while it becomes negligible if the lifetimes are shorter than 5 ns. For sensing applications based on dynamic quenching, phosphorescent molecules are hence the fluorophores of choice [47, 48]. Due to the extended unquenched lifetime and the ubiquity of various quencher molecules (most of all, oxygen, even in traces), the quantum yields vanish and phosphorescent emission is usually not observed in fluid solution near room temperature [47 {p. 317}].

Quenching data are usually presented as a plot of F_0/F as a function of Q. In ideal cases, thus, if a single class of fluorophores which are all equally accessible to the quencher is present, the resulting Stern-Volmer plot is expected to be linear. If two fluorophore populations are present and one is (even only partially) inaccessible to the quencher, deviations from linearity in the form of a downward curvature are observed. If static quenching occurs simultaneously to dynamic quenching, the obtained Stern-Volmer-Plots show an upward curvature (in this context see section 4.3.1.3 and section 5.5.2) [47].

2.3 CHARACTERISATION OF LUMINESCENCE PROPERTIES

Please note that this section and subsections are essentially a condensed excerpt of [47] focusing on the most relevant aspects of the comprehensive textbook which represents a massive toolset in the field of opto-chemical sensing applications.

The experimental observation of luminescence properties is of importance for a number of scientific applications. In some cases, the luminescence mechanisms and properties of a fluorophore itself are subject to investigation. More often, however, luminescent substances are used as *sensors* for the indirect characterisation of completely different properties of a sample. Specific interactions of the sample of interest and the fluorescent behaviour of the observed fluorophore are exploited to reveal the information of interest. For example, fluorophores are used to measure the concentration of a wide field of analytes in any medium or to determine the location or movement of intracellular biologic molecules. Any other property, for which a correlation to the luminescence behaviour may be defined, is, in theory, also accessible via fluorescence spectroscopy.

The exploitable luminescence properties include excitation and emission spectra, lifetime, quantum yield, a change of the decay laws and, in fluorescence microscopy, the location of the fluorophore. Except for cases where the luminescent substance is exclusively used as a "marker" to visualize the location of the marked molecule, the impact of the chemical and physical environment of the fluorophore on the parameters of the observed luminescence is of central interest. The interactions may involve a more rapid depopulation of the excited state (quenching, see section 2.2.1.5.2) or the creation of an additional excited species (resonance energy transfer, see section 2.2.1.5.1), to name a few. In any case, the changes of the luminescence emission of the sample are reflected by changes of the two most important observables *luminescence intensity I* and *lifetime τ*. These properties are, in addition, highly correlated to each other (see Equation 2-10). It

depends on the method of determination, whether the result is obtained in terms of intensities or lifetimes.

The principles of the fluorimetric methods introduced in the following sections are mathematically discussed on the basis of the single exponential decay law, which is given in Equation 2-10. Thus, the decrease of the luminescent emission of a fluorophore in the excited state (e. g. after a short pulse of excitation light) is described as a function of time. The predicted behaviour is indeed found if a single fluorophore is present in the sample.

$$I(t) = I_0 \cdot e^{-t/\tau}$$

$I(t)$	luminescence intensity at time t
I_0	luminescence intensity at t=0
t	time
τ	luminescence lifetime

Equation 2-10: The luminescence intensity decay after a short excitation pulse as a function of time.

It must not be forgotten, however, that there are more complex mechanisms and decay laws such as the multi-exponential or non-exponential decays, for whose description the single exponential decay function forms an important building block. In general, the intensity of a multi-exponential decay is described as in Equation 2-11. The multi-exponential decay model is very powerful and can account for virtually any decay law. The parameters α_i and τ_i, thereby do not necessarily have a physical meaning. However, the sum $\Sigma\alpha_i$ is normalised to unity.

Strictly speaking, some of the mathematical relations for single decays (discussed in the following sections) cease to be valid in case of multi-exponential decays. Nevertheless, *apparent lifetimes* can always be formulated and measured, representing an average of the multiple, simultaneous decays. Care must be taken, however, in the interpretation of such apparent lifetime values, because they may be a complex function of the parameters describing the actual behaviour of the luminescence intensity. Furthermore, the measured apparent lifetimes are generally depending on the method of determination.

$$I(t) = \sum_i \alpha_i e^{-t/\tau_i}$$

$I(t)$	luminescence intensity at time t
α_i	preexponetial factor of component i
$\Sigma\alpha_i$	normalised to unity
t	time
τ_i	luminescence lifetime of component i

Equation 2-11: The intensity of a multi-exponential decay as a function of time.

In the presented project, the property of interest, namely the analyte concentration, is determined via the lifetime of a luminescent sensor dye. In the following, the according fluorimetric methods and their background, as relevant, are discussed. Generally, the experimental observation of luminescence is classified into *steady-state* measurements and *time-resolved* measurements.

2.3.1   Steady-State Fluorimetry

In steady-state measurements the fluorophore is irradiated with constant illumination. In this way, the intensity and the spectrum of the luminescent light can be observed. Because of the relative simplicity of the experimental setups, steady-state measurements are the more frequently encountered ones. The parameters typically detected include the absorption, excitation and emission spectra of the fluorophores or the intensity of the emission. Commonly, the versatile *spectrofluorometers* provide the technical infrastructure for steady-state measurements [47].

The results obtained in the experiments basically represent an *average* of the luminescence intensity decays which are observable in time-resolved measurements (see section 2.3.2). After a single, imaginary, short-pulsed excitation, the intensity decay is mathematically described as in Equation 2-10. The steady-state illumination can be thought as a very large number of subsequent "pulses", following each other after an infinitely short period of time. Each of these pulses generates its own imaginary exponential decay, and many of such "individual" decays occur simultaneously at different stages of advancement. The observed, averaged intensity of such an imaginary sequence of pulse decays is related to the lifetime τ, as it is expressed in Equation 2-12. Thereby, I_0 (representing the initial intensity in time-resolved measurements) represents a barely predictable parameter which is depending on a number of factors such as the type of fluorophore, its concentration and a several instrumental properties. However, the observed steady-state intensity is proportional to the luminescence lifetime τ.

$$I_{SS} = \int_0^\infty I_0 \cdot e^{-t/\tau} dt = I_0 \cdot \tau$$

I_{SS}	steady-state intensity
I_0	parameter depending on fluorophore, concentration, instrumental properties
t	time
τ	luminescence lifetime

Equation 2-12: The Luminescence intensity observed in steady-state measurements.

If multi-decay systems are investigated using steady-state experiments (see the decay law in Equation 2-11), each component in the combination of decays has a fractional contribution to the observed overall intensity, which is described by Equation 2-13.

$$f_i = \frac{\alpha_i \tau_i}{\sum_j \alpha_j \tau_j}$$

f_i	fractional contribution of component i
α_i	preexponetial factor of component i
τ_i	luminescence lifetime of component i

Equation 2-13: The fractional contribution to the steady-state intensity of a multi-exponential decay.

The most comprehensive information about a luminescent sample obtained in a steady-state experiment is expressed in terms of excitation and emission spectra. Generally, they are the result of the combination of multiple absorption and emission bands displayed by the fluorophore(s). The individual bands may have their origin in the same fluorophore, but they can also be emitted by completely different species present in the sample. The spectra may thus be also considered as an "average" result of the individual decay processes [47].

The most versatile instruments for the measurement of steady-state properties in general and excitation/ emission spectra in particular are spectrofluorometers, which are discussed in the following section.

2.3.1.1   Instrumentation for Steady-State Fluorimetry: Spectrofluorometers

The "working horse" instrument in research dealing with luminescence is the so-called *spectrofluorometer*. With most of these instruments, both excitation and emission spectra of fluorophores can be recorded. Emission spectra are the representation of the luminescence intensity as a function of the wavelength of the emitted light and are recorded using a single constant wavelength for the excitation. An excitation spectrum is, in analogy, the intensity plotted as a function of the excitation wavelength, measured at a single emission wavelength. In the spectra, the wavelength (units: *nm*) is often represented in terms of wavenumbers with units cm^{-1} [47].

Spectrofluorometers comprise a number of crucial components, each of which directly affects the quality of the recorded spectra. Therefore, the spectra acquired have to be interpreted with care and some knowledge about the functionality of the technical units is required to take full advantage of the instrument performance. It is noted that the majority of fluorimeters do not provide the true spectrum directly [48].

Generally, the main application field of spectrofluorometers is found in steady-state experiments, although more versatile instruments are available. In the presented project, spectrofluorometers were not employed, since an appropriate sensor dye/ instrumentation system for lifetime measurements was developed and proofed in earlier projects and the spectral characterisation of fluorophores was thus not in demand. The discussion of spectrofluorometers should consequently be restrained to a brief description of their setup and functional parts. However, many of the components are also vital for lifetime measurement setups.

Typical spectrofluorometers comprise a light source, followed by a monochromator for a selection of the excitation wavelength. The monochromatic light is passed through an (optional) polarisation filter and a beam splitter, before irradiating the sample cuvette. The second beam generated by the splitter is passed to another cuvette containing a reference sample ("blank"). Fluorescent light emitted from the cuvettes is collected by an according optical module, passed through (optional) polarisers, filters and a further monochromator for a selection of the emission wavelength, before it is detected by so-called photomultiplier tubes. In the following, these components are briefly discussed [47].

Light sources:

In an "idealised" spectrofluorometer, a light source delivering a constant photon output at all wavelengths is used for the excitation of the luminescence of the sample. The most versatile source to date are high-pressure xenon arc lamps, which provide a relatively continuous output from 250 nm to 700 nm but produce large amounts of infrared and heat. According filters are therefore required. Alternatively, pulsed xenon flash lamps are used. The continuum is emitted upon recombination of electrons with ionised xenon atoms. Besides xenon lamps, high-pressure mercury lamps, mercury-xenon lamps, and, for calibration purposes, low pressure mercury and mercury argon lamps are used. Quartz-tungsten-halogen lamps provide a continuous output also in the IR, but are not useful for the excitation of UV absorbing fluorophores.

Recently, LEDs and laser diodes are beginning to be used as light sources in spectrofluorometers. They are available for a wide range of wavelengths. A continuum is obtained by combination of several LEDs of different wavelengths in arrays, while laser diodes are chosen for their sharp single-wavelength emission in specific experiments. The advantage of LEDs and laser diodes over arc lamps is that they can be pulsed or modulated. Hence they are preferably employed in time-resolved measurements. In the presented project, an LED was chosen as the light source in the measuring setup.

Monochromators:

Monochromators are used to disperse polychromatic light into various wavelengths. An idealised monochromator must pass photons of all wavelengths with equal efficiency, and the dispersion must furthermore be independent of the polarisation of the light. The separation of wavelengths is accomplished using prisms or diffraction gratings, with the latter being encountered much more regularly. The light to be dispersed is passed through an entrance- and exit slit, whose widths are adjustable in most cases. The slit width determines the resolution of the dispersion. The narrower the slit, the higher the resolution, but at the cost of light intensity, which is a function of the square of the slit width. Important performance specifications of monochromators include dispersion, efficiency and stray light levels. Stray light refers to radiation passed through the monochromator besides the desired wavelength. One of the sources of stray light is found in imperfections of the diffraction gratings used. The use of double-grating monochromators drastically reduces stray-light levels, but also the overall efficiency. A regularly encountered problem in this context is the overlap of the second-order transmissions of the monochromator with the desired wavelengths. Bandpass filters preventing the second order diffraction wavelengths to enter or leave the monochromator are used in such cases.

Optical Filters:

Not only due to second-order diffraction effects an employment of optical filters in addition to monochromators is often necessary. When the spectral properties of a fluorophore are known, the use of filters without monochromators can lead to largely increased sensitivity. Filters employed include coloured glass filters, some of which are called long-pass filters because they transmit all wavelengths above a particular wavelength. Also band-pass and short-pass filters are known. Care must be taken in the employment of coloured glass filters because often they emit luminescent light themselves when irradiated at certain wavelengths. The names of filters classify them into groups which refer to the colour of the transmitted light (BG for "blue glass", GG for "green glass", RG for "red glass", etc.). In addition to coloured filters, neutral density filters ("grey filters") equally reduce the light intensity, regardless of the wavelength.

Although a wide variety of coloured glass filers is available, the absorption spectra do not display sharp cut-off edges. If a more precise separation of wavelengths is desired, so-called thin-film or interference filters, which may be customised for virtually any wavelength and application, are a good choice. Thus, long-pass, short-pass, band pass and notch filters are known. Even if these filters can be tailored for any application, such a custom design is not practical for every experiment. If a certain filter is not suitable for a given requirement, the combination of two or more filters can lead to the desired spectral properties. In the presented project, a combination of optical filters instead of a much more complicated monochromator was used to separate the emission bands from the excitation light.

Polarisers:

When the anisotropic behaviour of fluorescence shall be observed, polarisers form a vital component of the measuring setup. Polarisers are a sort of filters, which transmit light when the electrical vector of the radiation is aligned with their polarisation axis and block the transmission when the vector is rotated by 90°. In spectrofluorimetry, Glan-Thompson polarisers consisting of birefringent calcite prisms are typically used. The calcite crystals are cut at a certain angle so that one polarised component of the light beam undergoes total internal reflection at the interface, whereas the other one continues along its optical path. Alternatively, thin-film polarisers made of a stretched polymer are used. The stretched polymer transmits light only if the electrical vector is oriented in the polymer's direction of polarisation. Because light which is not in the plane of polarisation is absorbed (unlike in Glan-Thompson polarisers, where it is reflected), these polarisers are easily destroyed by laser beams.

Detectors:

In analogy to light sources and monochromators, an idealised detector employed in a spectrofluorometer must detect photons of all wavelengths with equal efficiency. In almost all devices, photomultiplier tubes (PMTs) are used as detectors for the luminescent light. In an electronic context, a PMT is best seen as a current source. Single photons can be counted in the form of current pulses, or an average of the pulses is measured as a current which is proportional to the light intensity. A PMT is an evacuated tube comprising a photocathode and a series of dynodes forming the so-called amplification stages. The cathode, which is held at a negative potential of typically 1000 - 2000 V, is a thin film of metal on the inside of the tube window. The dynodes are also held at a negative potential, but the voltages decrease towards zero along the cascade. Incident photons eject electrons from the metal surface of the cathode with the efficiency depending on the wavelength.[14] The electrons are accelerated by the applied potential difference towards the first dynode, and upon impact 5 - 20 additional electrons are ejected from the surface for each impinging electron. The additional electrons are again accelerated towards the next dynode and so forth. Thus, an electron avalanche, triggered by the incident photon, is eventually arriving at the anode and can be measured as a current. The PMT is therefore a low-noise photo-current amplifier, and the amplification is depending on the applied potential. Commonly, alloys of alkali metals are used as the cathode material.

In recent years, so-called charge-coupled devices (CCDs) with their remarkable sensitivity were increasingly used in fluorescence spectroscopy. They are encountered particularly in small and portable devices containing no moving parts. Imaging CCDs with several millions of pixels may be realised. Each pixel acts as a detector where a charge accumulates in proportion to the light exposure. The charges are read out by an according analogue/ digital circuit and processed into a spectrum. Because CCDs are capable of producing 2-dimensional images, they are used in fluorescence microscopy.

2.3.2 Time-Resolved Fluorimetry

Time-resolved measurements are carried out to record the intensity decay of the luminescence, and hence provide more direct clues about the kinetic properties of the emission. In the experiment, the fluorophore is exposed to a short pulse of light (with a pulse width preferably shorter than the luminescence lifetime). Following the instant excitation, the exponential decay function of the emission intensity is recorded. However, since the typical lifetimes of fluorescence are around 10^{-8} s or even shorter, a high-speed detection system is required to resolve the nanosecond-scale decay of the intensity [47, 48].

---

[14] The efficiency is wavelength-dependent because of the intrinsic absorption spectrum of the window, and, most of all, a non-constant quantum efficiency of the cathode materials.

Despite the necessary instrumentation complexity, time-resolved measurements offer valuable advantages over steady-state measurements. In the averaging process, much of the attainable information about the nature and environment of the fluorophore is lost. Time-resolved measurements are therefore superior to steady-state experiments when luminescence lifetimes and quantum yields shall be detected. As it was explained, the observed, averaged intensity is proportional to the lifetime and quantum yield. However, it is also proportional to I_0, which is the sum of a number of parameters, some of which may be difficult to control or keep constant. From the course of the exponential decay, the lifetime can be extracted regardless of the absolute value of I_0, and hence the mentioned parameters do not affect the result. Consequently, lifetime measurements are usually accomplished without much concern about the actual intensity.

Time-resolved fluorescence measurements are feasible in two different ways. They can be carried out in the *time-domain* or in the *frequency-domain* [47, 48].

2.3.2.1   Time-Domain Fluorimetry

In *time-domain* measurements, the luminescence intensity decay is recorded as a function of the time elapsed after a very short excitation pulse of light. The technique is therefore also referred to as *pulse fluorimetry*.

For a discussion of lifetime measurements, the physical "origin" and meaning of the lifetime τ shall be remembered. Imagine an infinitely sharp pulse of light exciting the fluorophore under investigation. The initial population n_0 of fluorophores in the excited state decays with a rate $\Gamma+k_{nr}$ as described by Equation 2-14 [47, 48].

$$\frac{dn(t)}{dt} = \left(\Gamma + k_{nr}\right) \cdot n(t)$$

$n(t)$	population at time t
t	time
Γ	rate of emissive depopulation
k_{nr}	rate of non-radiative depopulation

Equation 2-14

Emission and non-radiative relaxation are random events, and each excited fluorophore has the same probability of undergoing a transition to the ground state in a given period of time. Integration of the latter equation expectedly leads to an exponential decay function (Equation 2-15).

$$n(t) = n_0 \cdot e^{-t/\tau}$$

$n(t)$	population at time t
n_0	population at t=0
t	time
τ	luminescence lifetime

Equation 2-15

In a fluorescence experiment not the population the excited state but rather the intensity of the emitted light is observed. However, the two are proportional to each other, and hence Equation 2-15 can be rewritten in terms of the time-dependent intensity *I(t)*, leading to an expression as it was introduced in Equation 2-10.

Thereby the lifetime τ is the inverse of the sum of depopulation rates. It furthermore expresses the average amount of time the fluorophore remains in the excited state before the transition back to the ground state. Alternatively, τ may be interpreted as the time at which the intensity has decreased to *1/e* of the intensity at *t=0*. It can be determined from the slope of a logarithmic plot of the intensity as a function of time (*log I(t)* vs. *t*) [47, 48].

The above statements are only valid if a single fluorophore displaying an exponential decay according to Equation 2-10 is present in the sample. In more general cases involving multiple simultaneous decays (a behaviour shown by most samples), the logarithmic plot of the intensity versus time is no longer linear, and neither does the time required to reach $I=I_0/e$ refer to any of the decay times involved. The lifetimes are extracted from the recorded data by fitting procedures to assumed decay models [47, 48]. Mostly the method of nonlinear least squares is employed in the analysis [52, 53].

If multi-exponential decays shall be resolved, very good signal to noise-ratios are necessary in the data acquisition to permit reasonable confidence levels. The reason for this demand is found in the mathematically inherent difficulty in recovering the amplitudes and lifetimes for overlapping exponentials, as it was known to mathematicians prior to the actual employment of time-resolved fluorescence measurements. Thus, two exponential decays with apparently different parameters can result in very similar intensity values over wide portions of the observable measurement range of the equipment, and may therefore become even indistinguishable. The problem has its origin in the high degree of correlation between the values α_i and τ_i, something that generally implies unfortunate circumstances in the context of least square fitting [47, 48]. However, the problem is inevitable, and thus the method defined by Grinvald is still in use to date [54, 55].

The numeric compensation for malign light emission, commonly termed "*background correction*", is straightforward in time-domain measurements. Background luminescence is usually stemming from scattering effects, luminescent impurities in the sample or auto-fluorescence of any component in the optical path. For the correction, the background luminescence decay of a blank sample is recorded. The thus acquired decay function is thereafter simply subtracted from the measured decay functions of the actual samples [47].

2.3.2.2 *Instrumentation for Time-Domain Fluorimetry*

The first time-domain life-time measurements were sampling the intensity in the course of the decay by *gated detection*. Thus, the sample is repeatedly irradiated by a stroboscopic lamp. A certain period of time after each pulse, the emission intensity is instantly measured, taking into account only a very short time window. In the course of the measurement, the time between the light pulse and

the intensity measurement is varied from very short to long periods. In this way, the decay of the emission is scanned and subsequently plotted as a function of time.

Meanwhile most of the time domain measurements are performed by means of the so-called *time-correlated single photon counting (TCSPC)*, a method based on a somewhat unique principle. Excitation is commonly achieved using picosecond of femtosecond laser light sources, although pulsed LEDs and laser diodes are increasingly used. Coaxial flash lamps with light pulse widths of typically 2 ns are of rather historical importance in this context. In the measurement, the conditions are adjusted so that typically 100 or more laser pulses must be repeatedly applied until one photon is detected. The time between the pulse and the detection of the photon is determined and stored in a histogram. After a sufficient number of photon counts the histogram represents the decay of the emission intensity. The recorded "waveform" of the decay is then subject to the data analysis procedure [47, 48].

2.3.2.3   Frequency-Domain Fluorimetry

Please note that this section and subsections are essentially a condensed excerpt of comprehensive textbooks [47, 48], thereby focusing on the most relevant aspects.

Frequency-domain or *phase modulation* measurements, which are realised using comparably simple instrumentation in most cases, represent an often employed alternative to time-domain measurements. In according experiments, the sample is irradiated with intensity-modulated light.[15] The frequency is chosen so that the frequency *v* is comparable to the reciprocal of the lifetime τ, thus about 100 MHz in case of fluorescence (lifetime ~10^{-8} s). A sine wave is ideally chosen as the modulation function, but rectangular functions are also encountered.

When a fluorophore is excited in this manner, the emission of the luminescent light is responding at the same modulation frequency. However, the luminescent response does not precisely follow the course of the incident excitation modulation. The lifetime of the excited state causes the emission to be delayed in time relative to the excitation. The time-delay is manifested in a phase shift Φ (commonly measured at the apparent zero-crossings of the modulation function), which is a function of the lifetime τ and modulation frequency ω (see Fig. 2-5).

Because the lifetime τ of the luminescence expresses an *average* and a number of excited states are still able to emit when a time $t=\tau$ has elapsed after a modulation maximum of the excitation light, complete absence of luminescence is not observed when the excitation is at its minimum. Consequently, the modulation depth of the luminescent response is decreased relative to the modulation depth of the excitation by a factor m_ω, and the extent of this *demodulation* is again depending on the lifetime and the modulation frequency. Not quite accurately, m_ω is frequently called *modulation*. In common terminology, *phase shift* and *modulation* are subsumed in the concept of the *frequency response* of the sample.

---

[15] The *amplitude-modulated intensity* must not be confused with the oscillating electromagnetic component of a light wave!
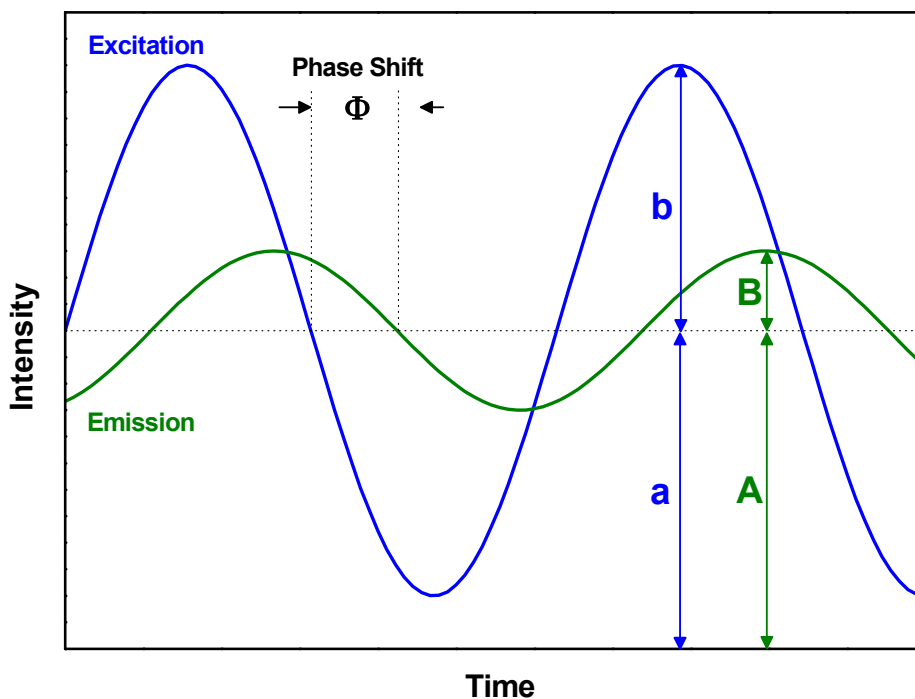
Fig. 2-5: Definition of phase angle and modulation of emission in frequency-domain measurements.

The frequency response is a function of the relative values of luminescence lifetime and modulation frequency of the excitation light source. The dependencies between phase angle Φ, modulation m_ω and modulation frequency ω are consequently used to recover the apparent lifetime τ. The according expressions are widely known and can be derived by several routes. The simplest approach is outlined in the following and utilises kinetic equations. In this context, the frequency is exclusively expressed in terms of the *circular modulation frequency ω* with unit *radians per second*. In usual scientific discussions, however, the units *cycles per second* (=Hertz) are used for the frequency, which is represented by the Greek letter *v* in this case. Thus, these units are converted according to *ω [Ra/s] = 2*π*v [Hz]*.

In a common frequency domain experiment, the incident excitation light is sinusoidally modulated and hence the intensity *L(t)* and depth of modulation m_L of the incident light are given by Equation 2-16.

$$L(t) = a + b \cdot \sin \omega t$$

L(t)	intensity of excitation at time t
a, b	parameters according to Fig. 2-5
ω	modulation frequency in radians/s
t	time
m_L	modulation of incident light

$$m_L = \frac{b}{a}$$

Equation 2-16

The fluorescence emission is forced to respond with the same frequency, but the phase of the oscillating intensity will be different, as will also the depth of modulation. For a description of the modulated emission, initially the population of the excited state *N(t)* is considered (Equation 2-17).

$$N(t) = A + B \sin(\omega t - \Phi)$$

N(t)	population of excited state at time t
A, B	parameters according to Fig. 2-5
ω	modulation frequency in radians/s
t	time
Φ	phase shift angle

Equation 2-17

The intensity of emission *I(t)* is at any time proportional to the number of fluorophores in the excited state *N(t)*. After an infinitely short pulse of excitation light, the intensity decreases according to Equation 2-18, given that the fluorophore is displaying a single exponential decay.

$$I(t) = I_0 \cdot e^{-t/\tau}$$

I(t)	luminescence intensity at time t
I_0	luminescence intensity at t=0
t	time
τ	luminescence lifetime

Equation 2-18

The time-dependent population of the excited state is, in case of a sinusoidal modulation, described in terms of a differential equation (Equation 2-19).

$$\frac{dI(t)}{dt} = -\frac{1}{\tau} I(t) + L(t)$$

I(t)	luminescence intensity at time t
t	time
τ	luminescence lifetime
L(t)	intensity of excitation at time t

Equation 2-19

Substitution of Equation 2-16 and Equation 2-17 into Equation 2-19 leads to the expression in Equation 2-20, which must be valid at all times. The relationship between the luminescence lifetime *τ* and the parameters *a, b, A* and *B* is found by expanding the trigonometric functions and equating the constant terms and terms in *sin (ωt)* and *cos (ωt)*. Thus, the expressions as in Equation 2-21 A - C are obtained.

$$\omega B \cdot \cos(\omega t - \Phi) = -\frac{1}{\tau} \cdot [A + B \cdot \sin(\omega t - \Phi)] + a + b \cdot \sin \omega t$$

ω	modulation frequency in radians/s
t	time
a, b, A, B	parameters according to Fig. 2-5
τ	luminescence lifetime
Φ	phase shift angle

Equation 2-20

$$\omega \cdot \cos \Phi - \left(\frac{1}{\tau}\right) \cdot \sin \Phi = 0$$

(A)

$$a - \left(\frac{1}{\tau}\right) \cdot A = 0$$

(B)

ω	modulation frequency in radians/s
a, b, A, B	parameters according to Fig. 2-5
τ	luminescence lifetime
Φ	phase shift angle

$$\omega \cdot \sin \Phi + \left(\frac{1}{\tau}\right) \cdot \cos \Phi = \frac{b}{B}$$

(C)

Equation 2-21

From Equation 2-21 (A) the familiar expression relating the phase shift Φ to an apparent lifetime τ_Φ is derived (Equation 2-22).

$$\frac{\sin \Phi}{\cos \Phi} = \tan \Phi = \omega \cdot \tau_\Phi$$

Φ	phase shift angle
ω	modulation frequency in radians/s
τ_Φ	apparent luminescence lifetime according to Φ

$$\tau_\Phi = \omega^{-1} \cdot \tan \Phi$$

Equation 2-22: Relation between apparent lifetime, modulation frequency and phase shift angle.

The modulation depth of the excitation m_L is given by the fraction b/a, (Equation 2-16) where a represents the average intensity and b is the difference between the maximum and average intensity of the modulated incident light. Likewise, the modulation depth of the emitted light is defined as the fraction B/A (the meaning of the parameters is illustrated in Fig. 2-5). From the two fractions, the demodulation factor m_ω (which is the modulation depth of the emission relative to the modulation depth of the excitation) is obtained according to Equation 2-24.

Calculation of the square of Equation 2-21 (B) and (C) and subsequent addition yields the expression in Equation 2-23. Remodelling of Equation 2-21 (B) furthermore reveals that $A = a\tau$. Consequently, a relationship between the demodulation factor m_ω (Equation 2-24) and an apparent lifetime τ_m is derived as in Equation 2-25.

$$\left[\omega^2 + \left(\frac{1}{\tau}\right)^2\right] = \left(\frac{b}{B}\right)^2$$

ω	modulation frequency in radians/s
b, B	parameters according to Fig. 2-5
τ	luminescence lifetime

Equation 2-23

$$m_\omega = \frac{B/A}{b/a}$$

m_ω	demodulation factor or "modulation"
B	modulation depth of emission
A	average intensity of emission
b	modulation depth of excitation light
a	average intensity of excitation light

Equation 2-24: Definition of the demodulation factor or "modulation".

$$m_\omega = \frac{1}{\sqrt{1 + \omega^2 \tau_m^2}}$$

$$\tau_m = \frac{1}{\omega} \cdot \sqrt{\frac{1}{m_\omega^2} - 1}$$

m_ω	demodulation factor or "modulation"
ω	modulation frequency in radians/s
τ_m	luminescence lifetime according to m_ω

Equation 2-25: Relation between lifetime, modulation frequency and demodulation factor.

As mentioned before, the decay of the luminescence may obey a law more complex than a simple exponential decay, a behaviour that is always observed with samples containing more than one fluorophore. Even single fluorophores may exhibit complex decays for countless possible reasons. Nevertheless, an apparent decay time can always be defined, irrespective of the complexity of the mechanism. Only in case of a single exponential decay, the measured lifetime corresponds to the time it takes for the intensity to decrease to *1/e* of the initial value and thus expresses the "real" lifetime. If multiple decay functions are overlapping, the *1/e* time is typically not equal to any of the contributing decay times [47, 48].

By measurements of such multi-exponential decays in the frequency domain, an *apparent* lifetime τ_Φ is calculated from the phase angle Φ_ω. From the determined depth of modulation, an apparent lifetime τ_m is obtained, which is, in such cases, not necessarily equal to τ_Φ. In fact, the apparent lifetimes depend on the method of determination. Each of these lifetimes represents a differently weighted average of the occurring decay processes. They are characteristic of the sample, but do not provide a detailed description of the intensity decay. Only a precise measurement of apparent decay times at a number of different modulation frequencies and according data processing allow the extraction of the individual lifetime contributions. However, it is often difficult to resolve the sum of

the individual exponentials, because the parameters are highly correlated. Very good signal-to-noise ratios are required in the measurements to recover the decay times with satisfactory confidence. Commonly, the recorded data are analysed by means of the nonlinear least squares fitting method [47 {p. 161}, 48 {p. 57}, 52, 53].

The frequency response of luminescent samples displays some important characteristics, which must be kept in mind when choosing the modulation frequency or a range of modulation frequencies for a given experiment.

Imagine an experiment, in which a fluorophore with a given decay time τ is irradiated with light which is modulated at a comparably low frequency. Since the peak-to-peak time of the excitation is much longer than the decay time τ of the fluorophore, the phase shift Φ of the luminescent response is virtually zero. The depth of modulation, on the other hand, is almost equal to the modulation depth of the excitation. Now the frequency of modulation is continuously increased. Initially, the phase angle hardly changes, and also the depth of modulation stays virtually not constant. However, when the peak-to-peak time of the modulation is approaching the magnitude of τ, the measured phase shift starts to increase more rapidly. When the reciprocal of the frequency is shorter than the lifetime, the phase shift asymptotically approaches a value of 90°. At the same time, the modulation decreases from 1 for very low frequencies to 0 for very high frequencies, with the most rapid change when the peak-to-peak time of the excitation is in the order of the lifetime. The "annihilation" of the modulation is due to the rapid "refilling" of the excited states at high frequencies. In such cases, the depopulation is not given time anymore to significantly reduce the emission intensity, before the next light pulse restores the initial population of the excited state. The phenomenon is similar in nature to the infinitesimal dense sequence of pulses used to explain a steady state illumination experiment (see section 2.3.1).

The 90° phase angle limit does not appear intuitive at a first glance (as one would assume a limit of 180°). However, for the mono- or multi-exponential decay functions of fluorophores it is also a theoretical limit, which is most easily accepted as a consequence of the tangent function in Equation 2-22. In the limit of 90°, the tangent becomes infinite. A phase angle of 90° is therefore only measured in case of an infinitely long lifetime τ or an infinitely high frequency ω [47].

In contrast to time-domain measurements, the numeric compensation of interfering background luminescence is somewhat complex in the frequency domain and furthermore degrades the resolution of the results. Therefore, frequency-domain measurements are preferably performed under conditions avoiding background luminescence to the best possible extent. For the correction, the phase angle $\Phi_{\omega B}$, modulation $m_{\omega B}$ and the average, steady-state intensity of the background are measured at each light modulation frequency employed for the actual sample characterisation. However, the recorded values cannot simply be subtracted from the frequency response of the sample. Instead, a more elaborate treatment involving vector analysis and trigonometric functions must be performed, which particularly complicates the description of error propagation into the corrected frequency response data. According procedures are found in literature [47 {p. 170}].

2.3.2.4   Instrumentation for Frequency-Domain Fluorimetry

The evaluation of phase delays for the measurement of short time intervals such as the decay of fluorescent processes has a history of about 100 years. In fact, the first lifetime measurements to be carried out in 1926 were performed on a phase fluorimeter [47 {p. 163}]. Many designs for according devices were suggested since then. The first generally useful device was presented in 1969 and comprised an ultrasonic modulator to obtain intensity-modulated light from an arc lamp source. In this technique, a periodic density gradient effectuated by ultrasonic sound waves is periodically diffracting the excitation light beam. However, an effective modulation is usually restricted to discrete resonance frequencies. Ultrasonic modulators were later on replaced by electro-optic units, which involve materials that rotate polarised light when exposed to an electrical field. Nowadays, pulsed LEDs and laser diodes became the preferred excitation source, since they can be modulated directly by the electrical input. While LEDs are employed up to frequencies of several hundred MHz, laser diodes can be modulated up to several GHz. A wide range of excitation wavelengths (meanwhile also in the UV) is available particularly for LEDs. Furthermore, LEDs are very cost-effective [47, 48].

With the short decay times of fluorescent processes in mind, the measurement of the phase angle and demodulation appears difficult, even more because accuracies of 0.2° in phase and 0.5 % in demodulation are required to resolve complex decays. In addition, these specifications have to be fulfilled over a wide range of modulation frequencies (typically 1 MHz to 200 MHz). However, the measurements are strikingly easy and furthermore free of interference due to a technique called *cross-correlation detection*. In this method the gain of the detector is modulated at a frequency $(F+\delta F)$ different by typically 10 to 100 Hz $(=\delta F)$ from the modulation frequency of the light source (F). The resulting interference leads to a low frequency signal with a frequency δF that carries the same phase and modulation information as the high frequency signal. Over the entire range of modulation frequencies, the phase and modulation are measured at the same *cross-correlation* or *difference frequency δF*. The low frequency oscillation is easily characterised by analogue or digital methods (e. g. Fast Fourier Transform). Furthermore, cross-correlation is surprisingly robust. In the process, harmonics and other common sources of noise are effectively suppressed. Therefore, neither the light modulation nor the gain modulation need to be a pure sine wave, and even a laser pulse train can be used as the excitation source. Because no concern about the shape of the modulation waveform is in demand, such frequency domain measurements are easily set up and used [47, 48].

The cross-correlation requires two frequencies up to 200 MHz with a resolution of less than 1 Hz that are synchronised but different by a small frequency offset δF. However, modern electronics readily cope with this task. Furthermore, the detectors typically used in TCSPC techniques are also useful in frequency domain measurements [47].

In a typical setup, two detectors (traditionally PMTs) are used. One of the two acts as the timing reference and observes reflected or scattered light or the emission of a reference, short-lifetime standard fluorophore. The second detector is alternately exposed to light emitted by the sample and light stemming from a so-called scatterer. Sample and scatterer are mounted in a rotating bracket. In

the measurement, the phase shifts of the two are measured relative to the reference detector and arbitrary phase angles Φ_1 and Φ_2 are obtained. However, the difference between Φ_1 and Φ_2 reveals the result of interest, the phase angle Φ_ω. The indirect route via the reference detector is necessary due to inevitable time delays in cables and electronic circuits [47, 48].

2.4 ANALYTE SENSING BY FLUOROPHORES

During the past decades, a number of analytical methods based on high-sensitivity fluorescence detection have been introduced. These include, besides the detection of "simple" analytes like oxygen or carbon dioxide, DNA fragment analysis and sequencing, immunoassays and others. Various mechanisms affecting the fluorescent behaviour enable analyte sensing [46, 50, 56]. Any phenomenon that results in a change of fluorescence intensity, lifetime, wavelength, or anisotropy may be utilised and the according change in the property evaluated accordingly [47].

Most commonly, resonance energy transfer processes (RET) are involved in the sensing strategies and thus represent the most general and versatile approach. Anything that brings the donor and acceptor into close proximity will result in a decrease of the luminescence intensity and lifetime. As it was mentioned, RET acts over wider distances as collisional quenching and is therefore particularly interesting in protein analysis. Common analytes detected via a RET mechanism include CO_2, cations, anions, pH and even glucose [47 {p. 633}].

Alternatively, the evaluation of fluorescence properties reveals analyte concentrations if the fluorophore exists in two states and the fraction of the states is analyte-dependent. Typically, the mechanism involves equilibria of the fluorophore free in solution and bound to the analyte. One of the two species may be completely non-fluorescent, or the two species may display different quantum yields or emission spectra. Such sensors are commonly used for the construction of pH probes, but also cations such as calcium may specifically be bound to special fluorophores. Sensors that bind specific analytes are often referred to as *probes of analyte recognition* [47 {p. 627}]. More sophisticated strategies measure a shift in the spectral properties as a function of the analyte concentration by means of wavelength-ratiometric probes. The technique is employed when the concentration of the fluorophore cannot be controlled (e. g. in intracellular plasma or due to severe photo-bleaching). Thus, the relative intensities of the fluorophore emissions in the absence and presence of the analyte are evaluated [47].

Mechanistically, the perhaps simplest of all depopulation processes is collisional quenching, but at the same time it is the most important one when thinking about oxygen detection. Almost any fluorophore is collisionally quenched by molecular oxygen, although only few are suitable for detection of oxygen traces. Other, less important collisional quenchers are chlorides, bromine and iodine atoms, sulphur dioxide, nitrous oxide, chlorinated hydrocarbons, and more specifically, halogenated anaesthetics [47 {p. 632}].

However, for collisional quenching the fluorophore and quencher must come into molecular contact. The effect of quenching rapidly vanishes (much more rapid than in case of RET) as the distance between the two molecules increases. Now, such encounters do, on a "fluorescent" timescale, not occur too often. It was found that the extent of quenching is proportional to the unquenched lifetime τ_0 of the fluorophore. The longer the lifetime, the longer the average time given to the excited state for a deactivating encounter with a quencher molecule, and hence the higher the probability for each excited state molecule for such an encounter. Therefore, particularly phosphorescent fluorophores with typical lifetimes in the microsecond regime are strongly sensitive, while collisional quenching becomes effectively negligible if the lifetime is shorter than 5 ns.

An ideal sensor shall not only be sensitive to the analyte, it shall also be selective. Selectivity is improved by maximisation of the probe response towards the analyte relative to the response towards other species present in the sample. In this context, an extension of the luminescent lifetime over-proportionally increases the sensitivity towards collisional quenching and hence supports selectivity. Besides the strong dependency on the luminescence lifetime, a number of additional aspects can improve the selectivity towards collisional quenchers. Thus, a number of analyte-quencher pairs (e. g. benzo(b)fluoranthene/ sulphur dioxide or carbazole/ chlorinated hydrocarbons) show a quite specific quenching behaviour while other quenchers have a minor effect. Large potential for tuning and optimisation lies also in the selection of a suitable matrix material immobilising the fluorophore. A matrix in which the quencher is able to move relatively freely while interfering molecules are prevented from penetration thus increases the selectivity. Finally, quite often the analyte shall be detected in media devoid of other interfering quenchers. This is commonly the case when oxygen shall be detected. Even if nitrous oxide (NO) is also a strong collisional quencher, it is not commonly present in the sample media (e. g. air) [47].

2.4.1 Fluorophores as Oxygen Sensors

As already mentioned various times, the most typical dynamic quencher is molecular oxygen, which is able to deactivate almost any excited state fluorophore. There is an ongoing debate about the exact mechanism responsible for quenching by oxygen. While it is commonly attributed to intersystem crossing of the fluorophore into an excited triplet state, in a number of reports mixed mechanisms involving intersystem crossing, charge transfer and electron exchange were suggested to account for the pronounced dynamic quenching behaviour [47 {p. 334}].

Although virtually all fluorophores are quenched, the sensitivity towards oxygen widely varies, depending on the fluorophore. If oxygen is the analyte in a sensing application, a suitable fluorophore is most likely found in the field of *transition metal complexes* (or *metal-ligand complexes*, MLCs). Such complexes usually have a long, phosphorescent lifetime in the microsecond regime. Many MLCs are easily embedded in a silicone matrix, a polymer with an extraordinary oxygen solubility and diffusivity. Hence, the phosphorescence of the sensor fluorophore is readily quenched by molecular oxygen present in the medium. Other fluorophores, which are not soluble in silicones, are frequently embedded in matrices of polystyrene. Although PS is much less permeable

to oxygen, some very sensitive fluorophores are out-weighting the loss of sensitivity attributed to the matrix material [47].

Since Kautsky reported the quenching of phosphorescence by small quantities of oxygen already in the 1930s, a large number of sensor dyes has been employed in the detection of oxygen [57]. The most widely used fluorophore used in oxygen sensors is probably $[Ru(Ph_2phen)_3]^{2+}$ (unquenched lifetime ~5 µs), although countless other long-lived MLCs are of large interest and, depending on the field of application, they are often superior. If oxygen must be detected in blood or through the skin, a fluorophore excited with red or near infrared light is most useful. A typical example is thereby platinum-(II)-octaethylporphyrin ketone (PtOEPK) with an unquenched lifetime as long as 61.4 µs. Other well-known sensors include platinum(II)- and palladium(II)-5,10,15,20-tetrakis-(2,3,4,5,6-pentafluorphenyl)-porphyrin (PtTFPP and PdTFPP, also see section 4.3.1.2) [47 {p. 629}].

A wide but selected variety of MLCs has been screened with respect to their applicability in oxygen trace analysis in a previous doctoral thesis [57]. Thus, properties like absorption and emission spectra, quantum yields, lifetimes, oxygen sensitivity, calibration characteristics, temperature-dependence, photo-bleaching behaviour and storage stability were investigated for the dyes immobilised in a polystyrene matrix. In addition, the mentioned properties were, in some cases, also investigated in a fluoropolymer (TeflonAF® 1600, see section 5.4.1).

The acquired information was, in later activities, used by Joanneum Research in the development of an OEM-scale oxygen trace detection system, which is a vital component in the presented OTR measurement method (see section 4.3.1).

Meanwhile, a number of ultra-sensitive fluorophores and matrix-fluorophore combinations for the detection of oxygen have been reported [46, 50, 58].

3 BARRIER TESTING METHODS

3.1 INTRODUCTION

First recorded experiments investigating the transport behaviour of gases in membranes, employing a permeation-rate measuring device [21 {p. 19}], were performed in 1829 by Thomas Graham. However, the diffusion of gases in membranes received little practical interest for about another century. With the emergence of industrialised foodstuff preparation and the advancement of membrane-based processes such as reverse osmosis or gas separation the demand for proper barrier testing of materials arouse, and thus a number of suppliers developed according instruments compliant with defined measuring standards [21, 22 {p. 272}]. The provided research tools served virtually all needs for decades.

However, as it is pointed out in numerous sections of this work, the commercial analytical instruments have limits of detection which are not sufficient for a quantification of the ultra-barriers meanwhile required for organo-electronics encapsulation, and alternative, more sensitive techniques are yet not very suitable for large-scale routine measurements.

This section addresses the principle of barrier testing setups in general and provides an overview of the available commercial instruments and well-established laboratory methods.

3.2 FUNDAMENTAL FUNCTIONAL PRINCIPLES

In this section, the general approach, as it is common to all imaginable methods for testing barrier properties, is discussed from a fundamental point of view. The physical principles concerned are, like in so many other cases, very straightforward and easily understood. However, it is the details which often emerge as the real challenge in the realization of a "high-resolution" barrier testing apparatus. As far as the characterisation of ultra-barriers is concerned, no-one has tolerably overcome these challenges thus far.

In analogy to every process taking place spontaneously, the driving force for permeation is the result of different chemical potentials at the opposite surfaces of the sample membrane, which forms the boundary between two different environments. The gradient in the chemical potential is, in this case, solely the result of a concentration gradient (or, more precisely, a partial pressure gradient) of the chemical species whose diffusive migration shall be tested (see also Fig. 3-1). Since permeation does not involve chemical reactions, the equilibrium in chemical potential can be achieved by diffusive migration of matter only.

The rate of equilibration (and thus the rate of diffusion of matter) is not only a function of the concentration gradient but also of the "resistance" or "drag" exerted by the membrane to be "perfused" (equivalent with the quality of the barrier). High resistance implicates low permeation

rates and vice versa. Actually, it is just this resistance which constitutes the magnitude of interest in permeation testing.
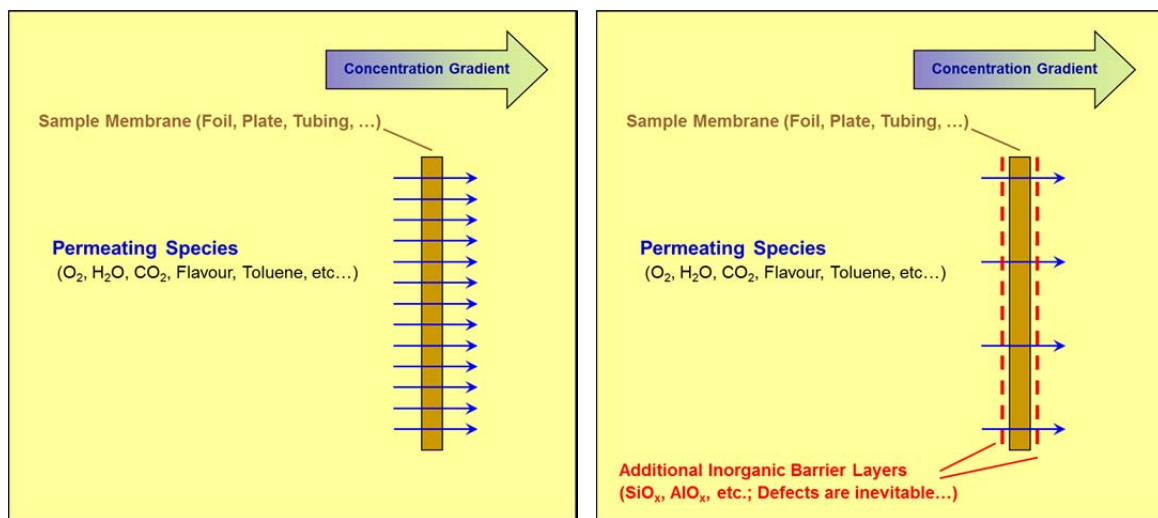
Fig. 3-1:   The driving force and antagonism for diffusive migration of matter through a membrane. Left: low barrier, resulting in high permeation rate. Right: high barrier, resulting in low permeation rate.

If the rate of permeation is to be measured, the sample is exposed to a defined, well-controlled concentration gradient. For this purpose, the membrane separates, in general, two differently conditioned cavities of a test apparatus. Most frequently, the permeating species is completely absent in one of the cavities at the beginning of the experiment, while the concentration is rather high in the remaining cavity, thus exerting a distinct gradient across the sample. In special but not even rare cases, one of the cavities may be represented by the surrounding air.

In at least one of the cavities, the *change in the amount* of the permeating species is monitored during the experiment by appropriate means and as a function of time. The observed change can either be positive (by permeation, matter is added to the monitored environment) or negative (by permeation, matter is removed), with the former being the prevailing mode of implementation.

For the detection of the amount of the chemical species of interest, every imaginable physical or chemical concept may be utilized, effectively. However, specificity of the measurement and the preclusion of cross-sensitivities are an issue in most cases, and consequently, the sensing principle or the conduct of the experiment (or a specific combination of the two) is selected as to comply with the requirements.

The physically perhaps most straightforward approaches include volumetric, barometric and gravimetric measurements of the permeation rate (see Fig. 3-2). With the goal of providing a fundamental understanding only, any further explanations in the context of the working principles are most likely obsolete.
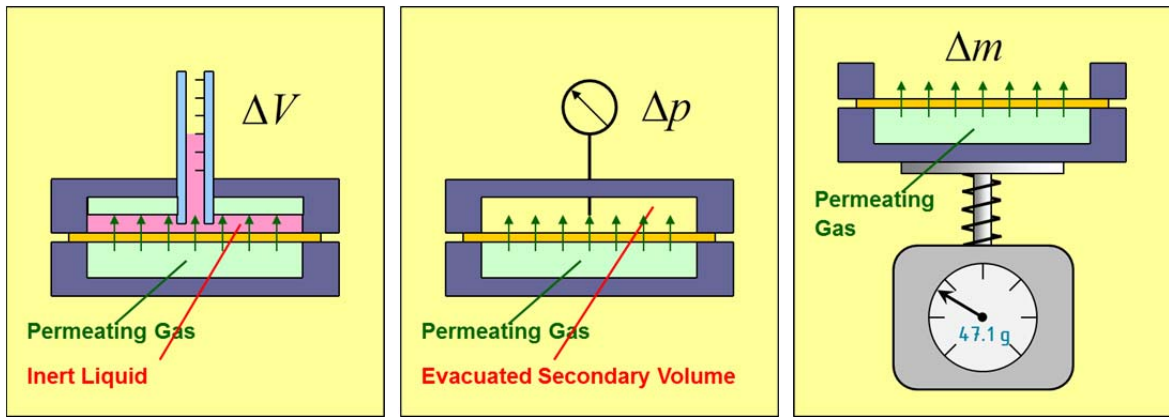
Fig. 3-2: The straightforward working principle of volumetric (left), manometric (centre) and gravimetric (right) permeation rate measurements.

Despite the seductive simplicity of the volumetric, manometric and gravimetric techniques, the employment of analyte-specific sensors in appropriately designed permeation setups is, in general, favoured, at least as far as commercial setups are considered. Not only specificity but also performance benchmarks such as the limit of detection are most often superior using tailored sensors. The respective schematic is indicated in Fig. 3-3.
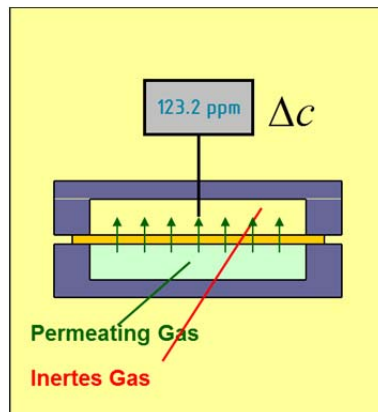
Fig. 3-3: The working principle of permeation measurements using a specific sensor.

Regarding the measurement variable (thus, the amount of permeating analyte detected) in the time domain (that is, with respect to the time-dependence of the detected parameter), all mentioned and imaginable methods for permeation measurement follow one out of two distinct chemical-physical modes of functionality.

In one mode, the secondary volume of the permeation apparatus represents an isolated system (see Fig. 3-2 and Fig. 3-3), as far as permeation through the membrane itself is ignored.[16] After the

---

[16] The secondary volume is, however, "initialized" to defined conditions at the beginning of the experiment by a purge flow of an inert gas. During the initialization, the secondary volume is therefore an open system.

initialization of the experiment, the permeating matter is *accumulating* in the volume at the secondary side of the membrane and the entire apparatus is never reaching a truly stationary state. It is, instead, aspiring after an equilibrium which is asymptotically approached, while the measurement parameter (volume, pressure, etc.) is *changing* as a function of time. In the process, the concentration gradient, representing the driving force for the diffusion of matter, is gradually declining and thus the rate of permeation is also to decrease. However, the equilibrium is very "distant" in most cases, and on a relevant time-scale, the system may be considered as pseudo-stationary. The rate of change of the measurement parameter *P, dP/dt,* can thus be considered constant over time in most cases. The permeation rate is calculated from the rate of change *dP/dt* which, mathematically, represents the first derivative of the measurement parameter. In general, volumetric, manometric and gravimetric techniques follow this scheme, and also setups based on sensors which are capable of non-destructive detection can be operated in this way. In ASTM E398 [59] the approach is referred to as "Dynamic Relative Measurement". As late as in 2015, ASTM 3136-15 covering opto-chemical oxygen detection in permeation setups was introduced. In the standard, the concept of analyte accumulation is referred to as "Dynamic Accumulation Method" [60].

In contrast to the "isolated system"-mode just discussed (or "dynamic accumulation method", respectively), the apparatus can be kept in a truly stationary state by permanent conditioning of the relevant environments (explicitly including the secondary volume) by a permanent purge flow of the respective operating gasses (see also Fig. 3-4). However, any matter migrating into the secondary volume is thus instantly and permanently removed by the purge flow. Before being discarded, the stream of the inert gas purging the secondary volume is passed to the detector, where a certain concentration level of the permeating species is detected. The level is depending on the permeation rate as well as the purge flow rate and possible impurities in the gas feed. It appears obvious that operational parameters such as the purge flow rate or, even more, the purity of the purge gas must be controlled more strictly. In the stationary state, the sensor signal does not change as a function of time. Instead, the recorded level is proportional to the rate of permeation [61], and no derivative needs to be computed. This "stationary state"-mode or "steady-state-method" [62] of operation is followed by the most recognized commercial OTR measuring instruments [12, 63, 64]. Noteworthy, when using a coulometric sensor, the mentioned requirements with respect to a very constant flow rate (but not the purity of the carrier gas) are modest [65].

3.3   STANDARDIZED BARRIER TEST METHODS

For the experimental determination of gases through polymeric materials, a number of ASTM[17], ISO[18] and DIN[19] standard procedures were defined. Common to almost all these standard definitions

---

[17] ASTM: *American Society for Testing and Materials.*
[18] ISO: *International Organization for Standardization.*
[19] DIN: *Deutsches Institut für Normung*

is a specified measuring range, within which they are valid (and outside which they are not, in consequence). And apparently, the demand for testing ultra-barriers has not made it into the rulebooks so far, since the defined ranges do not fully or not at all cover the relevant permeation rates.

For the manufacturers of according equipment, the compliance with one or more of these specifications is, in economic terms, anyhow essential, since the majority of the sold instruments are commonly applied in quality assurance rather than fundamental research, where traceability and absolute comparability are not so much an issue. Consequently, the principles and technologies implemented in the standard methods are rather conservative, from a researcher's point of view.

3.3.1 Standards Based on Straightforward Physical Relationships

There are a number of methods covered by ASTM and similar standards for the determination of gas permeation rates which follow very neat physical approaches but are not commonly encountered in commercial instruments.

In the ASTM D1434, for instance, the amount of permeant gas is recorded as a function of time either via the displaced volume of a liquid (volumetric method) or the increase of absolute pressure in a cavity evacuated prior to the measurement (manometric method) [66]. A manometric method is also defined in ISO 15105-1. Interestingly, a second procedure described in ISO 15105-1 uses a gas chromatograph as the detector, into which the amount of permeant gas accumulated over a certain period of time is flash-purged by a carrier gas.

Analogous standards for a number of gases are defined in DIN 53380-1 (volumetric, 23 °C, atmospheric pressure, range 3 - 20000 [cm^3 m^{-2} day^{-1} atm^{-1}]) [67], DIN 53380-2 (manometric, 10 - 40 °C, pressure not defined, range 0.5 - 20000 [cm^3 m^{-2} day^{-1} atm^{-1}]) [68], DIN 53380-3 (O_2 only, carrier gas method, external detector, temperature and pressure not defined, range 0.05 – 1000 [cm^3 m^{-2} day^{-1} atm^{-1}]) [69] and DIN 53380-4 (CO_2 only, detection of IR absorption, temperature and pressure not defined, range 0.05-5000 [cm^3 m^{-2} day^{-1} atm^{-1}]) [70].

Experimental laboratory setups measuring all imaginable sorts of permeating gases often rely solely on such physically simple and hence robust relationships or use them as a starting point and/ or backup reference for further development. Despite their physical simplicity, they may often prove inappropriate for the quantification of small permeation rates, not to think about the characterization of ultra-barriers.

3.3.2 Commercially Established Standard Methods

In case of oxygen being the permeant, the standard methods described in ASTM D3985 (at zero humidity) [71] and ASTM F-1927 (defined temperature and relative humidity) [72] are perhaps most often referred to by suppliers of permeability testing instruments and reference laboratories [1, 12,

73]. In both standards, the use of a carrier gas purging the permeant oxygen into a coulometric oxygen sensor is obligatory. Where applicable, humidification shall comply with ASTM E104 [74]. The listed standards are comparable to ISO 15105-2 and DIN 53380-3 [75-77].

In commercial instruments compliant with said standards, the sample membrane forms the boundary between two cavities of the test chamber (see Fig. 3-4). One of the cavities is purged by oxygen gas (which, depending on the standard, is conditioned to a defined relative humidity). The oxygen permeating through the sample into the second cavity is transported continuously into the detector by the flow of an inert gas (highly pure argon or nitrogen, humidified where applicable), where it produces an electrical current which is proportional to the amount of oxygen flowing into the detector per unit time [72].

Electrochemically, the measurements are *absolute*, because each oxygen molecule arriving at the detector generates a discrete electrical charge according to the faraday principle. Consequently, there is no need for calibration, which is possibly the driving force for the acceptance of coulometric detection as perhaps *the* standard method. However, the *oxygen is consumed* in the process of detection. Therefore, there is *no accumulation* of the analyte as a function of time and in addition, the permeating oxygen is diluted by the carrier gas to a certain extent. The "destructive" mode of detection presumably hampers the discrimination between oxygen stemming from permeation through the sample and oxygen intruding via "parasitic" processes such as apparatus leakage. In any case, there are strict requirements with respect to trace oxygen impurities in the carrier and therefore, O_2-absorbing catalyst beds are used in the gas feed [72]. From a mechanical point of view, the dimensions of such sensor units would not permit their direct integration into the permeation cavity of according instruments.

The sensors used reach impressive limits of detection in the ppb-regime. Despite the high performance of the sensor itself, the limit of detection of the overall method is limited to about $5*10^{-3}$ [cm^3 m^{-2} day^{-1} atm^{-1}] even for the best instruments available today. The defined standards provide for a measurement range of $0.05 - 1000$ [cm^3 m^{-2} day^{-1} atm^{-1}] only [69, 71, 72, 76].
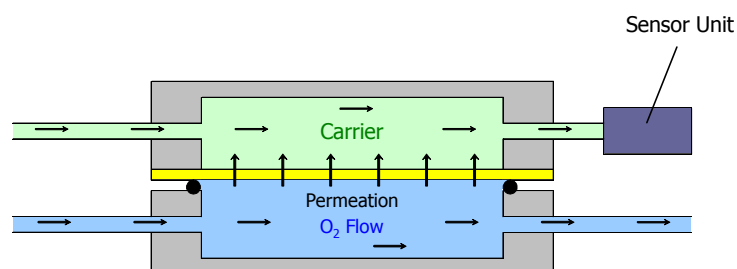
Fig. 3-4:   Working Principle of Commercially Available Instruments for OTR Measurements.

For some years now, a more broadly defined procedure is described in ASTM F2622-08, where no particular oxygen sensor is specified. The standard was created to enable the use of various oxygen sensors [78].

Noteworthy the analogy to the methods for oxygen barrier testing, the standards defined in ASTM E96 and ASTM F1249 commonly apply when the permeation of water vapour ("water vapour transmission rate", WVTR) is of interest [1].

3.3.3   Standards Based on Opto-Chemical Sensors

When the project associated with this thesis started in 2005, the use of opto-chemical sensors for the quantification of diffusion phenomena was merely described in literature [37, 79-81, 82 {p. 7}], while such sensors were completely absent in commercialized methods. Apparently, the institutions in charge of defining standardized methods thus saw no cause to explicitly include opto-chemical sensors in the procedures for permeation testing. Basically, the standard ASTM F2622-08 would have permitted the use of any suitable oxygen sensor in permeation measurement, including opto-chemical sensors [78].

In the last few years, however, the situation gradually changed and opto-chemical sensors received attention, also in the field of barrier property characterisation. The applicability of opto-chemical sensing had, for instance, already been demonstrated by 2005 for the non-invasive monitoring of oxygen in beer bottles [81] and food packages [79, 80]. In 2008 and covering such applications, the standard ASTM 2714-08 [83] was defined for the non-invasive, opto-chemical measurement of oxygen concentration in the headspace of food packages, enabling the calculation of a permeation rate.

Later, a technical committee concerned with the applicability of a dynamic accumulation method for flat-film permeation testing (ASTM WK43413 [84]) was convened. In 2015, eventually, ASTM F3136-15 [60] was created. The standard covers the concept of the development in this project.

3.4   MARKET SURVEY OF COMMERCIAL BARRIER TESTING EQUIPMENT

However well established the some of the named standards are in industry, hardly any to none of the commercially available systems based on these technologies has met the sensitivity requirements for the sought low permeation rates in the context of OLED encapsulation around 2005-2008 [11, 13]. Although this is meanwhile disputable [10 {pp. 26‑27}, 12, 14], the requirements have exceeded the performance by up to three orders of magnitude in the past. In the following, some selected examples of state-of-the art commercially available instruments, their limits of detection and possible particularities are mentioned.

Special attention should be paid to OxySense (see section 3.4.7) who appears to be the first commercial supplier offering an opto-chemical device for oxygen permeation testing, introduced in 2011.

3.4.1 MOCON Instruments

The perhaps most established supplier for permeability test instruments, MOCON from Minneapolis, Minnesota, specifies a limit of detection of 0.005 [cm^3 m^{-2} day^{-1} atm^{-1}] for its most sensitive oxygen transmission rate measuring system available in 2008 (OX-TRAN® Model 2/21) [11]. The product was, however, discontinued in 2016 [85] and replaced by OX-TRAN® Model 2/22 [12]. For the new system a limit of detection of 0.0005 [cm^3 m^{-2} day^{-1} atm^{-1}] is specified. Like the predecessor model it uses a patented coulometric sensor (COULOX®) and is compliant with the standards ASTM D-3985, ASTM F-1927, DIN 53380 and ISO 15105-2. Other products have inferior detection limits [63, 64]. As a budget option, a system (OX-TRAN® Model 2/10), which is non-compliant with ASTM D3985, is using a calibration-dependent electrochemical sensor and has a limit of detection of 0.1 [cm^3 m^{-2} day^{-1} atm^{-1}] [86].

It shall be mentioned that since 2006 [87], MOCON offered a water vapour transmission rate measuring device for whose design they advertise special consideration with respect to testing OLED encapsulation membranes. The device (Aquatran Model 1) reached a limit of detection of $5*10^{-4}$ [g m^{-2} day^{-1}] and used, similar to the ASTM-compliant OTR instruments, an absolute, coulometric sensor [13]. It was replaced in 2013 [87] by Aquatran Model 2 [14] which is specified for a limit of detection of $5*10^{-5}$ [g m^{-2} day^{-1}] and conforms to ISO 15106-3 [88]. The detection limit is meanwhile only one order of magnitude above the proposed worst-case demands of 10^{-6} [g m^{-2} day^{-1}] of water vapour transmission for OLED encapsulation [10] (see also Fig. 0-1 on page 13).

It is noteworthy that MOCON also used the concept of a "seal vestibule" that represents one of the key ideas in the instrument developed in this project (see section 5.3.2.2) but uses the trademark "TruSeal" and the terminus "Flush Ring" for the concentric arrangement of gaskets [65 {p. 13}]. According information of competitors was not obtained.

Furthermore, MOCON follows the concept of "Dynamic Relative Measurement" according to ASTM E398 [59] and of averaging multiple measurement cycles in one of their water vapour transmission rate measuring devices [89]. Again, this approach represents one of the key ideas implemented in the opto-chemical OTR measuring instrument developed.

In 2012, MOCON acquired PBI Dansensor [87], who previously sold their permeation line to Systech Illinois [90].

3.4.2 Systech Instruments and Illinois Instruments

The British manufacturer Systech Instruments and Illinois Instruments are selling their products with the marketing name Systech Illinois. The manufacturer specifies the limit of detection of their most sensitive OTR measuring device "Model 8001L" to 0.005 [cm^3 m^{-2} day^{-1} atm^{-1}] [73]. The device series complies with ASTM standards D3985, F1927 and F-2622 and uses a coulometric sensor. In the web resources, Systech Illinois is promoting the superior accuracy of their instruments in comparison to competitors [91] and the widest oxygen permeability measurement range in the market [73]. In

June 2010, Systech Illinois acquires the "Lyssy" oxygen permeation line from PBI Dansensor [90] and in July 2017 announces the "joining of forces" [92] with OxySense (see section 3.4.7), a supplier for opto-chemical oxygen sensing technology and apparently the first commercial supplier offering an opto-chemical system for OTR measurement.

In 2009 and following bilateral talks, a number of test samples provided by Systech Instruments were measured on the opto-chemical instrument developed within this project to evaluate the performance of the method. The attempt to establish a cooperative project with the target of technology transfer was not, however, successful.

3.4.3   PBI Dansensor

PBI Dansensor, a Danish manufacturer, produced a device (L100-5000 Manometric Gas Permeability Tester) capable of measuring the permeation rates of a number of gases via a manometric method according to ASTM D1434-82, DIN 53380-2 and ISO 15105-1. Performance data are, however, not given in the product brochure [93]. Another device ("OPT-5000") is designed for the measurement of oxygen transmission rates exclusively. The limit of detection is specified with 0.1 $[cm^3\ m^{-2}\ day^{-1}\ atm^{-1}]$. The system uses a ceramic solid state oxide oxygen sensor and does not comply with any of the standards mentioned in section 3.3 [94].

Effective with June 11, 2010, PBI Dansensor, sold their product line of permeability testers "Lyssy" to Systech Illinois [90, 95]. In 2012, the remainder of PBI Dansensor was acquired by MOCON (see section 3.4.1) and is now trading under the name "mocon DANSENSOR" [87].

In June 2006, the potential for cooperation between the Technical University of Graz, Joanneum Research and PBI Dansensor was discussed in the course of a visit of PBI Dansensor at Joanneum Research. The talks did, however, not lead into follow-up projects.

3.4.4   ExtraSolution

The Italian manufacturer ExtraSolution [96, 97], a spin-off evolved from the University of Pisa, offers flat film permeation testing devices for O_2 ("PermeO$_2$"), H_2O ("PermeH$_2$O"), CO_2 ("PermeCO$_2$") and a units ("Multiperm", "Totalperm") accommodating sensors for two or three of the listed analytes, respectively. In addition, devices to test complete packages ("Packperm", "CarboPack BT") are also available.

"PermeO$_2$" complies with DIN 53380-3 and ASTM F2622-08 and has a specified limit of detection of 0.01 $[cm^3\ m^{-2}\ day^{-1}\ atm^{-1}]$. The standards do not specify the kind of detector to be used; neither does ExtraSolution reveal the detection principle. The WVTR tester "PermeH$_2$O" uses an infrared sensor (ASTM F1249-06) and has a specified limit of detection of 0.002 $[g\ m^{-2}\ day^{-1}]$.

Worth being mentioned, ExtraSolution invented a method [98] to significantly reduce the equilibration time required by the sample to establish a steady-state permeation rate. This is achieved by smart adjustment of the oxygen concentration in the test gas. For a sample saturated

with air (as most samples are stored in air), the oxygen partial pressure of the test gas is set twice as high as the oxygen partial pressure of air. In this way, the material thickness which needs to equilibrate divides in effect by two, because the two imaginary "halves" now simultaneously and "independently" equilibrate to an identical partial pressure gradient. Thus, a steady-state permeation rate is attained more quickly.

In 2011, ExtraSolution visited Joanneum Research to explore the opportunities for exploiting the opto-chemical OTR measuring approach commercially. The idea was not realized and a co-operation not established, however.

3.4.5   Labthink International

The supplier Labthink used to sell an oxygen transmission rate tester ("TOY-C3 Film & Package Oxygen Permeability Tester") with a specified limit of detection of 0.007 [cm^3 m^{-2} day^{-1} atm^{-1}]. The device was compliant with the standards ASTM D3985, ASTM F1927 and ISO 15105-2 [99]. Meanwhile, the model is not in the product portfolio anymore [100]. In addition to devices functioning according to the "equal pressure" method, manometric gas permeation testers complying with the according standards with inferior limits of detection are sold [100].

3.4.6   PreSens

A comparably simple permeation cell based on an opto-chemical oxygen sensor is sold by PreSens, as the author learned at the "Braubeviale 2014" exhibition (Nürnberg, Germany). Detailed information on the function principle, performance and reliability is lacking in the web resources of the company [101], where the permeation cell is categorised as an "accessory". The cell itself does not comprise an oxygen sensing unit but merely a transparent window for the implementation of an opto-chemical sensor and a set of manual valves to control the gas fluxes. The specified detection limit for gaseous oxygen of 0.5 ppm expectedly makes a characterisation of ultra-barrier membranes difficult in the opinion of the author.

Apparently, the company is quite active in adverting the device in symposia and on the web [102, 103], but associated journal or proceedings papers discovered. Furthermore, no indication of associated communication to the public before 2011 was found.

3.4.7   OxySense

Presumably not yet existent in the period 2005 - 2008, when the development of the opto-chemical OTR instrument was conducted, particular attention must meanwhile be drawn to the American supplier OxySense [104]. Apparently, the Dallas-based company is involved in intensive cooperation with the University of Florida, focusses exclusively on opto-chemical oxygen sensing

systems [105] and claims to offer the first non-invasive oxygen measurement system for sealed packages. In the portfolio there are three different laboratory and field optical oxygen analysers, a process monitor and, most interesting, accessories sold under the trade name "OxyPerm System" for permeation/OTR analysis [106]. Particularly the permeation measuring technology based on opto-chemical oxygen sensors has a prominent position on the company website, and very recently Systech Illinois announced a joint venture with OxySense [92].

In the modular permeation measuring system, "Model 5250i" [107] can be supplemented by up to 250 permeation cells ("OxyPerm") [108], both for flat film analysis in compliance with the standard ASTM F3136-15 [60] created in 2015 – and presumably as a result of the companies initiative [109] - or of packages in compliance with ASTM F2714 [83].

In 2012, the University of Florida investigated the agreement of the flat-film device meanwhile covered by ASTM F3136-15 with steady-state method covered by ASTM D3985 (for which a MOCON Oxtran 2/20 device was used) and found comparable results [62]. However, the investigations only covered transmission rates greater than $1\,[\mathrm{cm^3\,m^{-2}\,day^{-1}\,bar^{-1}}]$ and covered several orders of magnitude. Note that the transmission rate of ultra-barriers is several orders of magnitude below.

The company is – at least to the knowledge of the author – the first supplier that entered the market with an opto-chemical permeation testing device functioning according to the "dynamic accumulation method". The earliest web resources available, however, date January 2011 when a permeation system was announced as a result of a university programme on packaging [110]. In July 2017, Systech Illinois announced the intention to "join forces" with OxySense, presumably in the field of permeation measurement [92].

A detection limit of the permeation testing equipment "OxyPerm" is not specified on the webpage. The oxygen analyser "Model 5250i" is able to detect oxygen between 0.03 % (corresponding to 30 Pa pO$_2$) and 30 % (30000 Pa pO$_2$), according to the specifications. Considering the dynamic range of about 0.01-10 Pa pO$_2$ of the opto-chemical sensor implemented in the ultra-barrier instrument developed within this project, the applicability of the OxySense system to ultra-barrier membranes appears highly unlikely. The device seems to be tailored for standard- and high-OTR measuring applications instead.

Nevertheless, the highest possible acknowledgement must be expressed for being the pioneer (to the knowledge of the author) introducing the technology into the market.

3.5 CALCIUM DEGRADATION TESTS

The urgent demand for much more sensitive analytical methods has led to the development of some procedures for barrier testing in the ultra-low-permeation-rate regime [1]. With few exceptions, they are based on the corrosion of metallic calcium by oxygen and water vapour. In the course of sample preparation, the substrate (which is the barrier material, in this case) is coated with a thin layer of calcium either in an inert atmosphere (glove box) or a vacuum chamber by appropriate

means [1, 4, 5, 111]. The thus prepared, reflecting calcium layers are then sealed between the substrate and a glass or metal cover, with the aid of sophisticated epoxy resins and gluing techniques, so that the ingression of oxygen and water vapour is ideally only possible through the substrate under investigation. The permeation experiment itself is commenced when the sample is brought into air or an atmosphere at controlled temperature and humidity.

Any permeating oxygen or water vapour arriving at the calcium layer is immediately adsorbed by the corrosive metal, forming calcium salts which are transparent and electrically insulating. The respective chemical reactions are assumed to occur as shown in Fig. 3-5 [111]:

$$
\begin{aligned}
1) \quad & 2\,Ca + O_2 \quad \rightarrow \quad 2\,CaO \\
2) \quad & Ca + H_2O \quad \rightarrow \quad CaO + H_2 \\
3) \quad & CaO + H_2O \quad \rightarrow \quad Ca(OH)_2
\end{aligned}
$$
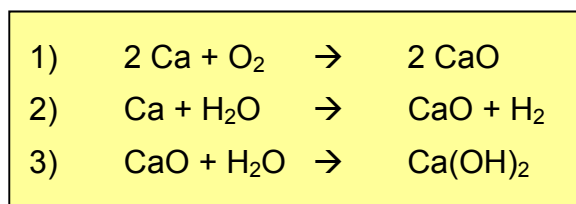
Fig. 3-5: **Assumed chemical reactions involved in the corrosion of metallic calcium by oxygen and water vapour [111].**

As the permeation experiment is going on and oxygen and water vapour are diffusing into the enclosure containing the calcium layer, the metal is thus gradually oxidised. For the assessment of the degree of corrosion, a number of strategies may be followed. Earlier developed calcium degradation tests utilise the transparency of the calcium salts (in contrast to the opacity of metallic calcium). With the aid of homogeneous light sources and CCD cameras, transmission photographs are obtained and processed by according imaging software to yield the fraction area of degraded calcium as a function of permeation time. From the thus recorded plots the gas transmission rate is calculated [4].

More commonly now, the degree of corrosion is assed via changes in the electrical resistance. For this purpose, the calcium layer is contacted using silver electrodes in the course of sample preparation. During the permeation measurement, the resistivity of the calcium layer is continuously recorded by a multimeter, applying only very small voltages to avoid electrochemically induced corrosion. Since calcium is a metallic conductor but calcium oxide and calcium hydroxide are insulators, the resistivity of the film increases as its degradation advances. From the recorded data, the gas transmission rate is calculated [111-114].

For good reason, the term "gas transmission rate" was used in the above explanations instead of either OTR or WVTR. As it may be concluded from the equations in Fig. 3-5, the calcium degradation tests do generally not discriminate between oxygen and water vapour permeation, despite the differences in the reaction stoichiometry of the two permeants with calcium. Only, if special conditions are established during the measurement (dry oxygen or humidified nitrogen atmospheres), the response of the method may be attributed to either an OTR or WVTR, respectively [1, 4, 111].

In some cases, the results of calcium degradation tests are *explicitly* reported in terms of an *effective WVTR* [4, 5, 112], while most commonly the result is simply (though not accurately) called WVTR. The property "effective WVTR" is understood as the sum of an actual WVTR and a further contribution to the calcium corrosion which is caused by permeating oxygen. Note again, that the stoichiometry of calcium corrosion is different for oxygen and water vapour. However, since the main impact of atmospheric gases on an OLED or OPV device is largely associated to the degradation of the corrosive cathode metals (calcium layers in many cases), the introduction the "effective WVTR" as a measurable property appears justifiable. Furthermore, the corrosion of calcium is generally assumed to be dominated by the reaction with water [112]. Terms like e. g. "decomposition equivalent" instead of OTR or WVTR would nevertheless be more accurate in case of a *composite property*, which is just exactly what is being measured in the calcium degradation test.

Optical calcium degradation tests are, in contrast to other techniques, able to discriminate between bulk-permeation and defect-based permeation [1, 4]. In according experiments, the substrates under investigation are coated with a thin calcium layer, which in turn is protected by subsequent deposition of an inert metal layer. The thus prepared sample is then sealed by an overcoat and a glass lid to protect the inert metal layer from mechanical damage. When the sample is brought into the atmosphere, water vapour and oxygen are permeating through the substrate and its defect sites. As a result, the sites of permeation (=defects) are reproduced as a discrete corrosion pattern in the calcium film. A microscope fitted with a CCD-camera is used to record images of the corrosion patterns, which can then be processed accordingly [4].

Many groups researching on ultra-barrier membranes have established their own derivations of these approaches to serve their demand for routine characterisations in barrier development [23, 24]. The measurement of water vapour transmission rates as low as $3*10^{-7}$ [g m^{-2} day^{-1}] has been reported in literature [1, 4], which indicates that the calcium degradation techniques are among the most sensitive manners for permeation detection.

Despite their sensitivity, the calcium methods are not particularly suitable for routine measurements due to the elaborate preparation of the substrates, involving sample handling in inert atmospheres or even vacuum. Furthermore, many derivations are used by different research groups, whereas a universally defined and accepted standard method is lacking [4].

Nevertheless, the importance and significance of calcium degradation tests must not be underestimated since they feature an inherent advantage over other methods for testing encapsulation materials of organo-electronics. It shall be kept in mind that the conditions, to which a calcium layer on a barrier substrate is exposed in such experiments, resemble those encountered by an actual electrode of an OLED or OPV device to the widest possible extent. In more elaborate stages of development, important and ultimate benchmark results such as the expectable service life, the identification of failure modes or location of blemishes may be obtained using these techniques. In more fundamental research activities associated with ultra-barrier development, where commonly a much larger number of membranes have to be tested, it is yet the almost only but far from ideal tool for barrier testing.

3.6   EXOTIC HIGH-SENSITIVITY BARRIER TESTS

Techniques using an ultra-high vacuum chamber for permeability measurements were reported in literature. The vacuum chamber is equipped with a residual gas analyser which accomplishes OTR measurements with a detection limit of 10^{-6} [cm^3 m^{-2} day^{-1} atm^{-1}]. The same technology is, however, much more complicated if water permeation shall be measured [1].

Perhaps the single most sensitive method to date for measurements of water vapour transmission rates is using tritium-doped water as the permeant. The permeation of water is detected *directly* on the basis of its intrinsic radioactivity. The technique reaches an impressive detection limit of 10^{-8} [g m^{-2} day^{-1}], but requires a certified radioactive laboratory, licensed for 10 Curie tritium and is therefore not suitable for large-scale routine measurements [115].

In other studies, the percentage of inactive OLED pixel area, destroyed by entrant water, was used to calculate the WVTR. However, this technique provides only an indirect conclusion about the permeation rate and requires significant development [1, 116].

PART II:

THE WORK

4 OPTO-CHEMICAL OTR MEASURING APPROACH

Almost all methods and devices for barrier characterisation outlined in the previous sections suffer from one inherent drawback that is found in the mode of oxygen detection. The sensors employed (whether a coulometric sensor or a thin layer of calcium) consume the analyte oxygen in the course of its detection. Thus, these sensors *do not* permit the permanent monitoring of the O_2 *concentration* inside a measuring cavity – *while* permeation occurs, and *while* the accumulation of the permeating gas inside the measuring cavity causes a gradual increase of concentration that follows a linear time-dependence in a first approximation. In addition to the "destructive" mode of detection, these sensors are either not re-usable (calcium film) or their physical dimensions counteract an integration into the (ideally small) permeation cavity of the instrument.[20]

In these aspects, opto-chemical oxygen sensors are superior by their principle. As already discussed in section 2.1, they are capable of *consumption-free analyte* detection [46]. The actual sensor of an opto-chemical setup consists of a small area of an appropriate, immobilised, luminescent dye, whose luminescent behaviour is dependent on the oxygen concentration of the surrounding atmosphere. The sensor's geometry is easily customized and furthermore permitting a large degree of minimization. Thus, the volume occupied by the sensor spot and, in consequence, its capacity for gas absorption should be practically zero, compared to the dimensions of a typical permeation cell. Moreover, the transmission of the measurement response occurs *optically* (via a transparent window or a waveguide, for instance) and does not require any electrical wiring penetrating the container boundaries, which is relieving the design complexity of an absolutely airtight apparatus and helping to preclude leakage issues.

In their entirety, these features enable a permeation setup in which the oxygen migrating through a sample membrane is accumulated in an otherwise hermetically sealed cavity. The accumulation causes a gradual, measureable increase of the oxygen concentration as a function of time, which is *simultaneously and permanently monitored* and from which the oxygen transmission rate is calculated.

The main benefit of consumption-free detection and permanent monitoring – compared with "destructive" detection schemes – is found in the relative robustness against inaccuracies of the sensor's zero point or impurities in the inert carrier gas. Provided the *gradient* of the sensor characteristic is accurately known and devoid of excessive drift, the rate of permeation can be correctly concluded from the recorded data, regardless of the sensor's readout at "true zero" or an actual, non-zero starting point of the analyte accumulation. In case of a "destructive" sensor, very high purity of the inert gas and thorough calibration of the sensor at zero level *and* with respect to

---

[20] It shall be noted that there are a number of devices on the market which function via the accumulation of the permeating analyte. However, continuous detection is also not attained with these instruments. Instead, the analyte is, after a certain period of accumulation, transported into an external detector by a short but efficient purge flow ("flash") of an inert gas. The use of the carrier gas "dilutes" the accumulated analyte to a certain extent prior the detection. Furthermore, impurities of the carrier or leakage of the apparatus may be difficult to identify. The sensitivity of the overall method is often affected, presumably for these reasons – despite the often impressive performances of the sensors employed.

the response gradient must be ensured for accurate results: small differences from "true zero" have to be quantified reliably in this case.

Using a consumption-free detection scheme (as with opto-chemical oxygen sensors), only time-dependent concentration changes are assessed in the data processing, and therefore, the technique is less vulnerable to oxygen impurities in the inert gas rather than conventional methods.[21] Moreover, since any gas transport to and from the cavity containing the sensor is, theoretically, taking place only through the membrane under investigation (the cavity is otherwise sealed during analyte accumulation), the potential for parasitic leakage is very small compared to a more complex apparatus. Using conventional coulometric sensors, such a setup would not be accessible, while opto-chemical sensors are literally tailored for this application. The approach meanwhile referred to as "dynamic accumulation" [60, 62] was introduced to the market in 2011. A standard covering the concept was created as late as 2015 [60].

The proof-of-principle of opto-chemical monitoring of oxygen permeation using a professional spectrofluorometer for sensor readout was already reported by the group of Winnik [37] who had previously used the effect of luminescence quenching to study diffusion and permeation kinetics inside polymer films [117]. The concept of permeation measurement based on luminescence quenching also attracted the attention of European researchers working with barrier membranes in the 2000 decade, as it is indicated by relatively scarce literature resources [118-120]. Apparently, a similar concept for the creation of a permeation measuring device was followed by the group more or less in parallel, but after 2009 no additional reports were published to the scientific community and a commercialization of the concept is has probably not been pursued. In any case, no indication was found that the advancement to an autonomously operating unit was attempted *prior* to the Flexonics project. Noteworthy that a number of diploma and doctoral projects were concerned with permeation rate measurement of analytes such as water vapour [49, 121] or BTEX[22] components [122].

Some years later, a comparably straight-forward device based on an opto-chemical oxygen sensor was presented by PreSens (see section 3.4.6) at the "Braubeviale 2014" exhibition (November 2014, Nürnberg, Germany). The sales personnel at the exhibition was, however, not able to provide the author with more detailed Information on the function principle, performance and reliability. According information is also lacking in the web resources of PreSens [101], where the unit termed "permeation cell" is categorised as an "accessory". The cell itself does not comprise an oxygen sensing unit but merely a transparent window for the implementation of an opto-chemical sensor and a set of manual valves to control the gas fluxes. The specified detection limit for gaseous oxygen of 0.5 ppm expectedly makes a characterisation of "real" ultra-barrier membranes difficult in the opinion of the author.

---

[21] From a mathematical point of view, the sensor's response attained with permanent flow of a carrier gas represents the first derivative of the sensor's response in case of oxygen accumulation.
[22] BTEX: Benzene, Toluene, Ethylbenzene, Xylene.

Web resources brought to light also an electronic article which was published on the webpage of a joint advertisement platform (this is an assumption, since no actual site notice is available) of manufacturers involved in the packaging industry, including also PreSens [102]. Again according to the web, a presentation of the same title was held a symposium [103]. An associated article in a scientific journal or in conference proceedings could not be found, neither any hint that activities were communicated by PreSens to the public before 2011.

Acknowledgments for being the pioneer to first commercialize opto-chemical oxygen permeation instruments must be expressed to OxySense (see section 3.4.7) who introduced such a system in 2011 [110].

4.1   OPTO-CHEMICAL OXYGEN DETECTION

4.1.1   A General Review

The employment of opto-chemical sensors is still growing in popularity [46]. In the last couple of years, the applicability of opto-chemical oxygen sensors has been demonstrated towards a wide range of different industrial applications [56, 80, 123-129]. Oxygen is, in any case, most easily accessible with opto-chemical sensors, and according research perhaps has the longest tradition in this field. Consequently, the technology is very well-engineered, compared with sensors for other analytes. Meanwhile, several manufacturers are offering optrodes as a substitute for conventional Clark-electrodes [130-136].

The sensing technique is based on the luminescence quenching effect caused by molecular oxygen. Similar mechanisms may be exploited to detect a number of analytes (carbon dioxide, ammonia, moisture, etc.) [126, 137]. The method has a number of remarkable advantages over electro-chemical oxygen detectors, some of which were already mentioned in the previous sections, and a number of oxygen-sensitive metal-complex dye formulations are available for different measuring ranges [57, 125]. Beneficial for industrial applications, the sensor stability is generally good and the calibration intervals are therefore long, there is no cross-sensitivity to carbon dioxide and, given a smart choice of the sensor formulation and protective coating, the sensors are sterilisable and resistant to CiP processes. Some of the sensors can be sterilized or laminated at temperatures of up to about 135 °C [138]. Because the sensors do not consume oxygen, the signal is furthermore largely independent of the flow rate of the medium. The technique is, after all, particularly useful for monitoring oxygen concentrations in the biochemical industry as well as in the food and beverage industry and has, for instance, been employed for the non-invasive monitoring of the oxygen concentration in beer bottles [81] (see also Fig. 4-3) and food packages [79, 80]. Covering the latter applications, the ASTM F2714-08 standard [83] was defined in 2008 for non-invasive, opto-chemical measurement of oxygen concentration in the headspace of food packages, enabling the calculation of a permeation rate. Only since 2015, ASTM 3136-15 [60] is covering permeation rate testing of flat films using opto-chemical oxygen sensors and according to the dynamic accumulation method.

4.1.2 Review on the Physics: Luminescence Quenching

The theory behind the opto-chemical oxygen measurement based on the luminescence quenching principle was first described by Stern and Volmer [51]. The respective topics, commonly allocated in the field of "spectrofluorimetry", are discussed in detail in section 2. Nevertheless, a brief review of the theoretical and technological framework shall be given in this section once more.

Luminescence is observed when a molecular or atomic system (luminophore or dye) in an excited state relaxes to the ground state, accompanied by the emission of light. However, various mechanisms lead to non-radiative relaxations of the luminophore, causing a change of the emitted luminescence with respect to intensity and lifetime. These processes are known as luminescence quenching [47, 51]. Oxygen behaves as a collisional (also said dynamic) quencher which can, theoretically, interact with the excited state every luminescent species. For sensing applications, however, the luminophore must be sufficiently sensitive and selective, which is the case with a number of dye families, such as heterocyclic compounds, polycyclic hydrocarbons, and, most important, metal-organic complexes. When molecular oxygen interacts with a luminophore in the excited state by means of collisions, the excitation energy is transferred to the oxygen molecules. Thus, the population of the excited state is diminished and a decrease of the luminescence intensity and lifetime is observed [47].

In the ideal case, the correlation between intensity, lifetime and oxygen concentration obeys the Stern Volmer law [51], as it is explained in section 2.2.1.5.2 in more detail.

$$\frac{\tau_0}{\tau} = \frac{I_0}{I} = 1 + K_{SV}[Q]$$

τ_0	unquenched lifetime
τ	quenched lifetime
I_0	unquenched luminescence intensity
I	quenched luminescence intensity
K_{SV}	Stern-Volmer constant
$[Q]$	concentration of quencher

Equation 4-1: The Stern-Volmer law.

where τ, I, τ_0, I_0 represent the luminescence lifetimes and intensities, in presence and in absence of the quencher, respectively, $[Q]$ is the quencher concentration and K_{SV} is the Stern-Volmer constant [51].

4.2 PROJECT PRE-CONDITIONS: THE STARTING POINT

The "Institute of Chemical Process Development and Control" of Joanneum Research Forschungsgesellschaft mbH[23] is involved in research on opto-chemical sensors for more than two

---

[23] JOANNEUM RESEARCH was re-organized in 2010. The research unit formed the division "Sensorsystems" of the Institute "MATERIALS" until another re-organisation in 2016 and is now referred to as "Sensors and functional printing".

decades and has built up comprehensive expertise in this field [139-141]. In the course of a vast number of preceding projects, a comprehensive, modular, phase-fluorimetric measuring chain, reaching from sensor chemistry to PC Software, had been developed, revised and thoroughly tested. Even though the group is working with a number of analytes, oxygen is the single most researched analyte with the most mature technology at disposal.

For research purposes, the components (sensors, optics, electronics and software) are produced in-house, or by manufacturers specialised on prototype construction on a pre-commercial scale. However, some parts of the technology are also licensed to OEM manufacturers, and one particular application (measuring oxygen in breweries) was in transition to series production in the period 2008 - 2014, before the enterprise was dismissed at the point of finalisation, mainly for political reasons.[24]

In general, the phase-fluorimetric, opto-chemical setup includes the opto-chemical sensor membrane itself, an optical setup tailored for the sensor dye and specific application, analogue opto-electronics and pre-amplification, digital FPGA-based driver- and readout circuits and LabView-based control software containing the routines for device communication, data acquisition and storage. Regarding the opto-chemical sensors, a large number of sensor dye/ matrix material formulations and printed or otherwise applied spots thereof were investigated by Joanneum Research in the past. Among the tested sensor variants, one particular formulation appeared to be suitable for trace oxygen detection.[25]

With the phase-fluorimetric sensing system and expertise at hand, the construction of an apparatus capable of the detection of very small oxygen transmission rates was attempted, with the first "proof of principle"-achievements made in 2003. On the basis of these results, the further development was embedded into the STREP-project "Flexonics" [15, 20], funded by the European Commission (6th EU-Framework Program). Remarkably, Flexonics was elected out of more than 50 EU-funded projects as one of the 11 finalists presented at the EuroNanoForum 2013 [142].

4.3   THE OTR MEASURING INSTRUMENT

In this section, the working principle, central features and data processing approach of the OTR measuring instrument are discussed. The familiarisation with the technological approach is in the focus of this chapter, while specific constructional details or remarks on development iterations are preferably avoided at this point, aiming for an easy comprehensibility of the principles, as it has been attempted also when presenting some of the achievements to the scientific community [143, 144].

---

[24] It was primarily the author of this work who was concerned with the research, product development and preparation of the series production at Joanneum Research where part of the manufacturing process was planned to happen. The extraordinary occupation resulting from these activities was substantially co-responsible for the discontinuity in the finalization of this thesis.

[25] Soon in the project, however, it turned out that the oxygen sensitivity of the sensing membrane was far behind the demands. In consequence, an improved alternative had to be found.

The illustration is reflecting the instrument's state of development after about two thirds of the project duration of Flexonics have had passed. By that time, the functionality of the instrument had been successfully demonstrated and the mechanical and electronic evolution of the device was completed to a wide extent.

However, countless minor and major improvements of the device have been attempted or attained and many aspects concerning e. g. unexpected behaviour were investigated, not only within the Flexonics context but also completely independent of it. These much more specific details are discussed in section 5, including remarks on the development process itself that resulted in the instrument in the present condition.

4.3.1 The Oxygen Measuring System

The measurement system comprises an oxygen-sensitive element and the opto-electronic instrumentation. The sensor membrane is prepared by dissolution and immobilization of an oxygen-sensitive dye in a suitable matrix material (commonly a reasonably permeable and soluble polymer). The opto-electronic setup has the task of exciting the dye molecules and detecting the luminescence of the sensitive membrane.

In a quantitative evaluation of luminescence, intensity and lifetime have their relevance, depending on the application [47]. However, monitoring luminescence lifetime rather than intensity has some important advantages when maximum signal stability is required. Intensity does not only depend on the analyte concentration but is also proportional to the luminophore content in the sensitive element. Therefore, leaching and photo-bleaching effects incurred by the dye indicator inevitably warp the intensity signal, as well as fluctuations of the light sources, photo-detectors and the quality of the optical coupling to the sensor membrane do [47, 137].

A determination of luminescence lifetime can be conducted either in the time domain or the frequency domain. Although the physical principle is simpler, time domain setups generally involve a more complex instrumentation and require fast electronic components to record the rapid dynamics of the luminescence emission (typically in the order of 10 - 100 µs).

Frequency domain measurements, in contrast, establish an indirect but powerful route to the lifetime of the luminescence decay, and the requirements with respect to the electronic setup are not as demanding. In this technique, the sensitive dye is excited by light of appropriate wavelength, which is modulated with a sinus function of proper frequency. The latter is chosen according to the range of decay times expected for the particular luminophore. The luminescent response shows a similar modulation, at the same frequency as the excitation light, but it occurs delayed by a phase angle which is related to the luminescent lifetime and thus inversely proportional to the degree of luminescence quenching (see Fig. 4-1). In analogy to the phase shift angle, also the amplitude ("intensity") of the modulated luminescence is reduced by quenching processes. However, intensity is in most applications not taken into consideration during data processing, despite some potential in algorithms for signal validation purposes. In contrast to the phase or decay time, the signal intensity is directly affected by fluctuations of the light source or even small changes in the optical path in *any*

luminescence measuring setup. It is thus not a very "robust" property for the evaluation of the degree of luminescence quenching caused by the analyte to be quantified.

Compared with time-domain acquisitions, the phase measurement technique only requires simpler and more cost-effective instrumentation. Light emitting diodes are used as the light source, and silicon-based photodiodes instead of PMTs detect the luminescence. Optical glass filters separate the luminescence signal from excitation light and parasitical radiation and – in a simplified illustration - complete the optical setup (Fig. 4-2), as it was already reported [80].
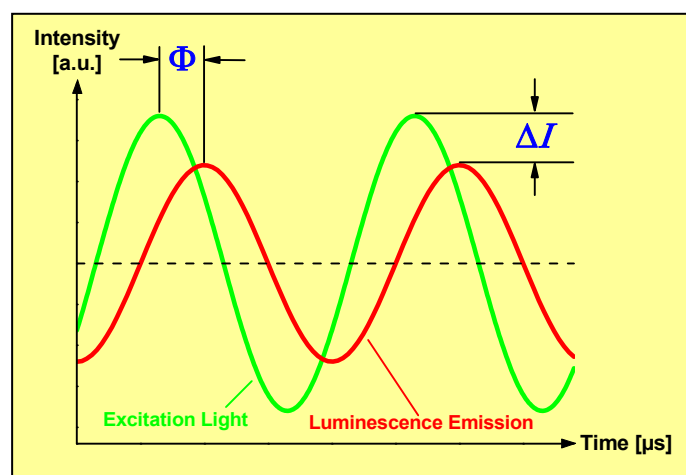
Fig. 4-1:   **The principle of frequency domain measurements of the luminescence lifetime.**
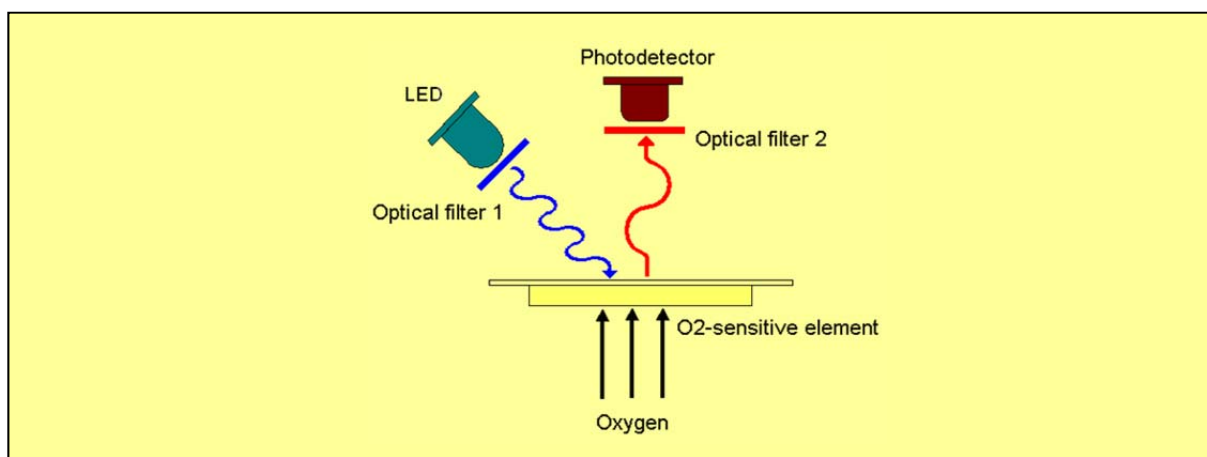
Fig. 4-2:   **The schematic optical setup of the oxygen detection method.**

Despite the targeted simplification it is worth noting also at this point, that the behaviour of the opto-electronic components (LED, photodiode) is significantly affected by temperature fluctuations, resulting in unstable signal readouts. For enhanced signal stability, a reference channel generating a phase shift *independent* of the sensor dye's luminescence is therefore implemented in the optical setup. Signal and reference channels are alternately evaluated by the readout electronics, and the difference between the two responses is used as the actual measurement result in the following data

processing. Important enhancements on the referencing quality have been achieved during the project (see section 5.3.7).

4.3.1.1 The Hardware

For the development of the OTR measuring instrument, Joanneum Research provided two opto-electronic setups (see Fig. 4-3), each comprising a "probe" (that is the internally used but not quite correct term; the "probe" comprises optical filters, prism optics, LED's, photodiode and an analogue pre-amplifier in a cylindrical steel housing) and a "vector board" (representing a digital, FPGA-based phase measuring and control unit, also including the LED-Drivers in an electronics enclosure; probe and vector board are linked through a multicore cable). Vector boards were implemented in two versions, namely "JoVec 03" and "JoVec 04", both of which were specifically modified to include additional temperature and pressure sensors for instrument monitoring.

Fig. 4-3: An opto-electronic setup as it was used in the development of the OTR measuring instrument. The setup comprises the "vector board" (digital readout electronics, grey enclosure left) and the "probe" (steel cylinder on top of a beer bottle, mid-right). The image illustrates the setup used for the measurement of oxygen in the headspace of beer bottles [81].

It is noted that development and evolution of FPGA-based phase measuring opto-electronics at Joanneum Research continue to this date and have resulted in a number of commercialised OEM

modules and devices. The analogue circuitry involved in LED-drivers and preamplifiers as well as the FPGA-code performing the asynchronous demodulation are representing core-know how of the research division "Sensorsystems" of Joanneum Research. According research was taken up already in the 1990s [145].

4.3.1.2 Sensor Membrane for Trace Oxygen Detection

The minute amounts of oxygen permeating through an ultra-barrier membrane require an accordingly performing sensor. In this application, the sensor dye of choice is Palladium(II)-5,10,15,20-tetrakis-(2,3,4,5,6-pentafluorphenyl)-porphyrin (abbreviated "PdTFPP", structure given in Fig. 4-4).

PdTFPP has an extraordinarily long unquenched luminescence lifetime in the order of one millisecond and thus allows an efficient diffusional interaction (quenching) with molecular oxygen, which explains the high sensitivity [46, 58]. Absorption maxima of the dye are found at 407 nm, 519 nm and 552 nm, luminescence emission has its maximum at 670 nm (see Fig. 4-5) [146].
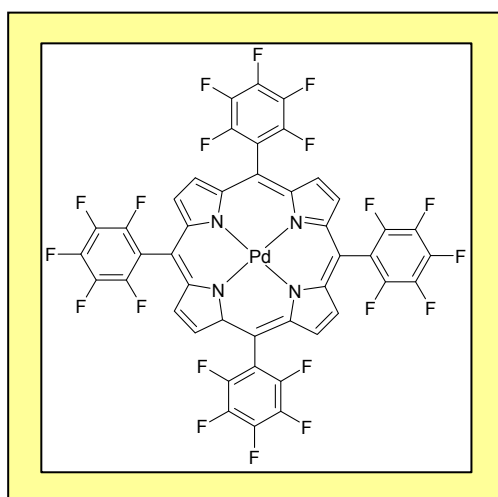
Fig. 4-4: **The Structure of Palladium(II)-5,10,15,20-tetrakis-(2,3,4,5,6-pentafluorphenyl)-porphyrin ("PtTFPP")**

As suggested by Joanneum Research in the course of the project proposal, PdTFPP was immobilised by doping a solution of polystyrene in toluene with the luminophore and casting the formulation onto 125 µm Melinex® foil. Circular spots were extracted from the coated PET substrate and glued into the OTR measuring cell.

Sensor membranes based on a polystyrene matrix were used throughout about the first two years of the development but soon proved to insufficiently sensitive for the intended application. Based on the work of Trinkel [57], the usability of membranes of PdTFPP immobilized in a highly permeable matrix material like soluble perfluoropolymers, particularly in TeflonAF® 2400 was investigated (see section 5.4.1). After some optimisations, the eventually chosen dye/matrix combination has a dynamic range 0 - 10 Pa of oxygen partial pressure (calibration characteristic in Fig. 4-6) with a resolution below 0.001 Pa in conjunction with the frequency domain instrumentation used. The

system has thus been among the most sensitive oxygen detectors available around 2006 [57]. Meanwhile, a number of luminophore/ matrix systems with even higher sensitivities have been reported [50, 58].

In contrast to the observations of Trinkel [57], the sensor membrane could be prepared in a quality that did not suffer from excessive signal drift due to ageing. The membranes currently used in the OTR instruments were prepared in 2009 and are in permanent service for 8 years now. Re-calibration turned out to be necessary only in intervals of more than 18 months.
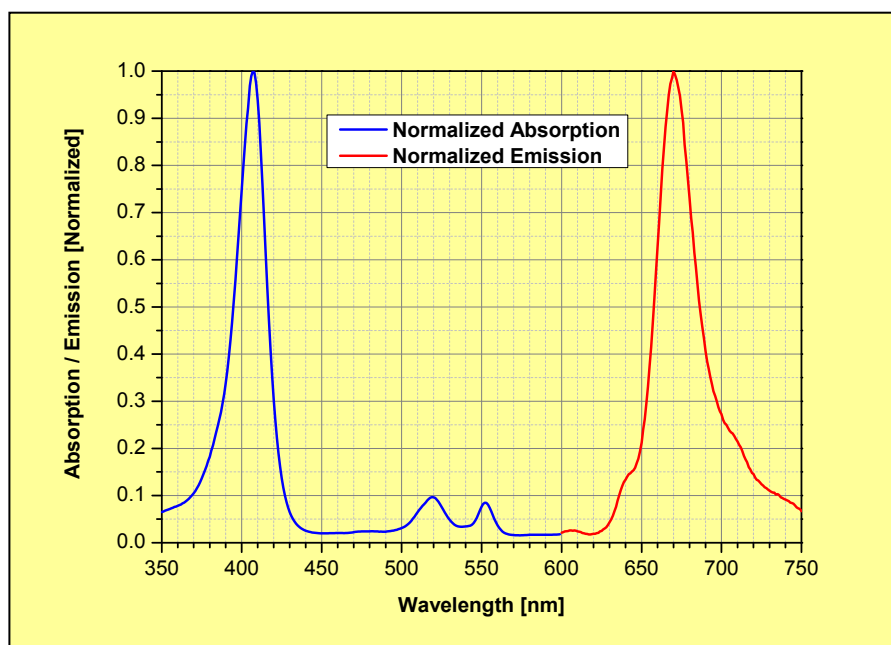
Fig. 4-5: Normalized absorption and emission spectra of PdTFPP, recorded in CHCl$_3$ at 20 °C. Spectral data were obtained from [146].

4.3.1.3   *Phase shift to pO$_2$: Stern-Volmer-Falselight Model*

In case of a frequency-domain setup, the oxygen concentration may be calculated from the measured and temperature-compensated phase shift Φ according to a rearrangement (see Equation 4-3) of the Stern-Volmer-Falselight model (Equation 4-2), as it was suggested in previous publications of Joanneum Research [147, 148] and where Φ_0 is the phase shift in absence of oxygen, K_{sv} is the Stern-Volmer constant and f_0 is the "false-light constant", representing parasitic luminescence and instrumental non-linearity.

For a given temperature of the sensor membrane, the model parameters are obtained in a non-linear regression, based on phase-shift data of calibration measurements, in which the sensor is exposed to oxygen/ nitrogen mixtures of well-defined concentrations at constant temperature (Fig. 4-6). Since the interaction of oxygen molecules with the sensor dye is based on diffusion-driven collisions and thus a function of temperature, the model parameters, in particular K_{sv}, are also temperature-dependent [47]. Consequently, the temperature behaviour of the membrane has to be mapped accordingly by recording the characteristic at multiple different temperatures and modelling

the temperature-dependence of the parameters. Alternatively, the measuring conditions may be constrained to the calibrated temperature by thorough thermo-stabilisation of the entire instrument. Since permeation measurements are commonly conducted at a defined temperature (23 °C in most cases), temperature stabilisation appeared to be the superior option.

A more fundamental consideration of the quality of the Stern-Volmer-Falselight model reveals some weaknesses, however. As discussed in section 5.5.2, a much more accurate mathematical model was implemented in 2016.

$$\frac{\Phi}{\Phi_0} = \frac{f_0}{1 + K_{SV} \cdot p_{O_2}} + \left[1 - f_0\right]$$

p_{O2} oxygen partial presure
Φ measured phase shift
Φ_0 phase shift at the absence of oxygen
K_{SV} Stern-Volmer constant
f_0 false-light constant

Equation 4-2:   **Stern-Volmer-Falselight model. [147, 148]**

$$p_{O_2} = \frac{\Phi_0 - \Phi}{K_{SV} \cdot \Phi + K_{SV} \cdot \Phi_0 \cdot (f_0 - 1)}$$

p_{O2} oxygen partial presure
Φ measured phase shift
Φ_0 phase shift at the absence of oxygen
K_{SV} Stern-Volmer constant
f_0 false-light constant

Equation 4-3:   **Calculation of pO$_2$ according to the Stern-Volmer-Falselight model.**
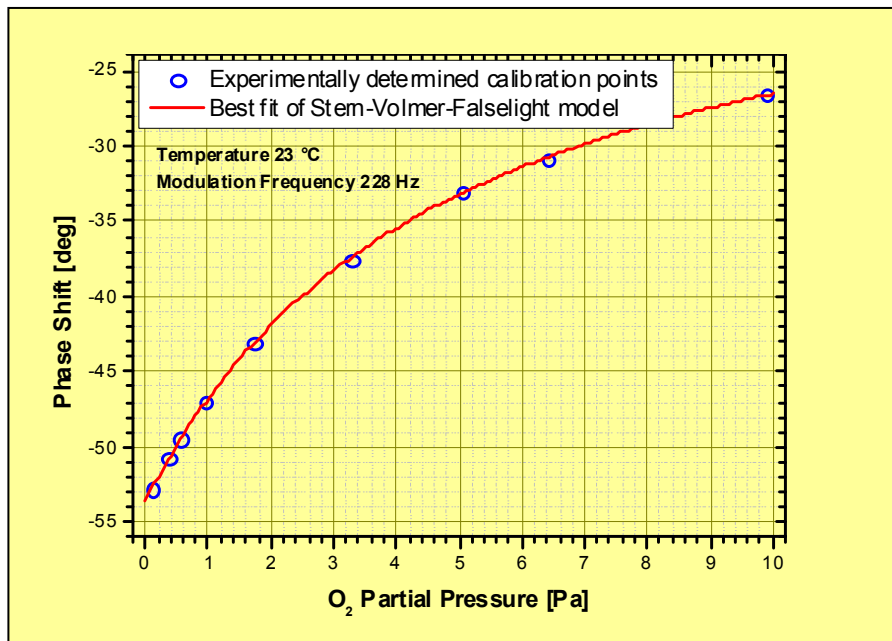
Fig. 4-6:   **The calibration characteristic of an oxygen sensor for trace analysis (PdTFPP immobilized in a highly permeable TeflonAF® 2400 matrix). Measuring range 0 - 10 Pa oxygen partial pressure, resolution <0.001 Pa.**

4.3.2   The Permeation Cell

As already mentioned in the introductory sections, the feasibility of OTR measurements based on an opto-chemical oxygen sensing scheme has been demonstrated on a laboratory scale by Rharbi et al. [37], involving a Pt-based sensor dye and a spectrofluorometer as readout instrumentation. In the presented work, a similar but independently sketched concept was cultivated to result in two autonomous, software-controlled stand-alone OTR testing units.

4.3.2.1   Setup and Working Principle

Based upon the expertise in high-performance opto-chemical oxygen sensors and ultra-stable frequency domain instruments of Joanneum Research, an apparatus comprising a test cell for measuring the oxygen transmission rate through ultra-barrier membrane samples was developed and continuously optimized (Fig. 4-7).

Essentially, the permeation cell consists of two defined volumes, separated by the sample membrane under investigation. One of the volumes (termed the "receiving cavity") accommodates the oxygen-sensitive dye/matrix spot, whose task is the quantification of oxygen that may have migrated through the sample membrane. Impinging the sample membrane with the test permeant is effected by a continuous purge flow of oxygen through the second volume ("reservoir cavity").[26]

During the initialization of the OTR measurement, a flow of an inert gas (nitrogen, quality grade >99.999 %) removes any oxygen from within the receiving cavity (see Fig. 4-8, left), with remaining impurities being in the order of 1 - 2 ppm O_2. By using additional point-of-use gas purification cartridges (ALPHAGAZ Purifier O_2-Free), the level of oxygen impurity is reduced to below 5 ppb [149], which is of relevance for the characterization of ultra-barriers (see section 5.4.3). When initialization is complete (5 - 10 min.), the highly leak-proof access valves of the receiving cavity are closed by software-controlled actuators, resulting in a hermetically sealed volume of precisely defined dimension.

Thus, the actual permeation experiment commences, and oxygen molecules that have migrated through the sample desorb from the membrane and start to accumulate in the receiving cavity (Fig. 4-8, right). By implication, the oxygen concentration gradually increases and progressively quenches the luminescence of the irradiated sensor dye. The luminescent response of the sensor is permanently monitored by the opto-electronic instrument through a glass window and according data are recorded.

---

[26] Depending on the sample properties, the test gas may be applied at elevated pressure to enhance the sensitivity of the overall device. Up to 5 bar were demonstrated.
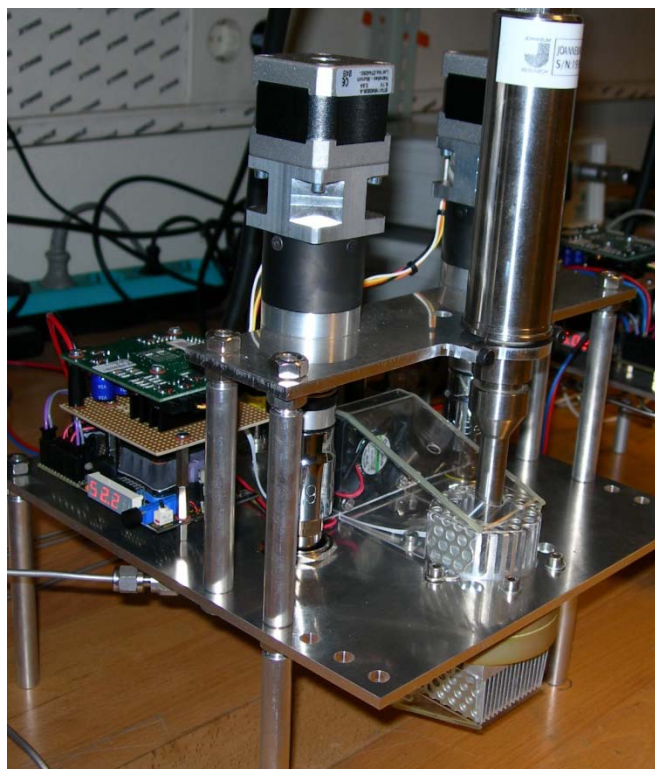
Fig. 4-7: **The laboratory demonstrator at the developmental stage of a reusable, software-controlled stand-alone device, as it is being used for ultra-barrier routine measurements for several years, meanwhile. Top right: Opto-electronic probe. Bottom right: The actual permeation cell is located underneath the main panel. Left: Temperature and valve actuators control electronics.**

Permeant accumulation is sustained for a certain period of time (typically 60 minutes). The chosen duration represents an empirically determined compromise between adverse effects which become pronounced at very short and very long permeation times, respectively. After the period has elapsed, the access valves of the receiving cavity are re-opened and the measurement is re-initialized by a purge flow of nitrogen according to the procedure above.

The process of accumulation and re-initialization is repeated until the sample has "equilibrated" to the concentration gradient between the reservoir cavity and the receiving cavity. In this final state which represents, in fact, a stationary non-equilibrium, a constant, steady-state migration of oxygen molecules and thus a constant oxygen transmission rate have established.

The time demand for this "equilibration" depends on sample properties like thickness, diffusivity and the "tortuosity" of the diffusion path through the membrane and ranges from a few minutes to several weeks. For a given sample, it is of just the same magnitude with the opto-chemical instrument as it is with conventional methods.[27]

---

[27] Frequently, the thickness of a homogeneous membrane enables a rough estimation concerning the time demand for equilibration already in advance. In case of multi-layer systems or if there is little or no knowledge at all about the "nature" of the sample under investigation (e. g. materials used, the exact configuration of a multi-layer system, etc.) such "predictions" may become very elusive.
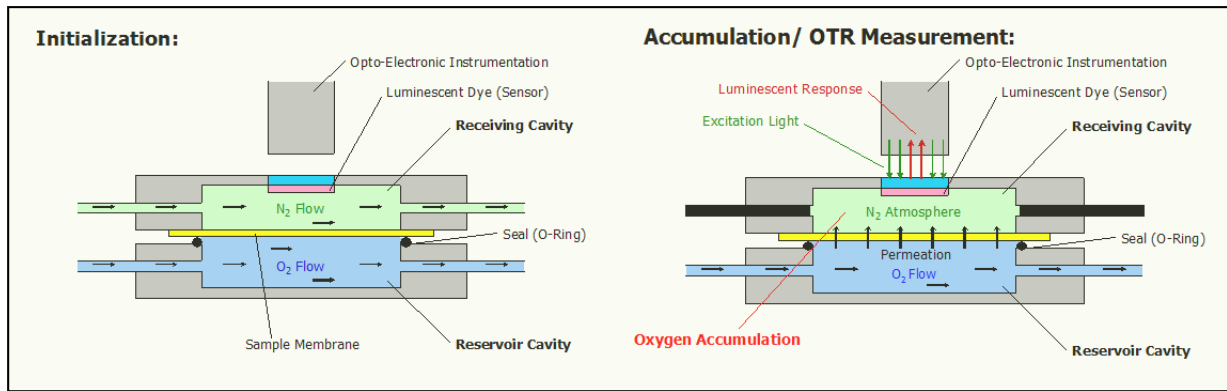
Fig. 4-8: The OTR test cell during initialization (left) and permeation/accumulation (right).

Mechanically, the membrane is held between the two moieties of the apparatus by a system of concentric O-rings. After chucking the sample, the O-rings seated around the reservoir cavity are exerting force on the membrane which, in turn, is pressed against the lapped surface of the cell half forming the receiving cavity. Leak-tightness is supported by application of small amounts of "Apiezon Grease T" [150] onto the O-rings and the contact area of the lapped surface. A continuous stream of nitrogen through the interstice between the O-rings is supposed to remove any traces of oxygen in the surroundings of the sample margin. In combination, these measures very effectively prevent the ingress of atmospheric oxygen as well as the leakage of oxygen from the reservoir cavity "around the edge" of the sample into the receiving cavity.

Mechanical support to the sample is accomplished by the insertion of discs of a porous material of well-defined free volume (sintered porous metal [151] or glass filters) into the reservoir and receiving cavity. In this way, an effectively "flat" surface is obtained for both moieties of the cell and the chucked membrane is mechanically constrained to a narrow domain. Sample "bending" or even rupture is thus prevented and a constant volume of the receiving cavity is ensured, regardless of the pressure gradients between the reservoir and receiving cavity.

4.3.2.2   Data Processing

From the data acquired by the opto-electronic instrument, the phase shift Φ is processed according to Equation 4-3 and the resulting oxygen partial pressure pO_2 is plotted as a function of time t. The plot is showing a saw-tooth like behaviour because of the alternating sequence of re-initialization and accumulation (Fig. 4-9).
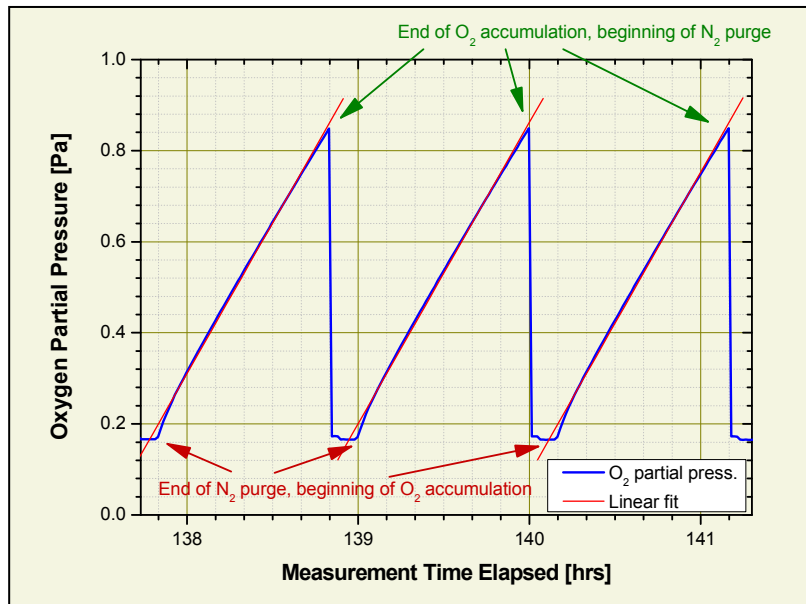
Fig. 4-9: The increase of oxygen partial pressure as a function of time elapsed. The accumulation process is repeatedly re-initialized by rinsing with nitrogen gas.

The progressively increasing O₂ partial pressure observed while the permeating oxygen accumulates in the receiving cavity is approximated by linear regression[28] and expressed in terms of the differential quotient dpO_2/dt. Due to the only minute and thus negligible amounts of oxygen in the receiving cavity, the partial pressure gradient between the two cavities is essentially equal to the absolute pressure $p_{reservoir}$ measured in the reservoir cavity. The absolute pressure in the receiving cavity cancels in the calculation. Consequently, the oxygen transmission rate is obtained according to Equation 4-4.

$$OTR = \frac{dp_{O_2}}{dt} \cdot \frac{V_{receiving}}{A_{sample} \cdot p_{std} \cdot p_{reservoir}}$$

OTR	oxygen transmission rate
dpO_2	change in O₂ partial pressure
dt	time elapsed
$V_{receiving}$	volume of the receiving cavity
A_{sample}	sample area
p_{std}	standard pressure
$p_{reservoir}$	pressure in the reservoir cavity

Equation 4-4: Calculation of the oxygen transmission rate

Since the interior volume of the receiving cavity ($V_{receiving}$), the sample area (A_{sample}) and the standard atmospheric pressure (p_{std}) are constants for a particular device, the calculation of a proportionality factor, including quantity calculus and unit conversion, further simplifies the

---

[28] In principle, the oxygen concentration should behave like the single-exponential step response to a Heaviside function. However, the time constant τ, which is proportional to the quotient $V_{receiving}/OTR$ is much larger than the accumulation time t. The error introduced by linear approximation is therefore negligible, particularly for small OTR's.

As discernible in Fig. 4-9, there is a non-linearity at the beginning of the accumulation, caused by the relatively slow migration of permeated oxygen molecules inside the receiving cavity (see section 5.5.3). Thus, the oxygen desorbing from the sample membrane does not evenly distribute into more remote sections of the volume immediately, pretending the initially somewhat higher rate of permeation.

calculation of the OTR. The parameters which have to be monitored during the OTR measurements include the O_2 partial pressure (p_{O2}), the pressure in the reservoir cavity ($p_{reservoir}$) and the time (t) elapsed since the end of the last initialization.

As already mentioned, the process of re-initialization and accumulation is repeated until the sample has equilibrated, a steady-state migration of oxygen has established and the OTR observed remains practically constant (Fig. 4-10). Typically, the steady state is accomplished after a day or two, depending on intrinsic sample properties. However, equilibration times of up to several weeks or months are also observed in some cases.[29]
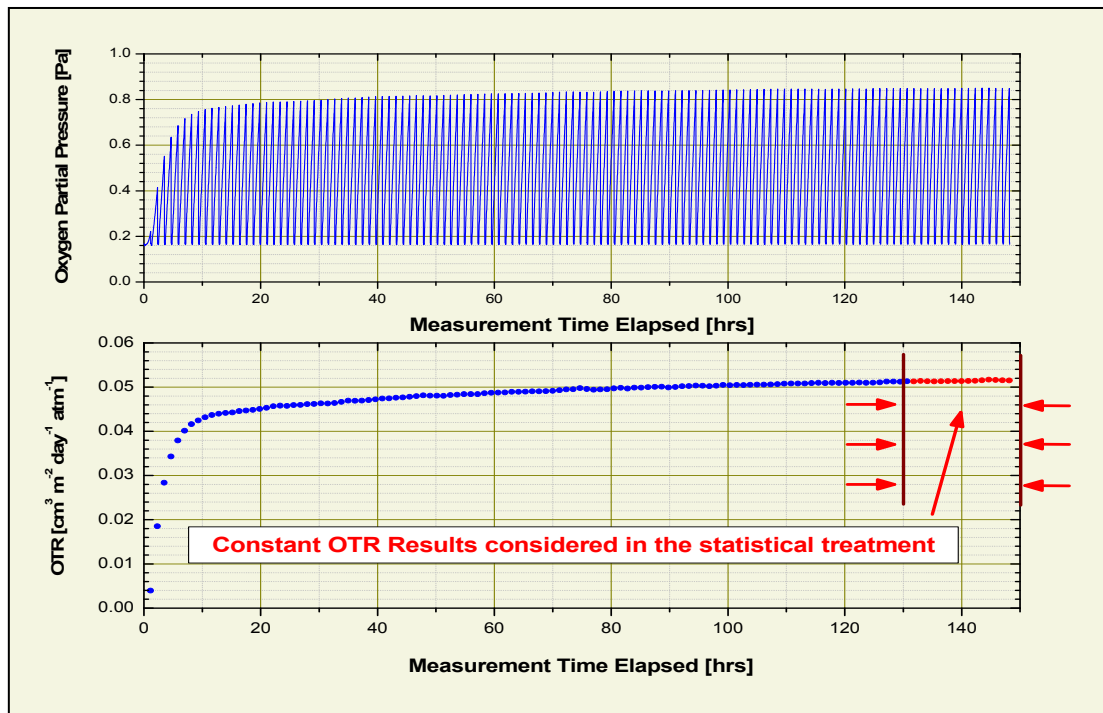
Fig. 4-10: **Top: The oxygen concentration recorded in a long-term measurement. Bottom: The calculated OTR. Data points marked with red colour are considered in the subsequent statistical treatment.**

As a sample's barrier improves and the according OTR becomes smaller, it becomes progressively relevant that the result uncertainty arising from residual temperature effects or pressure fluctuations is reduced by *averaging* several of such equilibrated OTR data points. The concept is comparable to the averaging/superimposing of multiple consecutive scans in spectroscopy to improve the signal-to-noise ratio.

---

[29] In 2011, the division "Statistical Applications" of Joanneum Research demonstrated the feasibility of an algorithm to predict the final equilibrium OTR after only 24 hours with a remarkable error margin of about 10 % for most of the samples, even if a steady state was obtained only after weeks with these samples (see section 5.5.5.2).

By superimposition and averaging of multiple measurements, the result uncertainty is reduced relatively to the uncertainty otherwise expressed in terms of a standard deviation according to Equation 4-5.

$$SEM = \frac{\sigma_{OTR}}{\sqrt{n}}$$

SEM   Stand Error of the Mean
σ_{OTR} standard deviation of OTR
n number of averaged results

Equation 4-5:   **Calculation of the Standard Error of the Mean ("SEM").**

Note that systematic errors are not removed in this way. These statistics explicitly disregard the process of sampling and sample placement in the cell. At least in case of coated or laminated barrier membranes the inhomogeneity of the sample itself generally outweighs the measuring uncertainty distinctly.

4.3.2.3 Evaluation of Device Performance

In total, some 500 barrier membranes with oxygen transmission rates over a wide range were characterized using the described demonstrator units in the course of a number of projects. A representative amount of data has thus been generated to enable an assessment of the device performance with respect to measurement repeatability, which is expressed by statistical parameters obtained during the data processing (*mean OTR*, standard deviation σ_{OTR}, standard error of the mean *SEM*, and the normalized uncertainty u_{OTR} in particular).

The normalized uncertainty of the attained results is calculated as in Equation 4-6 with $t_{95\%}$ representing the probability value of the *t*-distribution and *n* being the number of averaged results.

$$u_{OTR} = \frac{\sigma_{OTR} \cdot t_{95\%}}{\sqrt{n} \cdot \overline{OTR}}$$

u_{OTR} normalized uncertainty of OTR
σ_{OTR} standard deviation of OTR
$t_{95\%}$ 95 % probability value
n number of results
OTR oxygen transmission rate

Equation 4-6:   **Calculation of the normalized result uncertainty.**

The normalized uncertainty, plotted as a function of the corresponding mean OTR result, illustrates the device performance attained as a result of the development in a picturesque way (Fig. 4-11). Extrapolation of the data to unity indicates a limit of detection in the order of $2*10^{-5}$ [cm^3 m^{-2} day^{-1} atm^{-1}]. Thus, the device is outperforming the best instruments available on the market in 2008 by two orders of magnitude with respect to resolution. Meanwhile however, notably MOCON (see section 3.4.1) improved the detection limit of their instruments and now specifies a

number of $5*10^{-4}$ [cm^3 m^{-2} day^{-1} atm^{-1}] for OTR [12] and $5*10^{-5}$ [g m^{-2} day^{-1} bar^{-1}] for WVTR [14]. Note that accuracy of the opto-chemical instrument has been confirmed at substantially higher transmission rates only due to a lack of reference result near the detection limit. For a more detailed discussion about the accomplished performance of the instrument refer to section 6.
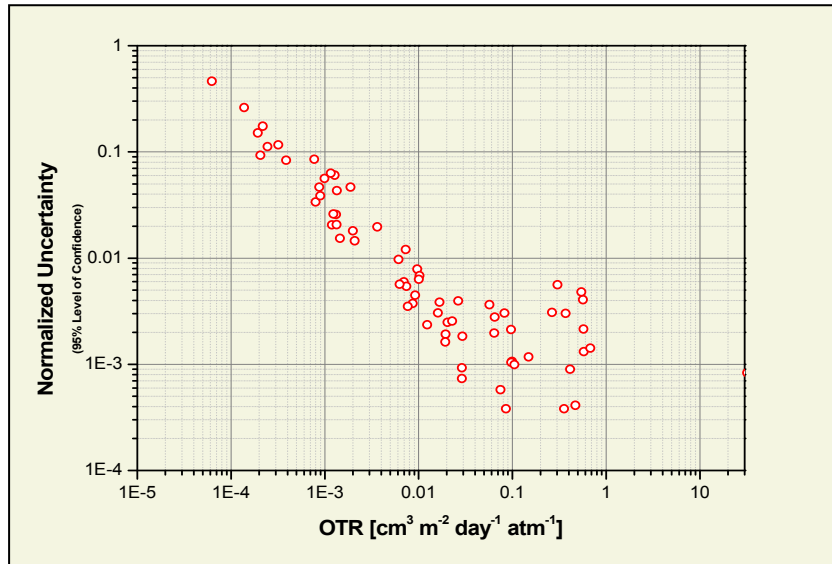
Fig. 4-11: Normalized OTR uncertainty of multiple results, calculated according to (Equation 4-6) as a function of the mean OTR. Extrapolation of the uncertainty to unity suggests a limit of detection of about $2*10^{-5}$ [cm^3 m^{-2} day^{-1} atm^{-1}].

5 THE OTR INSTRUMENT IN DETAIL

The fundamental working principle, the most important features and the general procedure of data analysis of the OTR measuring system are illustrated in section 4.3, thereby avoiding an excessive level of detail and putting the comprehensibility of the overall concept into the focus. Against this background, many aspects which are essential for the functionality *in practice* had to be sacrificed in the descriptions, however. Nevertheless, these deserve a discussion. Furthermore, the development of the instrument was involving the generation, trial and, if appropriate, implementation of countless concepts for a performance improvement of the instrument, which were, in turn, addressing countless different functional aspects of the device. Many of these ideas turned into successful development advances, while others were tested in vain and had to be discarded eventually.

In this section, all the details that would have blasted the general illustration of the instrument's functional scheme are discussed with all due attention. The comprehension of the general concept (section 4.3) is thereby presumed and a prerequisite. Since the interdependence of the majority of subjects in this section with each other is pronounced, the reader is advised to expect a large number of cross-references to other relevant sections whenever appropriate.

5.1 THE DESIGN PHILOSOPHY IN GENERAL

Soon in the Flexonics project, the goal of an economic, easy, reliable and user-friendly handling was kept in mind in the design of the OTR measuring instrument, in order to enable routine measurements to be carried out by assistant staff and to keep the operational costs low. In a long term objective, this approach should assist a possible technology transfer or the production of a small series of devices on a semi-commercialized scale. Some of the measures described in the following shall be seen in this context.

5.2 THE TOOLS AND SUPPORTERS

Briefly, the software tools used for design of the instrument as well as for processing data, programming the control and acquisition application and mathematical treatment of algorithms are listed.

- Computer-aided design of the mechanical components using Autodesk AutoCAD [152] strongly assisted the conception of the mechanical components. The layout of all versions of the instrument was drafted and evaluated on the screen before the design was forwarded for manufacture (see Fig. 5-1 for example images).

- Device control, data logging and data processing are conducted by an application which was programmed using National Instruments LabVIEW [153] as the developer environment.

- Data manipulation to obtain final results, statistical statements or graphic presentations of raw or pre-processed data was accomplished using OriginLabs "Origin" [154].

- Algebraic treatment of complex mathematical functions and modelling and testing of diffusion phenomena was aided by the toolkit "Mathematica" [155].

- Statistical treatment of data to establish termination criteria or prediction models (conducted by the division "Statistical Applications" of Joanneum Research) were based on the programming environment for statistical computing "R" [156].
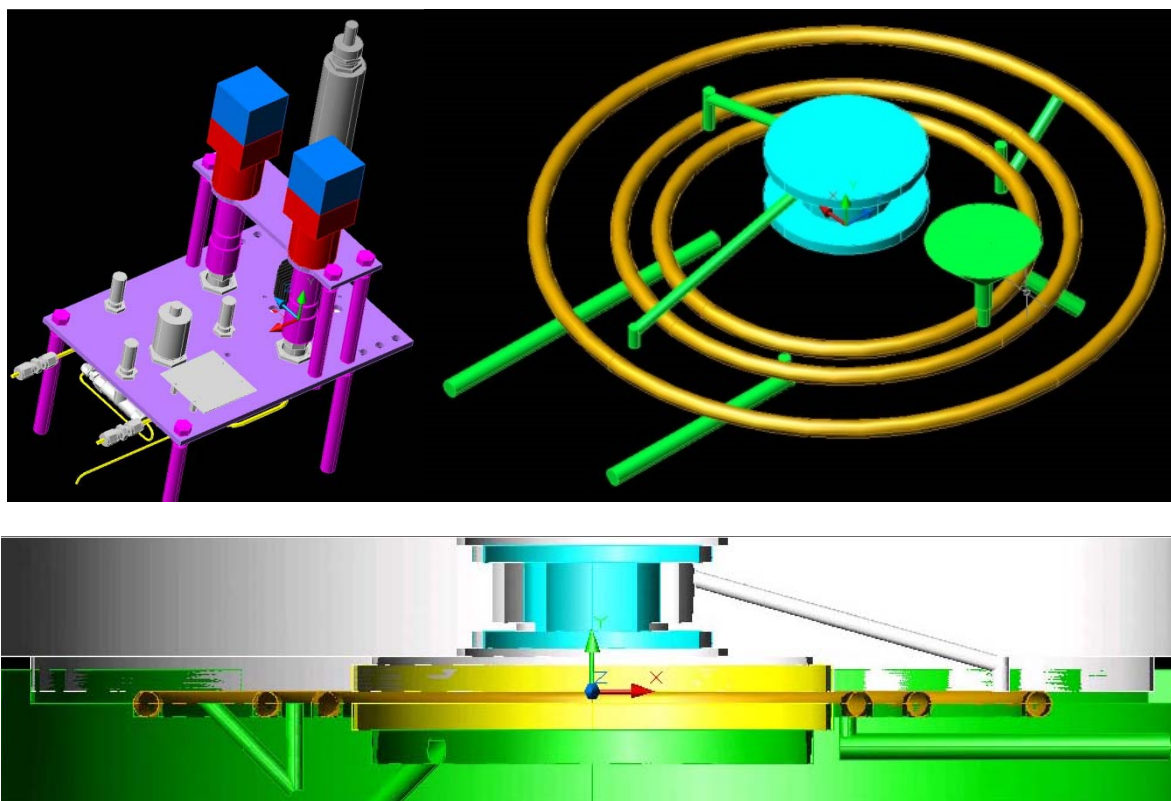
Fig. 5-1: Example images created during the CAD design of instrument version 2.0 (section 5.7.4). Top left: Overview. Top right: gas flux channels and O-rings forming part of the seal vestibule concept (section 5.3.2.2). Bottom: A cross-section of the cell.

A number of manufacturing tasks and the statistical treatment of a discrete issue were sub-contracted or conducted by third parties, respectively. The gratefully acknowledged contributions are listed below:

- Joanneum Research, Institute for Process Development and –Control: Provision of opto-chemical oxygen sensing technology, continuous support throughout the project.

- Joanneum Research, Institute for Laser- and Plasma-Assisted Vacuum Deposition Processes, Niklasdorf: Gold-plating of cell surfaces.

- Joanneum Research, Institute for Statistical Applications: Model development for termination criteria and result prognosis.

- Technical University Graz, Institute of Production Engineering: Manufacture of the cell bodies.

- Sappi, Gratkorn: Lapping of cell surface.

- Anton Paar GmbH, Graz: WIG-Welding of tube fittings.

- Anton Paar ShapeTech, Wundschuh: Milling of device panels.

5.3 THE HARDWARE

This section refers to any technical details concerning the OTR measuring device, such as mechanics, optics and electronics. The chemistry of sensors and consumables, algorithms or software are discussed in their own respective chapters.

5.3.1 Mechanical Dimensions

The two demonstrators existing by the end of the project were designed as entities separate from the opto-electronic readout instrumentation. Prior demonstrators were dismantled and some of their components used in the setup of enhanced replacements. The opto-electronics provided by Joanneum Research are applied in the form of an opto-electronic "probe" which rests in an according recess in the measurement cell.

The device shown in Fig. 5-33 (page 165) has the overall dimensions 30 cm x 20 cm x 15 cm, not including the opto-electronics ("probe") and the instrumentation driver unit ("vector board", see section 4.3.1.1). The actual cell (see Fig. 5-2) is located underneath the main panel and manufactured from stainless steel (1.4305) mainly by shape-cutting using a lathe. It has a diameter of 70 mm and a height of approx. 45 mm.
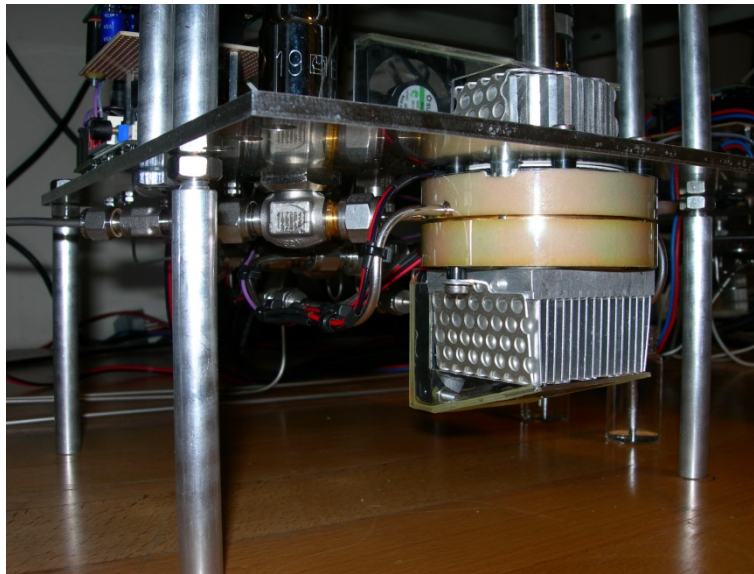
Fig. 5-2: The permeation cell of the OTR instrument (image of Version 3.0, see section 5.7.8) is located underneath the main panel and comprises two moieties. The receiving cavity is located in the top half, the reservoir cavity in the bottom. Peltier elements, heatsinks and fans thermo-stabilize the permeation cell.

The interior volume of the receiving cavity (see Fig. 5-3), to which the increase of the oxygen concentration has to be related in the calculation of the oxygen amount, is approx. 900 mm^3. This number includes the interior volume of the access valves which are sealing the receiving cavity.

Fig. 5-3: The top moiety of the permeation cell comprising the receiving cavity (recessed cylinder in the centre). A glass window enables the readout of the opto-chemical sensor, which is cast onto the window. The window is glued using an epoxy resin [157]. In- and outlet of the nitrogen purge flow, creating the "seal vestibule" (see section 5.3.2.2) are visible in the circular groove in the lapped surface around the receiving cavity. In case of permeation cell Version 3.0 (see section 5.7.8) the surface of the component was coated by pulsed laser deposition with a thin layer of gold for chemical passivation due to reasons explained in section 5.4.3.

Circular pieces with a diameter of 45 mm are cut from the sample membranes of interest by appropriate means (laser, punch, scissor or knife) and mounted/chucked between the two moieties of the cell. In the setup process of a measurement, the 3 screws (M5) that are joining the cell moieties with the sample in between are tightened with a torque of 4 Nm using a torque wrench.

The sample area actually subjected to the permeability measurement is circular, with a diameter of 30 mm, resulting in a permeation area of 706.9 mm^2 (see also Fig. 5-4, right).

5.3.2   Prevention of Atmospheric Oxygen Intrusion

Since the discrimination between oxygen permeating through the sample (the analyte of interest) and oxygen leaking into the cell from the surrounding atmosphere is difficult, any leakage effects are best eliminated from the beginning by constructive measures:

5.3.2.1   Access Valves of the Receiving Cavity

The access valves sealing the receiving cavity during the measurement are crucial components in context of the intrusion of atmospheric oxygen. Therefore highly leak-proof, bellow-sealed, pack-less valves of stainless steel (Hoke Type 4172 G4Y) were integrated in al demonstrators from version 1.1 (section 5.7.2) onwards. Unfortunately, these valves have a comparably large interior volume which is adding to the volume of the receiving cavity. Needle valves with a smaller interior volume are readily available but did, however, not satisfy the demands regarding leak-proof-ness.

5.3.2.2   "Seal Vestibule": N$_2$-Purged Interstice between Concentric O-Rings

Also, a lot of attention has been paid to the seal point between the sample membrane and the cell body. When the sample is mounted in the cell and the screws are tightened, it is pressed against a lapped steel surface of the upper cell body containing the receiving cavity by two concentric O-rings (FKM) at its circumference. In addition, a larger O-ring (FKM as well) is concentrically placed around the circumference of the sample (see Fig. 5-4 and also Fig. 5-1 on page 117). The system of O-rings creates circular volumes which shall be termed "seal vestibules". These volumes are continuously purged with a low flux of nitrogen. The purge flow effectively removes any oxygen leaking into the cell from the atmosphere before it can intrude the receiving cavity. Additionally, any oxygen stemming from the reservoir cavity which would otherwise be leaking "around" the edges of the sample membrane and might end up in the receiving cavity (that is, any oxygen that does not result from the permeation *through* the sample) is reliably removed. Leak-tightness is furthermore supported by application of small amounts of "Apiezon Grease T" [150] onto the O-rings and the contact area of the lapped surface.

Similarly, all components which penetrate the walls of the receiving cavity (e. g. the glass window for the luminescence readout, pressure sensors, etc.) are mounted in a manner that is creating an N_2-purged seal vestibules in between two distinct, circular adhesive zones for each component in instrument versions 2.x (see section 5.7.4 – section 5.7.7). In version 3 (see section 5.7.8), the efforts for creating seal vestibules was reduced as a result of the experience with version 2.

Noteworthy that MOCON also uses the concept (termed "TruSeal" or "Flush Ring") in their high-end permeation testers [65 {p. 13}].
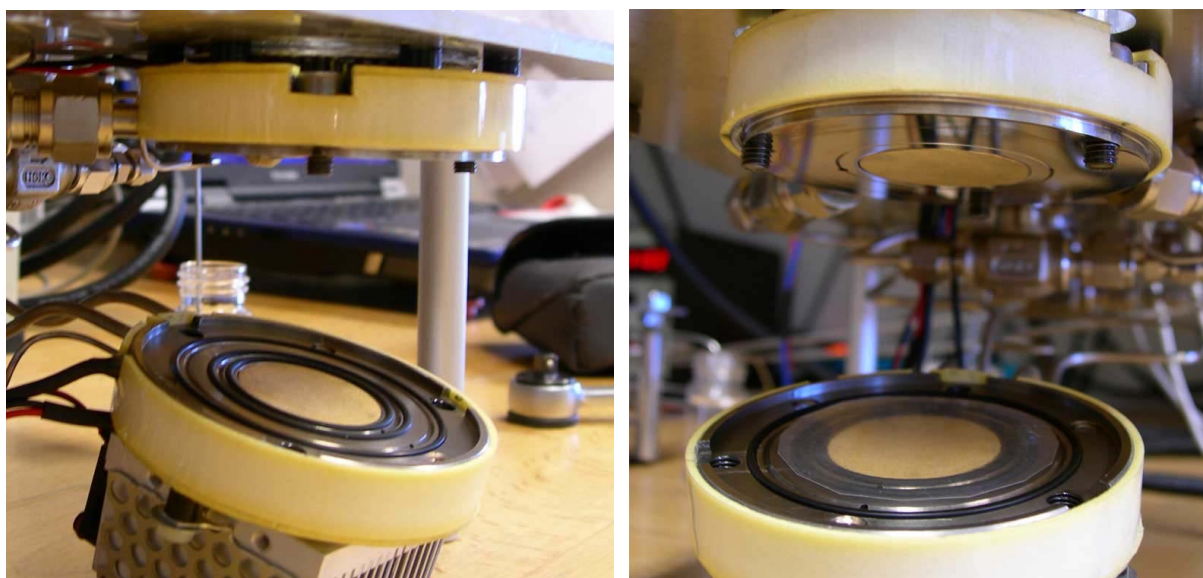
Fig. 5-4: **The concentric system of O-rings creating the "seal vestibule". The golden, circular areas are discs of sintered porous metal serving as a mechanical support for the sample. The position of the sample membrane is visible in the right hand image.**

5.3.3 Mechanical Support for the Sample Membrane

The driving force for the oxygen to permeate through the sample is the difference of the partial pressure in the two cavities of the cell. In commercial instruments, the measurements are commonly conducted using pure oxygen as the test gas at atmospheric pressure. The application of oxygen with elevated pressures (e. g. 5 bar) creates a larger partial pressure differential and hence a larger driving force, which shall assist the measurement of very low oxygen transmission rates. However, the elevated pressure exerts significant mechanical forces to the sample, which would rupture without further measures.

Also less distinct gradients in pressure across the membrane demand close consideration: the alternating sequence of N_2 purge and accumulation effects small fluctuations of the pressure in the receiving cavity in the order of 100 mbar. However, the fluctuations are sufficiently pronounced to exert significant force to sample membrane (100 mbar on an area of 7 cm^2 are corresponding to a force of about 7 N). The force will inevitably bend the membrane into one or the other direction by a few tens of a millimetre – depending on the *mechanical* properties of the sample. After all, the actual position/pressure offset of the membrane will be pretty undefined. Considering the height of the

cylindrical receiving cavity of only 2 mm, the numeric uncertainty of the resulting volume and hence the error introduced into the measurements would be unacceptable.

Hence, a means of mechanically confining the membrane to a defined position, regardless of the pressure force exerted, is highly advantageous. The mechanical support must, however, neither interfere with permeation processes nor damage or otherwise alter the sample. The solution to the issue was sought in a support material of sufficient mechanical strength, high porosity and a surface topography devoid of sharp features. In the course of development, a number of materials were tested.

5.3.3.1   Porous Metal Filters

In the construction of the demonstrators, circular discs (28.15 mm x 1.5 mm) of porous metal (GKN Sinter Metals "SIKA B8", a sintered brass powder [151], see Fig. 5-4) were integrated as a mechanical support in all demonstrators from version 1.1 onwards (section 5.7.2). The very fine grade (8 μm grain diameter) of the porous metal provides a very smooth surface which supposedly avoids the introduction of defect sites into superficial barrier layers of the sample. The pore size is sufficiently large in order not to obstruct the permeation into the receiving cavity, and the void volume of the material is certified by the manufacturer quite precisely (important since it contributes to the volume of the receiving cavity). The mechanical stability of the material is excellent.

Throughout the Flexonics project and, the mechanical support was based on this material exclusively. However, the high-surface-area brass was soon suspected to contribute to oxygen absorption phenomena which interfere with the measurement of very small oxygen transmission rates (see section 5.4.3) but a practicable alternative was not found immediately.

5.3.3.2   PTFE Filter Material

An attempt to overcome the parasitic absorption of oxygen at the interior surfaces of the cell involved the replacement of the sintered brass particle filters with a definitely inert material. Disc punched out of a 1.5 mm PTFE filter material [158] thus replaced the porous metal support. Significant improvement concerning the oxygen absorption behaviour was observed. However, the mechanical stability of the material is poor and the porosity is not precisely specified. Errors introduced by a badly defined volume of the receiving cavity have to be expected therefore.

The PTFE support was used in only one of the two demonstrators (version 3.0, see section 5.7.8) in the period 2009 - 2016.

5.3.3.3   *Glass Filter Material*

A favourable combination of chemical inertness and mechanical stability was soon expected from discs of sintered glass powder (as it is used as a filter material in every chemistry laboratory). During the Flexonics project, however, a manufacturer who would provide such material according to customer specifications at low quantity and/or cost was not found.

In the course of a commissioned research project in 2016, the quest for a suitable supplier was successful. Filter discs of sintered glass of precise mechanical dimensions and defined porosity and void volume were acquired (ROBU VitraPOR, porosity 4 = 10 – 16 µm, 28.25 mm x 1.5 mm, [159]) and thoroughly tested. The mechanical stability of the very inert material proved sufficient, and microscope images confirmed a smooth surface consisting of sintered glass spheres devoid of splintered features.

Considering the combination of the properties, the sintered glass filter discs are an advantageous replacement for the previously used porous bronze or PTFE supports and were installed in both laboratory demonstrators (Version 2.5 and Version 3.0, see section 5.7) by the end of 2016.

5.3.4   Temperature-Stabilization of the Permeation Cell

The permeation of gasses through polymers is a temperature-dependent process. Accordingly, measurements are commonly carried out at well-defined temperatures (typically 23 °C).

In addition, the collision processes causing the luminescence quench of the sensor dye are strongly temperature-dependent [47]. To account for the latter, the temperature behaviour of the opto-chemical sensor may be reflected by recording the characteristic at multiple different temperatures and modelling the temperature-dependence of the parameters. Alternatively, the operational conditions may be constrained to the calibrated temperature by thermo-stabilization of the entire instrument. In the context of permeation experiments that have to be conducted at a defined temperature, high-quality thermal stabilisation appears to be the superior option also in regard of the sensor performance. The tolerances are strict, however.

In the very first demonstrator setup (section 5.7.1), thermo-stabilization was attempted using a Lauda laboratory thermostat. The water cycle was passed through according channels in the bottom and the top of the permeation cell. However, the control loop characteristics of the thermostat proved inappropriate for stabilizing thermal loads as small as the permeation cell, resulting in an oscillation of the cell temperature with amplitudes of more than 1 °C.

Stabilization of the device furthermore appears feasible by accommodating the entire unit inside a climate chamber with appropriate temperature control characteristics, but at the expense of losing the comfortable accessibility of the cell, however. In addition, the investment for an appropriate climate chamber is considerable. The concept was discarded therefore.

Eventually, thermo-stabilization was accomplished using Peltier elements. First tests with demonstrator version 1.1 (section 5.7.2) involved a hexagonal array of 6 small, rectangular elements placed on top of the cell, a heatsink and a laboratory driver unit (Wavelength Electronics, "LFI-3751 Digital Temperature Control Instrument", [160]). The performance of the concept was convincing. In consequence, the bulky laboratory driver unit was replaced by a miniature temperature controller instrument (Wavelength Electronics "WTC3293-14001 2.2 A Temperature Controller", [161]) which is, according to the specifications of the manufacturer, able to stabilize the temperature within a tolerance band of +/- 0.1 °C.

In a fundamentally enhanced new demonstrator (version 2.0, see section 5.7.4), ring-shaped Peltier modules of appropriate dimension (No. MCR14003210L, Type "RH-1.4-32-10L MELCOR", [162]) were mounted as well on top as on the bottom of the cell. Thermal contact was established using thermal grease. Each Peltier module was equipped with an aluminium heatsink and a fan providing sufficient air flow. Temperature information for the miniature temperature controller was provided using a 10 kΩ thermistor immersed in thermal grease in a blind hole in the vicinity of the opto-chemical oxygen sensor in the top part of the cell. Thermal insulation of the cell using some 1 mm foam material adhesive tape completed the measures.

During the Flexonics project, the measurements were carried out at 25 °C. In later projects, 23 °C were chosen as the standard temperature, since many commercial laboratories are conducting their measurements at this temperature. Note that for each discrete temperature the acquisition of a calibration characteristic is obligatory, unless the parameter set of the opto-chemical sensor is augmented by appropriate temperature functions.

5.3.5 Parameter Monitoring

As the experience with the demonstrator grew the relevance of fluctuations of operational parameters such as temperature or pressure with respect to the OTR results became progressively obvious. Consequently, a number of sensors were installed to monitor or control the operational conditions.

5.3.5.1 Temperature Sensors

10 kΩ thermistors were used to monitor temperature at different locations of the instrument. One thermistor located in a blind hole in the top of the cell and in vicinity of the opto-chemical sensor provides the signal for the Peltier controller (see section 5.3.4). An additional thermistor in the direct vicinity delivers the same information for temperature monitoring purposes accomplished by the LabView control software. A third thermistor was accommodated inside the housing of the opto-electronic probe. The signal is recorded and used for temperature compensation algorithms regarding the thermal drift of the opto-electronic circuitry (see section 5.5.1).

5.3.5.2 Pressure Sensors

In demonstrator Version 2.0 (see section 5.7 for a version history), the pressures inside the reservoir cavity and the receiving cavity are directly monitored. The signal is obtained from sub-miniaturised analogue sensors (ENTRAN Model EPI-543-5B), whose signal is amplified by in line voltage pre-amplifiers and eventually transmitted to the control software by an A/D converter integrated in the phase measurement unit ("Vector Board"). To prevent leakage of atmospheric oxygen into the receiving cavity to the best possible extent, the respective sensor was glued into the cell using high-performance epoxy (Araldite 2012, [157]) at to distinct, ring-shaped zones. The interstice is part of the "seal vestibule" concept and purged by a flow of nitrogen (see section 5.3.2.2).

Unfortunately, the epoxy resin is transmitting any minute mechanical strain imposed on the cell (e. g. created simply by mounting the sample for measurement) to the sensor capsule and the pressure-sensitive silicon membrane. In consequence, proper calibration of the pressure sensors is effectively impossible and the magnitude of the readout is different by up to 100 mbar between different permeation experiments. The signals are still useful, however, to track fluctuations of the operational conditions, keeping in mind that the pressure signal must not be considered in terms of absolute numbers.

For the calculation of the oxygen transmission rate, the precise knowledge of the pressure inside the reservoir cavity is essential. In view of the incorrect readings of the analogue sensors, a digital pressure transducer (Keller "Pressure Transmitters Series 33 X", [163]) was integrated in the gas supply for the oxygen test gas. Since the flux through the reservoir cavity is adjusted to a very low flow rate using a needle valve at the outlet of cavity, the pressure signal obtained effectively equals the pressure inside the cavity. Data are transmitted via a RS-485 protocol to the computer controlling the instruments, where a LabView software module averages and publishes the feed pressure to the respective control programs of the two demonstrator units.

5.3.6 Software-Controlled Actuation of the Access Valves

In the concept of averaging multiple OTR results recorded from the same sample (see section 5.5.4), an alternating sequence of initialisation of the measurement and accumulation of the analyte is conducted. Each of these changes of operational stages requires the manipulation of the access valves of the receiving cavity and passing the information about the state change to the data acquisition software.

Regarding the extended time periods required by some samples for equilibration in combination with the duration of a single accumulation of only 60 minutes, it is obvious that a manual operation of the valves is far less than ideal. Nevertheless, throughout the first two years of development within the Flexonics project, manual operation was the only option available and a short visit of the author at the instrument was a frequent procedure, even at night or at weekends, whenever

practicable. Even though, since one OTR measurement requires 60 minutes only, a major portion of the time a sample was monitored did not generate any useful data.

In order to establish a practicable operation procedure and to support a more time-effective data acquisition scheme and hence increase the sample throughput, a means of automatically operating the cell (including night and weekend times) was highly desirable. By autonomous, software-controlled operation, a larger number of OTR data points are obtained within a given period of time, either reducing the "standard error of the mean result" by taking into account a larger number of individual results, or reducing the time-demand for the acquisition of a specified number of such OTR data points.

Automatic operation of the instrument, in turn, implies the necessity for actuators operation the access valves. In March 2007, a system was established which fully autonomously operates the cell. In combination with a high degree of automatic data processing, the device (version 2.2, see section 5.7.6) was thus on the verge of being a stand-alone instrument, requiring a minimum of manual intervention during OTR measurements, similar to commercial instruments.

For the access valves of the receiving cavity, no valve actuators were commercially available. In consequence, the entire drive train for valve actuation had to be designed from scratch. The OTR instrument modified by implementation of valve actuators is shown in Fig. 5-5. In the concept established, the torque produced by a stepper motor (Nanotec [164], Type ST4209L1704-B) is transmitted by a planetary gear train (Nanotec, Type GPLE40-1S-8), coupled into a bellow shaft (R+W, coupling Type BKL [165]) and finally transmitted to a standard 19-mm wrench which rests on the hexagonal "handle" of the access valve. Two of such actuator units, operating the inlet and outlet valve of the receiving cavity, are driven by a two-channel microelectronic controller (Nanotec, Type "SMCI21-1"). Communication with the controller is accomplished via a RS-485 protocol. The driver routines for the motor controller were implemented into the data acquisition and control software of the instrument.

As it turned out, the exact sequence and velocity of movements when operating the valves prior to the oxygen accumulation period influences the pressure inside the receiving cavity and has an impact on the overall measurement. Much effort was spent to investigate the ideal sequence of valve actuation to avoid these effects. On one hand, sealing the receiving cavity should be accomplished expeditiously. On the other hand, any flux-induced overpressure inside the receiving cavity should have degraded before the cavity is completely shut. Consequently, the inlet valve is closed rapidly, while the outlet valve is moved to the closing point in a sequence of three decreasing velocities. The sequence is modifiable and controlled by the data acquisition software.
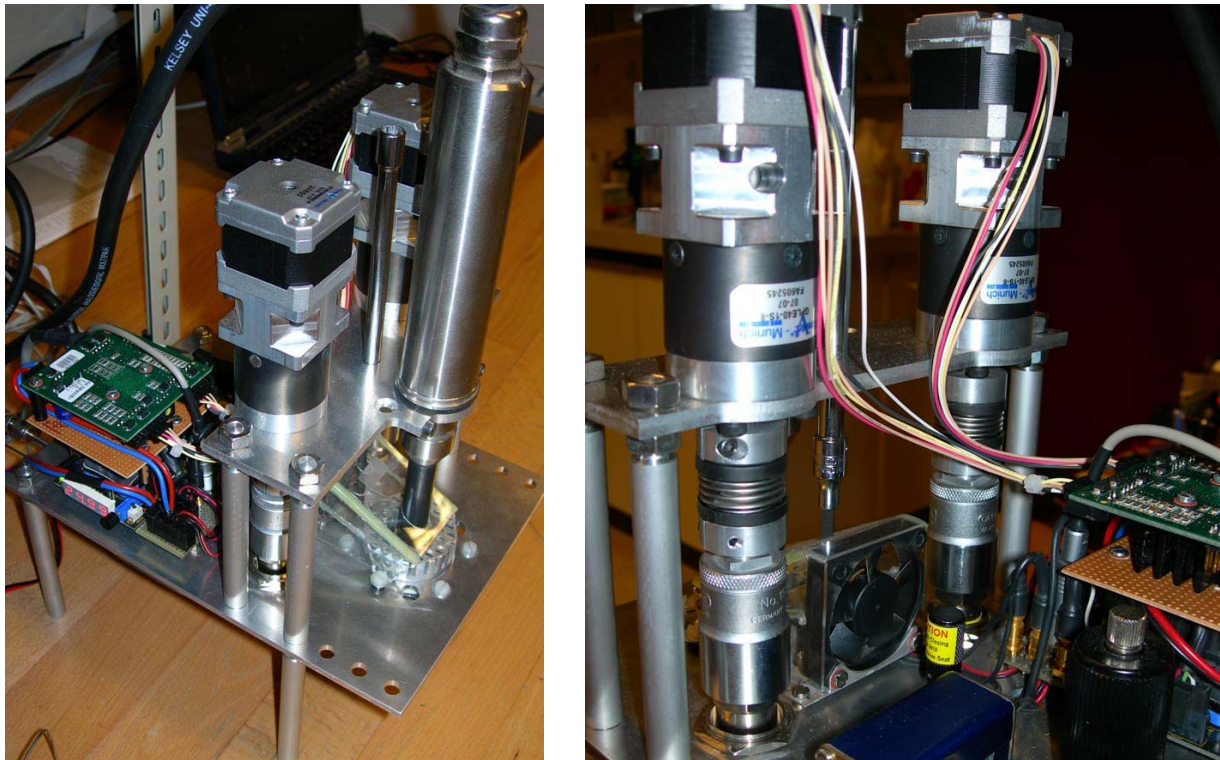
Fig. 5-5: **The OTR instrument with stepping motors implemented for autonomous, software-controlled actuation of the receiving cavity's access valves.**

5.3.7   Instrument Temperature Stability:
Self-Referencing of the Opto-Electronic System

Since, in case of ultra-barriers, very small concentration changes are to be recorded as a function of time, there are very challenging requirements to the stability of the system against fluctuations of parameters such as temperature or voltage. A radical improvement is accomplished, when a second LED is used for self-referencing the opto-electronic system, thus eliminating temperature effects to a wide extent. The two sources emit alternately, and the phase shift of the signal is referred to the phase angle measured for the reference. Traditionally, the excitation and reference light sources were selected from pairs of LED types which were thoroughly matched with respect to their temperature behaviour. The emission wavelength of the reference source (red LED) is chosen as to be insufficient for the excitation of any sensor luminescence, but it can pass the optical cut-off filter in front of the detector. The wavelength of the excitation source (typically a blue-green LED) is, in contrast, blocked by the filter and does not reach the photodiode.

In early stages of the project, such a "green-red"-setup (see Fig. 5-6) was used. However, the temperature stability soon turned out to be insufficient when low OTRs were to be measured. Triggered by the emerging stability demands, Joanneum Research invested some research efforts in the evolution of a latent idea for a superior referencing method in 2006.
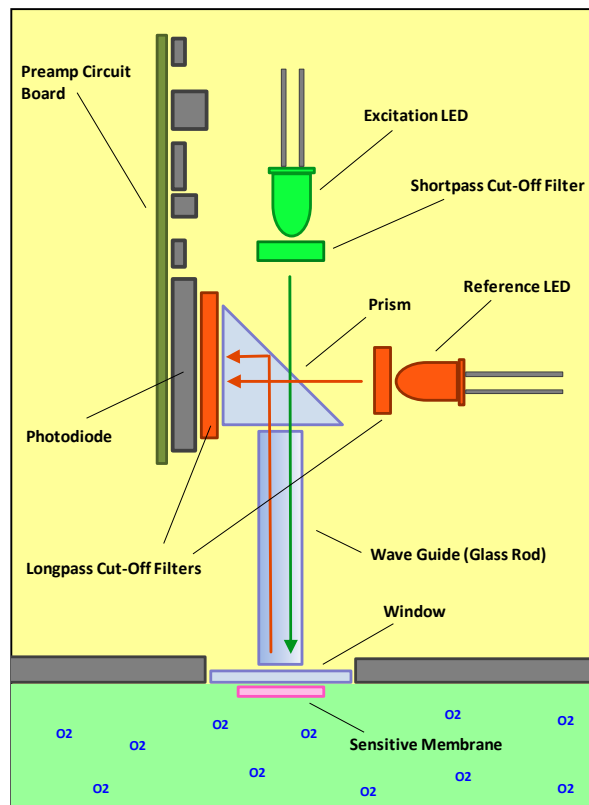
Fig. 5-6: Self-referencing opto-electronic setup using a matched pair of different LEDs.

When two identical LEDs ("green-green") are used, the signal stability is once more improved dramatically. In this case, the emission of the reference must be passed directly to the photo-detector without irradiating the opto-chemical sensor (see Fig. 5-7). An according patent was filed [166]. As it turned out in 2017, another group has worked on this principle in parallel but completely independently and applied for according IP protection only months earlier than Joanneum Research [167].

The enhancement accomplished by implementation of the modified opto-electronics in April 2006 had a very significant impact on the performance of OTR instrument, improving the limit of detection by orders of magnitude. It shall be noted, that, despite all referencing measures taken by Joanneum Research, there is a residing temperature dependence of the opto-electronic readout module, which becomes a significant obstacle in cases of very high-end performance demands to the equipment, that is, when very low OTRs shall be measured.

In the current setup, the opto-electronic probe is not temperature-stabilized, and thermo-stabilization of the existing equipment using Peltier elements is constructively difficult. In the construction of any follow-up OTR instrument, such measures can easily be taken into consideration, however. Fortunately, the temperature effects can be mathematically compensated to a large degree (see section 5.5.1).
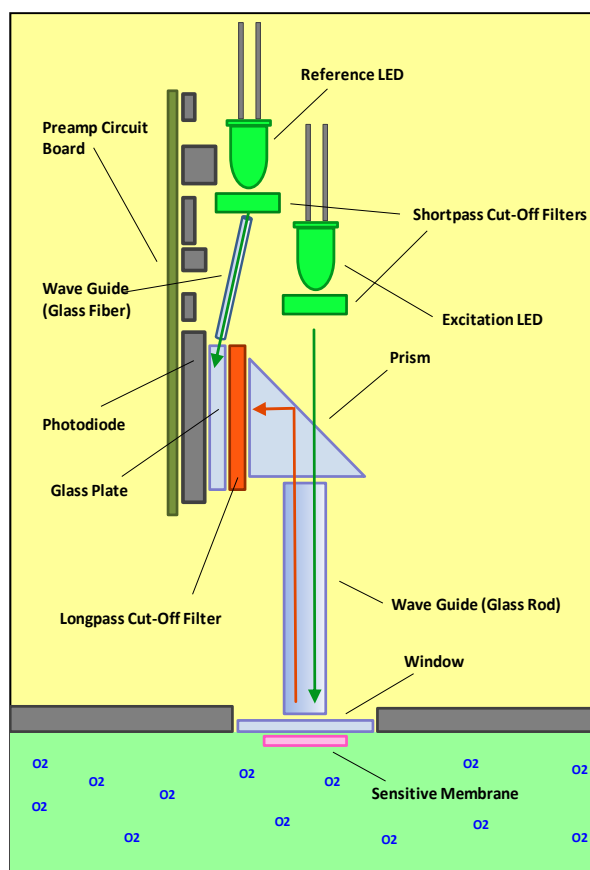
Fig. 5-7: Self-referencing opto-electronic setup using two identical LEDs.

5.4 THE CHEMISTRY

Relevant aspects about the nature of the opto-chemical sensor, the consumables and auxiliary materials are aggregated in this section.

5.4.1 Formulation of the Sensing Element

A functioning ultra-barrier membrane expectedly will permit the migration of only very small amounts of oxygen. An oxygen transmission rate of 10^{-3} [$cm^3\,m^{-2}\,day^{-1}\,atm^{-1}$] of a sample with an area of 707 mm^2 subjected to a pO$_2$ gradient of 5 bar will deliver only $1.47*10^{-7}$ cm^3 of oxygen per hour for accumulation inside the receiving cavity with a volume of 0.9 cm^3 (see also section 5.3.1), resulting in an oxygen partial pressure pO$_2$ of only 0.016 Pa or a fraction of 0.16 ppm, respectively. A typical overhead transparency PET film has an OTR of about 10 [$cm^3\,m^{-2}\,day^{-1}\,atm^{-1}$], thus higher by approximately 4 orders of magnitude. With such a sample, still only 16 Pa or 160 ppm of oxygen accumulate inside the receiving cavity within an hour. Considering these numbers, the demand for an accordingly performing oxygen sensor is evident.

For trace oxygen detection, a very suitable and widely used, commercially available sensor dye [46] is Palladium(II)-5,10,15,20-tetrakis-(2,3,4,5,6-pentafluorphenyl)-porphyrin ("PdTFPP", structure Fig. 4-4). As mentioned in 4.3.1.2 (spectra are given there), PdTFPP has an exceptionally long

unquenched luminescence lifetime (~ 1 ms), high oxygen sensitivity [46, 58], good photo-stability and absorption and similar emission maxima (552 nm and 670 nm, respectively [146]) as PtTFPP, the "working horse" for standard opto-chemical oxygen detection, permitting the use of the same optics. Thus, the opto-electronic equipment available at Joanneum Research could conveniently be integrated into the instrument with very minor modifications despite the lower quantum yield of PdTFPP. In the OTR instruments constructed, PdTFPP is being used exclusively until today.

Note that meanwhile there are a number of sensor dye molecules (such as fullerenes, for instance) with much longer luminescence lifetimes and, in consequence, higher sensitivities against oxygen [50, 58]. However, absorption and emission maxima are significantly different, and many of the dyes are not commercially available yet.
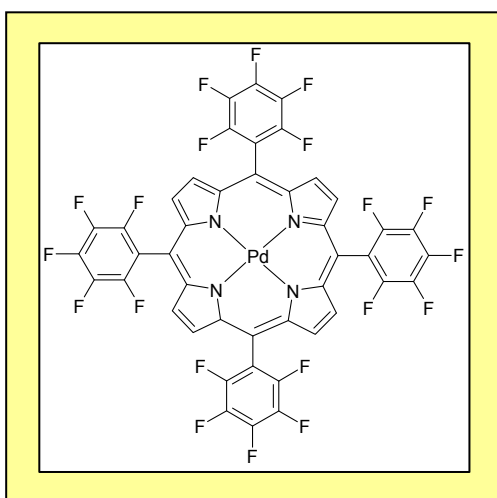
Fig. 5-8: **The Structure of Palladium(II)-5,10,15,20-tetrakis-(2,3,4,5,6-pentafluorphenyl)-porphyrin (PtTFPP).**

A sensor dye cannot be used in its pure form but must be immobilized in some sort of matrix material, commonly a dilute solid solution [47, 50]. Polystyrene was chosen as the immobilisation matrix in earlier projects of Joanneum Research due to the pronounced long-term ageing stability of the resulting sensors and the acquired expertise with the material. The thus obtained dye/ matrix formulations were thoroughly tested and are meanwhile well-established in a number of applications [46, 50].

Throughout the first two years of the Flexonics project, polystyrene was used as the matrix material for the opto-chemical sensing element. However, polystyrene is by far not the most permeable polymer with respect to oxygen, and a matrix promoting an easier penetration of oxygen molecules generally results in an improved sensitivity [46, 47, 50]. Nevertheless, it must be kept in mind that, depending on the matrix polymer, the behaviour of PdTFPP in terms of solubility, leaking, aggregation and ageing may be affected to a significant degree, when compared to polystyrene matrices. The matrix material hence requires careful selection involving some trade-offs between sensitivity, stability, dynamic range and general handling properties.

In 2007, a survey on high permeability polymers based on the work of Trinkel [57] and encouraged by patent literature [168] was conducted. The focus was laid on perfluorinated, soluble polymers such as TeflonAF® [169], Hyflon® [170] or Cytop® [171] which could potentially be used as a matrix (see also section 1.6). The chemical environment of the materials gave reason to expect excellent compatibility with PdTFPP. All these polymers are in their glassy state at room temperature, that is, well below their glass transition (see section 1.3.2) and have a high fraction of free volume (see section 1.3.3). In addition, the siloxane-based rubbery polymer PTMSP was tested.

On basis of the results and conclusions acquired in the matrix survey, a formulation comprising TeflonAF® 2400 (Fig. 5-9) as the matrix was chosen as the best compromise between sensitivity and ageing behaviour.
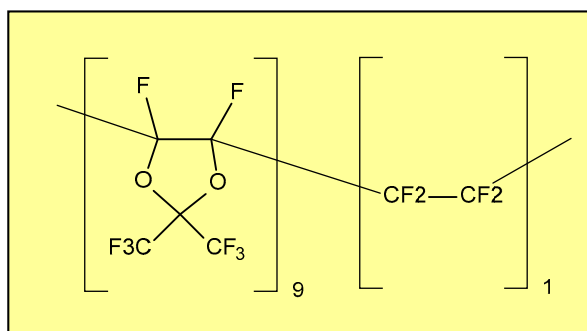
Fig. 5-9: TeflonAF® 2400 (2,2-bistrifluoromethyl-4,5-difluoro-1,3-dioxole/tetrafluorethylene copolymer)

First tests were performed on the manually operated demonstrator Version 1.5 (section 5.7.3). In the mathematically modelled calibration characteristics (see section 4.3.1.3), sensitivity is expressed by the magnitude of the Stern-Volmer quenching constant K_{SV}, which increases by a factor of ~100 when using TeflonAF® 2400 as the matrix instead of polystyrene (see Fig. 5-10). Using the enhanced frequency domain instrumentation provided by Joanneum Research (see section 5.3.7), a resolution below 0.001 Pa is furthermore accomplished. Around 2007, the system was thus among the most sensitive oxygen detectors available [57]. In consequence, a very substantial improvement of sensitivity of the overall instrument effectuated by using the PdTFPP/ TeflonAF® 2400 sensor formulation could be demonstrated.

Comparison of Sensitivity of PdTFPP with different Matrix Materials

TeflonAF 2400

PHI_0	-53.23905
F_{PC}	0.75524
K_{SV}	**0.02046**

TeflonAF 1600

PHI_0	-55.00786
F_{PC}	0.79427
K_{SV}	**0.0118**

Polystyrene (Reference)

PHI_0	-52,84233
F_{PC}	0,83365
K_{SV}	**0,000207**
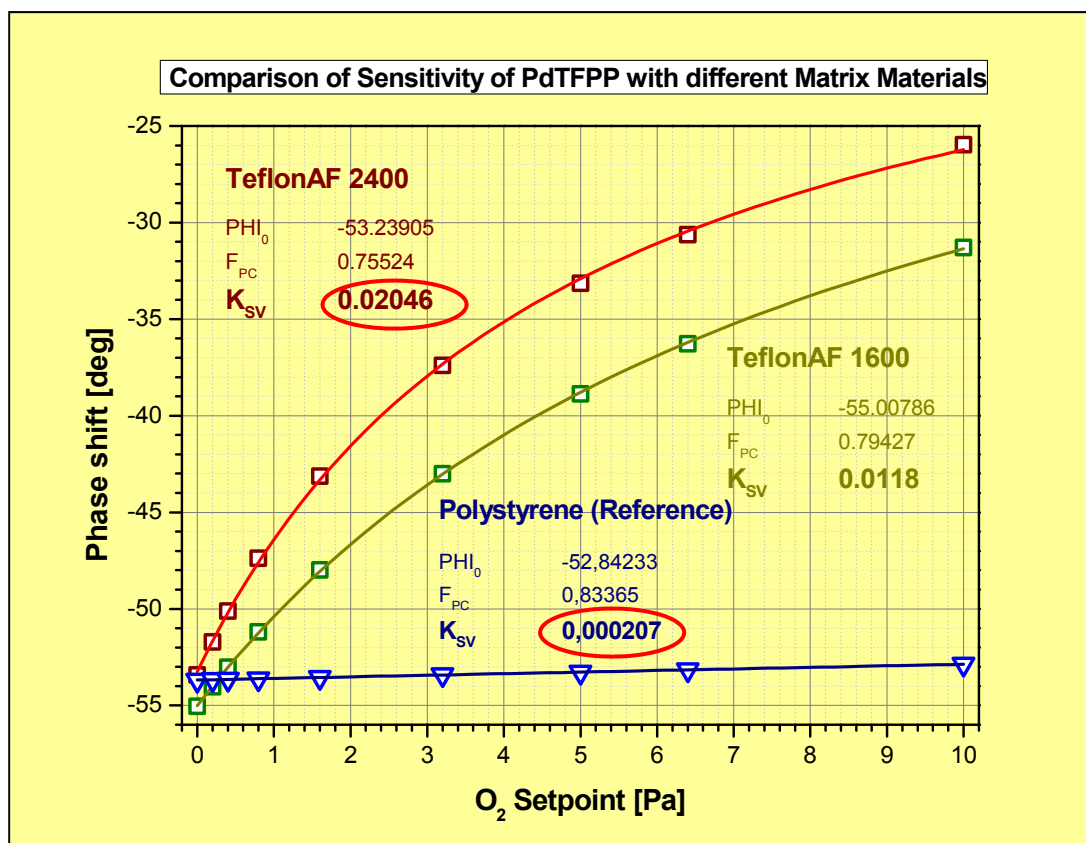
Fig. 5-10: The calibration characteristics for PdTFPP immobilised in a polystyrene matrix (blue), TeflonAF® 1600 (dark yellow) and TeflonAF® 2400 (red). K_{SV} of the TeflonAF® 2400-based senor is by a factor of 100 larger than with polystyrene

The improved sensor response renders the entire system much more immune against temperature fluctuations and electronic noise, which are, in case of the OTR measuring application, the main contributors to measurement uncertainty. However, the usable dynamic range of the sensor is, due to the extraordinarily effective luminescence quenching ability in this matrix, limited to 0 - 10 Pa or 0 - 100 ppm oxygen, respectively. Considering an accumulation period of 1 hour, the highest measurable OTR using this sensor is in the order of 6 [cm^3 m^{-2} day^{-1} atm^{-1}]. In 2016, however, the dynamic range of the sensor could be extended by implementation of an enhanced mathematical model for the calibration characteristic (see section 5.5.2), enabling the characterisation of OTRs exceeding this limit. Furthermore, the use of test gasses different from oxygen is an option (see section 5.4.2.3).

After the performance and ageing evaluation, the autonomous OTR measuring instrument Version 2.2 (see section 5.7.6) was upgraded by implementation of the new sensor formulation (Version 2.5, see section 5.7.7). Since the end of 2007, all OTR results were obtained using the improved PdTFPP/ TeflonAF® 2400 sensor.

As already indicated, the improvement in sensitivity of oxygen detection has a significant impact on the overall performance of the OTR measuring device. In Fig. 5-11, the standardised uncertainty (level of confidence: 95 %) for the results obtained is plotted as a function of the OTR. Thus, the

measurement uncertainty (measure of repeatability of data acquisition using the same sample) was improved by about a factor of 10.

Extrapolation of the cloud of red data points (corresponding to results acquired using the PdTFPP/ TeflonAF® 2400 sensor) suggests that oxygen transmission rates at the lower end of the 10^{-5} [cm^3 m^{-2} day^{-1} atm^{-1}] regime are measurable with respect to repeatability (uncertainty smaller than 1, level of confidence in the calculation of uncertainty 95 %).
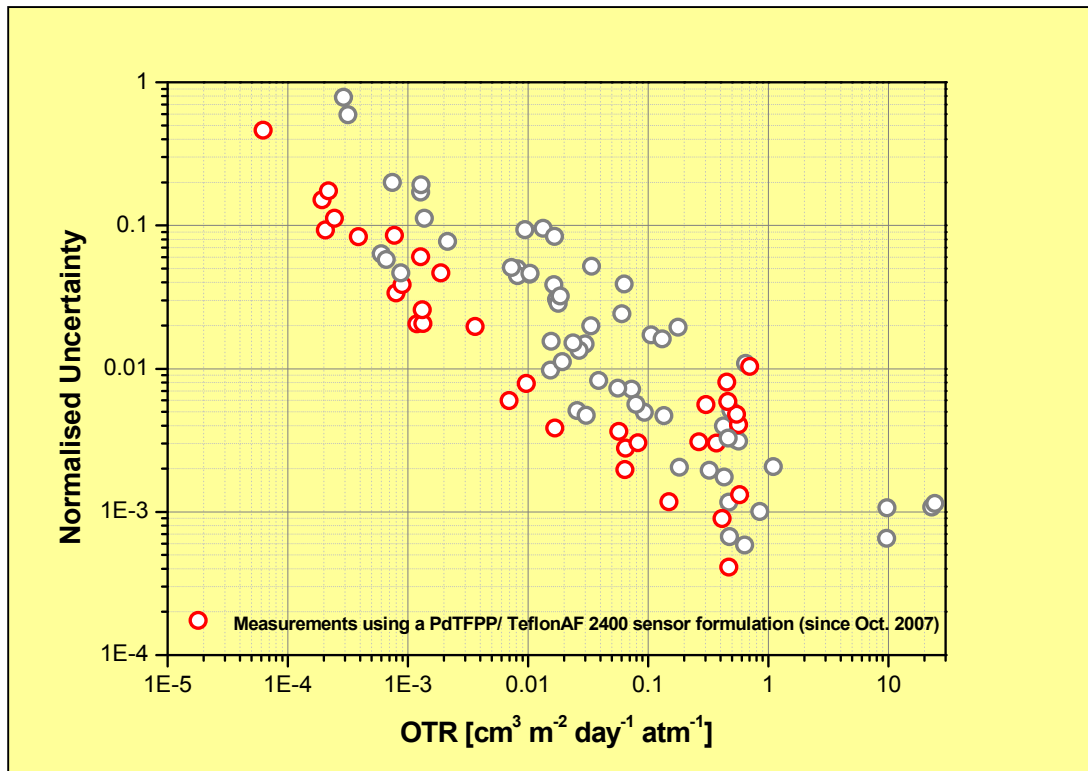
Fig. 5-11: **Normalised repeatability uncertainty (level of confidence: 95 %) of OTR results as a function of OTR. Red: Data acquired using a PdTFPP/ TeflonAF® 2400 sensor formulation. Grey: Previous data acquired using PdTFPP immobilised in polystyrene.**

As reported [57], the TeflonAF®-based sensor formulation exhibits a somewhat more distinct ageing behaviour than the previously used polystyrene matrix. However, the signal drift was found to be pronounced only for a freshly prepared sensor. After some period of ageing, the performance stabilized, which is attributed to the gradual removal of residual solvent by evaporation [172]. This is in contradiction to the observations of Trinkel [57] who did not attain stable sensors based on a TeflonAF® matrix at all. In this context it has to be acknowledged that the membranes currently used in the OTR instruments were prepared in 2009 and are in permanent service for 8 years now. Re-calibration turned out to be necessary only in intervals of more than 18 months.

In case of the OTR measuring application, only relative changes of oxygen are considered while absolute concentrations are of little relevance. Hence, the sensor drift is not so much an issue anyway as long as the inclination of the calibration characteristic is not affected. Fortunately, the characteristic is fairly stable in this context. The drift of the baseline itself (no oxygen present) of the

TeflonAF®-based sensor after one week of ageing would corresponds to an apparent oxygen transmission rate of about 10^{-6} [cm^3 m^{-2} day^{-1} atm^{-1}] and is thus negligible.

5.4.2   Gas Supply

The OTR measuring instrument is operated using nitrogen (quality grade >99.999 %) and oxygen gasses (quality grade >99.999 %), which are supplied from conventional laboratory steel containers. The gasses are passed into the devices through 1/8 inch stainless steel capillaries without further pre-conditioning measures (regarding an exception see the following section). The gas consummation of a few millilitres per minute is, compared to commercial instruments, quite low.

To date, there was no requirement for the implementation of cost-intensive mass flow controllers in order to measure and control the flow rates of the gasses. For an estimation of the fluxes through the different circuits inside the instrument, the ends of the gas outlets are immersed in water filled into small glass vials. In that way, a simple and cost-effective visual control ("bubble counter") of the gas flow is ensured.

5.4.2.1   Ultra-Pure Nitrogen

In general, the purity of nitrogen gas of quality grade >99.999 % is sufficient for an operation of the instrument. If membranes with very oxygen small transmission rates are investigated, a somewhat surprising behaviour can be observed. In particular, apparently *negative* OTRs are detected.

The reason for the phenomenon remained unclear until 2007. Eventually, the very slow chemical absorption of minute amounts of oxygen at the stainless steel surface of the receiving cavity was suspected to be the cause. When starting the "accumulation" of permeating oxygen (with a *very* small permeation rate in this case) at a "zero" level of about 0.1 Pa (typically the level of oxygen impurity in the nitrogen quality grade used), the rate of chemisorption of oxygen exceeds the ingress due to permeation, resulting in a gradual reduction of the concentration in the receiving cavity and hence an apparently negative OTR. In a series of experiments, the assumption could be confirmed.

One of the last concepts pursued in this context was the point-of-use purification of the feed gas to remove even last traces of oxygen impurities. Thus, gas purification cartridges (ALPHAGAZ Purifier O_2-Free) which accomplish a level of remaining oxygen impurity below 5 ppb [149] were inserted in the gas supply. In consequence, the phenomenon of apparently negative OTRs was not observed anymore.

Despite the fact that the chemisorption of oxygen inside the cell is an issue only when measuring very low OTRs and soon becomes insignificant if transmission rates increase, the instruments were exclusively operated with purified nitrogen since 2010. Due to the small flow rates withdrawn by the instrument the cartridges have a service life of more than two years before replacement is required.

The conclusions obtained in the experiments were incorporated in the construction of a further demonstrator instrument in 2008 in a number of constructional details (see sections 5.4.3 and 5.7.8).

5.4.2.2 *Measurements at Defined Relative Humidity*

So far, OTR measurements were carried out using dry oxygen and nitrogen gasses, thus at a relative humidity of 0 %. Measurements at a defined humidity should, in theory, be feasible. However, the integration of devices providing moist gasses with a well-defined relative humidity is a major cost issue and has therefore not been pursued yet.

Furthermore, attention must be paid to potential issues arising from electrochemical processes at the surfaces of cell components made of different metals (cell body and porous metal support, for instance). Although no real evidence has been obtained so far, an occasionally very unusual behaviour of the instrument in case of the ingress of excessive humidity or even liquid water supports according suspicions. The materials used for the construction of an instrument capable of operating with moist gasses should therefore be selected with consideration.

5.4.2.3 *Characterisation of Highly Permeable Membranes: A "Workaround"*

In section 5.4.1, the limitation of the reliably quantifiable OTR to a maximum of about 6 [$cm^3\,m^{-2}\,day^{-1}\,atm^{-1}$] is discussed in detail. In brief, the oxygen amount inside the receiving cavity must not exceed 10 Pa within the accumulation period of 1 hour in order to remain within the dynamic range of the opto-chemical oxygen sensor.

One option to circumvent the limitation is the substitution of the oxygen test gas with a gas containing smaller amounts of oxygen. Thus, the resulting partial pressure gradient across the membrane and, in consequence, the driving force for the migration of oxygen is reduced. In absolute numbers, oxygen is accumulating inside the receiving cavity at an accordingly smaller rate. Taking into account the reduced gradient, the oxygen transmission rate can be correctly calculated in the usual dimensions.

In a number of characterisations of highly permeable sample membranes, a test gas containing 10 Pa of oxygen was successfully used instead of pure oxygen. Considering the resulting partial pressure gradient, the OTRs computed by the software had to be multiplied by a factor of 10000 to obtain the correct transmission rates. In theory, the range of the instrument should be extended to a transmission rate of 60000 [$cm^3\,m^{-2}\,day^{-1}\,atm^{-1}$] with this test gas.

5.4.3 Oxygen Absorption at the Cell Surface

With an otherwise untreated high-quality nitrogen gas supply (see section 5.4.2.1), a slightly *negative* OTR result is quite surprisingly but reproducibly obtained in investigations regarding the

zero level noise. For such experiments, a massive and therefore securely airtight 100 μm aluminium or stainless steel membrane is used as the "sample". Similar behaviour is observed with transmission rates below 10^{-3} [cm^3 m^{-2} day^{-1} atm^{-1}]. The phenomenon was insinuated already with the initially used PdTFPP/ polystyrene sensors and became doubtlessly discernible with the introduction of the more sensitive PdTFPP/ TeflonAF® formulation.

Until the behaviour was fully understood, the negative "offset" was subtracted from the "raw" OTR result obtained for real samples during data processing. The standard deviation of the "zero"-OTR obtained with metal membranes was likewise added to the standard deviation of the OTR result of the sample. The combined standard deviation was then used for the calculation of the standard error of the mean.

This, with respect to the assumed measurement error, conservative procedure appeared as the most correct one – at the cost of increasing measurement uncertainty of smaller OTRs. However, the offset is of no relevance for OTR results > 10^{-2} [cm^3 m^{-2} day^{-1} atm^{-1}] and becomes significant in the 10^{-3} [cm^3 m^{-2} day^{-1} atm^{-1}] regime and below. Below 10^{-3} [cm^3 m^{-2} day^{-1} atm^{-1}], a slightly negative OTR result (but very reproducibly *less negative* than in case of the aluminium membrane) was obtained, substantiating that the chosen data processing procedure was reasonable.

5.4.3.1   *The Cause of the Phenomenon*

The reasons for the behaviour remained unclear until 2007, when the more sensitive TeflonAF®-based sensor membrane was implemented (see section 5.4.1). In data acquired with the less sensitive polystyrene-based sensor, the apparent decrease of oxygen amount was discernible only in the form of a slight negative inclination of the "ground level" noise recorded during the "permeation measurement" with a steel or aluminium membrane as the sample (red plot in Fig. 5-12). Lacking high-resolution data, the phenomenon was attributed to small temperature changes resulting from Joule-Thompson-effects during the re-initialisation purge of the cell, and it was expected to observe a fundamentally different magnitude of the effect using the new TeflonAF®-based sensor formulation, due to its different temperature response.

According experiments using the enhanced sensor, however, revealed just exactly the same negative inclination - but with much higher resolution - of the ideally flat and even "baseline" that should be obtained in the absence of oxygen permeation processes (blue plot in Fig. 5-12). Since the compared sensor membranes have intrinsically different temperature drift characteristics but the effect is observed in a similar magnitude in both cases, it is concluded that indeed a decrease of the oxygen amount is occurring. The Joule-Thompson-effect must therefore be excluded as the cause.
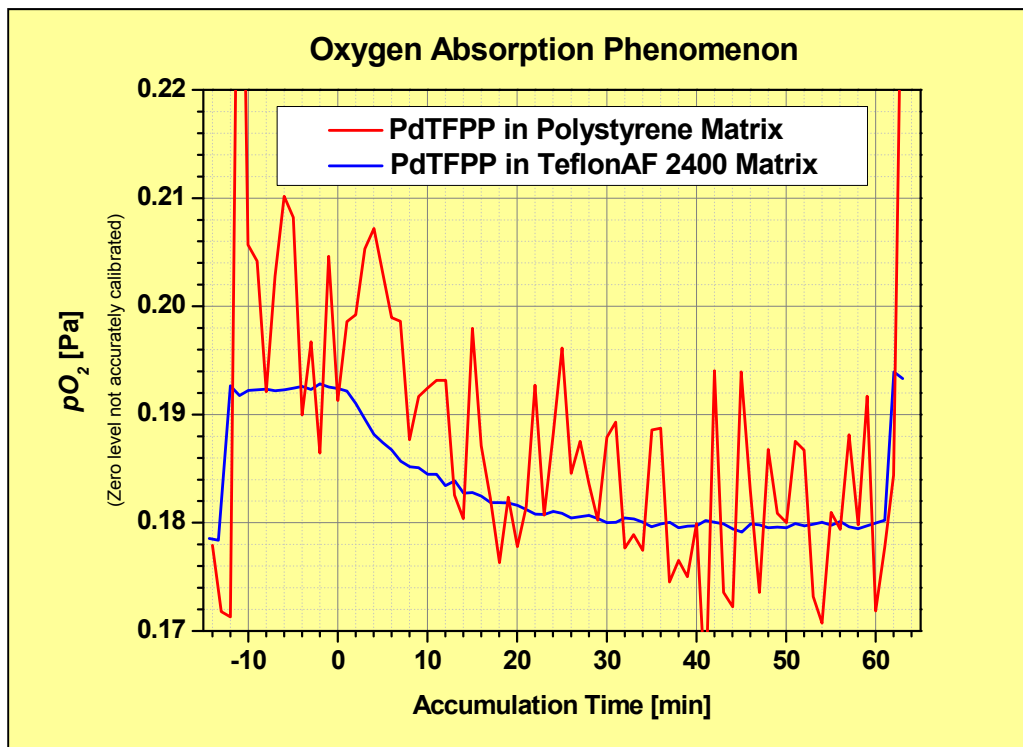
Fig. 5-12: Oxygen as a function of accumulation time. -12 min – 0 min: The receiving cavity of the cell is being purged with N_2 gas (<2 ppm O_2). At t=0 min, the access valves are closed and the receiving cavity is hermetically sealed. No ingression of O_2 is possible through the steel membrane used as the sample. 0 min-60 min: A detected decrease of O_2. The magnitude of decrease is equal for the two different sensors used in the experiments.

It was found that the rate of oxygen "disappearance" is reproducibly dependent on the surface-to-volume ratio of the receiving cavity of the device. In a number of experiments, the ratio was changed by e. g. removing the porous metal support (larger volume, smaller surface) or implementation of microscope glass slide pieces (smaller volume, glass surfaces considered inert). In addition, the two cells used for according experiments have different surface-to-volume ratios, and the observed "rate of disappearance" changes accordingly. The most distinct effect was observed, when 0.5 grams of powder prepared from exactly the same stainless steel used for manufacturing the cell (No. 1.4305) were accommodated in the receiving cavity. Accordingly obtained plots are shown in Fig. 5-13.
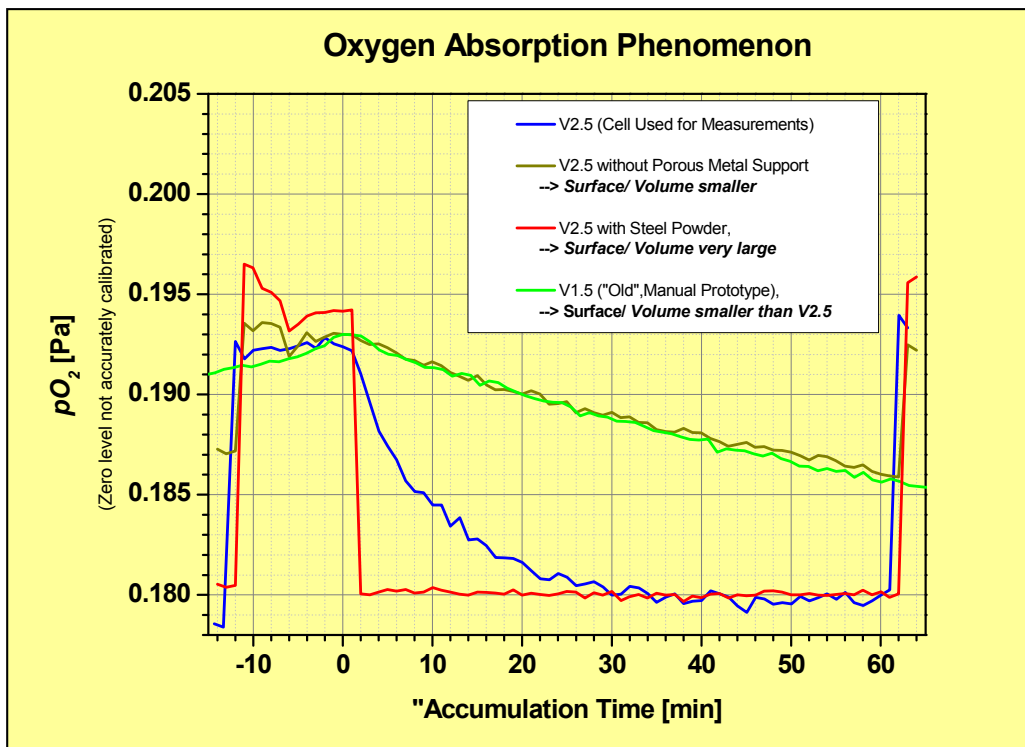
Fig. 5-13: Oxygen as a function of accumulation time. -12 min – 0 min: The receiving cavity of the cell is being purged with N$_2$ gas (<2 ppm O$_2$). At t=0 min, the access valves are closed and the receiving cavity is hermetically sealed. No ingression of O$_2$ is possible through the steel membrane used as the sample. 0 min-60 min: A detected decrease of O$_2$. Magnitude of decrease is dependent on the surface-to-volume ratio of the receiving cavity.

From a thorough analysis of the observations it is concluded, that even traces of oxygen present in the nitrogen gas used to operate the cell (< 1 ppm oxygen according to the specification) are chemically adsorbed by the steel surface of the receiving cavity.

During the initialisation, the cell is being purged with nitrogen gas, thus introducing said trace amounts of oxygen. When the valves are closed and the cell is hermetically sealed, the ingression of oxygen is only possible through the sample membrane itself. However, a massive 100 µm steel membrane (which can be considered absolutely airtight) was used as the "sample" in these experiments. In theory, the oxygen amount inside the cell should remain constant in the absence of leakage. In case of leakage or permeation, it should increase.

The reproducible "disappearance" of oxygen by adsorption to stainless steel surfaces does not appear suggesting at a first glance. However, since the rate of disappearance is strongly dependent on the surface-to-volume ratio of the cell, a certain form of adsorption or chemisorption of oxygen onto the surfaces present remains the only explanation. The adsorption effect was particularly impressive in case of the very large surface provided by the placement of steel powder inside the cell.

To assess the plausibility of the theory, stoichiometric considerations were carried out. Due to the extraordinary resolution of the new oxygen sensor, the disappearance of residual oxygen appears extreme. It must not be forgotten, however, that in fact only *minute* amounts of O$_2$ are adsorbed in

the cycle duration of 1 hour, that is, 0.013 Pa of oxygen in a volume of 902 mm³. With this amount of oxygen, only one out of about 100000 iron atoms located directly at the steel surface can be oxidised to Fe_2O_3.

The stainless steel used for the fabrication of the cell (No. 1.4305) receives its properties through a content of chromium of about 15 percent. Chromium is actually more ignoble than iron, it should therefore be prone to oxidation even more. However, chromium is, just like aluminium, forming oxide layers which act as a very effective diffusion barrier and thus prevent the oxidation of atoms further in the bulk of the material – a property not found in case of iron oxide. If the protecting layer of chromium oxide is damaged or even removed, a new barrier layer is immediately formed by oxidation of further chromium atoms. The oxidation barriers are therefore "self-healing", and stainless steel becomes "stainless", at least on a timescale relevant for common technical applications.

Very thin permeation barriers of metal oxides are brittle and therefore subject to damage by mechanical stress – and barrier defects are omnipresent, a fact that anyone researching ultra- barrier coatings can likely appreciate. Because the defects in chromium oxide are self-healing, there is always a slow oxidation process going on, repairing defect sites, but also consuming oxygen at a very gentle rate. There is a strong indication, that this effect causes the "negative OTR" phenomenon.

Mechanistically, it is a non-catalytic, heterogeneous reaction. In order to investigate the kinetics of the oxygen adsorption process, the experiments were repeated using an oxygen/ nitrogen mixture (10 Pa O_2 in N_2 gas) instead of pure N_2 to purge the cell. The rate of oxygen "disappearance" did not grow proportionally with the amount of O_2 in the gas. In contrast, a rather constant absorption rate (but not yet a perfectly linear function) was found at higher oxygen levels, while the typical "exponential decay"-like shape of a reaction approaching equilibrium gradually appeared as the oxygen level approached zero. Attempts to fit the recorded data with an exponential function were therefore only successful if very small O_2 levels were involved.

The observations indicate that the non-catalytic, heterogeneous reaction is, at least in the concentration regime involved in the barrier measurements, just in transition from diffusion control (=constant rate at higher O_2 levels) to reaction control (rate is a function of concentration at lower O_2 levels). Mathematically, a rate law accounting for such complex boundary conditions is analytically not accessible, and attempts to compensate numerically for the absorption effects from a kinetic point of apparently view have to fail. A literature survey was by no means encouraging in this context.

Reviewing, from this point of view, the previously practised treatment of the negative zero offset phenomenon, a few remarks on the acquired OTR results have to be made. OTRs close to the limit of detection should be devoid of a systematic error caused by this phenomenon, because the measured offset of the "zero" sample is recorded at similar kinetic conditions as it is the case with very small permeation rates. With large transmission rates (and thus higher amounts of O_2 in the cell), the absorption kinetics soon reach a nearly constant rate, and the "loss" of oxygen is negligible compared to the rate of oxygen ingression through the sample membrane. In the intermediate

range, however, a certain systematic error must be expected, pretending OTRs that are lower than the actual ones. The absorption rate is underestimated in the practised data processing procedure and, in the concentration regime involved, also a function of the amount of oxygen being present. An estimation of the magnitude of the systematic error appears difficult due to the absence of sufficient reference results across the entire measurable range and the difficulty of mathematical modelling.

5.4.3.2   The Solution approach: Surface passivation

After oxygen absorption effects were identified as the cause of the phenomenon of negative OTR results, a survey about improvement options was carried out. The "negative offset" adds a significant uncertainty to the OTR results if considered according to the data processing routine discussed in the introduction of section 5.4.3. The circumvention of the effect should therefore lead to an improvement of measurement repeatability and, in consequence, an improved limit of detection.

Since a purely numerical compensation for the effect is not practicable due to the complexity of the respective kinetic equations, a solution to the problem was sought in the passivation of the relevant surfaces of the cell. One of the most inert (with respect to oxidation) yet non-brittle materials is metallic gold. The deposition of the metal on the cell surfaces should thus prevent or at least reduce the observed absorption/ oxidation phenomena.

An ideal solution – from a purely chemical point of view – would be the construction of the permeation cell of an intrinsically inert yet absolutely airtight material such as glass. Considering, however, the challenge of having to integrate features like valve seats, O-ring groves, gas capillaries etc. into a monolithic workpiece of glass, the realisation did not appear viable.

The concept of gold-passivation was one of the key features in the design of a second, enhanced and autonomously operating laboratory demonstrator (Version 3.0, see section 5.7.8). The functional surfaces (see Fig. 5-14) were covered with a thin layer of gold (Fig. 5-15) by means of "pulsed laser deposition", conducted by Joanneum Research, Department "Laser- and Plasma-Assisted Vacuum Deposition Processes".
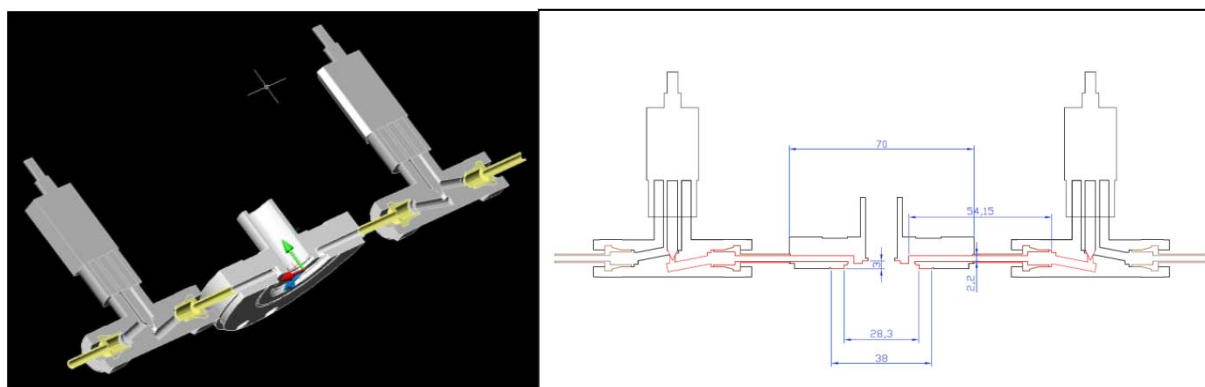
Fig. 5-14:   A cross-section through the receiving cavity and the access valves. In the sketch, the functional surfaces are marked red.

Fig. 5-15: The functional surfaces of the OTR measuring cell were gold-coated by means of "Pulsed Laser Deposition".

A galvanic deposition inside cavities is not feasible or at least very difficult due to the Faraday principle that prevents the penetration of an electric field into the interior of a hollow conducting body. Thus, most of the surfaces that are relevant in this context would not have been accessible at all.

With pulsed laser deposition, at least a part of these surfaces was successfully coated, not including, unfortunately, a significant surface fraction of the capillaries accessing the receiving cavity or the interior of the access calves. In consequence, a significant area of stainless steel surface still remained bare. In an alternative passivation strategy, it was attempted to protect the uncoated surfaces by induction of glass capillaries into the bores and padding the interstice with epoxy resin. However, the capillaries were fractured in the assembly process of the instrument (see the completed assembly in Fig. 5-16) due to mechanical stress (small yet sufficient torsion forces acting when the valve joints were mounted) and were therefore removed again.

The characterisation of "Zero-OTR", thus absolutely airtight metallic membranes[30] (steel or aluminium) has indicated *only some* improvement of the absorption behaviour. In addition to the cell surfaces, the large surface area of the porous bronze membrane support (see section 5.3.3.1) obviously contributes to the phenomenon by absorbing oxygen in a slow corrosion process. Apparently however, the bronze surfaces are less active in this regard than surfaces of stainless steel, considering the relatively large surface area in relation to a relatively small contribution to the phenomenon.

---

[30] Ideally, thin discs of glass or gold-coated metal membranes should be used as "Zero-OTR" samples to preclude absorption effects by the sample itself. Such samples were not obtained, however.

Fig. 5-16: The Completed Assembly of the OTR Measuring Device. In the Background of the Left-hand Image, the Device Used for Routine Measurements is also seen.

In 2010 and thus well after the end of the Flexonics project, the porous metal was replaced with intrinsically inert materials like Teflon (see section 5.3.3.2) and, in 2016, with sintered glass (section 5.3.3.3). The measures led to a further improvement but not to a complete elimination of the absorption phenomena.

By the end of Flexonics and with supports of porous bronze installed, the gold-coated instrument Version 3.0 was capable of OTR quantification with similar performance than the previously constructed Version 2.5, thus with satisfactory repeatability until the 10^{-5} [$cm^3\,m^{-2}\,day^{-1}\,atm^{-1}$] regime. Insufficient data of ultra-barriers have been generated by September 2017 to statistically asses the performance in this context with the sintered glass filters installed.

5.5 THE PROCEDURES AND ALGORITHMS

A major fraction of the efforts invested and performance improvements accomplished trace back to the processing of the data acquired by the instrument. The measures are addressing a number of different levels of the multi-stage cascade of data manipulation until an OTR result is generated. This section focusses on issues regarding the procedures and algorithms involved in the transformation of raw data to oxygen transmission rates.

5.5.1 Compensation for Electronics Temperature Fluctuations

In an electronic setup that is not thermo-stabilized, the temperature of circuit components will inevitably be a function of the room temperature. Particularly LEDs but also photodiodes, capacitors, transistors or resistors will, to a certain degree, change their behaviour with respect to steady-state properties as well as the timing behaviour in transient processes. In this context, an unreferenced phase-fluorimetric system is rather sensitive to temperature fluctuations and the resulting signal fluctuation is distinct. The referencing scheme for the opto-electronics followed at the beginning of

the project (see Fig. 5-6 in section 5.3.7) neutralized the majority of temperature-induced signal drift. In a setup demanding such extraordinary signal stability like the OTR instrument, however, the remaining interferences still are covering up the usable signal to an unacceptable degree. The accommodation of the instrument inside a climate chamber would be at the expense of losing accessibility and imply a significant additional investment, as discussed in section 5.3.4. Alternative solutions were therefore preferred.

A significant improvement in temperature stability of the opto-electronics was accomplished by Joanneum Research by development and integration of an enhanced and meanwhile patented self-referencing scheme [166] into the setup (see section 5.3.7). Despite the quality of the method, there is still a small residual temperature-induced drift of the phase signal which is totally irrelevant when samples of considerable transmission rates are being measured (that is, when a distinct ingress of oxygen into the receiving cavity is detectable) but interferes significantly near the limit of detection of the instrument.

The noise of an ensemble of otherwise "equal" results of the same sample (see the concept of averaging multiple data points to reduce the measurement uncertainty discussed in section 4.3.2.2 and 5.5.4.3) is once more reduced if the influence of temperature is considered in a linear correction term during data processing. Physically, merely the temperature inside the opto-electronics probe enclosure is measured by a thermistor, recorded together with the rest of the raw data and considered during data processing.

For the determination of the correction term, phase angle and temperature are recorded over a period of a few days while purified nitrogen is being passed through the receiving cavity, ensuring truly oxygen-free conditions at the opto-chemical sensor. The recorded phase shift is plotted as a function of opto-electronics temperature and the data are approximated by linear regression. In the processing of sample data, the phase shift reading is processed by the thus determined correction term before it is translated into an oxygen value. Despite the simplicity of this purely empiric compensation scheme, the signal-to-noise-ratio of OTR results near the detection limit improves impressively by almost one order of magnitude.

5.5.2 Extended Dynamic Range of the Sensing System: 2-Component-Stern-Volmer Model

Real-life opto-chemical oxygen sensors with perfectly linear Stern-Volmer-plots τ/τ_0 – as predicted by the theory – are much more an exception than the common rule [173]. An oxygen-sensitive dye dissolved in small amounts in a solvent or matrix material, respectively, is expected to behave uniformly across the bulk of the "solution" and should thus show an oxygen-dependent, single-exponential decay of the phosphorescence as a function of time. Such an "ideal" sensor would indeed yield linear Stern-Volmer-plots. Linear plots are, however, only observable for sensor dyes in *liquid* solutions with very dilute concentrations. As soon as the chromophores find themselves surrounded by a solid phase or exist in a more dense population, effects like self-aggregation or

micro-crystallisation, localized gas diffusivity changes, variations in O_2-accessibility, changes in the medium polarity or other interactions with the matrix material lead to deviations from linear behaviour by formation of multiple, distinct micro-domains. The micro-domains each may have a different photo-physical behaviour and, in particular, correspond to different phosphorescence decay times. In addition, the phosphorescence of some of the micro-domains may be a function of oxygen to a different degree while part of the phosphorescence does not depend on oxygen at all. The phosphorescence evaluation of the bulk material merely "sees" an averaged sum of multiple exponential decay components which are responsible for the more or less pronounced deviations of the Stern-Volmer-plots of real sensors from linearity [147, 174-177]. The existence of multiple populations of chromophores or micro-domains in a macroscopically homogeneous sensor film was previously proposed in literature [173, 178, 179], and lately the existence of distinct micro-domains could even be made visible by confocal fluorescence lifetime imaging spectroscopy [174].

When having to comply with even only slightly advanced requirements with respect to measurement accuracy, one must inevitably model the non-linear behaviour of the sensor films. Joanneum Research, who provided the opto-chemical sensing equipment used for the development of the barrier testing device had years of experience with the Stern-Volmer-Falselight model (see section 4.3.1.3) and processed the raw sensing data accordingly in the majority of their sensing applications, including a significant part of the development of the barrier testing device.

The Stern-Volmer-Falselight model captivates through the relative simplicity but reveals some shortcomings when the residuals of a "best fit" of actually recorded calibration data are considered in more detail. The curvature of the model is somewhat too convoluted to precisely describe the actual relationship between oxygen partial pressure and phase shift angle. In consequence, systematic errors of a certain extent are introduced when calculating pO_2 from the phase angle, no matter how thorough the calibration. Near zero values, the results obtained in the calculation are somewhat too low. In the intermediate range, there are regions with results that are systematically too high. However, within the calibrated range of pO_2 errors are manageable.

When very airtight samples are to be characterized in the barrier testing device, the oxygen partial pressure will remain at levels around or below 1 ppm. At such low pO_2, the characteristic of opto-chemical oxygen sensors shows a steep gradient, that is, small changes in pO_2 are reflected by relatively large changes in phase angle and errors thus remain reasonably small. At the upper end of the calibrated range, the characteristic shows a much smaller inclination. Small errors in the measured phase angle or such caused by modelling residuals introduce much larger errors in this case. By thoroughly trading off the targeted dynamic range with measuring accuracy, these errors remain only just acceptable as well. An extension of the calibrated range would increasingly introduce "measurement" errors (that is, modelling deficiencies) at low and intermediate oxygen levels.

When pO_2 exceeds beyond the highest calibrated value, the model quickly fails completely. The results of the calculation of oxygen are progressively deviating towards infinity, before the Stern-Volmer-Falselight function reaches a pole and gives *negative* results for even higher pO_2 at the

sensor. The dynamic range of the sensor is thus strictly limited to the actually *calibrated* range (which is essentially a trade-off), and extrapolation of the characteristic beyond the highest calibrated value is essentially impossible or at least useless.

Since the barrier testing device was explicitly designed for the characterisation of ultra-barriers initially, a sensor formulation with a very steep characteristic and thus an impressive resolution had to be used – at the cost of extent of the dynamic range, which has its upper limit at 10 Pa pO_2 in this case. Unfortunately, the restrictions in "permissible" oxygen amounts accumulated during barrier testing prevent the characterisation of membranes with oxygen transmission rates beyond those found for e. g. aluminised food packages – and thus exclude the majority of typical membrane samples from the scope of the instrument, unless special measures are taken. Such permeable membranes would cause the oxygen amount to significantly exceed the dynamic range of the sensor within the time of accumulation, in some cases even within minutes or seconds.

In the context of ultra-barrier development, the limitation to low oxygen transmission rates is not considered an obstacle. However, an instrument with the flexibility to test common polymer films as well as ultra-barriers would be much more attractive for commercialisation than a highly specialized testing device for ultra-barriers exclusively. There are work-arounds such as a shorter time-window of accumulation that would enable testing samples with OTRs exceeding the device limit, but care must be taken in regard of the kinetic effects explained in section 5.5.3.

In view of the limitations, the use of a mathematical model describing the real behaviour of opto-chemical oxygen sensors more accurately over a wider dynamic range would be highly beneficial. In the period 2010 - 2014, very positive experience was made with a 2-component-Stern-Volmer-model [178, 180] in the course of the product development for a beverage oxygen sensor with extraordinary requirements imposed by the customer regarding the measurement accuracy. In view of the observed performance and potential, the model was implemented into the control software of the barrier testing device in the course of a demanding commissioned research project carried out on the laboratory demonstrators in 2016.

The respective mathematical model is based on the assumption of two distinct, in fact both - but each to a different degree - oxygen-sensitive populations of sensor dye molecules. The oxygen-dependent behaviour of the "additional" population is modelled by introduction of an extra Stern-Volmer-constant into the equation. The complexity of the model itself (see Equation 5-1 and compare with Equation 4-2) hardly increases, while the rearrangement necessary to calculate pO_2 from the phase angle (Equation 5-2) becomes more elaborate.

At the cost of this one additional calibration parameter, the model reflects the characteristic of the sensor formulation much more accurately, as it is indicated by the smaller residuals of a "best fit" of calibration data (or the "measurement" error introduced solely by modelling deficiencies, respectively, see Fig. 5-17). The main advantage, however, is the relatively steady behaviour when oxygen amounts exceed the calibrated range (see Fig. 5-18). Furthermore, a pole where calculation results jump from +infinity to –infinity, as it is the case with the Stern-Volmer-Falselight model, is no issue in this case. Thus, extrapolation of the characteristic towards higher oxygen amounts is possible

accepting a reasonable degree of error while, at the same time, the model is significantly improving the measuring accuracy at lower oxygen levels.

$$\frac{\Phi}{\Phi_0} = \frac{f_0}{1 + K_0 \cdot p_{O_2}} + \frac{1 - f_0}{1 + K_1 \cdot p_{O_2}}$$

pO_2	oxygen partial pressure
Φ	measured phase shift
Φ_0	phase shift at the absence of oxygen
K_1	component 1 Stern-Volmer constant
K_2	component 2 Stern-Volmer constant
f_0	false-light constant

Equation 5-1: **2-Component Stern-Volmer-model [178, 180]**

$$p_{O_2} = -\frac{1}{2 \cdot \Phi \cdot K_0 \cdot K_1} \cdot \left\{ K_0 \cdot [\Phi - \Phi_0(1 - f_0)] + K_1[\Phi - \Phi_0 \cdot f_0] + \sqrt{4 \cdot \Phi \cdot K_0 \cdot K_1 \cdot (\Phi_0 - \Phi) + \{K_0 \cdot [\Phi - \Phi_0(1 - f_0)] + K_1[\Phi - \Phi_0 \cdot f_0]\}^2} \right\}$$

pO_2	oxygen partial pressure
Φ	measured phase shift
Φ_0	phase shift at the absence of oxygen
K_1	component 1 Stern-Volmer constant
K_2	component 2 Stern-Volmer constant
f_0	false-light constant

Equation 5-2: **Calculation of pO_2 according to the 2-Component Stern-Volmer-model [178, 180]**
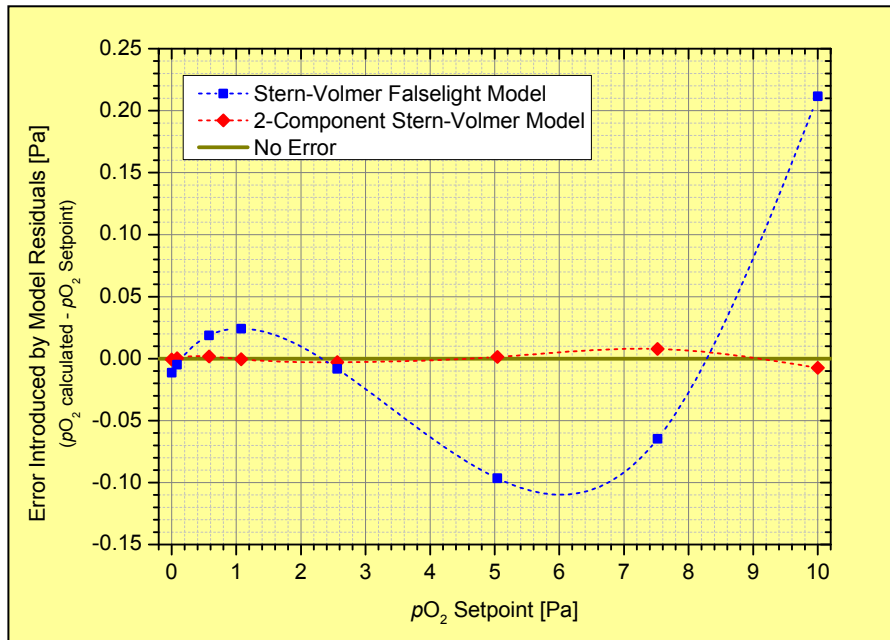
Fig. 5-17: Measurement errors introduced by calibration data fitting residuals of the Stern-Volmer-Falselight Model (blue), compared with those of the 2-Component-Stern-Volmer Model. The 2-Component Model is reflecting the behaviour of opto-chemical oxygen sensors much more accurately within the calibrated range.
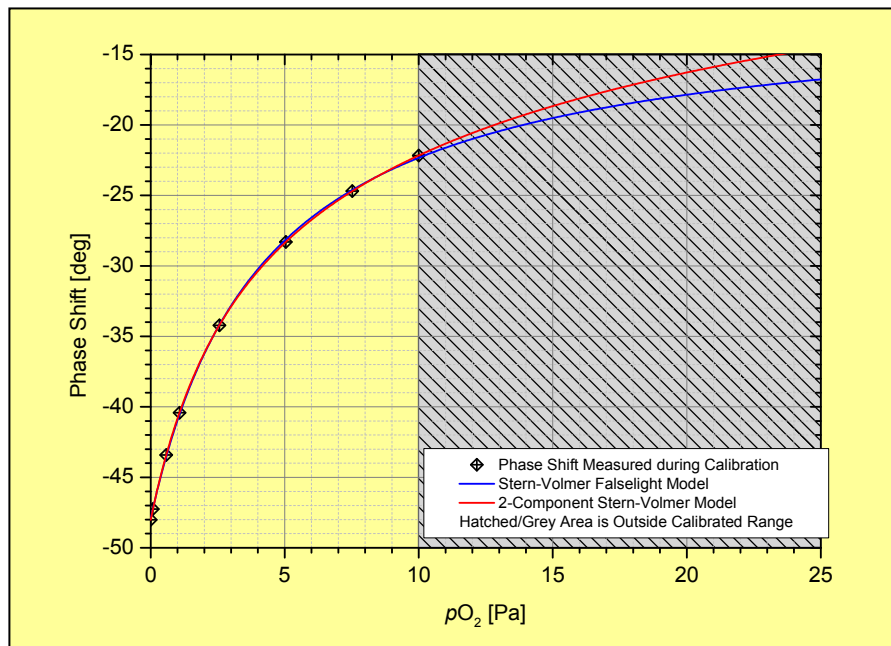
Fig. 5-18: Calibration data of the opto-chemical oxygen sensor mathematically modelled using the Stern-Volmer-Falselight model (blue) and the 2-Component-Stern-Volmer model (red). When the amount of oxygen exceeds the calibrated range of the sensor (hatched area), the differences between the models become increasingly pronounced. It was confirmed in experimental evaluation, that the 2-Component-Stern-Volmer model is reflecting the real behaviour much more accurately also when extrapolating the characteristic to ranges not covered by calibration.

As already mentioned, the 2-component-Stern-Volmer-function according to Equation 5-1 [178, 180] was implemented in 2016. Taking advantage of the resulting extended dynamic range of the oxygen sensor, most membranes which are typically used for food packaging are since included in the scope of the instrument without further measures.

5.5.3 Diffusion Kinetics and Their Impact on the Results

In measurements carried out with a more advanced version of the data acquisition software (automatically computing the apparent OTR in real-time), a certain non-linearity of the increase of the oxygen amount measured (see Fig. 5-21 left on page 151 and Fig. Fig. 5-28 on page 159) was progressively moving into the focus. The non-linear behaviour always occurs on the same timescale and is, at least when looking at the data thoroughly, found in every measurement.

A diligent interpretation of the phenomenon revealed that the non-linear behaviour has its origin in diffusion kinetics inside the volume forming the receiving cavity. Unfortunately, the diffusion processes in the gas volume occur on a time-scale that interferes with the permeability measurements. Two main diffusion processes were identified.

5.5.3.1   Diffusion through the Membrane Seal Point

A part of the boundaries of the receiving cavity is formed by the sample membrane which is firmly pressed against a lapped steel surface. The circumference around the "membrane seal point" is formed by the "seal vestibule", an interstice between concentric O-rings that is purged with a flux of nitrogen to prevent the intrusion of atmospheric oxygen into the receiving cavity (see section 5.3.2.2).

Before the OTR measurement is commenced, the relative oxygen amounts in the receiving cavity and the seal chamber are the same (about 1 ppm), since both volumes are being purged with nitrogen gas from the same supply. When the receiving cavity is sealed and the actual measurement begins, the amount of oxygen is increasing inside the receiving cavity but not in the seal chamber with its continuing purge flow. Therefore, a concentration gradient across the membrane seal point is developing and gradually acts as a driving force for oxygen accumulating in the receiving cavity to diffuse into the nitrogen atmosphere of the seal vestibule (see Fig. 5-19, left). The effect causes a decay of the detected increase rate of oxygen as the measurement proceeds over time until, eventually, a steady state and therefore a constant oxygen signal is observed (the effect is visible in Fig. 5-22, page 153). The result is an error of the calculated rate of oxygen ingress that is gradually growing as the measurement is proceeding. Mathematically, the process is easily described as an exponential approximation of the increase of oxygen partial pressure towards a steady state in which the out-flux of oxygen across the membrane seal point equals the ingress of oxygen through the sample membrane.

The magnitude of the diffusion process is different in each measurement and depending of parameters like the surface roughness and identity of the membrane material and the closing force of the test cell. The effect is a minor issue in most cases (intermediate OTR of the sample, smooth sample surface) and causes a negligible error of the result. In measurements of samples with very low OTRs or a very uneven surface the error is becoming significant. Without countermeasures this effect may, in theory, become the dominant parameter determining the limit of detection in the regime of very low OTRs.

Besides mathematical compensation (see section 5.5.3.3), an increase of the sample diameter and, in consequence, the fraction sample area/ seal point circumference may be used to counteract the effect. In the context of the effect, the systematic application of high-quality vacuum grease [150] proved to be essential.

5.5.3.2   Delayed Diffusion into Remote Valve Volumes

In the setup of the OTR demonstrator instruments, highly leak-proof, bellow-sealed valves are used to open or shut the nitrogen purge flow through the receiving cavity containing the oxygen sensor. In the closed state, the valves themselves have remaining interior volumes which are remote from the cylindrical "main" receiving cavity. However, all the named volumes are communicated via narrow steel capillaries and bores in the cell body. The valve voids (about 60 % of the volume of the

receiving cavity itself) thus contribute to the total volume of the receiving cavity in the data processing routine presented in section 4.3.2.2. As far as the design of the instrument at hand is regarded, this processing routine would only then be entirely accurate if an *immediate and uniform distribution* of oxygen permeating through the membrane in the total volume of the receiving cavity would occur - that is, among *all* compartments including the valve voids. That is, however, not the case.

Before commencing the oxygen accumulation forming the actual OTR measurement, the interior of the receiving cavity is purged with nitrogen. Therefore, a uniform concentration (about 1 ppm) in the entire volume is attained. When the valves are shut, the purge flow ceases and oxygen permeating through the sample starts to accumulate in the actual receiving cavity adjacent to the sample surface. Only gradually, however, the driving force for diffusion into the remote voids of the access valves is forming, as the amount of oxygen is already increasing to higher levels in the vicinity of the sensor (see Fig. 5-19, right). In an eventually established steady-state, the amount of oxygen in the valve volumes is increasing at the same rate as it is in the receiving cavity, but the absolute concentration is lagging behind (otherwise there would be no driving force for diffusion).
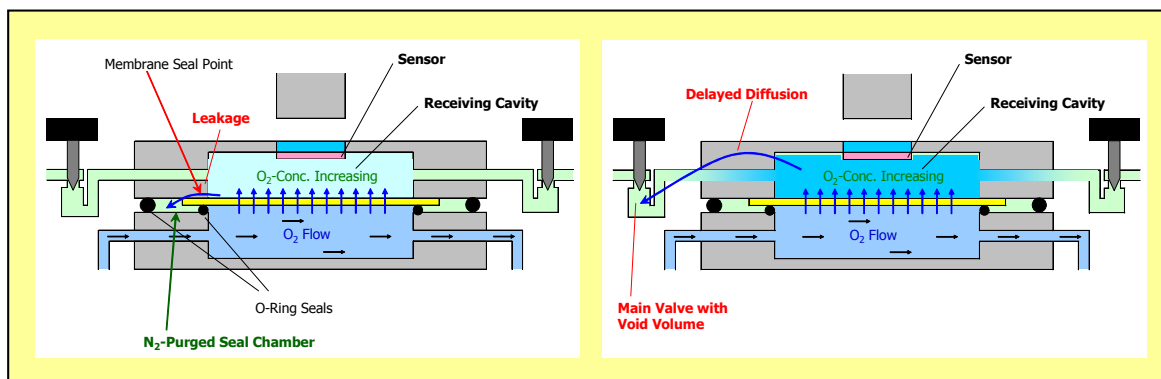
Fig. 5-19:   **Two kinetic effects interfering with the theoretically linear accumulation of oxygen during the OTR measurement were identified. Left: Leakage diffusion from the receiving cavity into the seal vestibule. Right: Delayed diffusion into the remote valve voids.**

The time until steady-state diffusion into the valve voids has established (approx. 15 min.) is intrinsic to the device. The phenomenon is affecting the linearity of the measurement data, introducing a distinct "kink" between the initial stages of accumulation and the steady state. In the first minutes of oxygen accumulation, an apparent OTR is found that is significantly higher than in the later stages of the permeation process. Initially, the permeant oxygen is distributing exclusively in the actual receiving cavity (but not into the valve voids), therefore the increase rate of oxygen would have to be referred to that volume only in the calculation of the OTR. Noteworthy that in 2014 similar considerations were reported by Abdellatief in the context of the dynamic accumulation method covered by ASTM 3136-15 [181].

The mathematical description of the process is somewhat more complicated than the leakage phenomenon explained in the previous section, but the determining parameters are device constants which, theoretically, permit the numeric compensation for the effect.

In a redesigned permeation cell, the issue can be circumvented at all by integration of the access valve seats directly into the main body of the measurement cell, that is, at the top of the cylindrical receiving cavity. Thus, the remote voids are completely avoided. The manufacture of such a device would likely require skilled and specialized mechanical engineering, however.

5.5.3.3   *Mathematical/ Numerical Treatment of the Combined Effects*

Considering the isolated processes defined in the preceding sections, mathematical modelling is leading to straight forward, 1st order differential equations with equally straight forward solutions. The combination of the effects, however, is more complicated.

In Fig. 5-20, the model describing the contributing kinetic effects is presented, indicating the origin of the individual terms of the statement. The system of 1st-order differential equations has an exact but cumbersome solution that is approachable by according software (Mathematica®, etc.). For reasons of space demand and the confusing complexity, the solution is omitted at this point.

$$\frac{dc}{dt} = \left(\frac{OTR}{V_{Receiving}}\right) - \left(\frac{LeakConst.}{V_{Receiving}} \times c[t]\right) - \left(\frac{Diff.Const}{V_{Receiving}} \times (c[t] - c_{Valve}[t])\right)$$

$$\frac{dc_{Valve}}{dt} = Diff.Const \times \left(\frac{c[t] - c_{Valve}[t]}{V_{tot} - V_{Receiving}}\right)$$
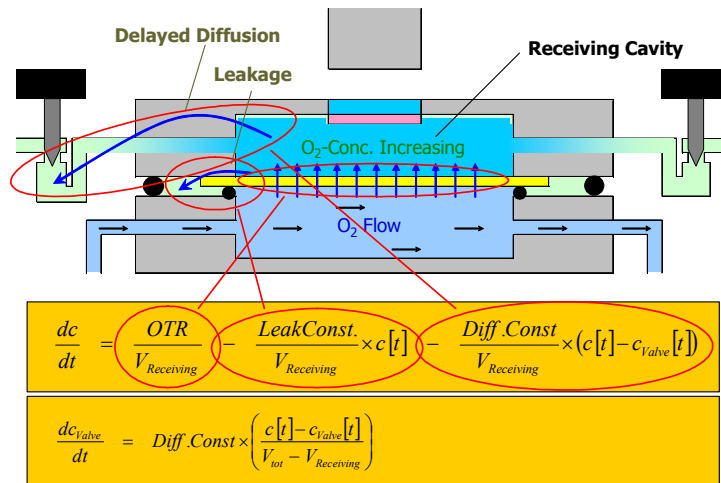
c	Oxygen concentration detected by the sensor
c_{valve}	Calculated oxygen concentration in the valve void
OTR	Mass flow according to the oxygen transmission rate
$LeakConst.$	Mass flow per unit gradient according to seal leakage
$Diff.Const.$	Mass flow per unit gradient according to diffusion into valve void
$V_{receiving}$	Volume of the actual "main" receiving cavity
V_{tot}	Total volume of the receiving cavity including valve voids
t	Time elapsed

Fig. 5-20:   The system of differential equations describing the diffusion processes interfering with the accumulation of permeating oxygen. The relevance of the individual terms is indicated by the red circles.

Fortunately, the quantities $V_{receiving}$, V_{tot} and *Diff.Const.* are representing device constants, which can be determined from a pool of measurement data and geometric properties of the cell. The remaining dependent fit variables are *OTR* (the property of interest) and *LeakConst.* With the set of 3 known and constant quantities, the solution of the differential equations simplifies to an expression that can likely be handled in real-time by a fitting routine of the data acquisition software.

The validity of the model is supported by simulations based on estimated device constants which were derived from the geometry of construction drawings and tabulated diffusion constants for oxygen/ nitrogen mixtures. The resulting function plots closely resemble the plots of the oxygen as a function of time recorded in real measurements, as shown in Fig. 5-21.

The model explained applies to permeation cells with the main valves being remote from the receiving cavity (such as the instruments set up in the Flexonics project). The establishment of accurate device constants and the implementation of a compensation algorithm was attempted but dismissed again.

A redesign of the permeation cell of a future instrument would eliminate effects arising from the diffusion into remote valve volumes, which, of the two processes, is more difficult to model mathematically. Cell leakage effects can be limited by constructive measures, but probably not completely eliminated. However, the according numerical treatment of the leakage effects alone would be straight forward.

In view of the effects interfering with the linearity of oxygen accumulation, attempts to use the instrument in transient permeation experiments as explained in section 1.4 appear obsolete also from this point of view.
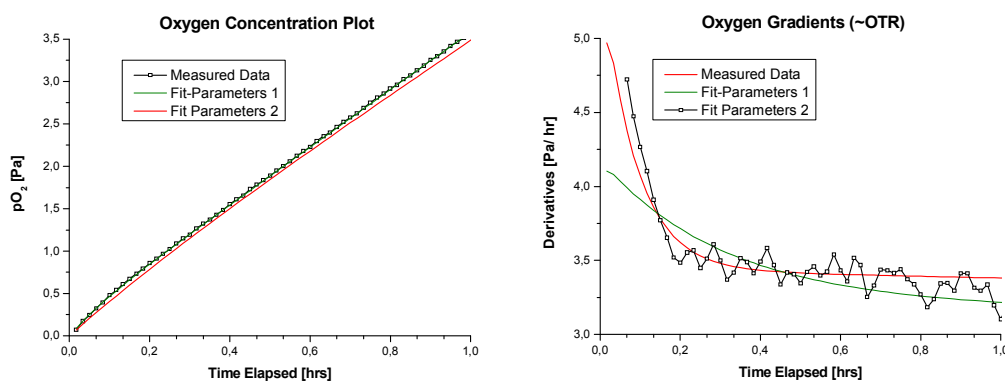
Fig. 5-21: Comparison of the kinetic model using estimated parameters with a measured data set. Left: Oxygen partial pressure as a function of time elapsed. Right: Derivatives thereof, which are related to the OTR in the simplified data processing routine described in section 4.3.2.2.

5.5.4   The Requirement for Repeated Data Acquisition

The general procedure of computing the oxygen transmission rate from the raw date of the opto-chemical oxygen sensor is illustrated in section 4.3.2.2. Very briefly, the transformation involves

plotting the increasing amount of oxygen as a function of time, obtaining the gradient of the increase and translating the gradient into a transmission rate by multiplication with a proportionality factor bundling device and operational parameters.

The explained procedure refers to a single sequence of measurement initialization and oxygen accumulation. A single result is, however, practically meaningless for reasons explained in the following section.

5.5.4.1   *Result Validity Monitoring and –enhancement*

One of the key concepts established in the project (refer to section 4.3.2.2 for a general overview) is the repetition of the permeation experiment with a sample to acquire a more or less large number of consecutive OTR results.

On one hand, the process of emergence of steady-state migration of oxygen is monitored in that way. With just a single accumulation experiment, no information about the sample's equilibrium state is obtained. However, the proper establishment of a steady-state permeation process is *essential* for the generation of transmission rate results that are meaningful *at all*. In consequence, the repeated re-initialisation, followed by analyte accumulation must be considered obligatory.

On the other hand, the procedure, once a steady-state has been reached, allows the acquisition and averaging of multiple data points in order to reduce the measurement uncertainty, which becomes increasingly important when operating the instrument near the limit of detection. Furthermore, statements about the measurement uncertainty with respect to repeatability and/or signal noise are thus possible. Note, however, that uncertainty originating in systematic errors remains disregarded in the context. The idea resembles the practice of superposition of multiple consecutively recorded scans to improve the signal-to-noise ratio in spectroscopy.

At a first glance, however, the advantage or even requirement for repeated accumulation cycles appears questionable. Why isn't the information required to assess the establishment of a steady state obtained by simply prolonging the accumulation process instead of considering merely the first hour for data processing? Referring to section 5.5.3, kinetic effects interfering with an ideally linear accumulation of oxygen in the receiving cavity enforce a compromise between a certain minimum (for reasons explained in 5.5.3.2) and a maximum duration (section 5.5.3.1) of a single permeation experiment. With the instruments set up in the project, 60 minutes for analyte accumulation, followed by re-initialization were empirically found to be a good compromise. In order to ensure comparability between measurements, this duration of a single permeation experiment was consequently defined within the standard operation procedure.

5.5.4.2   Manual Operation of the Cell Valves

In the first two years of development, no alternative but manual operation of the receiving cavity's access valves was a feasible option. Considering the requirement for a number of multiple acquisitions in combination with the duration constraint to an hour for a single permeation experiment, it appears redundant to underline the ineffectiveness of the measurement process, even if the author re-initialized the setup also during nights or at weekends when possible. Obviously, a procedure requiring manual action at such frequency is labour-intensive and tedious, particularly if equilibration times of several days or even weeks for some samples are kept in mind.

In consequence, results obtained by averaging a reasonable number of single data points have not been generated in large numbers. Furthermore, the process of equilibration might have been discontinued prematurely in many cases. In consequence, the reliability of results generated early in the project is low, compared with those generated by autonomous operation of the instrument (see the following section).

In Fig. 5-22, an example for data obtained by manual device operation is shown.
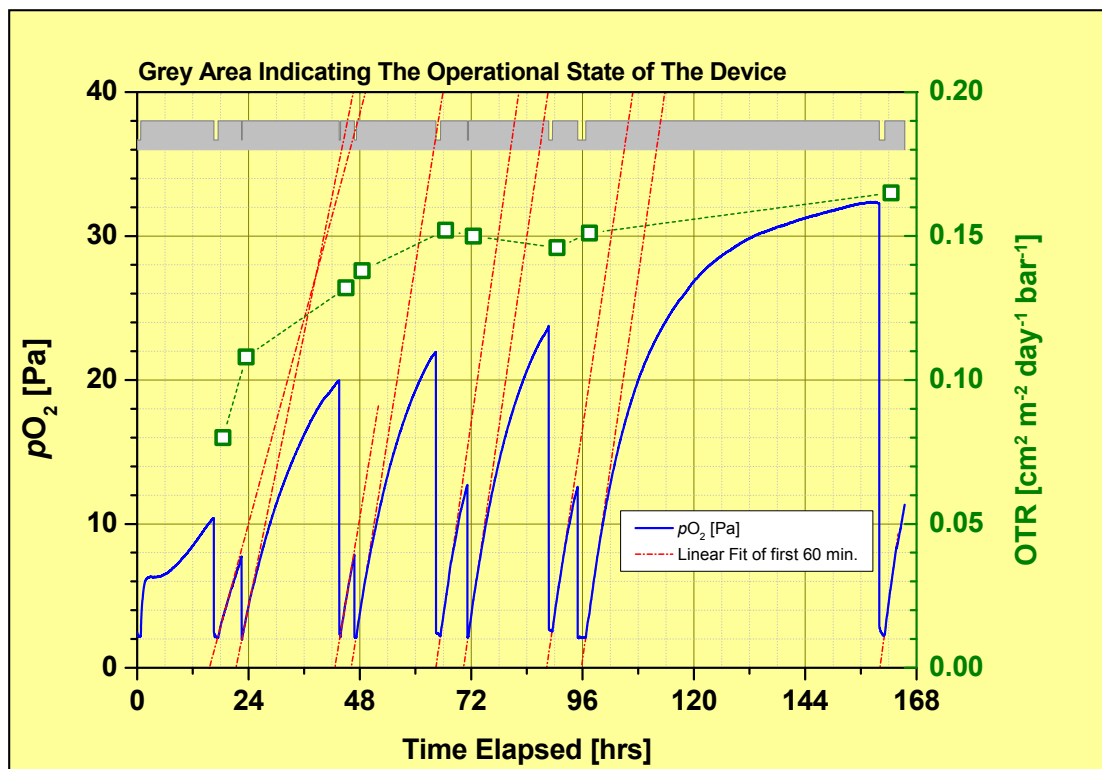
Fig. 5-22:   Typical example for data acquired by manual operation of the permeation instrument. Since only the first 60 minutes of accumulation are considered in the data processing, the major fraction of generated data is essentially useless. Manual data acquisition is therefore ineffective and furthermore labour-intensive.

5.5.4.3 Software-Controlled Valve Actuation

Unlike with manual operation, the automated, software-controlled operation of the receiving cavity access valves (see section 5.3.6) enables the seamless acquisition of permeation data. In the course of sample characterisation, a course of pO_2 inside the receiving cavity resembling saw teeth is obtained (see Fig. 5-23), and each of the "ramps" is linearly approximated and corresponds to one individual OTR result (Fig. 5-24). After the establishment of steady-state permeation is indicated by the onset of results remaining practically constant, acquisitions are continued until averaging a sufficient number of results has reduced the measurement uncertainty to the targeted value.
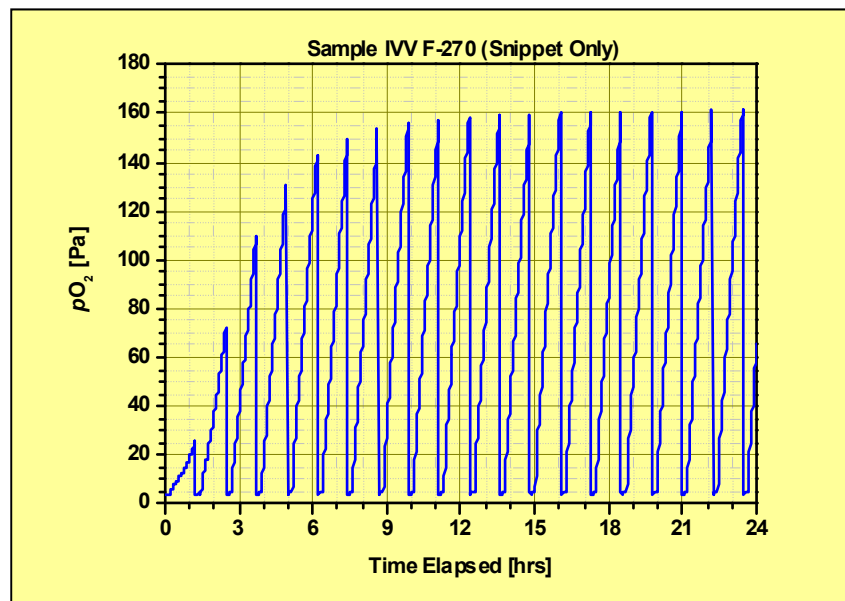
Fig. 5-23: The saw tooth-like course of detected pO_2 inside the receiving cavity obtained by autonomous instrument operation. Seamless acquisition of permeation data is thus ensured, interrupted merely by repeated re-initialization steps. Note that the graph is a snippet of the full measurement shown in Fig. 5-24 only.
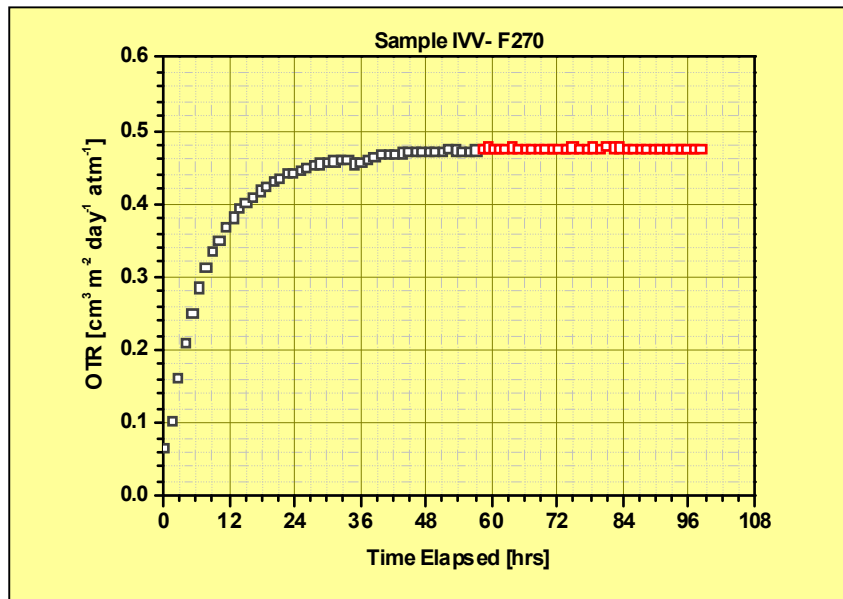
Fig. 5-24: The course of OTR results computed from the data in Fig. 5-23 as a function of acquisition time. The period required for sample equilibration at the beginning of the measurement is discernible by yet not stable readings (black data points). Results obtained after a steady state has established are used in the calculation of the mean OTR and the standard error.

5.5.5 Objectification of the Final OTR Result

During sample equilibration, which may be very time-consuming with some samples (weeks or even months), one of the hardest and patience-demanding decisions to make is the discontinuation of the measurement after a presumably positive assessment regarding the establishment of steady-state permeation. A defined procedure or algorithm assisting thereby would be highly advantageous.

5.5.5.1 Definition of Termination Criteria

5.5.5.1.1 First Attempt within the Flexonics Project

In an attempt to further reduce the manual effort associated with sample characterisation, an algorithm was defined to discriminate OTR data from an incompletely equilibrated sample from results obtained during fully developed steady-state permeation. The aim was, on one hand, to alert the operator in case of completion of the measurement sequence and, on the other hand, the ability to provide a complete automated report with averaged results and statements about the measurement uncertainty at the end of the measurement.

The concept is based on the comparison of the inclination of a linear fit through OTR results multiplied with the overall duration of the acquisition and weighted by an empirically determined factor with the standard deviation of the same data. Iteratively, one OTR result after the other is removed from the beginning of the data set and the procedure of comparing linear fit with standard deviation is repeated until the inclination is falling below the standard deviation.

Unfortunately, the algorithm is frequently overexerted by outliers (resulting from changes in the laboratory temperature which are too fast for the temperature compensation routine), prematurely "pretending" the completion of the measurement. This is the case particularly when small OTRs are measured.

The situation becomes very unclear for any algorithm if oxygen dissolved in superficial polymer layers of very airtight multi-layer samples gradually desorbs well before oxygen starts to break through the membrane. Before the establishment of a steady-state permeation rate *through* the sample, the combined processes pretend steady-state-behaviour which is mistaken by the algorithm for a complete measurement. However, with such complex samples this is not necessarily the case (see Fig. 5-25).

To date, the results are manually re-checked and, if appropriate, outliers are masked and the boundaries of the averaging range adjusted prior to the calculation of the mean OTR. The decision about the completion of the measurement is exclusively up to the operator.

Fig. 5-25: The course of OTR results obtained for a complex multi-layer barrier membrane. During the first 24 hours, oxygen dissolved in superficial layers of the membrane is desorbing and dominates the amount accumulating in the receiving cavity. The establishment of steady-state permeation requires about 10 days with this sample. In the transition between desorption of dissolved oxygen and actual permeation, intermediately constant results may be mistaken for the completion of the measurement.

5.5.5.1.2 *Exponentially Weighted Moving Average*

In the period 2009 - 2010, DI Ulrike Kleb and Mag. Dr. Michaela Dvorzak of the division "Statistical Applications" of Joanneum Research participated in an internal research project of Joanneum Research about high-performance barrier membranes. Soon in the project, the time demand for equilibration was recognized as a major obstacle in the screening of barrier samples, and consequently, in the development of barrier membranes. Initially, "Statistical Applications" were concerned with the problem of defining objective termination criteria discussed in the previous

section. The optimization of acquisition time should lead to an increased sample throughput. The chosen approach of definition of exponentially weighted moving average ("EWMA") quality criteria was superior to the approach explained in 5.5.5.1.1 but still not very robust against unusual sample behaviour. The algorithm was, however, not yet implemented into the data acquisition software. Nevertheless, a very brief explanation shall be given in this place. [31]

With every new OTR data point joining the set of data, the relative difference between consecutive data points is calculated. In the statistical process, past data are statistically weighted lower. The definition of lower and upper boundary conditions is the basis for the termination criterion.

Upper Boundary Condition = 0 + 3 * σ

Lower Boundary Condition = 0 - 3 * σ

where σ calculates according to Equation 5-3.

$$\sigma = \sqrt{\frac{\lambda}{(2-\lambda)}[1-(1-\lambda)^{2t}]\cdot s_{OTR}^2}$$

λ weight factor, $0 < \lambda < 1$

s^2_{OTR} variance of n=10 last OTR results

Equation 5-3:   **The weighting algorithm for past results.**

The weight factor λ determines the attenuation of past OTR results in the algorithm. If an empirically chosen number n=10 of consecutive and weighted differences remains within the boundary conditions, the establishment of a steady-state is assumed. The last 10 results are then averaged to give the final OTR result.
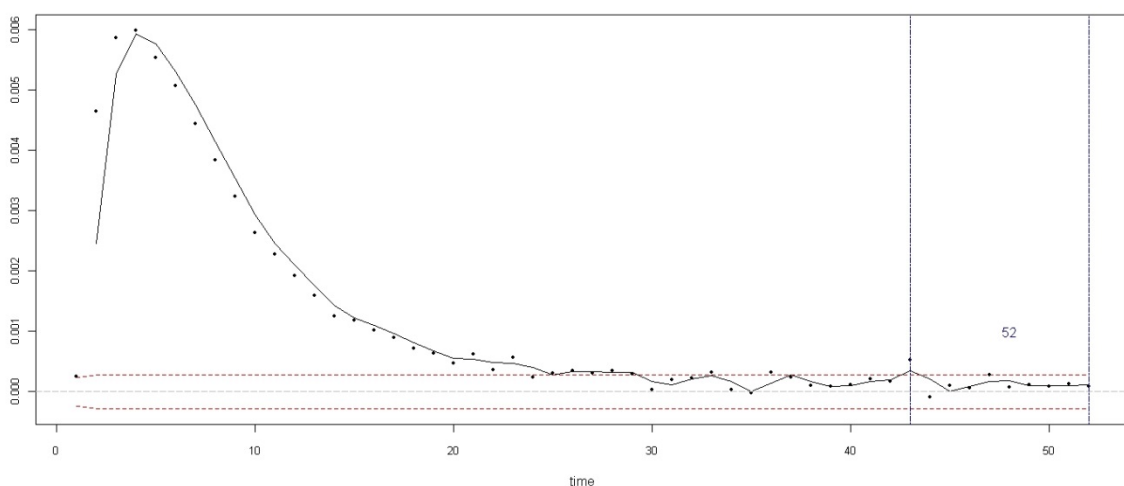
Fig. 5-26:   **A plot of the differences between consecutive measurements according to the discussed algorithm. In this example, data acquisition may be terminated after the 52nd data point.**

---

[31] The subjects discussed in this section are not part of the author's own research but have significance in the context of the presented work.

5.5.5.2   Prognosis of the Steady-State Transmission Rate

In an alternative approach to accelerate the process of obtaining a final result, "Statistical Applications" of Joanneum Research attempted the prognosis of the stable final result based on a purely empirical/statistical model which requires only 20 consecutive OTR data points – that implies a duration acquisition of little more than 20 hours only. Because the duration of the experiment is predefined, exorbitant testing times of several weeks are avoided and a high sample throughput is promoted at the cost of a few percent of accuracy of the predicted steady-state OTR.[32]

A prerequisite to establish the model is a large pool of data comprising the full course of sample equilibration and steady-state permeation. From the data, descriptive quantities as well as the OTR as a dependent variable are extracted, the latter according to the EWMA-algorithm explained in the previous section. The descriptive quantities are statistical coefficients like arithmetic mean, minimum, maximum, standard deviation, range and others and are calculated for the 20 first OTR data points of a measurement.

On the basis of the thus obtained descriptors, a linear statistical model estimating the steady-state OTR is estimated, using tools available included in the programming environment for statistical computing "R" [156]. If the initial 20 first data points of an "unknown" measurement are fed into the model, the steady-state OTR is predicted within an error tolerance of about 10 % for most samples, even if the steady state is obtained only after weeks of equilibration. Larger errors occur with very low OTRs in particular, as can be seen in Fig. 5-27.
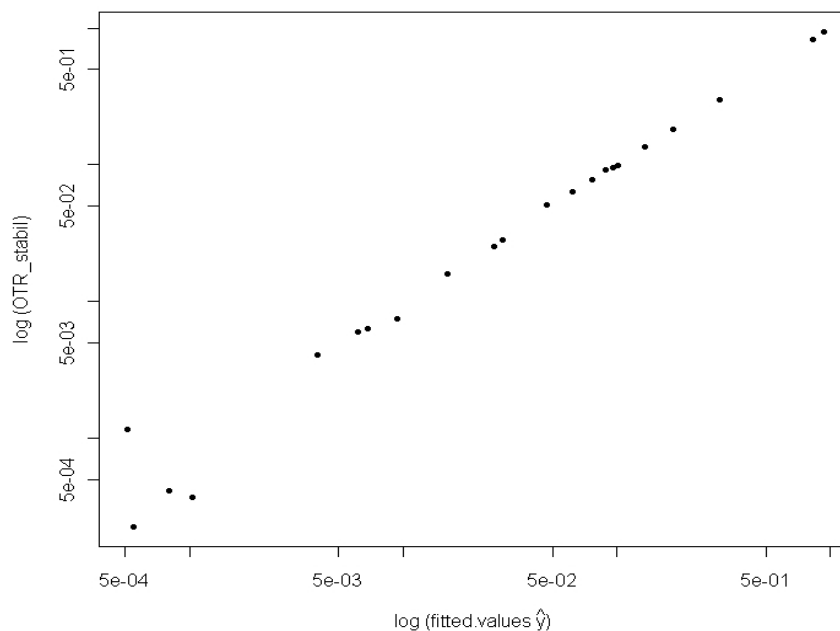
Fig. 5-27:   **A comparison of the predicted steady-state OTR (x-axis) obtained by a statistical model considering only the first 20 data points of a measurement with the experimentally determined steady-state OTR. Except for very low OTRs, the predicted values deviate by less than 10 % with most samples.**

---

[32] The subjects discussed in this section are again not part of the author's own research. Nevertheless, the conclusions obtained by the division "Statistical Applications" well after the Flexonics project may contribute to the further evolution of the OTR measuring instrument.

The performance of the model is impressive considering that it is based purely on statistical treatment of measurement data without taking into account any physical relationships or whatsoever. Since it is limiting the time requirement for a sample to predefined 20 OTR data point acquisitions, the possible increase in sample throughput is indeed remarkable. Note, however, that the model was tested solely with a large set of recorded data so far. Since some of the required routines are available in "R" but not in LabView (see section 5.6), the model has not been implemented into the data acquisition software yet. According routines would have to be programmed from scratch lacking such predefined tools in the software environment.

5.6 THE SOFTWARE

Device control, data logging and data processing are conducted by software which was programmed using National Instruments LabVIEW [153] as the programming environment. The evolution of the software bundle originated in routines provided by Joanneum Research which were created in a previous project ("Optogluc") and merely managed the communication with the phase measuring opto-electronics, logging of raw data and the control of mass flow controllers which are necessary for sensor calibration. Any processing of the raw data had initially to be done manually using tools like OriginLabs "Origin" [154].

As soon as the concept of repetitive acquisitions for a sample was followed, the requirement for data acquisition software tailored for the application became urging. In countless modifications, the original "Optogluc" application was modified, enhanced or supplemented with additional routines assisting data logging, data processing or the control of device components such as the actuators of the main valves. Mathematical algorithms or statistical models were implemented, tested and, if inappropriate, removed again. Practically, the application was in a process of permanent evolution and continues to be enhanced to this day (see Fig. 5-28 and Fig. 5-29). In the course, the author gained comprehensive skills in developing LabVIEW applications.
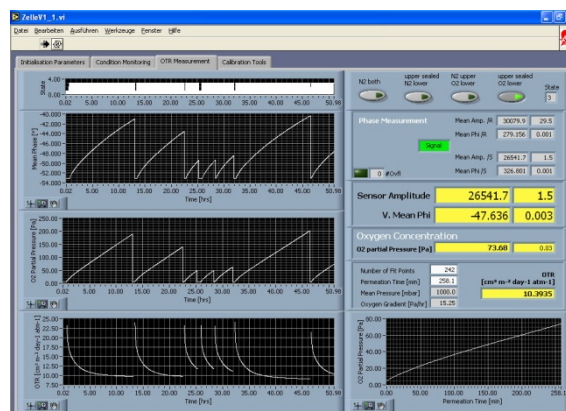
Fig. 5-28:   A screenshot of the data acquisition software in 2006 and after about 18 months of development.
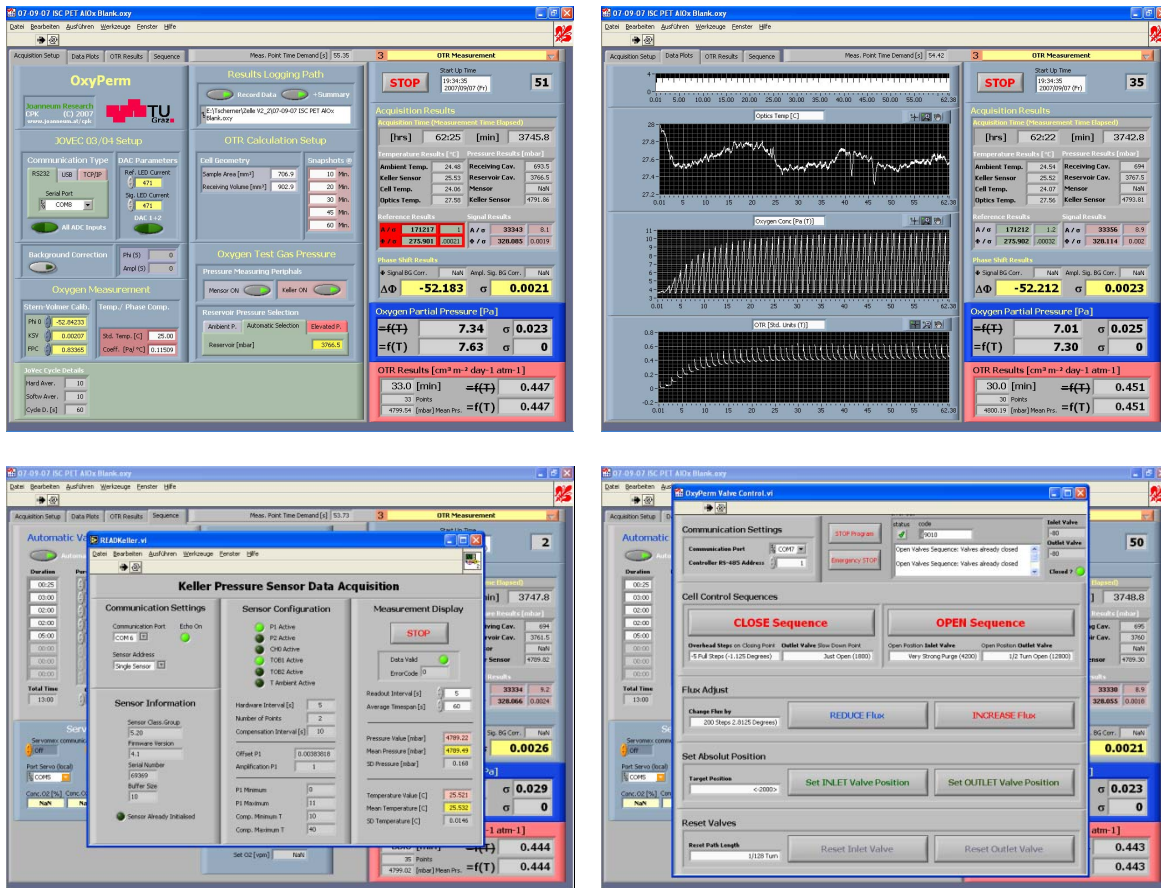
Fig. 5-29: **Screenshots of different windows of the data acquisition and device control software in September 2017. Device operation and data processing are done fully automatically, and many algorithms for data manipulation or compensation of interferences were implemented meanwhile.**

5.7 THE INSTRUMENT VERSION HISTORY

In the evolution of the OTR measuring concept to the demonstrator instruments in the present state (2017), some distinct steps regarding instrument "infrastructure" and performance have been made. In order to be able to address a certain stage of development, these distinct evolution steps have been given version numbers. Data were filed accordingly during the project for later correlation with the different instrument versions. The most important features of each version are briefly listed in this section.

5.7.1 Version 1.0

The very first laboratory demonstrator (see Fig. 5-30) was setup in 2003 and therefore prior to the Flexonics project and merely a permeation cell made of stainless steel. It consisted of two entities, one of which contained the receiving cavity, the other one the reservoir cavity. Thermo-stabilization was attempted in vein by cycling water from a laboratory thermostat through according channels in the top and bottom of the device.

The device did neither comprise high quality valves nor a system of O-rings forming a seal vestibule (see section 5.3.2.2). First attempts to seal the receiving cavity after initialization, in fact, involved bruising the steel capillaries of the in- and outlet of the receiving cavity using hammer and anvil. In prior projects of Joanneum Research, the method proved sufficient, and a certain degree of cold welding of the interior surface of the bruised capillaries was assumed.
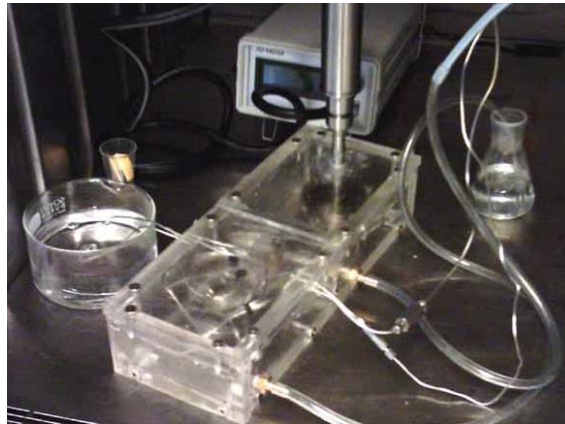
Fig. 5-30: **Demonstrator Version 1.0. The actual permeation cell is located inside a container purged with nitrogen to circumvent otherwise uncontrollable issues with atmospheric oxygen penetrating the cell.**

However, never-ending difficulties to demonstrate the feasibility of permeation experiments resulted in the construction of a container which was purged with nitrogen to create an oxygen-free atmosphere, and the entire device was accommodated inside. By migrating single components outside again, the method of bruising the capillaries was identified as the major issue concerning leak-tightness. In addition, the lack of a mechanical support for the sample membrane caused repeated problems.

Despite all weaknesses of this first demonstrator, important expertise was built up during the experiments. The conclusions led to distinct modifications and resulted in demonstrator version 1.1 (see the following section).

5.7.2   Version 1.1

Based on the conclusions obtained from first trials with version 1.0, the permeation cell was modified in the period May - July 2005 in a number of aspects:

- Highly leak-proof bellow-sealed valves (section 5.3.2.1) were integrated in the inlet and outlet of the receiving cavity.

- Mechanical support for the sample membrane (section 5.3.3.1) was integrated. Thus, the diameter of the receiving cavity was increased from 20 mm to 30 mm due to the dimensions (28.15 x 1.5 mm) of the porous metal discs available.

- Thermo-stabilization (section 5.3.4) using a hexagonal array of 6 Peltier elements, a heatsink, a thermistor and an according controller was integrated.

- Polymer tubing in the pipework was avoided completely and replaced by 1/16 inch or 1/8 inch stainless steel capillaries.

- Airtight joints between pipework components were accomplished using silver solder whenever practicable

Version 1.1 (Fig. 5-31) was the first demonstrator that was used routinely for sample characterisation within the Flexonics project. After a second demonstrator unit (version 2.0, section Version 2.0) has been built, the device was, however, mainly used for trials regarding new concepts. The major drawback of the demonstrator version was the initial lack of a seal vestibule (see section 5.3.2.2). Since no system of concentric O-rings with a nitrogen-purged interstice was integrated, atmospheric oxygen leaking into the cell frequently interfered with the measurements. First trials with the concept of a seal vestibule were conducted with this demonstrator. However, mechanical constraints did not permit an ideal solution.

In August 2007, the demonstrator was upgraded to version 1.5 (next section).
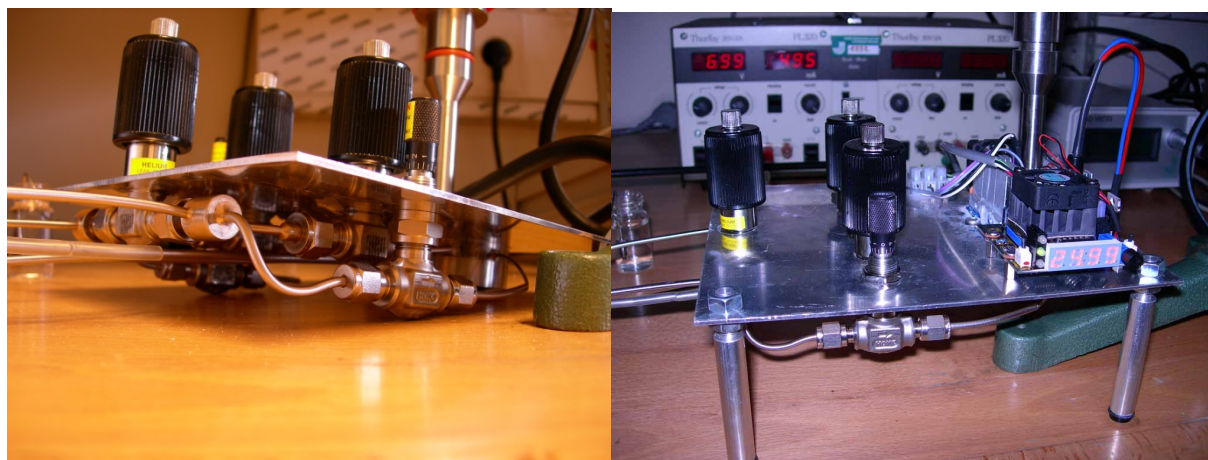
Fig. 5-31: **Demonstrator Version 1.1, established in August 2005, during setup (left, yet no temperature control installed) and operation (right, including temperature stabilisation).**

5.7.3   Version 1.5

A distinctly enhanced, much more sensitive formulation of the opto-chemical sensor membrane (see section 5.4.1) was first tested on demonstrator version 1.1 (previous section) in August 2007. Acknowledging the significant performance improvement of the cell, the unit with the enhanced sensor membrane is referred to as version 1.5.

The demonstrator was in operation until January 2008, before some of the components were re-used in the setup of demonstrator version 3.0 (section 5.7.8).

5.7.4   Version 2.0

Based on the expertise acquired with versions 1.x (section 5.7.1 and section 5.7.2), a second demonstrator instrument was designed from the beginning and built in the period September – November 2005 (Fig. 5-32). In addition to the features of version 1.1, a number of improvements were implemented:

- An elaborate two-stage seal vestibule (section 5.3.2.2) surrounding the membrane seal point represented a key feature of the demonstrator. Components penetrating the walls of the receiving cavity (pressure sensors, window) were also integrated into the seal vestibule concept.

- Analogue pressure sensors (section 5.3.5.2) were integrated into the receiving cavity as well as the reservoir cavity.

- Thermo-stabilization (section 5.3.4) was accomplished using ring-shaped Peltier elements on top and bottom of the cell, heatsinks with fans, a thermistor and a miniature controller.

- A further thermistor was used to record the cell temperature together with the other raw data.

- The design of the main panel assisted cell accessibility and enabled the later addition of further components.

From November 2005 onwards, sample characterisation within Flexonics were primarily conducted on this demonstrator. However, manual device operation and data processing were still labour-intensive.

In April 2006, a distinctly improved opto-electronic referencing scheme developed by Joanneum Research (5.3.7) was implemented into the instrument, resulting in significantly improved temperature stability of the device.
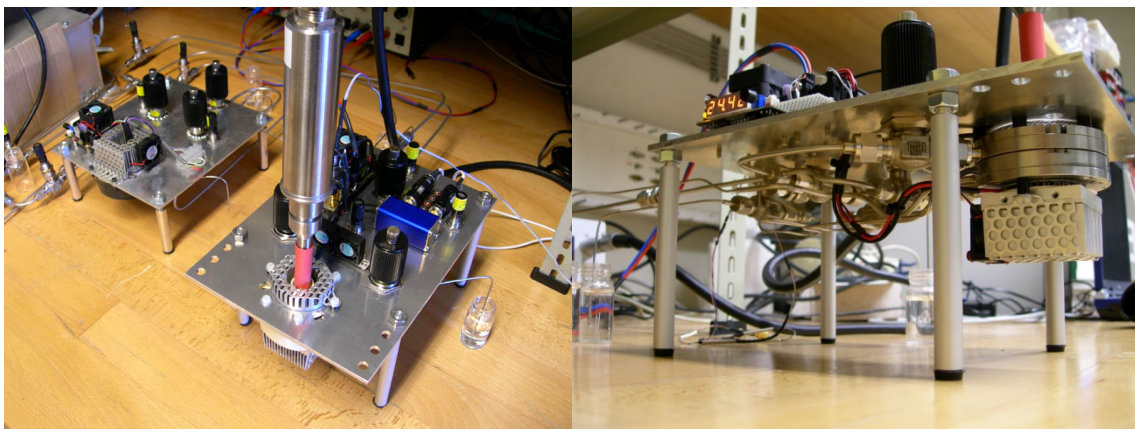
Fig. 5-32:   Images of demonstrator version 2.0, established in November 2005. In the background of the left image, version 1.1 can be seen in addition.

5.7.5   Version 2.1

The requirement for manual processing of data recorded in fairly confusing log-files increasingly became a problem due to the growing number of samples to characterize. In anticipation of version 2.2 (next section), the data acquisition software was modified and a log-file structure tailored for the application was introduced.

At the same time, a digital pressure sensor was integrated in the oxygen test gas supply line to overcome issues with the analogue pressure sensors (section 5.3.5.2) which turned out to be unreliable in terms of absolute readings.

Measurements conducted with the instrument in the period November 2006 – March 2007 are assigned to version 2.1.

5.7.6   Version 2.2

Regarding the requirement for frequent manual interference with the instrument, the most significant evolution step, based on demonstrator version 2.1 (previous section) was accomplished in March 2007 (Fig. 5-33):

- Software-controlled valve actuators (section 5.3.6) operating the receiving cavity's access valves were implemented. Thus, seamlessly repeated acquisition and re-initialization cycles at defined intervals became possible without any demand for intervention by the operator.

- Raw data of the accumulation acquisitions are since autonomously fitted and translated into an oxygen transmission rate result by the acquisition software (section 5.5.4.3). The results are recorded in an additional, neatly structured log-file. Merely the selection of data points corresponding to a fully established steady-state permeation rate and computing the according average result requires manual action.
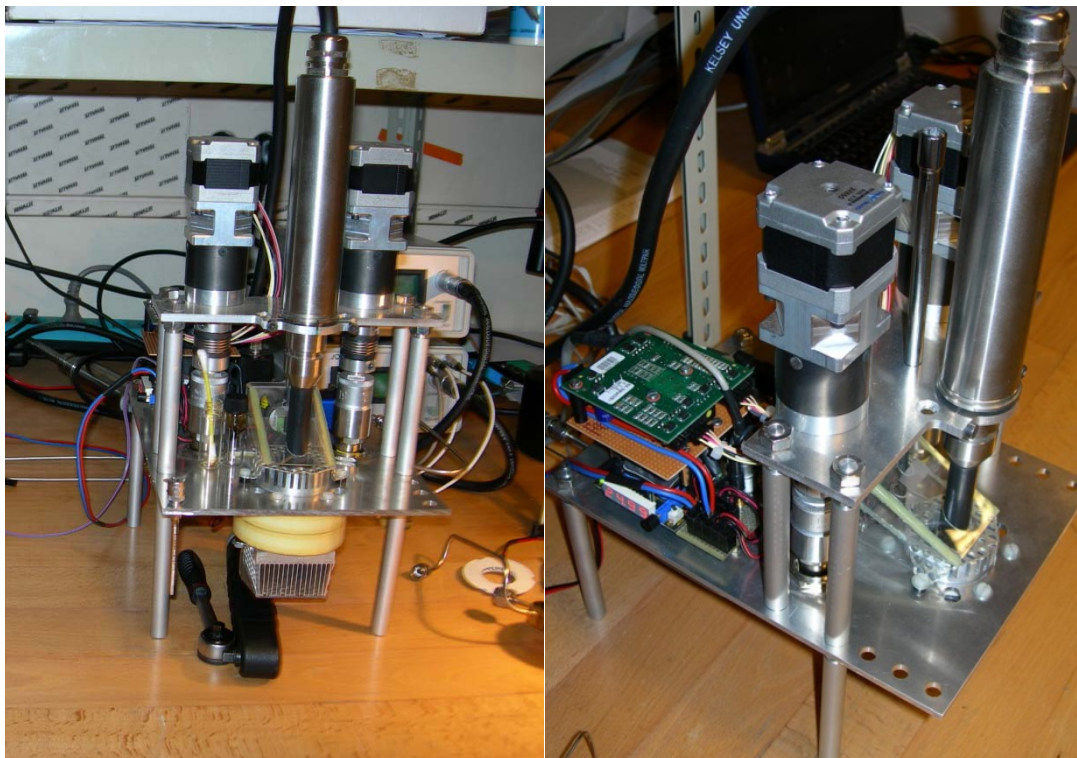
Fig. 5-33: Images of instrument demonstrator version 2.2, established in March 2007. Software-controlled valve actuators represent the most distinct new feature. After an upgrade with an enhanced sensor membrane (next section), the device is in permanent service to this day.

5.7.7 Version 2.5

In August 2007, an opto-chemical sensor membrane offering significantly improved sensitivity to oxygen (see section 5.4.1) was first tested on demonstrator version 1.5 (section 5.7.3) and, after positive evaluation, implemented into demonstrator version 2.2 (previous section) in September 2007. The change in sensor chemistry resulted in a very distinct improvement of device performance.

With a number of minor modifications after the Flexonics project (see section 5.3.3.3 or section 5.4.2.1, for instance), the instrument is in permanent service to this day and has been used in a number of commissioned research projects. After precisely 10 years of experience with the demonstrator it is noted that the instrument is, despite some weaknesses inherent to the design, an equivalent alternative to commercial instruments, yet performing with a lower limit of detection and permitting furthermore the experimental investigation of properties that would not be accessible with commercial units.[33]

---

[33] For instance, the amount of oxygen dissolved in a membrane stored under ambient conditions or the absorption capacity of oxygen scavengers can be quantified within limits if the operational conditions (gas supply, initialisation and measurement sequence, etc. are modified accordingly. Details are, however, not discussed in this thesis.

5.7.8   Version 3.0

The improved resolution of the oxygen sensing system introduced in demonstrator version 1.5 (section 5.7.3) and version 2.5 (previous section), surface-chemical effects (see section 5.4.3) were identified as the cause for apparently negative oxygen transmission rates if very airtight samples are measured.

The observations and conclusions triggered the anew design of another laboratory demonstrator (Fig. 5-34) which was established by March 2008 and, with a number of minor modifications (see section 5.3.3.3 or section 5.4.2.1, for instance), is in permanent service to this date. In the process, demonstrator version 1.5 was dismantled and many components were re-used in the new setup. Based on version 2.5, the most distinct features of the instrument include:

- The critical cell component containing the "receiving cavity" was reconstructed, aiming for an improved geometry of the receiving cavity in order to reduce kinetic side-effects (section 5.5.3).

- Functional surfaces associated with the receiving cavity were gold plated by means of "pulsed laser deposition".

- The seal vestibule system (section 5.3.2.2) was designed in a less complex manner, simplifying the manufacturing process. The secure prevention of leakage effects requires, however, a somewhat increased purge flow of nitrogen in comparison to version 2.5 with its two-stage seal vestibule.

- Like version 2.5, the unit was equipped with valve actuators to perform autonomous routine measurements.

-

Despite the efforts taken regarding the prevention of surface-chemical oxygen absorption, the performance of the instrument is similar to version 2.5. Unfortunately, only minor improvements with respect to oxygen absorption at the cell surface were accomplished.
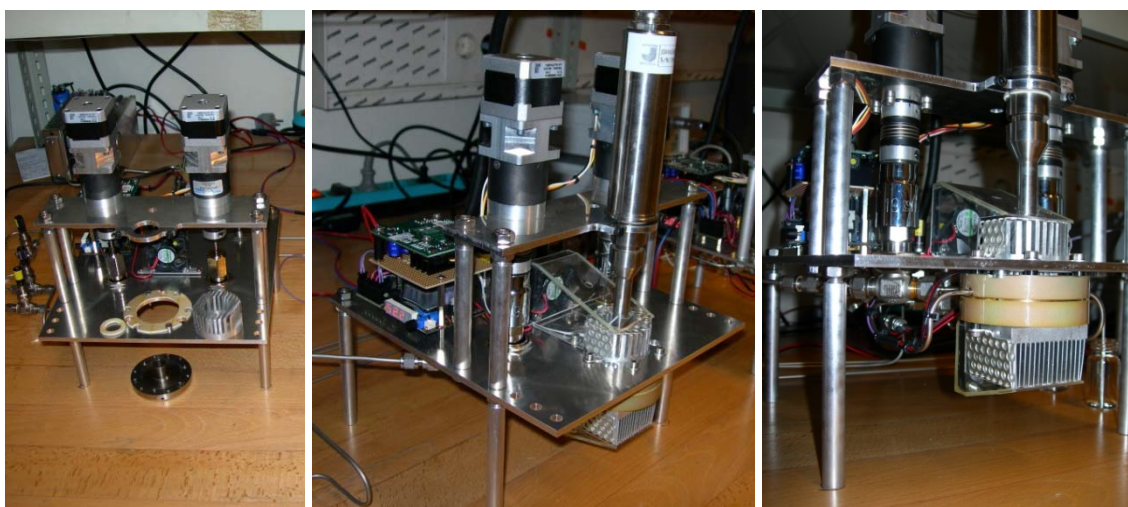
Fig. 5-34:   Images of demonstrator version 3.0, established in March 2008, during assembly (left) and operation (centre and right). Gold-plated functional surfaces and an optimized geometry of the receiving cavity represent the most distinct new features. The device is in permanent service to this day.

6 THE ACHIEVEMENTS: INSTRUMENT PERFORMANCE

6.1 INTRODUCTORY REMARKS

After the end of Flexonics; the remaining demonstrator instruments version 2.5 and version 3.0 (for the version history see section 5.7) continued to be in permanent service to this date, mostly in commissioned research projects. Thus, a large number of samples were characterized meanwhile:

- Until today, some 190 individual membrane samples have been investigated solely using the autonomously operating demonstrator instrument of versions 2.2 – 2.5, some 90 of which were measured within the Flexonics project between March 2007 and April 2008.

- Demonstrator 3.0 was used for the characterisation of approximately 100 samples to this day. Since version 3.0 was set up in March 2008 and thus at the end of the project, very few samples in the context of Flexonics were investigated using this instrument.

- Another 190 measurements, approximately, were conducted from March 2005 – February 2007 on the manually operated demonstrator devices of versions 1.0, version 1.1, version 2.0 and version 2.1.

- Reference results measured by partners within the Flexonics consortium on commercial instruments or otherwise obtained reference numbers are available for 11 of the investigated samples. The transmission rates of the reference results range from $3*10^{-3}$ [$cm^3 \, m^{-2} \, day^{-1} \, atm^{-1}$] to 50 [$cm^3 \, m^{-2} \, day^{-1} \, atm^{-1}$].

- Two of these reference results have a large statistical database from a round robin test involving 29 different laboratories.

For the procedure followed in the processing of the data acquired with the autonomously operating demonstrator versions refer to section 4.3.2.2 and/or section 5.5.4.3, including the calculation of the standard error of the mean (SEM) and the normalized uncertainty (4.3.2.3). Note that all measurements were carried out using dry nitrogen and dry oxygen gasses (quality 5.0), thus at a relative humidity of 0 % (compare section 3.6).

In regard of the large number of results obtained, tabulated data are omitted. Results are illustrated in graphical form instead, taking advantage of the lucid nature of display, compared to the tabular form.

6.2 PERFORMANCE OF DEMONSTRATOR VERSION 2.x

Not only in the context of the Flexonics project was a majority of OTR results obtained using the demonstrator instrument of version 2.1 – 2.5. In particular, version 2.5 (see section 5.7.7) evolved into the "working horse" during the project and beyond. Incidentally, the most reliable operation and the best measurement uncertainties were accomplished with this instrument. It thus represents

benchmark for the performance achieved in the development of the opto-chemical method for OTR measurements among all the instrument versions involved.

6.2.1 Results in Absolute Numbers

In Fig. 6-1 , results recorded with version 2.1, 2.2 and 2.5 within the Flexonics project are presented in graphical form. Due to the large number of results, sample IDs are not shown in the graph. However, the data are grouped if more than one individual specimen of the same sample membrane was characterized in an independent measurement, which applies to the majority of the samples. Results referring to a specific instrument version are coded by colour, and blue error bars indicate the standard error of the mean obtained according to the data processing procedure explained in section 4.3.2.2. Note that results of such measurements in which no steady-state permeation rate was established are not included in the presentation. The results generated in the context of Flexonics span a wide range of transmission rates from as low as $6*10^{-5}$ [cm^3 m^{-2} day^{-1} atm^{-1}] to rates as high as 50 [cm^3 m^{-2} day^{-1} atm^{-1}].
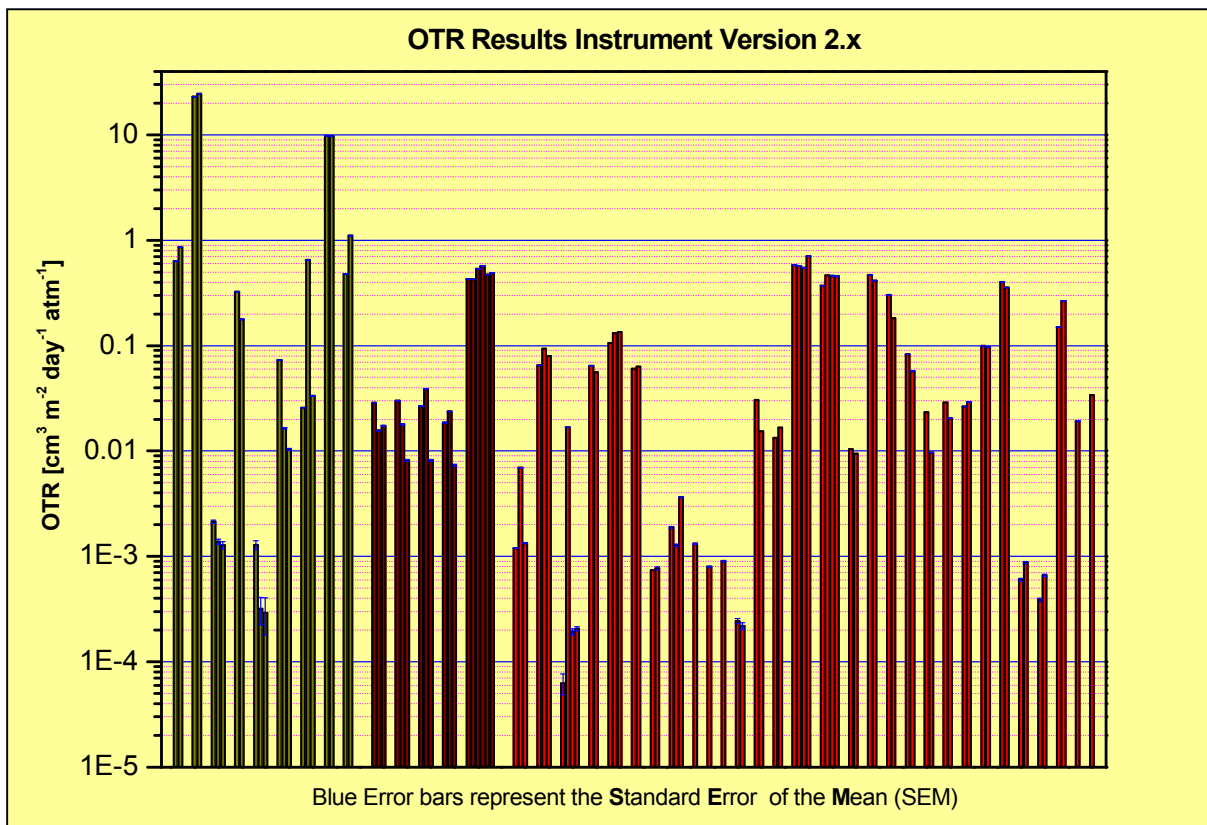
Fig. 6-1:   OTR results obtained using instrument version 2.1 - 2.5 within the Flexonics project. Error bars represent the standard error of the mean (= standard deviation divided by the square root of averaged data points). Results for different samples of the same membrane are grouped. Dark yellow: Results referring to instrument version 2.1 (manual operation). Brown: Results referring to instrument version 2.2 (autonomous operation, polystyrene-based oxygen sensor). Red: Results referring to instrument version 2.5 (autonomous operation, TeflonAF-based, distinctly enhanced oxygen sensor).

The error bars representing the standard error of the mean are hardly visible in case of OTRs exceeding 10^{-2} [cm^3 m^{-2} day^{-1} atm^{-1}] and become distinct only below. A detailed analysis of Fig. 6-1

reveals distinct improvements of the measurement uncertainty upon each instrument upgrade. Thus, results obtained with instrument version 2.1 (dark yellow bars) are tagged with error bars indicating a significantly larger uncertainty than it is the case with instrument version 2.5 (red bars).

More remarkable, however, is the fact that the standard error of the mean is smaller for every single measurement than is the variability between multiple independent measurements of different specimens of the same sample membrane (such measurements are grouped in the graph without any interstice). The observation implies a strong indication (but not an absolute evidence, however), that the repeatability of the permeation measurement itself significantly outweighs sample uniformity.[34]

Whereas some samples behaved quite reproducibly in independent tests, some others fluctuated almost over an entire order of magnitude. This, at a first glance, implausible variability is in fact quite common with organic-inorganic multilayer membrane composites, since random defects in the (commonly inorganic) barrier layer distinctly dominate the permeation behaviour. Particularly in case of polymer films coated with a superficial inorganic barrier layer (as frequently received for characterisation within Flexonics), the history with respect to shipping, handling and storage distinctly influences the barrier properties. As defects are often created in a pseudo-random distribution, specimens extracted e. g. near the edge of a DIN-A4 sheet of membrane may behave very differently from such taken from the middle.

In any case, the precision of the instrument itself appears to be sufficient for the characterisation of ultra-barrier membranes. For the least permeable sample measured successfully so far, 37 steady-state OTR data points were averaged to give a mean OTR of 6.25×10^{-5} [$cm^3\,m^{-2}\,day^{-1}\,atm^{-1}$] with a standard deviation of 8.5×10^{-5} [$cm^3\,m^{-2}\,day^{-1}\,atm^{-1}$]. Following the data processing procedure explained in section 4.3.2.2, a standard error of the mean of 1.4×10^{-5} [$cm^3\,m^{-2}\,day^{-1}\,atm^{-1}$] and a normalized result uncertainty of 0.46 are associated with the result. Even this single result alone already indicates the performance of the instrument which surpassed commercial instruments available in 2008 by two orders of magnitude. However, MOCON as the leading manufacturer for barrier testing equipment has meanwhile introduced new and more sensitive instruments for OTR measurement as well as for the analysis of WVTR. The specified limit of detection for oxygen transmission rate measurement is 5×10^{-4} [$cm^3\,m^{-2}\,day^{-1}\,atm^{-1}$].

6.2.2   Accuracy: Comparison with Reference Results

During Flexonics, reference results by measurements conducted in parallel on commercial instruments were obtained for 11 sample membranes only. However, these again span a relatively wide range of transmission rates from as low as 3×10^{-3} [$cm^3\,m^{-2}\,day^{-1}\,atm^{-1}$] to

---

[34] Theoretically, sample mounting may contribute to the result fluctuations. The fact that some membranes do not show such distinct fluctuations as others suggests that the main influence is by the samples themselves.

50 [$cm^3\ m^{-2}\ day^{-1}\ atm^{-1}$]. A particularly large database is available for two reference samples from an extensive round robin test involving 29 different laboratories.

The results obtained by the opto-chemical OTR instrument (version 2.5) are plotted as a function of the reference results obtained with commercial equipment in Fig. 6-2. Error bars represent the respective standard deviation (for such results where multiple measurements were averaged). Fig. 6-2 indicates good agreement of the compared measuring technologies over the entire range of OTRs measured.
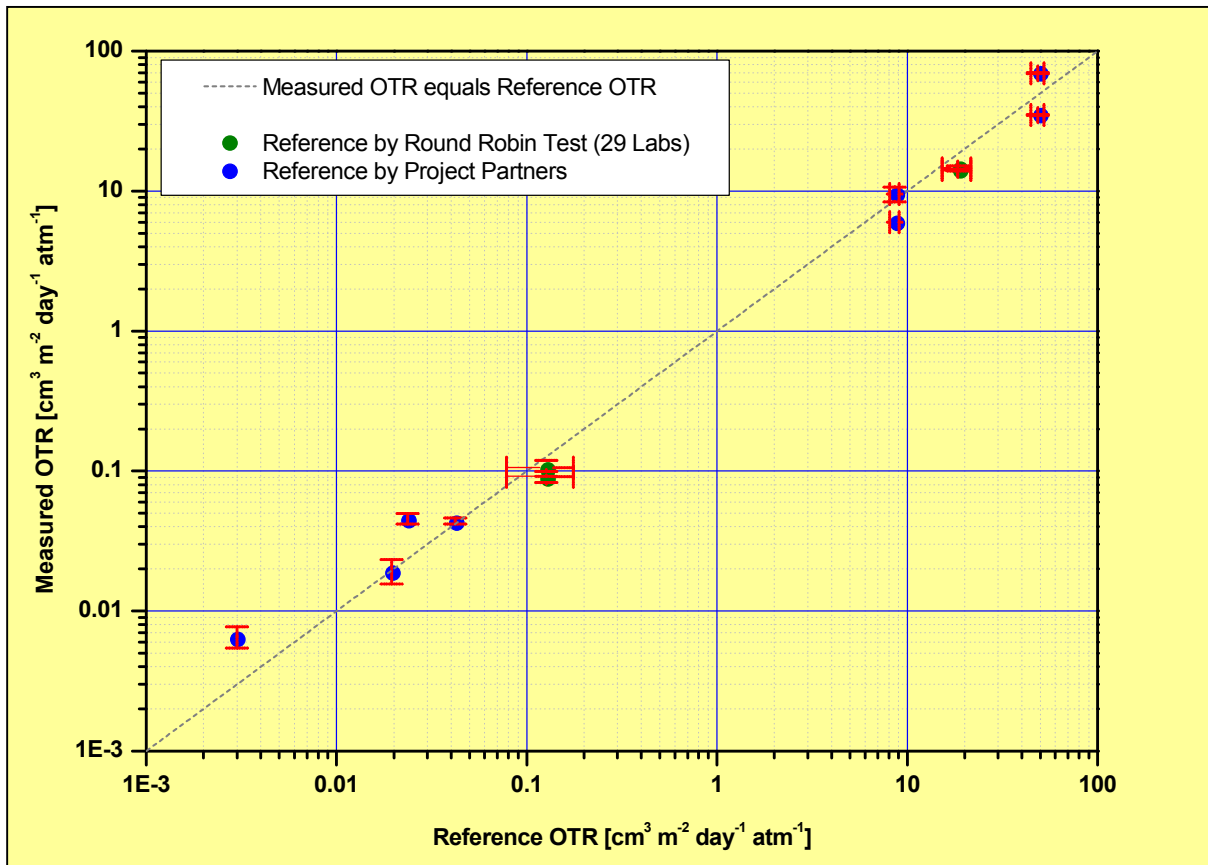
Fig. 6-2: The oxygen transmission rate measured with the opto-chemical instrument as a function of reference results obtained using commercial instruments. Error bars represent the standard deviation of results, where available. Dashed line: Measured OTR equals reference OTR. Reference results for two membranes (dark yellow) were obtained from a round robin test and are thus supported by a substantial statistical database.

Deviations of a few ten percent in some cases appear substantial at a first glance. Considering, however, the standard deviation produced by commercial equipment (which becomes even more pronounced between different instruments as in the round robin test, dark yellow results in Fig. 6-2), it is concluded that permeability measurements are generally tainted with a large variability (refer also to the discussion in the previous section).

An error bar representing one standard deviation implies that 31 % of the reference results would have fallen outside that error bar if plotted individually. Keeping in mind now the distribution of the reference numbers from the round robin test while noting that the opto-chemically obtained results

fall within approximately 1 standard deviation of the reference, the attained accuracy appears, in fact, well within acceptable limits.

Lacking reliable reference results of ultra-barrier membranes with transmission rates in the 10^{-5} [$cm^3\,m^{-2}\,day^{-1}\,atm^{-1}$] regime, the accuracy of the instrument could, however, not be substantiated experimentally near the limit of detection. In addition, particular attention must be paid to surface-kinetic effect (section 5.4.3) when deducing a similar accuracy behaviour as with the distinctly higher transmission rates of the reference results.

6.2.3   Limit of Detection: Normalized Uncertainty

The limit of detection attainable with the opto-chemical OTR measuring instruments is best discussed by reference to results obtained using demonstrator instrument version 2.5 exclusively, since it proved to be the most reliable version constructed, and a large number of results are available. Furthermore, only results shall be considered for which a steady-state permeation rate was fully and doubtlessly established in order to preclude prematurely terminated measurements to impair the assessment of the *feasible* performance.

In Fig. 6-3 , the normalized uncertainty of repeatability (level of confidence: 95 %) of the thus selected results is plotted as a function of the associated OTR.[35] Clearly, the uncertainty follows a linear dependence on the OTR in the double-logarithmic plot. Extrapolation of the data to unity (where uncertainty equals transmission rate) implies a limit of detection of the instrument at the lower end of the 10^{-5} [$cm^3\,m^{-2}\,day^{-1}\,atm^{-1}$] regime. The development goal set within the Flexonics project has, with respect to resolution, thus been fully accomplished.

---

[35] The database is the same as in case of Fig. 5-11 on page 140, but results obtained with instruments of a version other than version 2.5 were excluded.
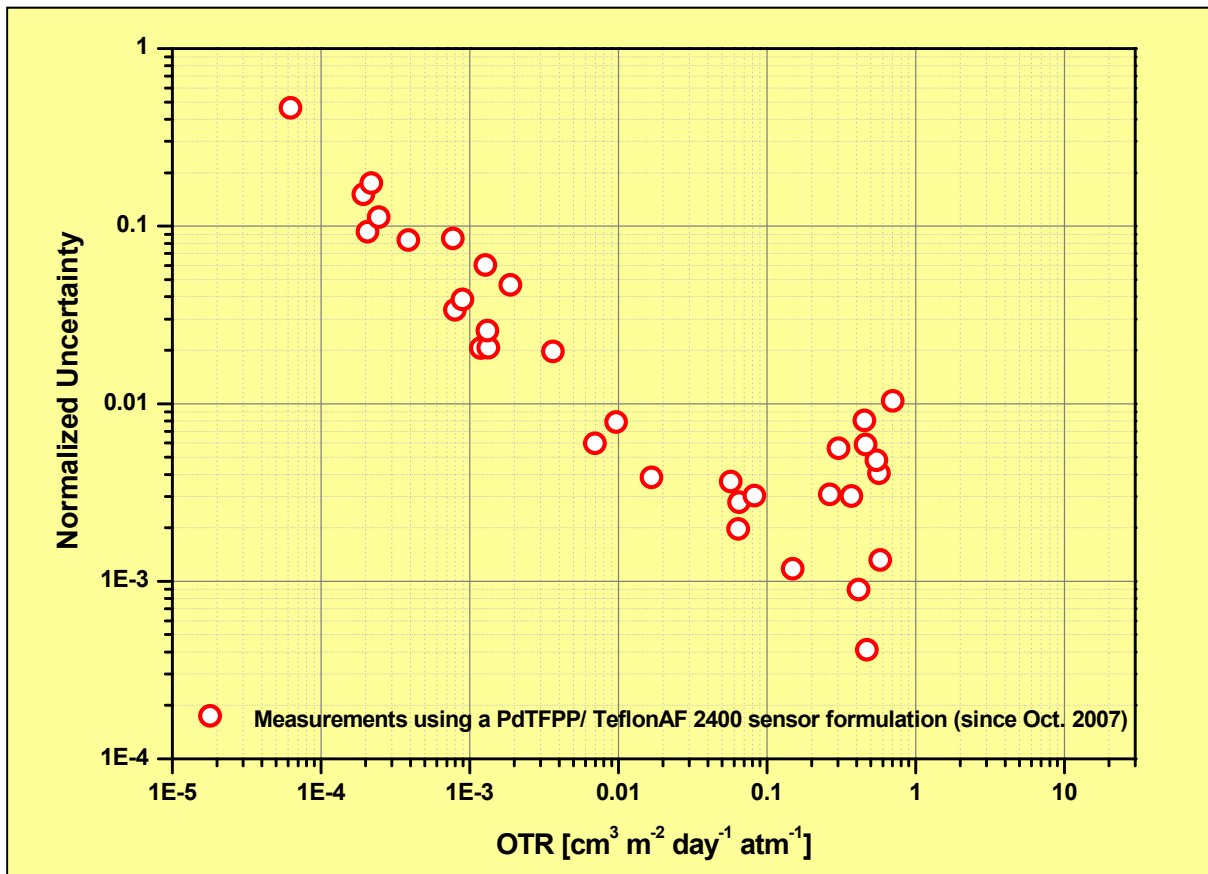
Fig. 6-3: Normalised measurement repeatability uncertainty (level of confidence 95 %) of OTR results as a function of associated OTR. Note that only results of measurements with an assured steady-state-permeation behaviour (sample membrane fully equilibrated) are included in the plot.

6.3 PERFORMANCE OF DEMONSTRATOR VERSION 3.0

Demonstrator Version 3.0 (see section 5.7.8) was set up for service in March 2008 and thus only few months before the end of Flexonics. In consequence, the number of results obtained within the project is, in consequence, much smaller than with demonstrator versions 2.x, and reference results have not been obtained with this device. However, it is the standard procedure since the entry to service to measure any sample on both devices in parallel, that is, demonstrator versions 2.5 and 3.0. In consequence, there are sufficient data to compare between the two devices.

A selection of results (ensured steady-state permeation) is shown in Fig. 6-4. Presumably due to imprecise calibration of the opto-chemical sensor and/or inaccuracies in the calculation of the receiving cavity volume, the results obtained with demonstrator instrument version 3.0 are on average higher by a factor of 1.6.
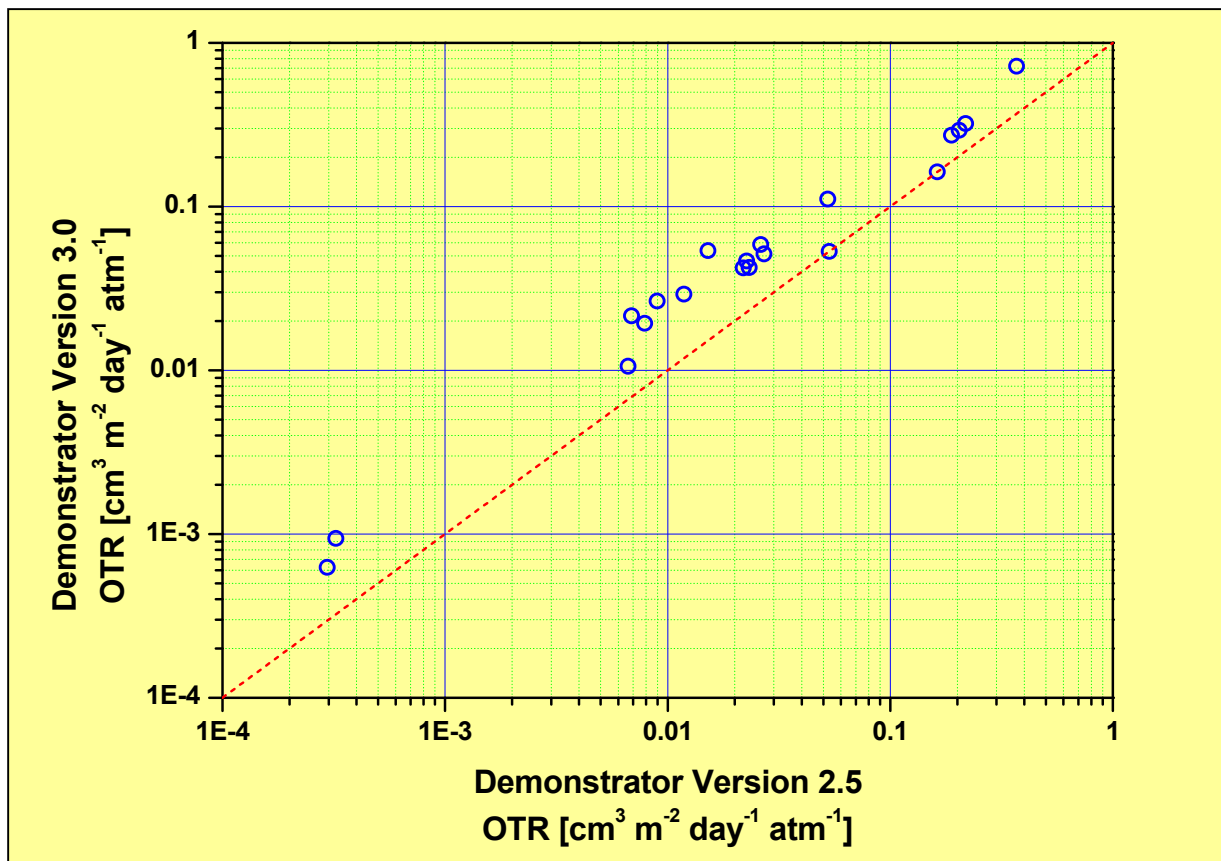
Fig. 6-4: Comparison of selected results obtained on demonstrator instruments of version 2.5 and version 3.0. Results obtained on version 3.0 are on average higher by factor of 1.6.

Unlike with instrument version 2.5, no sample with an OTR below 10^{-4} [cm^3 m^{-2} day^{-1} atm^{-1}] has ever been investigated. The normalized uncertainty of the results obtained is just slightly higher than in case of instrument version 2.5.

Despite all intentions to construct an instrument superior to demonstrator version 2.5, the attained performance is thus "only" similar. Note, however, that version 2.5 remains the somewhat more reliable instrument to this day with respect to handling, sample mounting and airtightness of the seal vestibule. In addition, the targeted elimination of surface absorption effects by gold-plating of the functional surfaces was only partially successful.

7 CONCLUSIONS AND OUTLOOK

The principle of very sensitive, high-resolution measurements of oxygen transmission rates based on an opto-chemical oxygen sensing system has been successfully demonstrated in the project conducted within this thesis. Two laboratory demonstrator instruments were constructed and remain in continuous service to this day. They thus represent a powerful alternative to conventional instruments measuring oxygen transmission rates through ultra-barrier membranes, as encountered in the field of organo-electronics encapsulation. The goal set within the Flexonics project was accomplished.

- Meanwhile, about 500 membranes were successfully tested with respect to their oxygen transmission rates. A significant fraction of the samples were related to Flexonics or follow-up projects conducted by Flexonics partners. Measurements in the course of commissioned research and internal projects related to ultra-barriers or the improvement of the instruments themselves supplemented the expertise in the field of transmission rate measurement by means of opto-chemical oxygen detection.

- The results indicate good repeatability and resolution over a wide range of transmission rates, and meanwhile the dynamic range of the instruments was extended to enable the characterisation of highly permeable polymer membranes as well.

- For the lowest transmission rate ever measured with these instruments a result of $6.25*10^{-5}$ [$cm^3\,m^{-2}\,day^{-1}\,atm^{-1}$] with an uncertainty with respect to precision of $1.4*10^{-5}$ [$cm^3\,m^{-2}\,day^{-1}\,atm^{-1}$] was obtained.

- The evaluation of the result uncertainty of a large number of measurements over a wide range of transmission rates indicates a limit of detection at the lower end of the 10^{-5} [$cm^3\,m^{-2}\,day^{-1}\,atm^{-1}$] regime. Thus, the opto-chemical concept is outperforming commercial instruments, with respect to the limit of detection, by two orders of magnitude.

- The accuracy of the instrument has been reasonably substantiated by comparison with reference results obtained in parallel on commercial instruments. Note, however, that near the limit of detection reference results were not available and that surface-chemical effects which are insignificant with higher transmission rates have the potential to distinctly impair the accuracy when testing ultra-barriers.

- The demonstrator instruments were designed as a stand-alone devices enabling similar convenience in operation as commercial instruments. Operational costs are low.

- Barrier testing at a defined, non-zero relative humidity has not been realized. All measurements are conducted at 0 % humidity.

- Diffusion phenomena taking place inside the permeation cell due to unfavourable geometric boundary conditions affect the linearity of the instruments. They may be circumvented, however, in a redesign of the permeation cell involving highly skilled mechanical engineering.

- The commercialisation or technology transfer, respectively, was attempted in the course of a number of according encounters with companies. In regard of the costs expected for product development and the expected market volume of merely a few thousand units worldwide, such attempts remained unsuccessful at the end.

It shall be noted that until 2015 the technique was not compliant with ASTM, ISO or DIN standards, which required the permeating oxygen to be passed to a coulometric sensor. Alternatively, volumetric or manometric measuring principles were described. The opto-chemical oxygen determination in the headspace of food packaging has been covered since 2008 by ASTM F2714-08. As late as 2015, ASTM 3136-15 [60] was introduced to explicitly cover the concept of dynamic accumulation and opto-chemical oxygen detection.

At the present stage, the capability of detecting ultra-low OTRs is not limited by the performance of the oxygen sensing system, as the resolution of the sensor is by far sufficient, and drift effects resulting from temperature fluctuations can be eliminated by constructive measures such as temperature stabilization.

Remarkably, surface-chemical processes which irreversibly adsorb minute amounts of oxygen onto the stainless-steel surfaces of the permeation cell at a slow rate appear to constrain the detection of even smaller transmission rates. Below a certain point, the rate of adsorption progressively competes with the rate of migration through the sample membrane, unacceptably contributing to the measurement error (see section 5.4.3). This, at first glance surprising, phenomenon was supported by according experiments and appears plausible in view of stoichiometric considerations.

The adverse effects do not apply solely to the opto-chemical methodology but supposedly impair the performance of other devices which are manufactured of aluminium or stainless steel as well. Since no commercial instrument is capable of detecting such low transmission rates, however, said effects may not have been recognized at all or do not impair the performance significantly and did thus not get into the focus.

In any way, the oxygen absorption phenomena must inevitably be addressed in the development of an instrument capable of detecting ultra-low transmission rates, regardless of the methodology, since minute amounts of permeating oxygen must be reliably preserved for detection.

The limit of detection of the opto-chemical OTR measuring method may be further improved and suspected accuracy issues circumvented if alternative materials, devoid of or less afflicted with such surface effects are used for manufacturing the permeation cell.

With the expertise gathered in years of experience with the methodology, the most important measures for any future development of an even more sensitive instrument appear to be:

- The use of intrinsically inert yet airtight materials for manufacturing the cell or a method to effectively passivate the relevant surfaces.

- Design and manufacture of a permeation cell of a more favourable geometry to prevent adverse diffusion phenomena. This includes the integration of the access valves directly into the cell body to avoid the creation of void volumes.

- Temperature stabilization for all critical components (opto-electronics) to a degree implied by the targeted device performance.

- Development and implementation of algorithms compensating for interfering temperature and kinetic effects

Finally, the practical establishment of statistical methods for a prognosis of the steady-state permeation rate as it has been demonstrated is recommended, since it would enable a distinct acceleration of the measurements, which can, particularly in case of multi-layer ultra-barrier membranes, take weeks or even months to complete.

APPENDIX

8 DISSEMINATION ACTIVITIES

The achievements accomplished in the development of the instrument for ultra-low oxygen transmission rate measurement were communicated to the scientific community:

Conference Talks

- M. Tscherner, C. Konrad, A. Bizzarri, V. Ribitsch, F. Stelzer, "*Opto-chemical Oxygen Permeability Measurements*", 7th Int. Conf. on Optical Technologies., Optical Sensors & Measuring Techniques (OPTO). Nürnberg (DE), 31.05.2006.

- M. Tscherner, C. Konrad, A. Bizzarri, M. Suppan, M. Cajlakovic, V. Ribitsch, F. Stelzer, "*Opto-chemical method for ultra-low oxygen transmission rate measurement*", IEEE Sensors, 2009, Christchurch (NZ), 27.10.2009.

- M. Tscherner, M. Buder-Stroissnigg, C. Bodor, G. Pinter, V. Ribitsch, F. Stelzer, „*Messung der Permeations- und Barriereeigenschaften von Kunststoffen*", PCCL-Symposium, Leoben (AT), 20.05.2011.

Conference Proceedings

- M. Tscherner, C. Konrad, A. Bizzarri, V. Ribitsch, F. Stelzer, "Opto-chemical Oxygen Permeability Measurements", Proceedings of the 7th Int. Conf. on Optical Technologies, Optical Sensors & Measuring Techniques (OPTO), Nürnberg (2006) 79-84.

- M. Tscherner, C. Konrad, A. Bizzarri, M. Suppan, M. Cajlakovic, V. Ribitsch, F. Stelzer, "Opto-chemical method for ultra-low oxygen transmission rate measurement", IEEE Sensors (2009) 1660-1665. DOI: 10.1109/ICSENS.2009.5398515.

In addition, the initiation of technology transfer for commercialisation was attempted in the course of a number of bilateral negotiations with renowned manufacturers of analytical equipment. Unfortunately, none of the attempts resulted in the actual commercialisation of the methodology.

- Anton Paar GmbH (Continuous informal communication, 2005-2008)

- PBI Dansensor (Personal meeting in Graz, June 2006)

- Systech Instruments (Electronic communication and characterisation of test samples in 2009)

- ExtraSolution (Personal meeting in Graz, 2011)

In 2006 furthermore, measures for intellectual property protection were discussed and the according potential was evaluated. Due to "prior art" represented by the work of Rharbi et al. [37], however, protection of the overall methodology is no longer possible.

9 LIST OF ABBREVIATIONS

AlO$_x$	Non-stoichiometric aluminium oxide
ASTM	American Society for Testing and Materials
CCD	Charge-coupled device
CiP	Cleaning in Place
DIN	Deutsches Institut für Normung
EWMA	Exponentially weighted moving average
FFV	Fractional free volume
FKM	Fluoroelastomers as defined in ASTM D1418
FPGA	Field programmable gate array
FRET	Förster resonance energy transfer, often mistakenly interpreted as "fluorescent resonance energy transfer"
ISC	Inter-system crossing
LED	Light-emitting diode
LOD	Limit of detection
MFC	Mass flow controller
MLC	Metal-ligand complex
OEM	Original equipment manufacturer
OLED	Organic light-emitting diode
OPV	Organic photovoltaics
OTR	Oxygen transmission rate
Pa	Pascal
PALS	Positron annihilation lifetime spectroscopy
PDMS	Poly(dimethylsiloxane)
PdTFPP	Palladium(II)-5,10,15,20-tetrakis-(2,3,4,5,6-pentafluorphenyl)-porphyrin
PET	Poly(ethylene terephthalate)
PMT	Photomultiplier tube
pO2	Oxygen partial pressure
ppb	Parts per billion
ppm	Parts per million
PS	Polystyrene
Pt	Platinum
PTFE	Poly(tetrafluoroethylene)
PTMSP	Poly[1-(trimethylsilyl)-1-propyne]
PtOEPK	Platinum-(II)-octaethylporphyrin ketone
PtTFPP	Platinum(II)-5,10,15,20-tetrakis-(2,3,4,5,6-pentafluorphenyl)-porphyrin
PVC	Polyvinylchloride
RET	Resonance energy transfer
RH	Relative humidity
SEM	Standard error of the mean
SiO$_x$	Non-stoichiometric silicon oxide (glass-like)
STP	Standard Temperature and Pressure
TCSPC	Time-correlated single photon counting
Tg	Glass transition temperature
WVTR	Water vapour transmission rate
WLF-Equation	Williams-Landel-Ferry-Equation
τ	Luminescence lifetime
Φ	Phase shift angle

10 REFERENCES

[1]   J. S. Lewis and M. S. Weaver, *"Thin-film permeation-barrier technology for flexible organic light-emitting devices"*, IEEE Journal of Selected Topics in Quantum Electronics 10/1 (2004) 45-57.
DOI: 10.1109/JSTQE.2004.824072

[2]   J. Lewis, *"Material challenge for flexible organic devices"*, Materials Today 9/4 (2006) 38-45.
DOI: 10.1016/S1369-7021(06)71446-8

[3]   P. E. Burrows, G. L. Graff, M. E. Gross *et al.*, *"Gas permeation and lifetime tests on polymer-based barrier coatings"*, International Symposium on Optical Science and Technology, San Diego, US (2001).
DOI: 10.1117/12.416878

[4]   G. Nisato, P. C. P. Bouten, P. J. Slikkerveer *et al.*, *"Evaluating High Performance Diffusion Barriers: the Calcium Test"*, Proc. of the International Display Workshop/ Asia Display, San Jose, US (2001) 1435–1438.

[5]   G. Nisato, M. Kuilder, P. Bouten *et al.*, *"Thin Film Encapsulation for OLEDs: Evaluation of Multi-layer Barriers using the Ca Test"*, SID Symposium Digest of Technical Papers (2003) 550-553.
DOI: 10.1889/1.1832335

[6]   E. Guenther, R. S. Kumar, F. Zhu *et al.*, *"Building blocks for ultrathin flexible organic electroluminescent devices"*, International Symposium on Optical Science and Technology, San Diego, US (2002).
DOI: 10.1117/12.457476

[7]   J. Fahlteich, M. Fahland, S. Straach *et al.*, *"Transparente Barriereschichten auf flexiblen Polymersubstraten"*, Vakuum in Forschung und Praxis 23/4 (2011) 29-37.
DOI: 10.1002/vipr.201100464

[8]   P. E. Burrows, G. L. Graff, M. E. Gross *et al.*, *"Ultra barrier flexible substrates for flat panel displays"*, Displays 22/2 (2001) 65-69.
DOI: 10.1016/S0141-9382(00)00064-0

[9]   G. Dennler, C. Lungenschmied, H. Neugebauer *et al.*, *"A new encapsulation solution for flexible organic solar cells"*, Thin Solid Films 511/Supplement C (2006) 349-353.
DOI: 10.1016/j.tsf.2005.12.091

[10]   Jeffry Funk, "**Flexible OLED Displays**" (Presentation Slides, Last Access 09/2017).
URL: www.slideshare.net/Funk98/flexible-oled-displays

[11]   MOCON, "**OX-TRAN® Model 2/21**" (Product Brochure, Last Access 03/2008).
URL: www.mocon.com/pdfperm/OXTRAN%202-21Nov07.pdf

[12]   MOCON, "**OX-TRAN® Model 2/22 Series**" (Product Brochure, Last Access 09/2017).
URL: www.mocon.com/assets/documents/mocon-ox-tran-222-data-sheet-pps.ds.0100.v1.3-web.pdf

[13]   MOCON, "**AQUATRAN® Model 1**" (Product Brochure, Last Access 03/2008).
URL: www.mocon.com/pdfperm/AQUATRANPDF.pdf

[14]   MOCON, "**AQUATRAN® Model 2**" (Product Brochure, Last Access 09/2017).
URL: www.mocon.com/assets/documents/aquatran2.pdf

[15]   Flexonics Consortium (Project Web Page, Last Access 09/2017).
URL: www.flexonics.org/

[16]   J. Fahlteich, *"Transparente Hochbarriereschichten auf flexiblen Substraten"*, Doctoral Thesis, Fakultät für Naturwissenschaften, University of Chemnitz (2010).
URL: www.qucosa.de/fileadmin/data/qucosa/documents/6451/DissFahlteich_online_A1b.pdf

[17]   M.P. Rosenblum (Vitex Systems Inc.), "**Barrier Film, Technology and Scaling**" (Electronic Article, Last Access 10/2007).
URL: http://cips.mit.edu/documents/5_03_06.RosenblumFinall.Vitex.pdf

[18]   N. Rutherford (Vitex Systems Inc.), "**Flexible Displays – A Low Cost Substrate/ Encapsulation Packaging Solution**" (Electronic Article, Last Access 10/2007).
URL: www.vitexsys.com/new/downloads/USDC_Flex_2005_Vitex.pdf

[19]   L. Moro (Vitex Systems Inc.), "**Integrated encapsulation of bottom and top emission OLED displays**" (Electronic Article, Last Access 10/2007).
URL: www.vitexsys.com/new/downloads/SPIE_2004_presentation.pdf

[20]   European Commission, FP6 Programme, Specific Targeted Research Project No. NMP3-CT-2005-013883 "**Flexonics**" (39 months).
URL: www.flexonics.org/index.php

[21]   R. E. Kesting and A. K. Fritzsche, *"Polymeric gas separation membranes"*, John Wiley & Sons Inc. (New York, 1993).

[22]   R. Baker, *"Membrane Technology in the Chemical Industry: Future Directions"* in "*Membrane Technology*", pp. 268-295, Wiley-VCH Verlag GmbH (2001).
DOI: 10.1002/3527600388.ch13

[23]   R. Gensler (Siemens) in personal communication about Calcium Degradation Tests (2007).

[24]   J. Hauch (Konarka) in personal communication about Calcium Degradation Tests (2007).

[25]   J. Brandrup, E. H. Immergut and E. A. Grulke, *"Polymer handbook"*, 4th ed., Wiley (New York, 1999).

[26]   E. L. Cussler, S. E. Hughes, W. J. Ward *et al.*, *"Barrier membranes"*, *Journal of Membrane Science* 38/2 (1988) 161-174.
       DOI: /10.1016/S0376-7388(00)80877-7

[27]   L. E. Nielsen, *"Models for the Permeability of Filled Polymer Systems"*, *Journal of Macromolecular Science: Part A - Chemistry* 1/5 (1967) 929-942.
       DOI: 10.1080/10601326708053745

[28]   N. Toshima, *"Polymers for gas separation"*, VCH (New York/Weinheim/Cambridge, 1992).

[29]   S. P. Nunes and K. V. Peinemann, *"Gas Separation with Membranes"* in *"Membrane Technology"*, pp. 39-67, Wiley-VCH Verlag GmbH (2001).
       DOI: 10.1002/3527600388.ch6

[30]   J. G. Wijmans and R. W. Baker, *"The Solution–Diffusion Model: A Unified Approach to Membrane Permeation"* in *"Materials Science of Membranes for Gas and Vapor Separation"*, pp. 159-189, John Wiley & Sons, Ltd (2006).
       DOI: 10.1002/047002903X.ch5

[31]   P. Mercea, *"Models for diffusion in polymers"* in *"Plastic Packaging Materials for Food"*, pp. 125-157, Wiley-VCH Verlag GmbH (2000).
       DOI: 10.1002/9783527613281.ch05

[32]   O. Piringer, *"Transport equations and their solutions"* in *"Plastic Packaging Materials for Food"*, pp. 183-219, Wiley-VCH Verlag GmbH (2000).
       DOI: 10.1002/9783527613281.ch07

[33]   S. Matteucci, Y. Yampolskii, B. D. Freeman *et al.*, *"Transport of Gases and Vapors in Glassy and Rubbery Polymers"* in *"Materials Science of Membranes for Gas and Vapor Separation"*, pp. 1-47, John Wiley & Sons, Ltd (2006).
       DOI: 10.1002/047002903X.ch1

[34]   O. Piringer, *"Permeation of gases, water vapor and volatile organic compounds"* in *"Plastic Packaging Materials for Food"*, pp. 239-285, Wiley-VCH Verlag GmbH (2000).
       DOI: 10.1002/9783527613281.ch09

[35]   *"Appendix I"* in *"Plastic Packaging Materials for Food"*, pp. 479-530, Wiley-VCH Verlag GmbH (2000).
       DOI: 10.1002/9783527613281.app1

[36]   D. W. Van Krevelen, *"Chapter 18 - Properties Determining Mass Transfer in Polymeric Systems"* in *"Properties of Polymers (Third, completely revised edition)"*, pp. 535-583, Elsevier (Amsterdam, 1997).
       DOI: 10.1016/B978-0-444-82877-4.50025-1

[37]   Y. Rharbi, A. Yekta and M. A. Winnik, *"A Method for Measuring Oxygen Diffusion and Oxygen Permeation in Polymer Films Based on Fluorescence Quenching"*, *Analytical Chemistry* 71/22 (1999) 5045-5053.
       DOI: 10.1021/ac990193c

[38]   A. Alentiev and Y. Yampolskii, *"Prediction of Gas Permeation Parameters of Polymers"* in *"Materials Science of Membranes for Gas and Vapor Separation"*, pp. 211-229, John Wiley & Sons, Ltd. (2006).
       DOI: 10.1002/047002903X.ch7

[39]   O. Piringer, *"Prediction of diffusion coefficients in gases, liquids, amorphous solids and plastic materials using an uniform model"* in *"Plastic Packaging Materials for Food"*, pp. 159-181, Wiley-VCH Verlag GmbH (2000).
       DOI: 10.1002/9783527613281.ch06

[40]   Y. Yampolskii and V. Shantarovich, *"Positron Annihilation Lifetime Spectroscopy and Other Methods for Free Volume Evaluation in Polymers"* in *"Materials Science of Membranes for Gas and Vapor Separation"*, pp. 191-210, John Wiley & Sons, Ltd. (2006).
       DOI: 10.1002/047002903X.ch6

[41]   M. Macchione, J. C. Jansen, G. De Luca *et al.*, *"Experimental analysis and simulation of the gas transport in dense Hyflon® AD60X membranes: Influence of residual solvent"*, *Polymer* 48/9 (2007) 2619-2635.
       DOI: 10.1016/j.polymer.2007.02.068

[42]   M. G. De Angelis, T. C. Merkel, V. I. Bondar *et al.*, *"Gas Sorption and Dilation in Poly(2,2-bistrifluoromethyl-4,5-difluoro-1,3-dioxole-co-tetrafluoroethylene): Comparison of Experimental Data with Predictions of the Nonequilibrium Lattice Fluid Model"*, *Macromolecules* 35/4 (2002) 1276-1288.
       DOI: 10.1021/ma0106090

[43]   T. C. Merkel, V. Bondar, K. Nagai *et al.*, *"Gas Sorption, Diffusion, and Permeation in Poly(2,2-bis(trifluoromethyl)-4,5-difluoro-1,3-dioxole-co-tetrafluoroethylene)"*, *Macromolecules* 32/25 (1999) 8427-8440.
       DOI: 10.1021/ma990685r

[44]   T. C. Merkel, I. Pinnau, R. Prabhakar *et al.*, *"Gas and Vapor Transport Properties of Perfluoropolymers"* in *"Materials Science of Membranes for Gas and Vapor Separation"*, pp. 251-270, John Wiley & Sons, Ltd (2006).
       DOI: 10.1002/047002903X.ch9

[45]   A. Y. Alentiev, V. P. Shantarovich, T. C. Merkel *et al.*, *"Gas and Vapor Sorption, Permeation, and Diffusion in Glassy Amorphous Teflon AF1600"*, *Macromolecules* 35/25 (2002) 9513-9522.
       DOI: 10.1021/ma020494f

[46] O. S. Wolfbeis, *"Luminescent sensing and imaging of oxygen: Fierce competition to the Clark electrode"*, *BioEssays* 37/8 (2015) 921-928.
DOI: 10.1002/bies.201500002

[47] J. R. Lakowicz, *"Principles of Fluorescence Spectroscopy"*, 3rd ed., Springer (New York, 2006).

[48] W. R. G. Baeyens, D. D. Keukeleire and K. Korkidis, *"Luminescence techniques in chemical and biochemical analysis"*, Marcel Dekker (1991).

[49] A.-C. Knall, *"Synthesis and Characterisation of Functional Materials for Water Vapor Sensors"*, Doctoral Thesis, Institute for Chemistry and Technology of Materials, *Technical University Graz* (2008).

[50] X.-d. Wang and O. S. Wolfbeis, *"Optical methods for sensing and imaging oxygen: materials, spectroscopies and applications"*, *Chemical Society Reviews* 43/10 (2014) 3666-3761.
DOI: 10.1039/c4cs00039k

[51] O. Stern and M. Volmer, *"Über die Abklingzeit der Fluoreszenz"*, *Physikalische Zeitschrift* 20 (1919) 183-188.

[52] Wikipedia, "*Levenberg–Marquardt algorithm*" (Last Access 09/2017).
URL: https://en.wikipedia.org/wiki/Levenberg%E2%80%93Marquardt_algorithm

[53] W. H. Press, S. A. Teukolsky, W. T. Vetterling *et al.*, *"Numerical Recipes in C: The Art of Scientific Computing, Second Edition"*, Cambridge University Press (Cambridge/New York/Port Chester/Melbourne/Sydney, 1992).

[54] A. Grinvald and I. Z. Steinberg, *"On the analysis of fluorescence decay kinetics by the method of least-squares"*, *Analytical Biochemistry* 59/2 (1974) 583-598.
DOI: 10.1016/0003-2697(74)90312-1

[55] J. R. Lakowicz, G. Laczko, H. Cherek *et al.*, *"Analysis of fluorescence decay kinetics from variable-frequency phase shift and modulation data"*, *Biophysical Journal* 46/4 (1984) 463-477.
URL: www.ncbi.nlm.nih.gov/pmc/articles/PMC1435017/

[56] O. S. Wolfbeis, *"Chemical Sensing Using Indicator Dyes"* in "*Optical fiber sensors 4. Applications, analysis, and future trends*", 8, eds. J. Dakin and B. Culshaw, pp. 53-107, Artech House (Boston, 1997).
URL: epub.uni-regensburg.de/21556/

[57] M. Trinkel, *"Optochemical sensors for trace oxygen analysis"*, Faculty of Natural Scieces, *Karl-Franzenz-University of Graz* (1998).

[58] M. Quaranta, S. M. Borisov and I. Klimant, *"Indicators for optical oxygen sensors"*, *Bioanalytical Reviews* 4/2-4 (2012) 115-157.
DOI: 10.1007/s12566-012-0032-y

[59] ASTM International, *"Standard Test Method for Water Vapor Transmission Rate of Sheet Materials Using Dynamic Relative Humidity Measurement"*, Document ASTM E398-13 (2013).
DOI: 10.1520/E0398

[60] ASTM International, *"Standard Test Method for Oxygen Gas Transmission Rate through Plastic Film and Sheeting using a Dynamic Accumulation Method"*, Document ASTM F3136-15 (2015).
DOI: 10.1520/F3136-15

[61] R. A. Pasternak, J. F. Schimscheimer and J. Heller, *"A dynamic approach to diffusion and permeation measurements"*, *Journal of Polymer Science Part A-2: Polymer Physics* 8/3 (1970) 467-479.
DOI: 10.1002/pol.1970.160080312

[62] A. Abdellatief and B. A. Welt, *"Comparison of New Dynamic Accumulation Method for Measuring Oxygen Transmission Rate of Packaging against the Steady-State Method Described by ASTM D3985"*, *Packaging Technology and Science* 26/5 (2013) 281-288.
DOI: 10.1002/pts.1974

[63] MOCON, "*OX-TRAN® Model 702*" (Product Brochure, Last Access 09/2017).
URL: www.mocon.com/assets/documents/oxtran702.pdf

[64] MOCON, "*OX-TRAN® Model 2/61*" (Product Brochure, Last Access 09/2017).
URL: www.mocon.com/assets/documents/oxtran261.pdf

[65] MOCON, "*Permeation in Flexible Electronics*" (Presentation Slides, Last Access 09/2017).
URL: www.slideshare.net/guywray/wvtr-otr-in-flexible-electronics-moconincv02ss-39202169

[66] ASTM International, *"Standard Test Method for Determining Gas Permeability Characteristics of Plastic Film and Sheeting"*, Document ASTM D1434-82 (2003).
DOI: 10.1520/D1434-82R03

[67] Mecadi, "*Gasdurchlässigkeit (volumetrisch) nach DIN 53380-1 bzw. nach DIN 53380-V*" (Last Access 09/2017).
URL: www.mecadi.com/de/permeationsmessungen/gasdurchlaessigkeit/gas-permeation-volumetrisch-din-53380-1-bzw-din-53380-v

[68] Mecadi, "*Gasdurchlässigkeit (manometrisch) nach DIN 53380-2 bzw. DIN 53380-M*" (Last Access 09/2017).
URL: www.mecadi.com/de/permeationsmessungen/gasdurchlaessigkeit/gas-permeation-manometrisch-din-53380-2-bzw-din-53380-m

[69] Mecadi, "*Gasdurchlässigkeit (Trägergas-Verfahren) nach DIN 53380-3 bzw. DIN 53380-S*" (Last Access 09/2017).
URL: www.mecadi.com/de/permeationsmessungen/gasdurchlaessigkeit/gas-permeation-tr%C3%A4gergas-verfahren-din-53380-3-bzw-din-53380-s

[70] Mecadi, "*Gasdurchlässigkeit (IR-Absorptionsverfahren) nach DIN 53380-4 bzw. DIN 53380-I*" (Last Access 09/2017).
URL: www.mecadi.com/de/permeationsmessungen/gasdurchlaessigkeit/gas-permeation-ir-absorptionsverfahren-din-53380-4-bzw-din-53380-i

[71] ASTM International, *"Standard Test Method for Oxygen Gas Transmission Rate Through Plastic Film and Sheeting Using a Coulometric Sensor"*, Document ASTM D3985-05 (2005).
DOI: 10.1520/D3985-05

[72] ASTM International, *"Standard Test Method for Determination of Oxygen Gas Transmission Rate, Permeability and Permeance at Controlled Relative Humidity Through Barrier Materials Using a Coulometric Detector"*, Document ASTM F1927-07 (2007).
DOI: 10.1520/F1927-07

[73] Systech Illinois, "*8000 Series - Oxygen Permeation Analyzers* " (Product Brochure, Last Access 09/2017).
URL: www.systechillinois.com/assets/uploads/products/8001-oxygen-analyzer/8000%20U.S.pdf

[74] ASTM International, *"Standard Practice for Maintaining Constant Relative Humidity by Means of Aqueous Solutions"*, Document ASTM E104-02 (2007).
DOI: 10.1520/E0104-02R07

[75] International Organization for Standardization, *"Plastics -- Film and sheeting -- Determination of gas-transmission rate -- Part 2: Equal-pressure method"*, Document ISO 15105-2:2003 (2003).
URL: www.iso.org/standard/37514.html

[76] Deutsches Institut für Normung, *"Prüfung von Kunststoffen - Bestimmung der Gasdurchlässigkeit - Teil 3: Sauerstoffspezifisches Trägergas-Verfahren zur Messung an Kunststoff-Folien und Kunststoff-Formteilen"*, Document DIN 53380-3 (1998).
URL: www.din.de/de/mitwirken/normenausschuesse/fnk/normen/wdc-beuth:din21:3725281

[77] Systech Illinois (Company Website, Last Access 09/2017).
URL: www.systechillinois.com/en/

[78] ASTM International, *"Standard Test Method for Oxygen Gas Transmission Rate Through Plastic Film and Sheeting Using Various Sensors"*, Document ASTM F2622-08e1 (2008).
DOI: 10.1520/F2622-08E01

[79] H. Voraberger, *"Novel opto-chemical methods for non-invasive oxygen measurement in transparent packages or containers and their performance during application"*, *Europtrode VII*, Madrid, ES (2004).

[80] A. Bizzarri, W. Gruber, W. Trettnak *et al.*, *"Opto-chemical sensor for oxygen measurements in sealed packages"*, *4th International Conference and Exhibition on Optoelectronics, Optical Sensors and Measuring Techniques (OPTO 2000)*, Erfurt, DE (2000) 193-198.

[81] C. Konrad, G. Zanker, A. Bizzarri *et al.*, *"Novel optochemical method for the non destructive determination of oxygen in encapsulated beer bottles"*, *30th EBC Congress*, Prague, CZ (2005).
URL: getinfo.de/app/Novel-optochemical-method-for-the-non-destructive/id/BLCP%3ACN057805521

[82] G. P. Crawford, *"Flexible Flat Panel Display Technology"* in "*Flexible Flat Panel Displays"*, pp. 1-9, John Wiley & Sons, Ltd (2005).
DOI: 10.1002/0470870508.ch1

[83] ASTM International, *"Standard Test Method for Oxygen Headspace Analysis of Packages Using Fluorescent Decay"*, Document ASTM F2714-08 (2008).
DOI: 10.1520/F2714-08

[84] ASTM International, "*Technical Committee F02 (15-01); Test Method For Oxygen Gas Transmission Rate through Plastic Film and Sheeting using a Dynamic Accumulation Method WK43413*" (Last Access 09/2017).
URL: www.astm.org/SOCIETY_REVIEW/F02%20(15-01).htm

[85] MOCON, "*OX-TRAN® Model 2/21 Series*" (Announcement about discontinuation, Last Access 09/2017).
URL: www.mocon.com/instruments/ox-tran-model-2-21.html

[86] MOCON, "*OX-TRAN® Model 2/10*" (Product Brochure, Last Access 09/2017).
URL: www.mocon.com/assets/documents/oxtran210.pdf

[87] MOCON (Information on the Company History, Last Access 09/2017).
URL: www.mocon.com/about-mocon/history.html

[88] International Organization for Standardization, *"Plastics - Film and sheeting - Determination of water vapour transmission rate - Part 3: Electrolytic detection sensor method"*, Document ISO 15106-3:2003 (2003).
URL: www.iso.org/standard/29783.html

[89] MOCON, "*PERMATRAN-W Model 1/50*" (Product Brochure, Last Access 09/2017).
URL: www.mocon.com/mocon-model-1.50-bundle-web.pdf

[90] Systech Illinois, "*About Systech Illinois: Gas Analysis Experts*" (Company Information, Last Access 09/2017).
URL: www.systechillinois.com/de/company/about-us/

[91] Systech Illinois, "*All oxygen permeation instruments are created equal*" (Commercial, Last Access 09/2017).
URL: www.systechillinois.com/en/news-and-events/news/2017/07/03/all-oxygen-permeation-instruments-are-created-equal/

[92] Systech Illinois, "***OxySense and Systech Illinois join forces***" (Announcement, Last Access 09/2017).
URL: www.systechillinois.com/en/news-and-events/news/2017/07/26/oxysense-and-systech-illinois-join-forces/

[93] PBI Dansensor, "***L100-5000 Manometric Gas Permeability Tester***" (Product Brochure, Last Access 03/2008).
URL: www.pbi-dansensor.com/Products/Permeability%20Testers/L100-5000.aspx

[94] PBI Dansensor, "***OPT-5000 Oxygen Permeability Tester***" (Product Brochure, Last Access 09/2017).
URL: www.pbi-dansensor.com/Products/Permeability%20Testers/OPT-5000.aspx

[95] PBI Dansensor, "***News 2010: Divesting of Lyssy Line***" (Announcement, Last Access 12/2010).
URL: http://dansensor.de/News/2010/Divesting%20of%20Lyssy%20Line

[96] ExtraSolution (Company Website, Last Access 09/2017).
URL: www.extrasolution.it/en

[97] ExtraSolution in personal communication about Product Information Brochures (2011).

[98] A. Piombini and M. Lucchesi, ***"Method for Measuring the Gas Permeability of Containers and Sealing Members in General"***, Patent No. WO 2008/032170 A3, to "ExtraSolution S.R.L." (Italy, 2006).

[99] Labthink, "***TOY-C3 Film&Package Oxygen Permeability Tester***" (Product Brochure, Last Access 03/2008).
URL: www.labthink.cn/upimages/20080318110312984.pdf

[100] Labthink International, "***Gas Permeability Tester, Overview***" (Product Portfolio, Last Access 09/2017).
URL: www.labthinkinternational.com/products/test-property/gas-permeability-tester.html

[101] Presens, "***Permeation Cell***" (Product Information, Last Access 08/2017).
URL: www.presens.de/products/detail/permeation-cell.html

[102] D. Timineri, G. T. John, K. Müller *et al.*, GuiaEnvase PackGuide, "***Oxygen Permeation Measurement with Chemical Optical Sensors***" (Last Access 09/2017).
URL: envases-barrera.guiaenvase.com/en/articles-packaging-innovation/test-equipments-measuring-permeation/oxygen-permeation-measurement-with-chemical-optical-sensors/

[103] Meeting Pack 2013, "***Daniela Timineri: Oxygen permeation measurement with chemical optical sensors***" (Conference Programme, Last Access 09/2017).
URL: http://2013.meetingpack.com/eng/programa_sesion2.html

[104] OxySense (Company Website, Last Access 09/2017).
URL: www.oxysense.com/

[105] OxySense, "***How Oxygen is Measured Within a Package / PET Bottle***" (Supplementary Product Information, Last Access 09/2017).
URL: http://oxysense.com/how-oxysense-works.html

[106] OxySense, "***Optical Oxygen Analyzers, Scalable Permeation System for Films, Bottles and Packages and Inline Oxygen Monitoring***" (Product Portfolio, Last Access 09/2017).
URL: http://oxysense.com/oxygen-analyzers-permeation-testing.html

[107] OxySense, "***Optical Oxygen Analyzer - OxySense 5250i***" (Product Information, Last Access 09/2017).
URL: www.oxysense.com/oxygen-measurement-system-5250i.html

[108] OxySense, "***OxyPerm Permeation/OTR System***" (Product Information, Last Access 09/2017).
URL: www.oxysense.com/permeation-analyzer-OTR-testing.html

[109] OxySense, "***New ASTM Standard Approved For Dynamic Accumulation OTR***" (Announcement, Last Access 09/2017).
URL: http://oxysense.com/oxysense-news-Dynamic-Accumulation-OTR.html

[110] OxySense, "***Advancement in Permeation Measurement Technology***" (Announcement, Last Access 09/2017).
URL: http://oxysense.com/oxysense-news-permeation-measurement.html

[111] R. Paetzold, A. Winnacker, D. Henseler *et al.*, *"Permeation rate measurements by electrical analysis of calcium corrosion"*, *Review of Scientific Instruments* 74/12 (2003) 5147-5150.
DOI: 10.1063/1.1626015

[112] R. Paetzold, D. Henseler, K. Heuser *et al.*, ***"High-sensitivity permeation measurements on flexible OLED substrates"***, *Proc. SPIE 5214, Organic Light-Emitting Materials and Devices VII, 73* (2004) 73-82.
DOI: 10.1117/12.510027

[113] J. H. Choi, Y. M. Kim, Y. W. Park *et al.*, *"Evaluation of gas permeation barrier properties using electrical measurements of calcium degradation"*, *Review of Scientific Instruments* 78/6 (2007) 064701.
DOI: 10.1063/1.2747168

[114] P. Jin-Seong, C. Heeyeop, C. Ho Kyoon *et al.*, *"Thin film encapsulation for flexible AM-OLED: a review"*, *Semiconductor Science and Technology* 26/3 (2011) 034001.
URL: stacks.iop.org/0268-1242/26/i=3/a=034001

[115] R. Dunkel, R. Bujas, A. Klein *et al.*, *"A new method for measuring ultra-low water-vapor permeation for OLED displays"*, *Journal of the Society for Information Display* 13/7 (2005) 569-573.
DOI: 10.1889/1.2001214

[116] M. S. Weaver, L. A. Michalski, K. Rajan *et al.*, *"Organic light-emitting devices with extended operating lifetimes on plastic substrates"*, *Applied Physics Letters* 81/16 (2002) 2929-2931.
DOI: 10.1063/1.1514831

[117] A. Yekta, Z. Masoumi and M. A. Winnik, *"Luminescence measurements of oxygen permeation and oxygen diffusion in thin polymer films"*, *Canadian Journal of Chemistry* 73/11 (1995) 2021-2029.
DOI: 10.1139/v95-250

[118] S. Hess, A. Becker, S. Baluschev *et al.*, *"A Comparative Study of Oxygen Permeabilities of Film-Forming Polymers by Quenching of Platinum Porphyrin Phosphorescence"*, *Macromolecular Chemistry and Physics* 208/19-20 (2007) 2173-2188.
DOI: 10.1002/macp.200700196

[119] S. Hess, M. M. Demir, V. Yakutkin *et al.*, *"Investigation of Oxygen Permeation through Composites of PMMA and Surface-Modified ZnO Nanoparticles"*, *Macromolecular Rapid Communications* 30/4-5 (2009) 394-401.
DOI: 10.1002/marc.200800732

[120] Sandra Hess, "*Measurement of Extra-Low Permeation Rates*" (Electronic Article, Last Access 09/2017).
URL: www2.mpip-mainz.mpg.de/groups/wegner/Research/pdf/permeationrates.pdf

[121] M. Knausz, *"Einfluss polymerer Einkapselungsmaterialien auf die Qualität und Zuverlässigkeit von PV Modulen "*, Doctoral Thesis, Lehrstuhl für Werkstoffkunde und Prüfung der Kunststoffe, *Montanuniversität Leoben* (2015).
URL: https://online.unileoben.ac.at/mu_online/wbAbs.showThesis?pThesisNr=51877&pOrgNr=15055

[122] C. Bodor, *"Entwicklung einer In-Situ-Permeations-Mess-Apparatur für die Detektion von flüchtigen Kohlenwasserstoffen und die Messung der Permeationsrate an thermoplastischen Kunststoffrohren"*, Master Thesis, Lehrstuhl für Werkstoffkunde und Prüfung der Kunststoffe, *Montanuniversität Leoben* (2011).
URL: https://online.unileoben.ac.at/mu_online/wbAbs.showThesis?pThesisNr=26376&pOrgNr=15163

[123] M. Trinkel, W. Trettnak and C. Kolle, *"Oxygen trace analysis utilising a miniaturised luminescence lifetime-based sensor instrumentation"*, *Quimica Analitica* 19 (2000) 112-117.
URL: acnpsearch.unibo.it/singlejournalindex/7696103

[124] S. M. Borisov and I. Klimant, *"Ultrabright Oxygen Optodes Based on Cyclometalated Iridium(III) Coumarin Complexes"*, *Analytical Chemistry* 79/19 (2007) 7501-7509.
DOI: 10.1021/ac0710836

[125] D. B. Papkovsky and T. C. O'Riordan, *"Emerging Applications of Phosphorescent Metalloporphyrins"*, *Journal of Fluorescence* 15/4 (2005) 569-584.
DOI: 10.1007/s10895-005-2830-x

[126] O. S. Wolfbeis, *"Fiber-Optic Chemical Sensors and Biosensors"*, *Analytical Chemistry* 78/12 (2006) 3859-3874.
DOI: 10.1021/ac060490z

[127] C. McDonagh, C. Kolle, A. K. McEvoy *et al.*, *"Phase fluorometric dissolved oxygen sensor"*, *Sensors and Actuators B: Chemical* 74/1 (2001) 124-130.
DOI: 10.1016/S0925-4005(00)00721-8

[128] C. O'Donovan, J. Hynes, D. Yashunski *et al.*, *"Phosphorescent oxygen-sensitive materials for biological applications"*, *Journal of Materials Chemistry* 15/27-28 (2005) 2946-2951.
DOI: 10.1039/b501748c

[129] A. Mills, *"Oxygen indicators and intelligent inks for packaging food"*, *Chemical Society Reviews* 34/12 (2005) 1003-1011.
DOI: 10.1039/b503997p

[130] Hach, "*Orbisphere M1100 Oxygen Sensors*" (Product Information, Last Access 08/2017).
URL: www.hach.com/dissolved-oxygen-sensors/orbisphere-m1100-oxygen-sensors/family?productCategoryId=35546907003

[131] Presens, "*Optical Oxygen Measurements in Scientific & Industrial Applications*" (Product Portfolio, Last Access 08/2017).
URL: www.presens.de/products/o2.html

[132] Ocean Optics, "*Oxygen Sensors*" (Product Portfolio, Last Access 08/2017).
URL: https://oceanoptics.com/product-category/oxygen-sensors/

[133] Pyro Science (Company Website, Last Access 08/2017).
URL: www.pyro-science.com/

[134] Mettler, "*Dissolved Oxygen Sensors*" (Product Portfolio, Last Access 08/2017).
URL: www.mt.com/at/de/home/products/Process-Analytics/DO-CO2-ozone-sensor/dissolved-oxygen-meter.html

[135] Neotek-Ponsel (Product Brochure, Last Access 08/2017).
URL: http://docs.wixstatic.com/ugd/40ca60_dd6a801456fb45ec8789635a22b450de.pdf

[136] TecSense (Company Website, Last Access 08/2017).
URL: www.tecsense.com/

[137] M. Cajlakovic, A. Bizzarri, C. Konrad *et al.*, *"Optochemical Sensors Based on Luminescence"* in *Encyclopedia of Sensors*, eds. C. A. Grimes, E. C. Dickey and M. V. Pishko, pp. 291-314, American Scientific Publisher (Pennsylvania State University, 2005).

[138] H. S. Voraberger, H. Kreimaier, K. Biebernik *et al.*, *"Novel oxygen optrode withstanding autoclavation: technical solutions and performance"*, *Sensors and Actuators B: Chemical* 74/1 (2001) 179-185.
DOI: 10.1016/S0925-4005(00)00730-9

[139] W. Trettnak, *"Optical Sensors Based on Fluorescence Quenching"* in "*Fluorescence Spectroscopy: New Methods and Applications*", ed. O. S. Wolfbeis, pp. 79-89, Springer Berlin Heidelberg (Berlin, Heidelberg, 1993).
DOI: 10.1007/978-3-642-77372-3_7

[140] B. H. Weigl, S. Draxler, D. Kieslinger *et al.*, *"Optical sensor instrumentation using absorption- and fluorescence-based capillary waveguide optrodes"*, *Proc. SPIE 2508, Chemical, Biochemical, and Environmental Fiber Sensors VII*, Munich, DE (1995) 199-209.
DOI: 10.1117/12.221733

[141] K. Biebernik, F. Reininger and W. Trettnak, *"Opto-chemischer Sensor sowie Verfahren zu seiner Herstellung"*, Patent No. EP 1 114 309 B1, to "Joanneum Research Forschungsgesellschaft mbH" (Austria, 1999).

[142] Nano, "*Just how is your money spent?*" (Electronic Article, Last Access 08/2017).
URL: www.ltfn.gr/images/projects/nano_magazine_Feb2014.pdf

[143] M. Tscherner, C. Konrad, A. Bizzarri *et al.*, *"Opto-chemical method for ultra-low oxygen transmission rate measurement"*, *2009 IEEE Sensors*, Christchurch, NZ (2009) 1660-1665.
DOI: 10.1109/ICSENS.2009.5398515

[144] M. Tscherner, C. Konrad, A. Bizzarri *et al.*, *"Opto-chemical oxygen permeability measurements"*, *Sensor and test 2006 proceedings :OPTO 2006*, Nürnberg, DE (2006) 79-84

[145] C. Kolle, *"Development and Evaluation of a Phase Fluorimetric Instrumentation for Luminescence Based Optical Oxygen Sensors"*, PhD Thesis, Institute for Automation, *Montanuniversität Leoben* (1999).

[146] Applied Sensors Group, TU Graz, "*fluorophores.org*" (Database, Last Access 09/2017).
URL: www.fluorophores.tugraz.at/

[147] P. Hartmann and W. Trettnak, *"Effects of Polymer Matrices on Calibration Functions of Luminescent Oxygen Sensors Based on Porphyrin Ketone Complexes"*, *Analytical Chemistry* 68/15 (1996) 2615-2620.
DOI: 10.1021/ac960008k

[148] W. Trettnak, M. J. P. Leiner and O. S. Wolfbeis, *"Optical sensors. Part 34. Fibre optic glucose biosensor with an oxygen optrode as the transducer"*, *Analyst* 113/10 (1988) 1519-1523.
DOI: 10.1039/an9881301519

[149] AirLiquide, "*ALPHAGAZ O2-Free, Point-of-Use Gas Purification*" (Product Information, Last Access 09/2017).
URL: http://produkte.airliquide.de/loesungen/produkte/armaturenkatalog/sonstigedok/1983.pdf

[150] Apiezon, "*Grease T*" (Product Information, Last Access 09/2017).
URL: www.apiezon.com/products/vacuum-greases/t-grease

[151] GKN Sinter Metals, "*Sika B*" (Product Brochure, Last Access 09/2017).
URL: www.gkngroup.com/sintermetals/media/Brochures%20Library/Capabilities%20-%20Porous%20Metal%20Filters/GKN%20Filter%20Technology%20SIKA-B%20EN.pdf

[152] Autodesk, "*AutoCAD*" (Product Information, Last Access 09/2017).
URL: www.autodesk.com/products/autocad/overview

[153] National Instruments, "*LabVIEW*" (Product Information, Last Access 09/2017).
URL: www.ni.com/en-gb/shop/labview/buy-labview.html

[154] OriginLab, "*Origin*" (Product Information, Last Access 09/2017).
URL: www.originlab.com/

[155] Wolfram Research, "*Mathematica*" (Product Information, Last Access 09/2017).
URL: www.wolfram.com/mathematica/index.en.html?footer=lang

[156] GNU Project, "*R*" (Last Access 09/2017).
URL: www.r-project.org/

[157] Huntsman, "*Araldite 2000+ Adhesives*" (Product Information, Last Access 09/2017).
URL: www.huntsman.com/advanced_materials/Media%20Library/global/files/US%202000%2B%20Adhesives%20Selector%20_Guide%20for%20Bonding_Assembly_Repair_Araldite.pdf

[158] BOLA, "*PTFE Filtering Tiles*" (Product Information, Last Access 09/2017).
URL: www.bola.de/en/products/filtration/detail/kapitel/90/kategorie/10/num/N_1610_16/ext/detail.html

[159] ROBU, "*Special-Design Sinter Filters*" (Product Information, Last Access 09/2017).
URL: www.robuglas.com/en/products/sintered-filters/special-designs/special-design-sinterfilter.html

[160] Wavelength Electronics, "*LFI3751 5A Digital Temperature Control Instrument*" (Product Information, Last Access 09/2017).
URL: www.teamwavelength.com/products/product.php?part=20

[161] Wavelenght Electronics, "*WTC3293-14001 2.2A Temperature Controller*" (Product Information, Last Access 09/2017).
URL: www.teamwavelength.com/products/product.php?part=120

[162] Knap, "***Peltier Modules with Through Holes***" (Product Information, Last Access 09/2017).
URL: www.knap.at/products/heatpipes-peltiers/peltier-modules/sh-rh-ot

[163] Keller, "***Pressure Transmitters***" (Product Information, Last Access 09/2017).
URL: www.keller-druck.com/home_e/paprod_e/33x_35x_e.asp

[164] Nanotec, "***Stepping Motors, Planetary Gears and Controller Units***" (Product Portfolio, Last Access 09/2017).
URL: https://en.nanotec.com/products/

[165] R+W, "***Precion Bellow Couplings, Series BKL***" (Product Information, Last Access 09/2017).
URL: www.rw-couplings.com/products/precision-couplings/metal-bellows-couplings/bkl/

[166] A. Bizzarri, C. Konrad and V. Ribitsch, ***"Method and device for determining the fluorescence of a sample and use thereof"***, Patent No. WO 2007068021 A1, to "Joanneum Research Forschungsgesellschaft mbH" (Austria, 2005).

[167] A. Soeren, ***"A method and fluorometer for measuring the phase shift induced in a light signal by fluorescence emission by a sample"***, Patent No. WO2006010604 (A1), to "Precisense AS" (Denmark, 2005).

[168] T. Trapp, K.-D. Anders, C. Huber *et al.*, ***"Optischer Sensor zur Bestimmung eines Analyten und Verfahren zu dessen Herstellung"***, Patent No. EP 1 199 556 A1, to "Mettler-Toledo GmbH" (Germany, 2001).

[169] Chemours, "***Teflon™ AF amorphous fluoroplastics***" (Product Information, Last Access 09/2017).
URL: www.chemours.com/Teflon_Industrial/en_US/products/product_by_name/teflon_af/index.html

[170] Solvay, "***Hyflon AD***" (Product Information, Last Access 09/2017).
URL: www.solvay.com/en/markets-and-products/featured-products/hyflon-ad.html

[171] AGC Chemicals, "***Amorphous Fluoropolymer Cytop***" (Product Information, Last Access 09/2017).
URL: www.agcce.com/cytop/

[172] J. C. Jansen, M. Macchione and E. Drioli, *"On the unusual solvent retention and the effect on the gas transport in perfluorinated Hyflon AD® membranes"*, *Journal of Membrane Science* 287/1 (2007) 132-137.
DOI: 10.1016/j.memsci.2006.10.031

[173] E. R. Carraway, J. N. Demas and B. A. DeGraff, *"Photophysics and oxygen quenching of transition-metal complexes on fumed silica"*, *Langmuir* 7/12 (1991) 2991-2998.
DOI: 10.1021/la00060a015

[174] J. López-Gejo, D. Haigh and G. Orellana, *"Relationship between the Microscopic and Macroscopic World in Optical Oxygen Sensing: A Luminescence Lifetime Microscopy Study"*, *Langmuir* 26/3 (2010) 2144-2150.
DOI: 10.1021/la902546k

[175] D. R. James and W. R. Ware, *"A fallacy in the interpretation of fluorescence decay parameters"*, *Chemical Physics Letters* 120/4 (1985) 455-459.
DOI: 10.1016/0009-2614(85)85640-2

[176] E. R. Carraway, J. N. Demas and B. A. DeGraff, *"Luminescence quenching mechanism for microheterogeneous systems"*, *Analytical Chemistry* 63/4 (1991) 332-336.
DOI: 10.1021/ac00004a006

[177] P. Hartmann, M. J. P. Leiner and M. E. Lippitsch, *"Luminescence Quenching Behavior of an Oxygen Sensor Based on a Ru(II) Complex Dissolved in Polystyrene"*, *Analytical Chemistry* 67/1 (1995) 88-93.
DOI: 10.1021/ac00097a015

[178] W. Xu, R. C. McDonough, B. Langsdorf *et al.*, *"Oxygen Sensors Based on Luminescence Quenching: Interactions of Metal Complexes with the Polymer Supports"*, *Analytical Chemistry* 66/23 (1994) 4133-4141.
DOI: 10.1021/ac00095a004

[179] X. Lu and M. A. Winnik, *"Luminescence Quenching in Polymer/Filler Nanocomposite Films Used in Oxygen Sensors"*, *Chemistry of Materials* 13/10 (2001) 3449-3463.
DOI: 10.1021/cm011029k

[180] E. R. Carraway, J. N. Demas, B. A. DeGraff *et al.*, *"Photophysics and photochemistry of oxygen sensors based on luminescent transition-metal complexes"*, *Analytical Chemistry* 63/4 (1991) 337-342.
DOI: 10.1021/ac00004a007

[181] A. Abdellatief, B. A. Welt, J. Butler *et al.*, *"Modelling Gas Transmission in Cylindrical Dynamic Accumulation Oxygen Transmission Rate Chambers to Explore Implications of Oxygen Sensor Location Relative to Samples"*, *Packaging Technology and Science* 27/8 (2014) 651-662.
DOI: 10.1002/pts.2059

11. CURRICULUM VITAE

Personal Data

NAME	Martin Tscherner
ACADEMIC DEGREE	Dipl.-Ing.
DATE/PLACE OF BIRTH	4th of September, 1975 (Wagna /Austria).
PERSONAL STATUS	Unmarried, daughter Luisa Pöttler-Tscherner (born 7th of October 2016).

Education

SEPTEMBER 1986 – JUNE 1994	Secondary education at „Naturwissenschaftliches Realgymnasium BG und BRG Leibnitz". A-levels with excellent success.
SEPTEMBER 1994 – JUNE 1996	Studies of "Industrial Mechanical Engineering", Technical University Graz.
MARCH 1995 – APRIL 2005	Studies of "Industrial Chemistry", Technical University Graz.
SEPTEMBER 1997 – JUNE 1998	Studies within the ERASMUS-programme at the University of Sheffield, UK.
OCTOBER 2001 – JANUARY 2004	Diploma Project at the Institute for Chemistry and Technology of Organic Materials at the Technical University Graz and under supervision of Ao. Univ. Prof. Mag. rer. nat. Dr. techn. Wolfgang Kern.
20TH OF APRIL 2005	Diploma in "General Industrial Chemistry" completed with excellent success.
APRIL 2005 – JULY 2008	Practical research within doctoral studies at the Institute for Chemistry and Technology of Organic Materials, Technical University Graz, under supervision of Univ.-Prof. Dipl.-Ing. Dr. techn. Franz Stelzer and in co-operation with the Institute for Chemical Process Development and -Control of Joanneum Research.
JULY 2017	Advanced Study Course on Optical Chemical Sensors (ASCOS), Trst (CZ).
29TH OF NOVEMBER 2017	Planned Date for Doctoral Viva.

Working Experience within Scientific Context

JULY 1998 – AUGUST 1998	Internship at "Institut Dr. Jäger", Tübingen (DE). Environmental Analytics.
JUNE 1999 – JULY 1999	Project Internship at the Institute for Organic Chemistry, Technical University Graz. Biocatalysis.
JULY 1999 – SEPTEMBER 1999	Internship at "Hoechst Schering Agrevo", Frankfurt (DE). Research and Synthesis of Herbizides.
SEPTEMBER 1999 – JANUARY 2000	Project Internship at the Institute for Organic Chemistry, Technical University Graz. Biocatalysis.
OCTOBER 1999 – DECEMBER 2001	Occasional organisational assistance for congresses.
JANUARY 2004 – FEBRUARY 2004	Project "Methodenentwicklung für Permeationsmessungen", Institute for Chemical Process Development and –Control, Joanneum Research.
APRIL 2004 – MAY 2004	Project "Literaturrecherche für die Ausschreibung NANONET", Institute for Chemical Process Development and –Control, Joanneum Research.
APRIL 2005 – APRIL 2008	Scientific employee at the Institute for Chemistry and Technology of Organic Materials, Technical University Graz. STREP-Project "Flexonics" (6th EU Framework Programme). Development of highly sensitive methodology for the characterization of oxygen permeation rates of ultra-barriers.
SINCE AUGUST 2008	Scientific employee at Joanneum Research. Management and execution of research and development projects for customers including Anton Paar GmbH, Resom GmbH, OMV Production&Exploration, Fraunhofer IVV, Constantia Teich.
MARCH 2013 – NOVEMBER 2013	Educational Leave and reduction of engagement with Joanneum Research to 4 hrs weekly. Preparation of substantial parts of doctoral thesis.

Additional Activities (Selection)

1991 – 1997	Annual employment at various enterprises during vacations.
1992 – 1999	Tutorial teaching lessons in mathematics, descriptive geometry, chemistry and English as well as drums & percussion lessons.
1996 – 1999	Voluntary assistance at the culture department of the township Leibnitz (organisation of the annual Jazz festival.
NOVEMBER 1999 – DECEMBER 2001	Sound & Light engineer in the theatre- and culture centre "Theatro", Graz
SEPTEMBER 2000 - DECEMBER 2001	Technical coordination in the theatre- and culture centre "Theatro", Graz
SINCE JUNE 2000	Increasing activities in sound engineering and event management, thereby working with a number of artists, organisations and recording studios.
SINCE OCTOBER 2001	Trade certificate for „Sound Engineering and Event Management". Work for and with artists like Joe Zawinul, Opus, Marla Glen, Rebekka Bakken, Al Jarreau, Hans Theesink, Mike Stern, Jose Feliziano, Roger Chapman, Simon Phillips, Manu Katche, Steve Smith, TM Stevens, Papermoon, Klimmstein and countless local artists. Technical management also for large scale events (>10.000 visitors).

Skills and Interests

LANGUAGES	German (native language) English (proficient) Spanish (Intermediate)
IT	NI LabView, C++ (Fundamentals), Origin, Mathematica, AutoCAD, MS Access/Word/Excel/PowerPoint/Project/VBA, Adobe Photoshop/ Premiere/ Audition, Windows, Linux, system- and network administration.
HANDCRAFT	Distinct electronics, mechanics and device knowledge. High artisanal skills and ability for technical improvisation. Processing of wood and metal. Maintenance of manned glider planes and sound engineering equipment. Maintenance and construction of guitars.
RECREATIONAL ACTIVITIES	Flying gliders (cross-country and aerobatics; glider pilot license obtained in June 2003) and powered aircraft Sport Climbing/ Bouldering. Music active (drums/ guitars) and passive. Alpine- and Endurance-dependent sport activities. Nature/ Languages/ Countries/ Cultures.

LIST OF PUBLICATIONS

Papers

M. Hollauf, P. W. Zach, S. M. Borisov, B. J. Müller, D. Beichel, M. Tscherner, S. Köstler, P. Hartmann, A.-C. Knall, G. Trimmel., "*Dye functionalized-ROMP based terpolymers for the use as a light up-converting material via triplet-triplet annihilation*", Journal of Materials Chemistry C, 5 (2017) 7535-7545.
DOI: 10.1039/C7TC01639E

M. Hollauf, M. Cajlakovič, M. Tscherner, S. Köstler, A.-C. Knall, G. Trimmel, „*Synthesis and characterization of naphthalimide-functionalized polynorbornenes*", Monatsh. Chem. 148 (2017) 121–129.
DOI: 10.1007/s00706-016-1887-3

A. Rudorfer, M. Tscherner, C. Palfinger, F. Reil, P. Hartmann, I. E. Seferis, E. Zych, F. P. Wenzl, „*A study on Aerosol jet printing technology in LED module manufacturing*", Proc. SPIE 9954, Fifteenth International Conference on Solid State Lighting and LED-based Illumination Systems, 99540E (2016).
DOI: 10.1117/12.2237737

C. Wolf, M. Tscherner, S. Köstler, „*Ultra-fast opto-chemical sensors by using electrospun nanofibers as sensing layers*", Sensors and Actuators B: Chemical, 209 (2015) 1064–1069.
DOI: 10.1016/j.snb.2014.11.070

C. Wolf, M. Tscherner, S. Köstler, V. Ribitsch, „*Optochemical sensors based on polymer nanofibers with ultra-fast response characteristics*", IEEE Sensors (2014) 950-953.
DOI: 10.1109/ICSENS.2014.6985159

A.-C. Knall, M. Tscherner, N. Noormofidi, A. Pein, R. Saf, K. Mereiter, V. Ribitsch, F. Stelzer, C. Slugovc, "*Nonradiative deactivation of europium(III) luminescence as a detection scheme for moisture*", Analyst 137 (2012) 563-566.
DOI: 10.1039/C1AN15987A.

E. Kraker, B. Lamprecht, A. Haase, G. Jakopic, T. Abel, C. Konrad, S. Köstler, M. Tscherner, B. Stadlober, T. Mayr, "*Optochemical sensor based on screenprinted fluorescent sensorspots surrounded by organic photodiodes for multianalyte detection*", Proc. SPIE 7779 (2010) 777904 Organic Semiconductors in Sensors and Bioelectronics III.
DOI: 10.1117/12.859857.

B. Lamprecht, T. Abel, E. Kraker, A. Haase, C. Konrad, M. Tscherner, S. Köstler, H. Ditlbacher, T. Mayr, "*Integrated fluorescence sensor based on ring-shaped organic photodiodes*", physica status solidi (RRL) - Rapid Research Letters 4 (2010) 157-159.

DOI: 10.1002/pssr.201004096.

T. Mayr, T. Abel, E. Kraker, S. Köstler, A. Haase, C. Konrad, M. Tscherner, B. Lamprecht, "*An optical sensor array on a flexible substrate with integrated organic opto-electric devices*", Procedia Engineering 5 (2010) 1005-1008.
DOI: 10.1016/j.proeng.2010.09.279.

M. Cajlakovic, A. Bizzarri, M. Suppan, C. Konrad, M. Tscherner, V. Ribitsch, E. Beran, I. Knez, "*Simultaneously monitoring of tissue O2 and CO2 partial pressures by means of miniaturized implanted fiber optical sensors*", IEEE Sensors (2009) 1930-0395.
DOI: 10.1109/ICSENS.2009.5398126.

M. Tscherner, C. Konrad, A. Bizzarri, M. Suppan, M. Cajlakovic, V. Ribitsch, F. Stelzer, "*Opto-chemical method for ultra-low oxygen transmission rate measurement*", IEEE Sensors (2009) 1660-1665.
DOI: 10.1109/ICSENS.2009.5398515.

M. Tscherner, C. Konrad, A. Bizzarri, V. Ribitsch, F. Stelzer, "*Opto-chemical Oxygen Permeability Measurements*", Proceedings of the 7th Int. Conf. on Optical Technologies, Optical Sensors & Measuring Techniques (OPTO), Nürnberg (2006) 79-84.

K. Dax, M. Albert, D. Hammond, C. Illaszewicz, T. Purkarthofer, M. Tscherner, H. Weber, "*Rearrangements in the Course of Fluorination by Diethylaminosulfur Trifluoride at C-2 of Glycopyranosides: Some New Parameters*", ChemInform, 33/31 (2002).
DOI: 10.1002/chin.200231220

K. Dax, M. Albert, D. Hammond, C. Illaszewicz, T. Purkarthofer, M. Tscherner, H. Weber, "*Rearrangements in the Course of Fluorination by Diethylaminosulfur Trifluoride at C-2 of Glycopyranosides: Some New Parameters*", Monatshefte fuer Chemie/Chemical Monthly; 133 (2002) 427-448.
DOI: 10.1007/s007060200019.

K. Dax, M. Albert, D. Hammond, C. Illaszewicz, T. Purkarthofer, M. Tscherner, H. Weber, "*Rearrangements in the Course of Fluorination by Diethylaminosulfur Trifluoride at C-2 of Glycopyranosides: Some New Parameters*" in: W. Schmid, A. Stütz, "*Timely Research Perspectives in Carbohydrate Chemistry*", Vienna (2002).
DOI: 10.1007/978-3-7091-6130-2_5.

Patents

M. Tscherner, V. Ribitsch, "*Optochemischer Sensor*", Patent Family AT512498 (B1), EP2859333 (B1), TW201415002 (A), US2015147231 (A1), WO2013181679 (A1).

Conference Talks

C. Wolf, M. Tscherner, S. Köstler, V. Ribitsch, „*Optochemical sensors based on polymer nanofibers with ultra-fast response characteristics*", IEEE Sensors, 2014, Valencia (ES), 04.11.2014.

M. Tscherner, M. Buder-Stroissnigg, C. Bodor, G. Pinter, V. Ribitsch, F. Stelzer, „*Messung der Permeations- und Barriereeigenschaften von Kunststoffen*", PCCL-Symposium, Leoben (AT), 20.05.2011.

M. Tscherner, C. Konrad, A. Bizzarri, M. Suppan, M. Cajlakovic, V. Ribitsch, F. Stelzer, "*Opto-chemical method for ultra-low oxygen transmission rate measurement*", IEEE Sensors, 2009, Christchurch (NZ), 27.10.2009.

M. Cajlakovic, A. Bizzarri, M. Suppan, C. Konrad, M. Tscherner, V. Ribitsch, E. Beran, I. Knez, "*Simultaneously monitoring of tissue O2 and CO2 partial pressures by means of miniaturized implanted fiber optical sensors*", IEEE Sensors, 2009, Christchurch (NZ), 26.10.2009.

A.-C. Knall, A. Pein, N. Noormofidi, M. Tscherner, F. Stelzer, C. Slugovc, „*Preparation, characterization and applications of europium-containing copolymers*", 1st Joint Austrian & Slovenian Polymer Meeting ASPM 2008 and 9th Austrian Polymer Meeting, 2008, Graz (AT), 26.3.2008.

A.-C. Knall, A. Pein, N. Noormofidi, M. Tscherner, F. Stelzer, C. Slugovc, „*ROM-polymerizable europium complexes and their application in sensing layers*", 5. Workshop Anorganische Chemie in Österreich (5. WACÖ), 2008, Graz (AT), 18.3.2008.

M. Tscherner, C. Konrad, A. Bizzarri, V. Ribitsch, F. Stelzer, *"Opto-chemical Oxygen Permeability Measurements"*, 7th Int. Conf. on Optical Technologies., Optical Sensors & Measuring Techniques (OPTO). Nürnberg (DE), 31.05.2006.

Conference Posters

M. Tscherner, R. Resch, M. Schweiger, S. Köstler, *"Permanent Oxygen Monitoring in the Fermentation Atmosphere of Grass Silage using Optochemical Sensing Technology"*, Poster at the "Sensors in Food and Agriculture 2016" Conference, Cambridge (UK), 29.-30.11.2016.

M. Tscherner, A. Dolezal, B. Feketeföldi, H. Pressler, A. Tschepp, M. Suppan, V. Ribitsch, P. Hartmann, „*Optochemical oxygen sensors for chemically harsh environments*", Poster at the "Europtrode XIII" Conference, Graz (AT), 21.-23.03.2016.

C. Wolf, M. Tscherner, S. Köstler, „*Ultra-fast opto-chemical sensors by using electrospun nanofibers as sensing layers*", Poster at the Europtrode XII" Conference, Athens (GR), 13.–16.04.2014.

A.-C. Knall, A. Pein, N. Noormofidi, M. Tscherner, C. Konrad, V. Ribitsch, G. Uray, F. Stelzer, C. Slugovc, „*Lifetime-based optical humidity measurements using europium-containing materials*", Poster at the "Europtrode IX" Conference, Dublin (IRE), 31.03. - 02.04.2008.

A.-C. Knall, A. Pein, N. Noormofidi, M. Tscherner, C. Konrad, V. Ribitsch, G. Uray, F. Stelzer, C. Slugovc, „*Optical humidity sensor materials based on europium*", Poster at the "10th Conference on Methods and Applications of Fluorescence", Salzburg (AT), 09. – 12.09.2007.

A.-C. Knall, M. Tscherner, C. Konrad, A. Bizzarri, V. Ribitsch, F. Stelzer, G. Uray, „*Optical humidity sensor using europium luminescence*", Poster at the "Materials Research Society Fall Meeting", Boston (USA), 27.11. – 1.12.2006.

Press Articles

„*Fehler erschnüffeln mit Gas*", Kleine Zeitung, 06. 03 2014.
URL: http://www.kleinezeitung.at/nachrichten/chronik/uni/3567086/fehler-erschnueffeln-gas.story

Series „*Innovative Geister*" in „Steirische Wirtschaft" No. 23 (04.07.2014), p.35, about a joint development with the project partner „Resom GmbH".
URL: http://www.stwi.at/stwi_2014-23/files/assets/basic-html/page35.html

„*Der High-Tech-Sensor im Viehfutter*", Die Presse, 15.09.2017.
URL: http://diepresse.com/home/science/5286495/Der-HighTechSensor-im-Viehfutter